Universidad Autónoma de Madrid
Facultad de Ciencias
Departamento de Física Teórica

Imprints of heavy Majorana neutrinos and their SUSY partners in Higgs physics

Memoria de Tesis Doctoral realizada por
Ana María Rodríguez Sánchez
presentada ante el Departamento de Física Teórica
de la Universidad Autónoma de Madrid
para la obtención del Título de Doctor en Ciencias

Trabajo dirigido por
María José Herrero Solans,
Catedrática del Departamento de Física Teórica
y miembro del Instituto de Física Teórica, IFT-UAM/CSIC

Madrid, Noviembre de 2011

A mi abuela Clara
que te envolvía con su calidez

Contents

Introduction **1**

Introducción **15**

1 SUSY models **29**

1.1 The Minimal Supersymmetric Standard Model 29

1.2 Interactions and particle content of the MSSM 33

1.2.1 Squark sector 38

1.2.2 Slepton sector 41

1.2.3 Chargino sector 42

1.2.4 Neutralino sector 43

1.2.5 The Higgs boson sector at tree-level 44

1.2.6 Radiative corrections to the lightest Higgs boson in the MSSM . . . 46

1.3 Constrained MSSM scenarios and experimental bounds 50

1.3.1 Constrained SUSY models 50

1.3.2 CMSSM/mSUGRA model 52

1.3.3 NUHM scenarios 52

1.3.4 Experimental status of the MSSM 53

2 Majorana neutrinos, their SUSY partners and their interactions **57**

2.1 Majorana neutrinos 57

2.2 The MSSM-seesaw: the three generations case 59

2.2.1 The neutrino mass Lagrangian 61
2.2.2 The sneutrino mass Lagrangian 66
2.2.3 The neutrinos interaction Lagrangian 68
2.2.4 The sneutrinos interaction Lagrangian 69
2.3 The MSSM-seesaw: the one generation case 70
2.3.1 The neutrinos and sneutrinos interaction Lagrangian 72
2.3.2 Relevant parameters and limits 74

3 Radiative corrections to m_h in the MSSM-seesaw model 79
3.1 Higher-order corrections to m_h 80
3.1.1 Regularization and renormalization 80
3.1.2 The concept of higher order corrections in the Feynman-diagrammatic approach 81
3.1.3 One-loop renormalization 82
3.1.4 Renormalization schemes 84
3.2 Results 87
3.2.1 One-loop calculation of the renormalized self-energies 87
3.2.2 Analysis of the renormalized self-energies 88
3.2.3 Estimate of the one-loop corrections from neutrino/sneutrino sector to M_h within the MSSM-seesaw 104

4 LFV processes mediated by Higgs bosons within constrained MSSM-seesaw scenarios 113
4.1 Flavor mixing in the slepton sector within the MSSM-seesaw 114
4.2 LFV in Higgs mediated processes 118
4.3 Framework for the LFV decays 120
4.4 Hadronisation of quark bilinears 127
4.5 Results for BR($\tau \to \mu\eta$) 133
4.6 Results for BR($\tau \to \mu f_0(980)$) 135

Conclusions **147**

Conclusiones **153**

A New Feynman rules **161**

B Majorana case. One-loop neutrino/sneutrino corrections to the self-energies and tadpoles **169**

C Dirac case. One-loop neutrino/sneutrino contributions to the h Higgs boson self-energy **175**

Bibliography **177**

Introduction

The Standard Model (SM) [1–5] is a 4 dimensional quantum field theory, based on the gauge symmetry $SU(3)_C \times SU(2)_L \times U(1)_Y$. The SM describes three of the four fundamental interactions, the strong interaction (QCD), that binds quarks within hadrons, such as protons and neutrons, the electromagnetic interaction (QED), responsible, for instance, of the propagation of radio waves and the weak interaction that triggers the β decay. Gravitation is the only fundamental force that is not included in the SM since up to date no quantum field theory of gravity has been developed. This model describes with amazing success most of the known phenomena and, indeed, the agreement between its predictions and the data is excellent, tested in some cases to a precision greater than 1%.

The matter content of the SM corresponds to the fermionic sector (spin 1/2), leptons and quarks, which are organized in a three-fold family structure. The gauge sector of the SM corresponds to gauge bosons (spin 1-vector particles), $W^{\pm}$ and Z, 8 gluons and one photon, which are exchanged when a weak, strong and electromagnetic interaction, respectively, occurs.

For consistency reasons, the SM contains also a complex scalar doublet, the Higgs doublet, which is the only fundamental scalar field of the model. The introduction of this Higgs doublet at the electroweak scale, $v \sim \mathcal{O}(100)$ GeV, is needed in order to preserve unitarity in the scattering of four gauge bosons with longitudinal polarization. As a consequence of the introduction of this Higgs field, the $SU(3)_C \times SU(2)_L \times U(1)_Y$ gauge symmetry of the SM Lagrangian (can be) is broken by the vacuum, which triggers the Spontaneous Symmetry Breaking (SSB) of the electroweak group to the electromagnetic subgroup: $SU(2)_L \times U(1)_Y \to U(1)_{QED}$. This mechanism of electroweak symmetry breaking (EWSB) is known as the Higgs mechanism [6–9] and it provides a general framework to explain the observed masses of the $W^{\pm}$ and Z gauge bosons by means of charged and neutral Goldstone bosons that end up as the longitudinal components of the gauge bosons. Fermions also acquire mass through this mechanism via the Yukawa couplings.

Moreover, the Higgs mechanism predicts the existence of a physical scalar particle, the so-called Higgs boson, which has not yet been detected. Finding this particle and understanding the underlying dynamics of EWSB is one of the most important challenges of experimental and theoretical particle physics nowadays. The Higgs boson mass in the SM is proportional to the quartic Higgs self coupling, λ . Since λ is presently unknown, the value of the SM Higgs boson mass m_h is not predicted. However, there are bounds on the mass of this particle coming both from theory, for instance unitarity and triviality bound, and from experiment, due to the contribution of the Higgs boson to observables that are measured with high precision, such as M_Z or M_W. For example, the upper bound from perturbative unitarity is $m_h \leq \sqrt{\frac{8\pi\sqrt{2}}{3G_F}} \sim 1\,\text{TeV}$ [10]. For values of m_h above this upper bound, weak interactions become strong in the TeV regime and perturbation theory is no longer valid. From electroweak precision data, a 95% C.L. upper bound on m_h can be set, $m_h \leq 169$ GeV for a standard fit, and $m_h \leq 143$ GeV for the complete fit including the constraints from the direct Higgs searches at LEP, Tevatron and LHC [11]. Regarding the experimental bounds, prior to the LHC, the best direct information on the mass of the Standard Model Higgs boson was a lower limit of 114.4 GeV at the 95% confidence level, set using the combined results of the four LEP experiments [12] and an excluded band of 158 GeV to 173 GeV from the combined Tevatron experiments [13, 14]. During the present year 2011, the LHC has improved quite substantially the previous bounds. The ATLAS experiment has excluded at 95% CL a very wide range of Higgs boson mass in the two mass ranges from 155 GeV to 190 GeV and 295 GeV to 450 GeV [15]. The CMS experiment, has excluded the SM Higgs boson at 95% C.L. in the two mass ranges 149-206 and 300-440 GeV [16]. The Higgs boson mass limits are indeed improving very rapidly at the LHC. At the time this thesis is coming to an end, a very recent ATLAS and CMS combined analysis has been performed, where a Higgs boson like mass in the range from 144 to 476 GeV is excluded at at 95% C.L.. This analysis, combined with the LEP lower bound on the SM Higgs mass, leaves a quite narrow window left for the SM Higgs mass: $114 < m_h < 141$ GeV at 95% C.L. [17].

Furthermore, in the SM the Higgs boson mass has an instability under radiative corrections, known as the hierarchy problem. All low-energy couplings and fermion masses are logarithmically sensitive to the scale of new physics Λ. In contrast, scalar squared-masses are quadratically sensitive to Λ. This implies that the Higgs boson can get huge radiative corrections if the scale of new physics is large. Therefore, in order to obtain a light Higgs boson mass of $\mathcal{O}(100)$ GeV, compatible with the present bounds, there has

to be a cancellation between the tree level mass and higher order contributions. If Λ is considerably larger than 1 TeV, then an "unnatural" cancellation must occur. This cancellation is what physicists refer to as fine tuning and, although it may be considered a prejudice more than a real problem, many theories have been developed in order to avoid this improbable coincidence.

A very positive aspect of going beyond tree level is that, quantum corrections offer the possibility to be sensitive to heavy particles, which cannot be kinematically accessed, through their virtual loop effects. The importance of these virtual effects from the heavy particles at low energies depends critically on the decoupling or non-decoupling properties of these heavy particles and these, in turn, depend on the particular features of the Quantum Field Theory considered. For instance, in QED and QCD the vacuum polarization contribution of a heavy fermion pair is suppressed at low energies by inverse powers of the fermion mass. Therefore, at low energies, the information on the heavy fermions is then lost. This decoupling of the heavy fields happens in theories with only vector couplings and an exact gauge symmetry [18], where the effects generated by the heavy particles can always be reabsorbed into a redefinition of the low-energy parameters. The SM involves, however, a broken chiral gauge symmetry. This has the very interesting implication of avoiding the decoupling theorem [18]. Thus, for instance, the vacuum polarization contributions induced by a heavy top generate corrections to the $W^{\pm}$ and Z self-energies, which increase quadratically with the top mass [19]. Therefore, a heavy top does not decouple and its quantum effects are relevant even at very low energies compared with its mass.

The most stringent SM test comes from the high-precision measurements of the electron and the muon anomalous magnetic moments, $a_l = (g_l - 2)/2$, with $l = e, \mu$. Radiative corrections contributing to these anomalous magnetic moments are fully known to $\mathcal{O}(\alpha^4)$, and some $\mathcal{O}(\alpha^5)$ corrections have been computed. In fact, a_e provides the most accurate determination of the fine structure constant, $\alpha^{-1} = 137.035999084 \pm 0.000000051$ [20]. The anomalous magnetic moment of the muon has been measured at Brookhaven National Laboratory to a precision of 0.54 parts per million. The current average of the experimental results is given by $a_\mu = (1165920.80 \pm 0.63) \times 10^{-9}$, which is different from the SM prediction by $2.2\,\sigma$ to $2.7\,\sigma$ [21], $\Delta a_\mu = a_\mu^{\rm exp} - a_\mu^{\rm SM} = (22.4 \pm 10 \text{ to } 26.1 \pm 9.4) \times 10^{-10}$ [1]. This discrepancy between prediction and experiment seems to be a hint of new physics that would contribute with positive sign to a_μ, but it could also be explained by higher

[1] The main source of uncertainty in the SM prediction comes from the hadronic vacuum polarization. The above result is determined directly from the annihilation of $e^- e^+$ into hadrons. If the hadronic decay of the τ is also taken into account, a_μ^{hadr} becomes bigger and this reduces the discrepancy to about $1.6\,\sigma$.

order QCD corrections that have not been calculated yet. This is the power of precision measurements, as the experimental sensitivity increases, the required precision of the theory prediction becomes higher. Therefore, the calculation of higher order quantum corrections to a certain observable is needed in order to check the agreement with the experimental value. If there is a discrepancy, then extensions of the SM can try to explain it, but their parameter space might be very constrained in order to account for such a precise measurement.

Processes involving Flavor Changing Neutral Currents (FCNC) provide excellent opportunities to search for evidence of new physics since in the SM they are forbidden at tree level, and can only occur through higher order loop diagrams. For instance, the decay $B_s \to \mu^+\mu^-$ has been identified as a very interesting potential constraint on the parameter space of models for physics beyond the SM. The present upper limit to this decay, measured by the CMS and LHCb collaborations [22], is given by, $\mathrm{BR}(B_s \to \mu^+\mu^-)_{\mathrm{exp}} < 1.1 \times 10^{-8}$ at 95% C.L. However, the SM prediction is computed to be $\mathrm{BR}(B_s \to \mu^+\mu^-)_{\mathrm{SM}} = (3.6 \pm 0.4) \times 10^{-9}$ [23]. Within the SM, this decay is dominated by a Z/Higgs-penguin diagram. Hence it is very sensitive to any new physics with new scalar or pseudoscalar interactions, in particular to any model with an extended Higgs sector.

At present, the most evident signal of new physics beyond the SM is provided, however, by the neutrino data, which indicate that neutrinos are massive particles and oscillate in flavor, contrarily to the SM prediction. The experiments with solar, atmospheric and reactor neutrinos [24–36] have provided compelling evidence for the existence of neutrino oscillations [37, 38], transitions in flight among the different neutrino flavors ν_e, ν_μ, ν_τ (antineutrinos $\bar{\nu}_e, \bar{\nu}_\mu, \bar{\nu}_\tau$), caused by nonzero neutrino masses and neutrino mixing. Strong evidence for oscillations of muon neutrinos were obtained also in the long-baseline accelerator neutrino experiments K2K [39] and MINOS [40, 41]. It follows from the existing data that at least 3 of the neutrinos mass eigenstates ν_j, say ν_1, ν_2, ν_3, must be light, $m_{1,2,3} < 1$ eV, and must have different masses, $m_1 \neq m_2 \neq m_3$.

Since the SM does not include neutrino masses, the measured masses and mixings of the neutrinos are clear signals of new physics and, therefore, a mechanism to generate neutrino masses and mixings is needed. The simplest possibility to include neutrino masses is to extend the SM by the introduction of 3 right-handed neutrinos in parallelism with all the other fermions of the SM. Then, neutrinos as any other fermion would acquire their masses via their Yukawa interactions with the Higgs field, concretely when EWSB

takes place and the Higgs field acquires an expectation value. However, in contrast to all the other fermions of the SM, right-handed neutrinos have the special property of being singlets under all the gauge groups of the SM, and that implies that neutrinos with definite mass ν_j can be Dirac fermions (with particles and antiparticles being different, $\nu \neq \nu^c$) or Majorana particles (with particles and antiparticles being the same, $\nu = \nu^c$). All the other fermions of the SM are Dirac particles.

Regarding the theoretical description of neutrino flavor oscillations, the neutrino mixing can be described by an unitary mixing matrix U, which can be parameterized by 3 angles, and, depending on whether the massive neutrinos ν_j are Dirac or Majorana particles, by 1 or 3 CP violating phases, respectively [42, 43]. The only way to forbid neutrino Majorana mass terms, i.e. explicit mass terms, is to impose the conservation of total lepton number, which is a global symmetry that is accidentally conserved in the SM. Establishing whether neutrinos with definite mass are Dirac or Majorana fermions is of fundamental importance for understanding the origin of neutrino masses and mixings and the underlying symmetries of neutrino interactions.

The Majorana nature of massive neutrinos manifests itself, for instance, in the existence of processes in which the total lepton charge L changes by two units. At present, the only feasible experiments having the potential of establishing that massive neutrinos are Majorana particles are the ones searching for the neutrinoless double beta decay ($(\beta\beta)_{0\nu}$ -decay): $(A, Z) \rightarrow (A, Z + 2) + e^- + e^-$. The observation of this $(\beta\beta)_{0\nu}$ -decay and the measurement of the corresponding half-life with sufficient accuracy, would not only be a proof that the total lepton charge is not conserved, but might also provide unique information on the i) type of neutrino mass spectrum [44], ii) Majorana phases in the neutrino mixing matrix U [45, 46] and iii) the absolute scale of neutrino masses [44, 46–49].

For the rest of this study, we will work within the hypothesis that neutrinos are of Majorana type. In this context a natural explanation of the smallness of neutrino masses is provided by the seesaw mechanism of neutrino mass generation [50, 51]. This mechanism, referred usually as seesaw type I, assumes the existence of right handed neutrinos with very large Majorana mass m_M compared to the electroweak scale, $M_{EW} \sim \mathcal{O}(100)$ GeV, coupled to the left-handed neutrinos via Yukawa couplings. Moreover, the right handed neutrino masses are chosen so that one obtains the three light neutrino masses, m_{ν_i} ($i = 1, 2, 3$), and the three neutrino mixing angles, θ_{12}, θ_{23}, θ_{13}, in agreement with present data [20].

An interesting property of Majorana neutrinos generated by a seesaw mechanism is

that the Yukawa couplings can be large, $Y_\nu \sim \mathcal{O}(1)$, if m_M is large, say $m_M \sim (10^{14} - 10^{15})$ GeV, in contrast to Dirac neutrinos, with $Y_\nu \sim \mathcal{O}(10^{-12})$. In the first case, the heavy neutrinos have a chance of being detected indirectly through quantum effects induced to observables that are measured with high precision. However, in the Dirac case, the contribution of right-handed neutrinos is negligible.

Another appealing feature of the seesaw mechanism is that a Majorana mass term provides the violation of lepton number which might lead to the explanation of baryogenesis via leptogenesis. Within the framework of leptogenesis, the observed baryon asymmetry of the Universe (BAU) is explained by the out-of-equilibrium CP-violating decays of the heavy right-handed neutrinos. The lepton symmetry violation converts into baryon asymmetry due to the sphalerons that conserve B-L but violate B+L. If the heavy neutrinos, N_j ($j = 1, 2, 3$), have a hierarchical spectrum, $m_{N_1} \ll m_{N_2} \ll m_{N_3}$, the observed baryon asymmetry can be reproduced, provided the mass of the lightest one satisfies $m_{N_1} \gtrsim 10^9$ GeV [52].

Nevertheless, in the SM extended with three heavy right handed neutrinos, the existence of two separate mass scales, the electroweak scale M_{EW} and the Majorana scale m_M, usually chosen in the range, $10^{10} - 10^{15}$ GeV, leads to a severe hierarchy problem. Thus, one needs a proposal of new physics beyond the SM that can solve this puzzle. One of the most appealing solutions to the hierarchy problem is provided by the introduction of a new symmetry, called supersymmetry (SUSY) [53–55]. This symmetry relates fermions and bosons in such a way that the contribution of the new SUSY particles exactly compensates all the undesired quadratic contributions to scalar squared masses, therefore, stabilizing the value of Higgs mass at the electroweak scale. On the other hand, any SUSY extension of the SM may also incorporate the seesaw mechanism to generate the neutrino masses. Therefore, these SUSY-seesaw models successfully accommodate neutrino data and at the same time they do not suffer from the hierarchy problem.

The Minimal Supersymmetric Standard Model (MSSM) [56–58] is the minimal supersymmetric version of the SM which incorporates one supersymmetric partner per SM particle with the same mass and quantum numbers but with spin differing in one half unit. Thus, a new boson partner is assigned to each SM fermion and, correspondingly, a new fermionic SUSY partner is added to each SM boson particle. It is called minimal because it has the minimal number of possible supersymmetries ($N = 1$) and therefore, the minimal SUSY particle content. In order to implement the seesaw mechanism within the MSSM, one introduces, in addition to the usual MSSM spectra, three right-handed

neutrinos and the three corresponding superpartners, the sneutrinos.

However, it is well known that supersymmetry can not be an exact symmetry of the observed particle spectrum and, therefore, it must be broken in Nature, since no SUSY particles have been found so far in the experiments [20]. Although the SUSY breaking mechanism is not well known yet, if we do not want to spoil the cancellation of quadratic divergences the SUSY breaking terms must be *soft* [59]. In addition, they must provide proper masses for the SUSY particles in order to make them heavier than their SM partners.

The MSSM and the MSSM-seesaw have an extended Higgs sector that contains five physical Higgs bosons: two charged particles $H^{\pm}$, 1 neutral CP-odd particle A^0 and 2 neutral CP-even particles, h^0 and H^0. The lightest Higgs boson h^0 mass, m_{h^0}, is not a free parameter. In contrast with the Higgs of the SM, m_{h^0} has an upper bound at tree level given by M_Z, but it receives higher order corrections from loops of the SM particles and its superpartners, which are logarithmically dependent on the soft breaking SUSY masses and increase the tree level value. The main corrections to m_{h^0} in the MSSM come from the tops/stops sector because the Yukawa couplings are proportional to the corresponding fermion masses, and the top mass is bigger than any of the other fermion masses of the SM. The upper bound on m_{h^0} is then shifted above M_Z and the precise bound depends on the specific choice of soft parameters. For soft SUSY masses $\leq 2\,\text{TeV}$ the upper bound on m_{h^0} is ~ 135 GeV [60–62].

As we can appreciate, in the MSSM the Higgs boson mass is predicted to be relatively light, close to the EW scale, which makes it a phenomenological interesting theory because its predictions can be discarded or corroborated in the experiments, and particularly in the LHC. Many areas of the Higgs mass region have already been excluded, as it was shown above for the SM Higgs boson case. In the region of the parameter space where $m_{A^0} \gg M_Z$ and the masses of supersymmetric particles are large (the decoupling limit), the decay rates of the lightest MSSM Higgs boson h^0 into SM particles are nearly indistinguishable from those of the SM Higgs boson and, therefore, the exclusion bounds for h_{SM} can be applied to h^0. However, the low Higgs mass region has not been tested yet at the LHC because in this zone the most promising discovery decay mode of the Higgs is the diphoton channel, which needs more luminosity due to the smallness of the corresponding branching ratio with respect to other channels ($b\bar{b}$, $\tau\bar{\tau}$), which, on the contrary, suffer from a large background, resulting very difficult to disentangle signal from background.

In order to reduce the large number of free parameters introduced by the soft SUSY

breaking terms one often assumes constrained SUSY models. For instance, the well known constrained supersymmetric standard model (CMSSM) [63] minimizes the number of these parameters by assuming universal values at the gauge unification scale, leaving only five free parameters: the universal soft scalar mass, M_0, the universal soft gaugino mass, $M_{1/2}$, the universal trilinear coupling, A_0, the ratio of the two Higgs vevs, $\tan\beta$, and the sign of the Higgsino mass term, sign(μ). An interesting departure from the CMSSM can be obtained by relaxing the universality hypothesis for the soft SUSY breaking masses of the Higgs sector, M_{H_1} and M_{H_2}, so that they are independent of the soft scalar mass M_0. This partially constrained MSSM has seven free parameters, M_{H_1}, M_{H_2}, M_0, $M_{1/2}$, A_0, $\tan\beta$ and sign(μ), and is commonly referred to as the Non Universal Higgs Mass (NUHM) scenario [64]. The enlarged version of the CMSSM and the NUHM (including right handed neutrinos and sneutrinos) will be here designated as CMSSM-seesaw and NUHM-seesaw, respectively.

No SUSY particles have been detected yet and the LHC as well as Tevatron are setting bounds on the parameter space of constrained SUSY models, in particular the CMSSM. For instance, the CMS detector has excluded squark and gluino masses below ~ 1 TeV for a common value of the scalar mass at the GUT scale of $M_0 < 0.5$ TeV and for certain fixed values of the model parameters [65, 66]. Complementary to the direct search for SUSY particles, the indirect effects of those particles via radiative corrections to high precision observables is a very useful tool to test whether SUSY is compatible with data, and therefore a good candidate of new physics, or not, and thus SUSY (or some region of the parameter space) could be ruled out.

This thesis is devoted to the study of some of the indirect effects of Majorana neutrinos and sneutrinos via their radiative corrections to low energy observables that are planned to be measured with high precision and that have a potential sensitivity to the Higgs sector. Concretely, we have focused on two of the most relevant loop effects, namely: 1) the radiative corrections to the lightest Higgs boson mass of the MSSM-seesaw due to Majorana neutrinos and their SUSY partners, the sneutrinos, and, 2) the contributions induced by the Majorana neutrinos and sneutrinos to Higgs mediated lepton flavor violating decays within constrained SUSY-seesaw models. In the following we shortly introduce both studies.

In the first part of this thesis we study the indirect effects of Majorana neutrinos and sneutrinos in Higgs physics, via their radiative corrections to the MSSM Higgs boson masses. The main motivation for this study is that we expect these effects to be relevant

for sufficiently large Majorana mass, $m_M \gg m_{EW}$, due to the large size of the involved neutrino couplings, $Y_\nu \sim \mathcal{O}(1)$. In fact, in Ref. [67] the one-loop corrections to the lightest MSSM Higgs boson mass, M_h, were first estimated within a different scenario, the so-called split SUSY, and by the use of several approximations, and they already found a large and negative correction from the neutrino/sneutrino sector. Here we will present a full one-loop diagrammatic computation of the neutrino/sneutrino contributions to M_h and we will work in general MSSM-seesaw scenarios with no universality conditions imposed to the neutrino/sneutrino sector. Our study will also explore the role played by the large Majorana scale in the numerical size of the Higgs mass corrections. Furthermore, we will focus particularly in the features of these corrections with regard to the issue of decoupling or non-decoupling of the heavy Majorana neutrinos in Higgs physics. This will allow us to find out the interesting values of the Majorana mass where the size of the Higgs mass corrections enter into the measurable range. Although not fully set yet, the expected accuracy on the M_h measurement is challenging. The LHC expected precision on the measurement of a Standard Model (SM)-like Higgs boson is ~ 200 MeV [68–71] , while the ILC expected precision could reach the 50 MeV level [72–75]. On the other hand, the current precision in the predicted value of the MSSM Higgs corrected mass is estimated to be $\sim 2-3$ GeV [76]. Any correction comparable or larger than this current precision, should, therefore, be taken into account. We will show in this thesis that corrections from the Majorana neutrinos and their SUSY partners can be, indeed, of this order or even larger.

The second part of this thesis is devoted to the study of indirect effects of Majorana neutrinos and sneutrinos in Lepton Flavor Violating processes that can be mediated by Higgs bosons. In the context of indirect searches, Lepton Flavor Violating (LFV) processes provide one of the most challenging windows to test supersymmetric extensions of the standard model and also to test the neutrino sector beyond the SM [77–83]. The reason for this relies on the fact that Lepton Flavor Violating interactions are forbidden in the SM and, therefore, the SM predicts zero rates for those LFV observables. When extending the SM to include neutrino masses and mixings via a seesaw-type-I mechanism with no SUSY, LFV processes occur via loops of neutrinos, but they are extremely suppressed due to the small masses of the light neutrinos. However, this might not be the case in other low scale seesaw models (see for instance [84]).

In a MSSM-seesaw framework the situation is completely different. Besides the SM-seesaw contributions, supersymmetry provides new direct sources of flavor violation,

namely the possible presence of off-diagonal soft terms in the slepton mass matrices and in the trilinear couplings at low energies. In practice, flavor violation originates from the misalignment between fermion and sfermion mass matrices, that cannot be diagonalized simultaneously. Even if the scalar masses are universal at high energy, flavor mixing in the Yukawa couplings of the Majorana neutrinos induces, through renormalization effects, flavor mixing in the slepton masses at low energies and these sleptons, in turn, when propagating in the loops can, therefore, generate large rates in LFV processes [77–81].

The LFV process that is the most sensitive to the neutrino Yukawa couplings, in the SUSY-Seesaw context, is $\mu \to e\gamma$, where the present experimental sensitivity is at 2.4×10^{-12} [85]. Also $\mu - e$ conversion in heavy nuclei, with present bounds at $\mathrm{CR}(\mu - e, \mathrm{Ti}) < 4.3 \times 10^{-12}$ [86] and $\mathrm{CR}(\mu - e, \mathrm{Au}) < 7 \times 10^{-13})$ [87], and $\mu \to 3e$ with $\mathrm{BR}(\mu \to 3e) < 1.0 \times 10^{-12}$ [88], are quite sensitive to LFV in the $\mu - e$ sector.

In the $\tau - \mu$ sector the upper bound in the decay $\tau \to \mu\gamma$ is now set to 4.4×10^{-8} by the BABAR collaboration [89]. Moreover, the sensitivity to LFV in $\tau \to 3\mu$ has improved remarkably in the last years. The present upper bounds from BELLE and BABAR collaborations are 2.1×10^{-8} [90] and 3.3×10^{-8} [89], respectively. In the last years, the semileptonic τ decays have already become competitive with the pure leptonic decays [91, 92].

In this thesis we perform a comparative study of the semileptonic decays $\tau \to \mu f_0(980)$ and $\tau \to \mu\eta$. Both channels have competitive upper bounds $\mathrm{BR}(\tau \to \mu\eta) < 2.3 \times 10^{-8}$ [93] and $\mathrm{BR}(\tau \to \mu f_0(980)) < 3.4 \times 10^{-8}$ [94]. The advantage of $\tau \to \mu\eta$ [95–97] and $\tau \to \mu f_0(980)$ [98] over the $\tau \to \mu\gamma$ channel is their potential sensitivity to the Higgs sector. It is known that within SUSY-seesaw scenarios $\tau \to \mu\gamma$ is not sensitive to the Higgs sector at the one-loop level. On the other hand, $\tau \to 3\mu$ is sensitive to the Higgs sector via the one-loop Higgs penguin diagrams [99]. However, the Higgs mediated contribution in this $\tau \to 3\mu$ channel is usually overwhelmed by the γ penguin diagrams in most of the constrained MSSM-seesaw scenarios. Therefore, to reach some sensitivity to the Higgs sector one must consider semileptonic τ decays [97]. The two semileptonic channels $\tau \to \mu\eta$ and $\tau \to \mu f_0(980)$ do not have γ mediated contributions and, therefore, they have direct access to the Higgs sector. Whereas the $\tau \to \mu\eta$ can be mediated by a Z boson and a CP-odd Higgs boson A^0, and it is dominated by the A^0 just at large $\tan\beta \gtrsim 20$ [97, 100], the $\tau \to \mu f_0(980)$ decay is exclusively mediated by the exchange of the neutral CP-even Higgs bosons H^0 and h^0. Therefore, through the $\tau \to \mu f_0(980)$ channel one is testing directly the neutral CP-even Higgs sector at all $\tan\beta$ values.

Our computation of the BR($\tau \to \mu f_0(980)$) improves the estimate of [98] in several aspects. First, we demand compatibility with present data on light neutrino masses and mixings. Second, we do not use the mass insertion approximation, we take into account the full set of SUSY one-loop diagrams in the LFV vertex $\tau\mu H$ ($H = h^0, H^0$), and include the two contributions mediated by the h_0 and H_0 respectively. Consequently, we explore the full $5 \leq \tan\beta \leq 60$ interval. Besides, the hadronization of quark bilinears into the $f_0(980)$ meson is performed here quite differently than in [98], where a simplified quark-flavour scheme was used to express these bilinears in terms of phenomenological meson decay constants. We instead pay close attention to the chiral constraints, following the standard Chiral Perturbation Theory (χPT) [101–103] and the Resonance Chiral Theory (RχT) [104–108] to incorporate resonances. Concretely, we follow the description of $f_0(980)$ in [107], where it is defined by a mixing between the octet and singlet components of the nonet of the scalar resonances which are included in RχT.

In our calculation, we focus on the constrained SUSY-seesaw scenarios described above, i.e. CMSSM-seesaw and NUHM-seesaw. In this later case the physical Higgs boson masses, m_{h^0} and m_{H^0}, can be both light, $\sim 100 - 250$ GeV, indeed close to their present experimental lower bounds and, therefore, the corresponding Higgs mediated contribution to the previous LFV processes can be relevant, even for large soft SUSY masses at $\sim \mathcal{O}(1\,\text{TeV})$. This is precisely the main interest of the channel $\tau \to \mu f_0(980)$, namely, the fact that the decay rates can be sizable even for large SUSY masses, $M_{\text{SUSY}} \sim \mathcal{O}(1\,\text{TeV})$, in clear contrast with other competitive tau flavor violating channels like $\tau \to \mu\gamma$, whose rates decrease as $1/M^2_{\text{SUSY}}$ and lie below the present experimental bound for such a heavy SUSY spectrum. In this thesis we will find that these two semileptonic channels, $\tau \to \mu f_0(980)$ and $\tau \to \mu\eta$ are indeed very competitive to test the three relevant sectors: SUSY, Higgs and the neu/sneu sectors.

The present thesis is organized as follows. In Chapter 1 the main aspects of the MSSM are reviewed paying special attention to the Higgs sector of this model. The relevance of radiative corrections to the lightest Higgs boson mass in the MSSM is shown, both analytically and numerically. Afterwards, we describe the main features of two constrained SUSY models of relevance for our work: CMSSM/mSUGRA and NUHM. Finally, we comment about the experimental status of the MSSM.

In Chapter 2, we review the need of enlarging the MSSM spectrum to accommodate neutrino masses. The benefits of the seesaw mechanism for generating neutrino masses are pointed out. The new ingredients of the MSSM-seesaw with respect to the MSSM,

which are original of this thesis, will be presented in this chapter. In particular, the mass spectrum of neutrinos and sneutrinos and their interactions with the neutral Higgs bosons of the MSSM and the Z gauge boson will be derived, being the relevant ones for the calculation in Chapter 3 of the radiative effects of heavy Majorana neutrinos and sneutrinos in the neutral $\mathcal{CP}$ even Higgs boson masses. The corresponding Feynman rules will also be presented.

The following chapters contain the central work of this thesis.

In Chapter 3 we present the calculation of the 1-loop radiative corrections to the lightest $\mathcal{CP}$ even Higgs boson mass from the neutrino/sneutrino sector within the MSSM-seesaw framework. We work here in general MSSM-seesaw scenarios with no universality conditions imposed, and explore the full parameter space of the neutrino/sneutrino sector. We restrict our calculation to the 1 generation case of neutrinos/sneutrinos for simplicity and to fully understand the effect of just a single Majorana scale, although we know that at least two right handed neutrinos are needed in order to accommodate neutrino data. The complete set of one-loop neutrino/sneutrino contributing diagrams will be taken into account, with both Yukawa and gauge couplings switched on. We also analyze the results in different renormalization schemes, which will be shown to provide remarkable differences. In addition to the exact results, we present some analytical and numerical results in the interesting limit of very large m_M as compared to all other scales involved. Finally, we will discuss to what extent the radiative corrections computed here enter into the measurable range.

In Chapter 4 we perform a comparative study of the LFV semileptonic decays $\tau \to \mu\eta$ [95–97] and $\tau \to \mu f_0(980)$ within constrained MSSM-seesaw scenarios. Firstly, the generation of flavor mixing in the lepton sector of SUSY-seesaw models is explained. Then the framework used for the calculation of the mentioned decays is introduced, namely, the CMSSM-seesaw and the NUHM-seesaw. The numerical predictions of the neutral Higgs boson masses with respect to the other SUSY parameters is shown. Moreover, the connection between neutrino physics and LFV is illustrated in different contour plots. The full one-loop computation of the $\tau\mu H_i$ vertex is presented. The hadronization of quark bilinears is performed within the Chiral framework. We further present an approximate formula of the decays, which will provide very good results as it will be shown in the numerical estimates of the branching ratios. Finally, a comparison of the predictions with the experimental bounds will be addressed.

This thesis is based on the results published in the articles, [109], [110] and [111] and

in the conference proceedings [112], [100], [113], and [114].

Introducción

El Modelo Estándar (SM) [1–5] es una teoría de campos en cuatro dimensiones, basada en la simetría gauge $SU(3)_C \times SU(2)_L \times U(1)_Y$. El SM describe tres de las cuatro interacciones fundamentales, la interacción fuerte (QCD), que mantiene unidos a los quarks dentro de los hadrones, como pueden ser los protones o neutrones, la interacción electromagnética (QED), que es, por ejemplo, la responsable de la propagación de ondas de radio y las interacciones electrodébiles que desencadenan la desintegración β. La gravitación es la única fuerza fundamental, que no está incluída en el SM, ya que hasta la fecha no se ha desarrollado ninguna teoría cuántica de la gravedad. Este modelo describe satisfactoriamente la mayoría de los fenómenos conocidos y, de hecho, la concordancia/el acuerdo entre sus predicciones y los datos experimentales es excelente, habiéndose comprobado algunas veces hasta una precisión mayor del 1%.

El contenido de materia del SM consiste en el sector fermiónico (spin 1/2), leptones y quarks, que están organizados en una estructura de tres familias. El sector gauge del SM está formado por los bosones gauge (partículas vectoriales de spin 1), $W^{\pm}$ and Z, 8 gluones y un fotón, que son intercambiados cuando tiene lugar una interacción débil, fuerte y electromagnética, respectivamente.

Por argumentos de consistencia, el SM contiene también un doblete escalar complejo, el doblete de Higgs, que es el único campo escalar fundamental del modelo. La introducción de este doblete de Higgs a la escala electrodébil, $v \sim \mathcal{O}(100)$ GeV, es necesaria para preservar la unitariedad en la interacción de cuatro bosones gauge con polarización longitudinal.

Como consecuencia de la introducción del campo de Higgs, la simetría gauge $SU(3)_C \times SU(2)_L \times U(1)_Y$ del Lagrangiano del SM no es una simetra del vacío, provocando la ruptura espontánea de simetría (SSB) del grupo electrodébil en el subgrupo electromagnético: $SU(2)_L \times U(1)_Y \rightarrow U(1)_{QED}$. Este mecanismo de ruptura de la simetría electrodébil

(EWSB), es conocido como el mecanismo de Higgs [6–9] y proporciona un marco teórico para explicar las masas observadas de los bosones de gauge $W^{\pm}$ y Z, a través de los bosones de Goldstone cargados y neutro que se convierten en las componentes longitudinales de los bosones gauge. Los fermiones también adquieren su masa gracias al mecanismo de Higgs a través de los acoplamientos de Yukawa.

A su vez, el mecanismo de Higgs predice la existencia de una partícula física escalar, el bosón de Higgs, que todavía no ha sido detectado. Encontrar esta partícula y comprender la dinámica subyacente de EWSB es, en la actualidad, uno de los retos más importantes de la física de partículas, tanto teórica como experimental. La masa del bosón de Higgs es proporcional al auto acoplamiento cuártico del Higgs, λ. Puesto que λ es un parámetro desconocido hoy en día, el valor de la masa del bosón de Higgs del SM no está fijada por el modelo. No obstante, hay cotas a la masa de esta partícula que provienen tanto de la teoría, por ejemplo la cota de trivialidad y unitariedad, como de los experimentos, relacionadas con la contribución del bosón de Higgs a observables que se miden con gran precisión, como son M_Z o M_W.

Por ejemplo, la cota superior impuesta por unitariedad perturbativa es $m_h \leq \sqrt{\frac{8\pi\sqrt{2}}{3G_F}} \sim$ 1 TeV [10]. Para valores de m_h por encima de esta cota las interacciones débiles se convierten en fuertes a la escala del TeV y la teoría de perturbaciones deja de ser válida. De los datos de precisión electrodébiles, podemos extraer una cota superior sobre m_h al 95% de nivel de confianza, $m_h \leq 169$ GeV para un ajuste estándar y $m_h \leq 143$ GeV para un ajuste completo incluyendo las cotas de búsqueda directa del Higgs en LEP, Tevatron y el LHC [11].

Respecto a las cotas experimentales, antes del LHC, la mejor información directa sobre la masa del bosón de Higgs del SM era un límite inferior de 114.4 GeV al 95% de nivel de confianza, que se había obtenido gracias al resultado conjunto de los cuatro experimentos de LEP [12] y una banda excluída desde 158 GeV a 173 GeV, resultado de un estudio conjunto de los experimentos de Tevatron [13, 14]. En el presente año 2011, el LHC ha mejorado considerablemente las cotas previas. El experimento ATLAS ha excluído al 95% de nivel de confianza un amplio abánico de masas del bosón de Higgs en los dos intervalos de masas, de 155 GeV a 190 GeV y de 295 GeV a 450 GeV [15]. El experimento CMS, ha excluído el bosón de Higgs del SM al 95% de nivel de confianza en los dos intervalos 149-206 GeV y 300-440 GeV [16]. De hecho, los límites a la masa del bosón de Higgs están mejorando a gran velocidad en el LHC. Cuando esta tesis estaba a punto de ser finalizada,

se ha realizado un estudio conjunto ATLAS y CMS muy reciente, donde excluyen, al 95% de nivel de confianza, un bosón de Higgs como el del SM con una masa comprendida en el intervalo 144-476 GeV. Este análisis, combinado con la cota inferior de LEP a la masa del bosón de Higgs, deja una estrecha ventana de valores posibles para el bosón de Higgs del SM: $114 < m_h < 141$ GeV al 95% C.L. [17].

Por otra parte, en el SM la masa del bosón de Higgs es inestable frente a correcciones radiativas, conociéndose esta inestabilidad como el problema de las jerarquías. Todos los acoplamientos de baja energía y las masas de los fermiones son logarítmicamente sensibles a la escala de nueva física Λ. Sin embargo, las masas al cuadrado de los escalares son cuadráticamente sensibles a Λ. Esto implica que el bosón de Higgs puede recibir correcciones radiativas enormes si la escala de nueva física es grande. Por lo tanto, para obtener un bosón de Higgs ligero de $\mathcal{O}(100)$ GeV, compatible con las cotas actuales, debe haber una cancelación entre la masa a nivel árbol y correcciones de órdenes superiores. Si Λ es considerablemente más grande de 1 TeV, entonces debe tener lugar una cancelación "no natural". Esta cancelación es lo que los físicos denominan ajuste fino y, aunque pueda ser considerado un prejuicio más que un problema real, muchas teorías se han desarrollado para evitar esa improbable coincidencia.

Un aspecto muy positivo de ir más allá del nivel árbol es que las correcciones cuánticas tienen la posibilidad de ser sensibles a partículas pesadas, a las que no se puede acceder cinemáticamente, a través de sus efectos virtuales en loops (lazos). La importancia de estos efectos virtuales de partículas pesadas a baja energía depende fuertemente de las propiedades de desacoplamiento (*decoupling*) o no desacoplamiento (*non decoupling*) y éstas, a su vez, dependen de las características de la Teoría Cuántica de Campos (QFT) considerada. Por ejemplo, en QED y QCD la contribución de una par de fermiones pesados a la polarización del vacío está suprimida a bajas energías por potencias inversas de la masa del fermión. Por tanto, a bajas energías, se pierde la información de los fermiones pesados.

Este desacoplamiento de campos pesados se sabe que ocurre en teorías con acoplamientos vectoriales y con una simetría gauge exacta [18], donde los efectos generados por las partículas pesadas pueden ser siempre reabsorbidos en la redefinición de los parámetros a baja energía. No obstante, el SM posee una simetría gauge quiral que está rota. Este hecho tiene como consecuencia interesante que el teorema del *decoupling* [18] no es aplicable. Así, por ejemplo, las contribuciones a la polarización del vacío inducidas por un quark top pesado generan correcciones a las autoenergías del $W^{\pm}$ y Z, que crecen cuadráticamente

con la masa del top [19]. Es por ello, que un top pesado no se desacopla y sus efectos cuánticos son relevantes incluso a energías muy bajas comparadas con su masa.

El test más riguroso del SM proviene de las medidas de precisión electrodébiles del momento magnético anómalo del electrón y del muón, $a_l = (g_l - 2)/2$, con $l = e, \mu$. Las correcciones radiativas que contribuyen a estos momentos magnéticos anómalos se conocen por completo hasta $\mathcal{O}(\alpha^4)$, y algunas correcciones de $\mathcal{O}(\alpha^5)$ han sido calculadas. De hecho, a través de la medida de a_e se determina con la mayor precisión la constante de estructura fina $\alpha^{-1} = 137.035999084 \pm 0.000000051$ [20]. El momento magnético anómalo del muón ha sido medido en el Laboratorio Nacional de Brookhaven con una precisión de 0.54 partes por millón. El promedio actual de los resultados experimentales está dado por $a_\mu = (1165920.80 \pm 0.63) \times 10^{-9}$, que difiere de la predicción del SM en $2.2\,\sigma$ a $2.7\,\sigma$ [21], $\Delta a_\mu = a_\mu^{\rm exp} - a_\mu^{\rm SM} = (22.4 \pm 10 \text{ to } 26.1 \pm 9.4) \times 10^{-10}$ [2]. La discrepancia entre la predicción y el experimento parece un indicio de nueva física, que pudiese contribuir con signo positivo a a_μ, pero también podría ser explicado por correcciones de órdenes superiores en QCD, que no han sido calculadas todavía. Éste es el poder de las medidas de precisión, a medida que la precisión experimental aumenta, la precisión que se pide a la predicción teórica es mayor. Por lo tanto, el cálculo de correcciones cuánticas de órdenes superiores a un cierto observable es necesario para comprobar si está de acuerdo con el valor experimental. Si hay una discrepancia, entonces extensiones del SM pueden intentar explicarla, pero su espacio de parámetros puede verse muy restringido al intentar justificar una medida tan precisa.

Los procesos que involucran corrientes neutras con cambio de sabor (FCNC), proporcionan una oportunidad excelente para buscar evidencia de nueva física, ya que en el SM están prohibidos a nivel árbol y sólo pueden llevarse a cabo a través de diagramas de loop de órdenes superiores. Por ejemplo, la desintegración $B_s \to \mu^+\mu^-$ tiene un gran potencial restrictivo sobre el espacio de parámetros de modelos de física más allá del SM. El límite superior de esta desintegración, medido por las colaboraciones de CMS y LHCb [22], está dada por $\text{BR}(B_s \to \mu^+\mu^-)_{\rm exp} < 1.1 \times 10^{-8}$ al 95% de nivel de confianza. Sin embargo, se ha calculado que la predicción del SM es $\text{BR}(B_s \to \mu^+\mu^-)_{\rm SM} = (3.6 \pm 0.4) \times 10^{-9}$ [23]. En el SM, esta desintegración está dominada por el diagrama de pingüino del Higgs/Z. Por tanto, es muy sensible a nueva física con nuevas interacciones escalares o pseudoescalares,

[2] La mayor fuente de incertidumbre en la predicción del SM proviene de la contribución hadrónica a la polarización del vacío. El resultado citado arriba está determinado directamente por la aniquilación de e^-e^+ en hadrones. Si se tiene también en cuenta la desintegración hadrónica del τ, a_μ^{hadr} aumenta y esto reduce la discrepancia a $\sim 1.6\,\sigma$.

en concreto a cualquier modelo con un sector de Higgs extendido.

Actualmente, la señal más evidente de nueva física más allá del SM la proporcionan, no obstante, los datos experimentales de neutrinos, que indican que estos son partículas masivas y que oscilan en sabor, en contraposición a la predicción del SM. Los experimentos con neutrinos solares, atmosféricos y de reactores [24–36] han proporcionado pruebas convincentes de la existencia de oscilaciones de neutrinos [37, 38], transiciones en vuelo entre los distintos sabores de neutrinos ν_e, ν_μ, ν_τ (antineutrinos $\bar{\nu}_e, \bar{\nu}_\mu, \bar{\nu}_\tau$), causadas por masas y mezclas no nulas de los neutrinos. También se ha obtenido evidencia de las oscilaciones de neutrinos muónicos en los experimentos de neutrinos en aceleradores long-baseline K2K [39] and MINOS [40, 41]. Se deduce de los datos existentes que, al menos 3 de los autoestados de masa de los neutrinos ν_j, digamos ν_1, ν_2, ν_3, tienen que ser ligeros, $m_{1,2,3} < 1$ eV, y deben tener distintas masas.

Puesto que el SM no contiene masas para los neutrinos, las masas y mezclas de los neutrinos son señales claras de nueva física y, por tanto, es necesario un mecanismo que genere las masas y mezclas de los mismos. La opción más sencilla para incluir las masas de los neutrinos, es ampliar el SM con la introducción de 3 neutrinos dextrógiros (*right-handed*), en paralelismo con el resto de fermiones del SM. Entonces, los neutrinos, como cualquier otro fermión, adquirirán sus masas a través de las interacciones de Yukawa con el campo de Higgs, concretamente cuando se produce EWSB y el campo de Higgs adquiere un valor esperado en el vacío. Sin embargo, en contraste con el resto de los fermiones del SM, los neutrinos dextrógiros tienen la característica peculiar de ser singletes bajo todos los grupos gauge del SM, y eso implica que los neutrinos con una masa definida ν_j pueden ser fermiones de Dirac (con partículas y antipartículas diferentes entre si, $\nu \neq \nu^c$) o partículas de Majorana (con partículas y antipartículas idénticas, $\nu = \nu^c$). El resto de fermiones del SM son partículas de Dirac.

En lo que respecta a la descripcción teórica de las oscilaciones de sabor de los neutrinos, la mezcla de los mismos puede ser descrita por una matriz unitaria U, que puede parametrizarse con tres ángulos, y, con 1 o 3 fases de violación de $\mathcal{CP}$ dependiendo de si los neutrinos pesados ν_j son partículas de Dirac o Majorana, respectivamente [42, 43]. La única manera de prohibir los términos de masa de Majorana, es decir, términos de masa explícitos, es imponer la conservación del número leptónico total, que es una simetría global, que se conserva accidentalmente en el SM. Establecer si los neutrinos con masa definida son fermiones de Dirac o Majorana es de fundamental importancia para entender el origen de las masas y mezclas de los neutrinos y la simetría subyacente a las interac-

ciones entre los mismos.

La naturaleza Majorana de los neutrinos masivos se manifiesta, por ejemplo, en la existencia de procesos en los que el número leptónico total L cambia en dos unidades. En la actualidad, los únicos experimentos factibles capaces de establecer si los neutrinos son partículas de Majorana, son áquellos que buscan la doble desintegración beta con ausencia de neutrinos (desintegración-$(\beta\beta)_{0\nu}$): $(A, Z) \to (A, Z+2) + e^- + e^-$. La observación de esta desintegración $(\beta\beta)_{0\nu}$ y la medida de la correspondiente vida media con suficiente precisión, no sería sólo una prueba de que el número leptónico total no se conserva, sino que, además, podría proporcionar información excepcional sobre i) el espectro de masas de los neutrinos [44], ii) las fases de Majorana de la matriz de mezcla de los neutrinos U [45, 46] y iii) la escala absoluta de masas de los neutrinos [44, 46–49].

Durante el resto de esta tesis, trabajaremos con la hipótesis de que los neutrinos son partículas de Majorana. En este contexto, el mecanismo seesaw de generación de masas [50, 51] proporciona una explicación natural para la pequeñez de las masas de los neutrinos. Este mecanismo, nombrado usualmente seesaw tipo I, asume la existencia de neutrinos dextrógiros con masas de Majorana muy grandes m_M comparadas con la escala electrodébil, $M_{EW} \sim \mathcal{O}(100)$ GeV, acoplados a los neutrinos levógiros a través de los acoplamientos de Yukawa. Además, las masas de los neutrinos dextrógiros son elegidas de manera que las masas de los tres neutrinos ligeros, m_{ν_i} $(i = 1, 2, 3)$, y los tres ángulos de mezcla de los neutrinos, θ_{12}, θ_{23}, θ_{13}, sean compatibles con los datos actuales [20].

Una propiedad interesante de los neutrinos de Majorana, cuya masa es generada a través del mecanismo de seesaw, es que los acoplamientos de Yukawa generados a través de dicho mecanismo pueden ser grandes, $Y_\nu \sim \mathcal{O}(1)$, si m_M es grande, digamos $m_M \sim (10^{14} - 10^{15})$ GeV, a diferencia de los neutrinos de Dirac, con $Y_\nu \sim \mathcal{O}(10^{-12})$. En el primer caso, existe la posibilidad de detectar los neutrinos pesados indirectamente a través de efectos cuánticos inducidos a observables que son medidos con gran precisión. Sin embargo, en el caso de neutrinos de Dirac, la contribución de los neutrinos dextrógiros es despreciable.

Otra característica atractiva del mecanismo de seesaw es que los términos de masa de Majorana proporcionan la violación de número leptónico que podría explicar bariogénesis vía leptogénesis. Dentro del marco de leptogénesis, la asimetría bariónica observada en el Universo (BAU) se explica por la desintegración de los neutrinos dextrógiros que tiene lugar fuera del equilibrio y que viola $\mathcal{CP}$. La simetría leptonica se convierte en asimetría bariónica debido a los esfalerones que conservan B-L pero violan B+L. Si los neutrinos

pesados, N_j ($j = 1, 2, 3$), tienen un espectro jerárquico, $m_{N_1} \ll m_{N_2} \ll m_{N_3}$ la asimetría bariónica observada puede generarse, siempre que la masa del neutrino mas ligero sea tal que $m_{N_1} \gtrsim 10^9$ GeV [52].

Sin embargo, en el SM extendido con tres neutrinos dextrógiros, la existencia de dos escalas de masas separadas, la escala electrodébil M_{EW} y la escala de Majorana m_M, que normalmente se elige en el intervalo, $10^{10} - 10^{15}$ GeV, da lugar a un problema de las jerarquías severo. Por tanto, es necesaria una propuesta de nueva física más allá del SM que pueda resolver este conflicto. Una de las soluciones más atractivas al problema de las jerarquías consiste en la introducción de una nueva simetría, denominada supersimetría (SUSY) [53–55]. Esta simetría relaciona bosones y fermiones de tal manera que la contribución de las nuevas partículas SUSY cancela las contribuciones cuadráticas a las masas de los escalares al cuadrado, estabilizando por tanto el valor de la masa del Higgs a la escala electrodébil. Por otra parte cualquier extensión del SM puede incorporar a su vez el mecanismo de seesaw para generar las masas de los neutrinos. De esta forma, los modelos SUSY-seesaw acomodan de forma satisfactoria los datos experimentales de los neutrinos y, al mismo tiempo, no sufren el problema de las jerarquías.

El Modelo Standard Supersimetrico Minimo (MSSM) [56–58] es la version supersimétrica mínima del SM, que incorpora un compañero supersimétrico por cada partícula del SM con la misma masa y números cuánticos pero con un spin que difiere en un 1/2. Asi, un nuevo compañero bosónico se asigna a cada fermión del SM y, de la misma forma, se asigna un nuevo compañero fermiónico SUSY a cada bosón del SM. Este modelo es llamado mínimo, porque tiene el mínimo numero de supersimetrías posibles ($N = 1$) y, por tanto, el mínimo contenido de partículas SUSY. Con el fin de implementar el mecanismo de seesaw dentro del MSSM, se introducen, además del espectro usual del MSSM, tres neutrinos dextrógiros y los tres supercompañeros correspondientes, los sneutrinos.

No obstante, es sabido que la supersimetría no puede ser una simetría exacta del espectro de partículas observado y, por tanto, debe estar rota en la naturaleza, puesto que hasta la fecha no se han encontrado partículas SUSY en los experimentos [20]. A pesar de que el mecanismo de ruptura de SUSY no se conoce todavía, si no queremos estropear la cancelación de las divergencias cuadráticas, los términos de ruptura de SUSY deben ser *suaves* [59]. Adicionalmente tienen que proporcionar masas apropiadas a las partículas SUSY de manera que sean más pesadas que sus compañeras del SM.

El MSSM y el MSSM-seesaw tiene un sector de Higgs extendido que contiene cinco bosones de Higgs fisicos: dos partículas cargadas $H^{\pm}$, una partícula neutra impar bajo

$\mathcal{CP}$ A^0 y dos partículas neutras pares bajo $\mathcal{CP}$, h^0 y H^0. La masa del bosón de Higgs más ligero, m_{h^0}, no es un parámetro libre. A diferencia del Higgs del SM, m_{h^0} tiene una cota superior a nivel árbol dada por M_Z, pero recibe correcciones de órdenes superiores provenientes de loops de partículas del SM y sus supercompañeras, que dependen logarítmicamente de las masas de ruptura de SUSY *suave* y aumentan el valor a nivel árbol. Las correcciones principales a m_{h^0} en el MSSM vienen del sector de tops/stops porque los acoplamientos de Yukawa son proporcionales a las masas de los fermiones correspondientes, y la masa del top es mayor que ninguna otra masa de los fermiones del SM. La cota superior de m_{h^0} se desplaza entonces por encima de M_Z y el límite preciso depende de la elección específica de los parámetros *suaves*. Para masas SUSY *suaves* $\leq 2\,\text{TeV}$ la cota superior de m_{h^0} es ~ 135 GeV [60–62].

Como se puede apreciar, el MSSM predice una masa del bosón de Higgs relativamente ligera, cerca de la escala EW , lo que la convierte en una teoría con interés fenomenológico porque sus predicciones pueden ser descartadas o corroboradas en los experimentos y, en concreto, en el LHC. Muchas zonas de la región de masas del Higgs han sido ya excluídas, como se mostró previamente para el caso del bosón de Higgs del SM. En la región del espacio de parametros donde $m_{A^0} \gg M_Z$ y las masas de las partículas SUSY son grandes (el límite del *decoupling*), las tasas de desintegración del bosón de Higgs más ligero h^0 en partículas del SM son prácticamente indistinguibles de las del bosón de Higgs del SM y, por tanto, las áreas de exclusión del h_{SM} pueden aplicarse al h^0. No obstante, la zona de masa ligera del Higgs no ha sido probada todavía en el LHC, porque en esta zona el canal de desintegración más prometedor es el canal a dos fotones, que necesita mucha luminosidad ya que su tasa de desintegración es baja comparada con otros canales ($b\bar{b}$, $\tau\bar{\tau}$), que sin embargo, tienen más ruido de fondo y en los que resulta más difícil, por tanto, separar la señal del ruido.

Con el fin de reducir el números de parámetros libres introducidos por los términos de rupturas *suave* de SUSY normalmente se asumen modelos SUSY restringidos. Por ejemplo, el conocido modelo estándar supersimétrico restringido (CMSSM) minimiza el numero de estos parámetros asumiendo valores universales de los mismos a la escala de unificación gauge, quedando sólo cinco parámetros libres: la masa escalar universal *suave*, M_0, la masa gaugino universal *suave*, $M_{1/2}$, el acoplamiento trilineal universal, A_0, el cociente entre lo valores esperados de los dos Higgses, $\tan\beta$, y el signo del término de masas de Higgsino, $\text{sign}(\mu)$. s Una interesante desviación del CMSSM se puede obtener relajando las condiciones de universalidad para las masas de ruptura *suave* del sector

de Higgs, M_{H_1} y M_{H_2}, de manera que sean independientes de la masa escalar universal *suave* M_0. Este MSSM restringido parcialmente tiene siete parámetros libres, M_{H_1}, M_{H_2}, M_0, $M_{1/2}$, A_0, $\tan\beta$ y sign(μ), y es conocido normalmente como el escenario de Masas del Higgs No Universales (NUHM) [64]. La versión ampliada del CMSSM y del NUHM (que incluye neutrinos y sneutrinos dextrógiros) será designada como CMSSM-seesaw y NUHM-seesaw respectivamente.

Ninguna partícula SUSY ha sido detectada todavía y el LHC al igual que Tevatrón están poniendo cotas al espacio de parámetros de modelos SUSY restringidos, en particular el CMSSM. El detector CMS ha excluído masas de squarks y gluinos por debajo de ~ 1 TeV para un valor común de la masa de los escalares a la escala GUT de $M_0 < 0.5$ TeV y para valores concretos del resto de parámetros del modelo [65, 66]. De manera complemetaria a la búsqueda directa de partículas SUSY, el estudio de los efectos indirectos de dichas partículas, a través de correcciones radiativas, a observables de precisión, es una herramienta muy útil para comprobar si SUSY es compatible con los datos y, por tanto, un buen candidato a nueva física, o no, y entonces SUSY o alguna región de su espacio de parametros puede ser descartada.

Esta tesis se ha centrado en el estudio de algunos de los efectos indirectos de los neutrinos de Majorana y sus compaeros supersimétricos, los sneutrinos, a través de sus correcciones radiativas a observables de baja energía que esta previsto sean medidos con gran precisión y que tienen capacidad de acceder al sector de Higgs. Concretamente, nos hemos centrado en dos de los efectos de loop más relevantes, a saber: 1) las correcciones radiativas a la masa del bosón de Higgs más ligero del MSSM-seesaw, debidas a los neutrinos de Majorana y sus compañeros SUSY, los sneutrinos, y, 2) las contribuciones inducidas por los neutrinos de Majorana y los sneutrinos a desintegraciones con violación de sabor leptónico (LFV) mediadas por el Higgs en modelos SUSY-seesaw restringidos. A continuación introduciremos brevemente ambos trabajos.

En la primera parte de esta tesis estudiamos los efectos indirectos de los neutrinos de Majorana y sneutrinos en la física del Higgs, a través de las correcciones radiativas a las masas de los bosones de Higgs del MSSM. La motivación principal de este estudio es que esperamos que estos efectos sean relevantes para masas de Majorana suficientemente grandes, $m_M \gg m_{EW}$, debido al gran tamaño de los acoplamientos de los neutrinos involucrados, $Y_\nu \sim \mathcal{O}(1)$. De hecho, en Ref. [67] las correcciones a un loop a la masa del bosón de Higgs del MSSM más ligero, M_h, fueron calculadas en un escenario diferente, conocido como split SUSY, haciendo uso de varias aproximaciones, y ya encontraron

correcciones grandes y negativas provenientes del sector de neutrinos y sneutrinos. Aquí nosotros presentaremos un cálculo diagramático completo a un loop de las contribuciones de neutrinos/sneutrinos a M_h y trabajaremos en escenerios genéricos MSSM-seesaw sin condiciones de universalidad impuestas al sector de neutrinos y sneutrinos.

Adicionalmente, nos centraremos particularmente en las características de estas correcciones con respecto al asunto del *decoupling* o *non decoupling* de los neutrinos pesados de Majorana y los sneutrinos en la física del Higgs. Esto nos permitirá averiguar los valores interesantes de la masa de Majorana donde el tamaño de las correcciones a la masa del Higgs son susceptibles de ser medidas experimentalmente. Aunque no esté completamente determinada, la precisión experimental esperada en la medida de M_h constituye un gran reto. La precisión esperada en el LHC sobre la medida de un bosón de Higgs como el del SM, es de ~ 200 MeV [68–71], mientras que la precisión esperada en el ILC podría alcanzar el nivel de 50 MeV [72–75]. Por otro lado, la precisión actual en el valor predicho teóricamente de la masa corregida del bosón de Higgs del MSSM, se estima que sea $\sim 2-3$ GeV [76]. Cualquier corrección comparable o más grande que la precisión actual, debería tenerse en cuenta. En esta tesis mostraremos que las correcciones de los neutrinos de Majorana y sus compañeros SUSY pueden ser, de hecho, de este orden o incluso mayor.

La segunda parte de esta tesis está dedicada al estudio de los efectos indirectos de los neutrinos de Majorana y sneutrinos en procesos con violación de sabor leptónico y que pueden ser mediados por bosones de Higgs. En el contexto de búsquedas indirectas, los procesos con violación de sabor leptónico (LFV) proporcionan una de las ventanas más importantes para probar extensiones supersímetricas del SM y tambien el sector de neutrinos más allá del SM [77–83]. La razón subyacente es que las interacciones LFV están prohibidas en el SM y, por tanto, el SM predice tasas nulas para estos observables LFV. Cuando se extiende el SM para incluir las masas y mezclas de los neutrinos a través de un mecanismo seesaw tipo I sin SUSY, existen procesos LFV a través de loops de neutrinos, pero están extremadamente suprimidos debido a las pequeñas masas de los neutrinos ligeros. Sin embargo, esto puede no ser así en otros modelos seesaw (see for instance [84]).

En el marco teórico del MSSM-seesaw la situación es completamente diferente. Ademas de las contribuciones del SM-seesaw, supersimetría proporciona nuevas fuentes directas de violación de sabor, a saber, la posible presencia de términos *suaves* no diagonales en las matrices de masa de los sleptones y en los acoplamientos trilineales a bajas energias.

En la práctica, la violación de sabor se origina por el desalineamiento entre las matrices de masa de fermiones y sfermiones, que no pueden diagonalizarse simultaneamente. Incluso si las masas de los escalares son universales a alta energía, la mezcla de sabor en los acoplamientos de Yukawa de los neutrinos de Majorana induce, mediante efectos de renormalización, mezcla se sabor en las masas de los sleptones a baja energía y estos sleptones, a su vez, cuando se propagan en loops pueden, por ello, generar grandes tasas en procesos LFV [77–81].

El proceso LFV que es más sensible a los acoplamientos de Yukawa del neutrino, en un contexto SUSY-seesaw, es $\mu \to e\gamma$, donde la sensibilidad experimental actual es 2.4×10^{-12} [85]. Tambien la conversión $\mu - e$ en nucleos pesados, con cotas actuales de $\mathrm{CR}(\mu - e, \mathrm{Ti}) < 4.3 \times 10^{-12}$ [86] y $\mathrm{CR}(\mu - e, \mathrm{Au}) < 7 \times 10^{-13})$ [87], y $\mu \to 3e$ con $\mathrm{BR}(\mu \to 3e) < 1.0 \times 10^{-12}$ [88], son bastantes sensibles a LFV en el sector $\mu - e$.

En el sector $\tau - \mu$ el límite superior de la desintegración $\tau \to \mu\gamma$ es ahora fijado a 4.4×10^{-8} dado por la colaboración de BABAR [89]. Adicionalmente, la sensibilidad a LFV in $\tau \to 3\mu$ ha mejorado notablemente en los últimos años. Las cotas superiores actuales de las colaboraciones de BELLE y BABAR son 2.1×10^{-8} [90] y 3.3×10^{-8} [89], respectivamente. En los últimos años las desintegraciones semileptónicas del τ han llegado a ser competitivas con las desintegraciones leptónicas puras [91, 92].

En esta tesis hemos llevado a cabo un estudio comparativo de las desintegraciones semileptónicas $\tau \to \mu f_0(980)$ y $\tau \to \mu\eta$. Ambos canales tienen cotas superiores competitivas $\mathrm{BR}(\tau \to \mu\eta) < 2.3 \times 10^{-8}$ [93] y $\mathrm{BR}(\tau \to \mu f_0(980)) < 3.4 \times 10^{-8}$ [94]. La ventaja del canal $\tau \to \mu\eta$ [95–97] y $\tau \to \mu f_0(980)$ [98] sobre el canal $\tau \to \mu\gamma$ es su potencial sensibilidad al sector de Higgs. Es sabido que dentro de los modelos SUSY-seeaw $\tau \to \mu\gamma$ no es sensible al sector de Higgs a nivel de un loop. Por otro lado $\tau \to 3\mu$ es sensible al sector de Higgs a través de diagramas de pinguino a un loop [99]. Sin embargo, la contribución mediada por el Higgs en este canal $\tau \to 3\mu$ es superada por la contribución de los diagramas de pingüinos del γ en la mayoría de los escenarios MSSM-seesaw restringidos. Por tanto para conseguir cierta sensibilidad al sector de Higgs se deben considerar desintegraciones semileptónicas τ [97]. Los dos canales semileptónicos $\tau \to \mu\eta$ y $\tau \to \mu f_0(980)$ no tienen contribucion mediada por γ y, por tanto, tienen acceso directo al sector de Higgs. Mientras el canal $\tau \to \mu\eta$ puede ser mediado por un bosón Z y un boson de Higgs impar bajo $\mathcal{CP}$ A^0, y está dominado por el A^0 solo a gran $\tan\beta \gtrsim 20$ [97, 100], la desintegración $\tau \to \mu f_0(980)$ está mediada exclusivamente por el intercambio de los bosones de Higgs neutros pares bajo $\mathcal{CP}$ H^0 an h^0. En consecuencia

mediante el canal $\tau \to \mu f_0(980)$ se está probando directamente el sector de Higgs neutro par bajo $\mathcal{CP}$ para cualquier valor de $\tan\beta$. Nuestro cálculo del BR($\tau \to \mu f_0(980)$) mejora la estimación de [98] en distintos aspectos. En primer lugar, nosotros exigimos compatibilidad con los datos actuales de las masas y mezclas de los neutrinos ligeros. En segundo lugar, no usamos la aproximación de la inserción de masa, tenemos en cuenta el conjunto completo de diagramas a un loop de SUSY en el vértice LFV $\tau\mu H$ ($H = h^0, H^0$), e incluimos las dos contribuciones mediadas h_0 y H_0, respectivamente. De este modo, exploramos todo el intervalo $5 \leq \tan\beta \leq 60$. Además, la hadronización de los bilineales de quarks en el mesón $f_0(980)$, se realiza aquí de forma diferente que en [98], donde se usa un esquema simplificado de sabor de quark para expresar estos bilineales en términos de constantes de desintegración del mesón fenomenológicas. Nosotros al contrario centramos nuestra atención en las restriciones quirales, siguiendo la Teoria de Perturbaciones Quiral (χPT) [101–103] estándar y la Teoria de Resonancias Quiral (RχT) [104–108] para incorporar las resonancias. Concretamente seguimos la descripción de $f_0(980)$ de [107], donde se define a través de la mezcla de las componentes singlete y octete del nonete de resonancias escalares que están incluídas en RχT.

En nuestro cálculo, nos centramos en dos escenarios SUSY-seesaw restringidos descritos previamente, a saber, CMSSM-seesaw y MSSM-seesaw. En el último caso las masas físicas de los bosones de Higgs m_{h^0} y m_{H^0}, pueden ser ligeras, $\sim 100 - 250$ GeV, de hecho cerca de los límites inferiores experimentales y, por tanto, la correspondiente contribución mediada por el Higgs a los procesos LFV previos puede ser relevante, incluso para masas SUSY *suaves* grandes $\sim \mathcal{O}(1\,\text{TeV})$. Éste es precisamente el interés principal del canal $\tau \to \mu f_0(980)$, a saber, el hecho de que las tasas de desintegracion pueden ser considerables incluso para masas SUSY grandes, $M_{\text{SUSY}} \sim \mathcal{O}(1\,\text{TeV})$, en contraste con otros canales LFV competitivos, como $\tau \to \mu\gamma$, cuyas tasas de desintegración decrecen como $1/M^2_{\text{SUSY}}$ y se encuentran por debajo de la cota experimental actual para un espectro SUSY tan pesado. En esta tesis mostraremos que estos dos canales semileptónicos $\tau \to \mu f_0(980)$ y $\tau \to \mu\eta$ son, de hecho, muy competitivos para testar los tres sectores relevantes: SUSY, Higgs y el sector neu/sneu.

Esta tesis esta organizada como sigue. En el Capítulo 1 los aspectos principales del MSSM son revisados poniendo especial atención en el sector de Higgs de este modelo. Se muestra la relevancia de las correcciones radiativas a la masa del bosón de Higgs más ligero en el MSSM, tanto analítica como numéricamente. A continuación se describen las características principales de dos modelos SUSY restringidos que serán relevantes

para nuestro trabajo: CMSSM/mSUGRA y NUHM. Finalmente comentamos la situación experimental del MSSM.

En el Capítulo 2 repasamos la necesidad de ampliar el espectro del MSSM para acomodar las masas de los neutrinos. Los beneficios del mecanismos de seesaw para generar las masas de los neutrinos son remarcados. Los nuevos ingredientes del MSSM-seesaw con respecto al MSSM, que son originales de esta tesis, son presentados. En particular el espectro de masas de neutrinos y sneutrinos y sus interaciones con los bosones de Higgs neutros del MSSM y el bosón gauge Z serán derivados, ya que son los relevantes para los calculos del Capítulo 3 de los efectos radiativos de neutrinos de Majorana y sneutrinos en las masas de los bosones de Higgs neutros pares bajo $\mathcal{CP}$. Las reglas de Feynman tambien seran mostradas.

Los siguientes Capítulos contienen el trabajo central de esta tesis.

En el Capítulo 3 presentamos el cálculo de las correciones radiativas a un loop a la masa del bosón de Higgs $\mathcal{CP}$ más ligero provenientes del sector de neutrinos y sneutrinos dentro del marco del MSSM-seesaw. Trabajamos en escenarios MSSM-seesaw genéricos sin condiciones de universalidad impuestas, y exploramos el espacio de parámetros completo del sector neutrino/sneutrino. Restringimos nuestro cálculo al caso de una generacion de neutrinos/sneutrinos por simplicidad y para entender en profundidad el efecto de una única escala de Majorana, aunque sabemos que al menos dos neutrinos dextrógiros son necesarios para acomodar los datos de los neutrinos. El conjunto completo de diagramas a un loop de neutrinos/sneutrinos serán tenidos en cuenta con los acoplamientos de Yukawa y gauge activos. Tambien analizamos los resultados en distintos esquemas de renormalización, que mostraran grandes diferencias. Adicionalmente a los resultados exactos presentamos algunos resultados analíticos y numéricos en el límite de m_M en comparación con el resto de escalas involucradas. Finalmente, discutiremos hasta que punto las correciones radiativas calculadas aquí entran en el rango que puede ser medido.

En el Capítulo 4 realizamos un estudio comparativo de las desintegraciones LFV semileptonicas $\tau \to \mu\eta$ [95–97] y $\tau \to \mu f_0(980)$ en escenarios MSSM-seesaw restringidos. En primer lugar la generación de mezcla de sabor en el sector leptónico de los modelos SUSY-seesaw es explicada. A continuación el marco teórico utilizado para nuestro cálculo de las mencionadas desintegraciones es introducido, a saber, el CMSSM-seesaw y el NUHM-seesaw. Las prediciones numéricas de las masas de los bosones de Higgs neutros con respecto al resto de parámetros SUSY son presentadas. Por otra parte, la conexión entre la física de neutrinos y LFV es ilustrada en diferentes diagramas de contorno. El

cálculo completo a un loop del vértice $\tau\mu H_i$ es explicado. La hadronización de bilineales de quarks es realizada dentro del marco teórico Quiral. Adicionalmente, presentamos una fórmula aproximada de las desintegraciones, que proporcionará muy buenos resultados como se mostrará en las estimaciones numéricas de las tasas de desintegración. Finalmente se realizará una comparación entre las predicciones con los límites experimentales.

Esta tesis está basada en los resultados publicados en los artículos, [109], [110] and [111] y en las presentaciones de las conferencias [112], [100], [113], y [114].

Chapter 1

SUSY models

In this chapter some of the main features of the Minimal Supersymmetric Standard Model (MSSM) are briefly reviewed. Moreover, the interactions and the particle content of the MSSM are described paying special attention to the Higgs sector of this model. The relevance of radiative corrections to the lightest Higgs boson mass in the MSSM is shown, both analytically and numerically. Afterwards, we describe the main features of two constrained SUSY models of relevance for our work: CMSSM/mSUGRA and NUHM. Finally, we comment about the experimental status of the MSSM.

1.1 The Minimal Supersymmetric Standard Model

Supersymmetry (SUSY) is a symmetry that relates boson and fermion fiels and it is generated by charges transforming like spinors under the Lorentz group:

$$Q|fermion\rangle = |boson\rangle \qquad\qquad Q|boson\rangle = |fermion\rangle \tag{1.1}$$

These spinorial charges give rise to a closed system of commutation-anticommutation relations, which may be called a "pseudo Lie algebra". It turns out that the energy-momentum operators appear among the elements of this pseudo Lie algebra, so that in some sense a fusion between internal and geometric symmetries occurs. The possible forms for such symmetries in an interacting quantum field theory are highly restricted by the Haag-Lopuszanski-Sohnius extension of the Coleman-Mandula theorem [115]. As a conclusion from these works [115], Supersymmetry is the only possible symmetry in a

non trivial interacting quantum field theory that relates a spacetime symmetry (Lorentz symmetry) with an internal symmetry. In theories that contain chiral fermions, like the Standard Model (SM), this theorem implies that the generators Q and $Q^\dagger$ must satisfy the followig algebra of anticommutation and commutation relations with the schematic form:

$$\{Q, Q^\dagger\} = P^\mu \tag{1.2}$$

$$\{Q, Q\} = \{Q^\dagger, Q^\dagger\} = 0 \tag{1.3}$$

$$\{P^\mu, Q\} = \{P^\mu, Q^\dagger\} = 0 \tag{1.4}$$

where P^μ is the four-momentum generator of spacetime translations. The single-particle states of a supersymmetric theory fall into irreducible representations of the supersymmetry algebra, called supermultiplets. Each supermultiplet contains both fermion and boson states, which are commonly known as superpartners of each other. Each of the partners of the supermultiplet have the same eigenvalues of the momentum and therefore equal masses. Moreover, the number of bosonic and fermionic degrees of freedom is the same in each supermultiplet.

$$n_B = n_F \tag{1.5}$$

The simplest possible supermultiplet consistent with Eq. (1.5) contains a fermion with two degrees of freedom and two scalar particles, with one degree of freedom each or, equivalently, one complex scalar particle. The next simplest supermultiplet contains a spin-1 vector boson and its superpartners are fermions of spin 1/2 because if they had spin 3/2 the theory would not be renormalizable. Gauge bosons as well as their superpartners, called gauginos, must transform as the adjoint representation of the gauge group.

The Minimal Supersymmetric Standard Model (MSSM) [56–58] is the minimal supersymmetric extension of the Standard Model, where minimal means that it contains the minimum number of supersymmetry generators Q and $Q^\dagger$ and it contains the minimum number of superfields. In principle, one could introduce extra copies of SUSY generators but it has been proven that four-dimensional field theories cannot allow for chiral fermions or parity violation as observed in the Standard Model. Therefore, the MSSM is the most realistic SUSY extension of the SM.

In order to supersymmetrize the SM one needs to introduce a superpartner for each of the particles of the SM, that has the same quantum numbers and mass but with a spin differing in 1/2. Each fermion has its corresponding scalar partner, the sfermion, one for the left-handed fermion and another one for the right-handed fermion, each gauge boson

has its fermionic partner, the gaugino, and each scalar Higgs particle has its fermionic partner, the Higgsino. One doubles the particle content of the SM. Moreover, one needs to extend the Higgs sector of the SM. An extra supermultiplet with its scalar Higgs and the corresponding Higgsino superpartner is needed for two reasons:

- In the supersymmmetrized version of the SM, the introduction of an extra chiral fermion, the Higgsino, contributes to the $SU(2) \times U(1)$ gauge anomaly making it inconsistent as a quantum theory. All the fermions of the theory contribute to the anomaly through the fermion triangle vertex. The conditions for cancellation of gauge anomalies include $\mathrm{Tr}[T_3^2 Y] = \mathrm{Tr}[Y^3] = 0$, where Y and T_3 are the weak hypercharge and the third component of the weak isospin, respectively, in a normalization where the ordinary electric charge is $Q = T_3 + Y$. The traces run over all of the left-handed Weyl fermionic degrees of freedom in the theory . In the SM these anomalies cancel by the known quarks and leptons. However, the introduction of the extra chiral fermion, the Higgsino, contributes to the anomaly and, in order to cancel it, we need another Higgs superfield with opposite hypercharge [116].

- Supersymmetry requires that the superpotential be an analytic function of the superfields. Therefore it cannot contain the hermitian conjugate of a Higgs superfield and it is then not possible to give masses to both up and down-type quarks without introducing a second Higgs doublet superfield. Here $\hat{\mathcal{H}}_1$ will be responsible for the masses of the down-type fermions and $\hat{\mathcal{H}}_2$ the corresponding one for the up-type fermions.

As a consequence of SUSY implying pairs of bosons and fermions with the same mass, their couplings to the Higgs boson are related and their corresponding radiative corrections to the Higgs mass cancel at all orders in perturbation theory. Consequently, the hierarchy problem disappears. As explained in the introduction, the SM suffers of a hierarchy problem related to the fact that the Higgs mass is sensitive to the scale of the new physics introduced. At one loop order in perturbation theory, the radiative corrections of fermions, with mass m_F and coupling to the Higgs boson with a term in the Lagrangian $-\delta_F H \bar{f} f$, to the self-energy of the Higgs have a quadratic and a logarithmic dependence on the cutoff Λ:

$$\delta m_H^2 = \frac{|\delta_F|^2}{16\pi^2}\left(-2\Lambda^2 + 6m_F^2 \log\frac{\Lambda}{m_F}\right) + ... \tag{1.6}$$

If this scale Λ is replaced by the Planck mass M_P, the resulting correction to the Higgs mass is 30 orders of magnitude larger than the tree level SM Higgs mass, which leads to

the required fine tuning to fulfill the upper bound of around 1 TeV on the Higgs mass in order to preserve unitarity and to be in agreement with the SM precision measurements. Supersymmetry solves this problem because the quadratic and logarithmic dependences in the cutoff Λ, are canceled due to the fact that one introduces scalar partners of the SM fermions with the same quantum numbers and mass and equal number of degrees of freedom. The contribution of each scalar partner S with mass m_S which couples to the Higgs boson with a Lagrangian term $-\delta_S|H|^2|S|^2$ is given by:

$$\delta m_H^2 = \frac{\delta_S}{16\pi^2}\left(\Lambda^2 - 2m_S^2 \log\frac{\Lambda}{m_S}\right) + \dots . \tag{1.7}$$

The cancellation is then produced due to relation implied by SUSY, $\delta_S = |\delta_F|^2$, so that the fermions and their superpartners have the same masses. This cancellation of radiative corrections happens at all orders of perturbation theory.

As no SUSY particles have been observed so far, it is clear that supersymmetry must be broken. Nevertheless, if we want supersymmetry to continue being a good candidate to solve the hierarchy problem, the SUSY breaking part of the Lagrangian must be soft. With this requirement the cancellation of quadratic divergences is not spoiled but the cancellation of logarithmic divergences is no longer achieved. These logarithmic corrections to the Higgs mass grow with the masses of the sfermions. This is one of the most convincing arguments in favor of low energy superparticles, with masses $M_S \leq \mathcal{O}(1\text{ TeV})$ such that they do not lead to too large logarithmic radiative corrections to the Higgs mass. Although the SUSY breaking mechanism is not known, this mechanism must give masses to the superpartners of the SM particles, as well as allowing the electroweak symmetry breaking, that is not achieved in an exact SUSY version of the SM because the minimum of the Higgs potential occurs at $\mathcal{H}_1 = \mathcal{H}_2 = 0$.

There is one additional property of the MSSM which makes it be less constraint than the SM. In the SM the most general, invariant under $SU(3)_C \times SU(2)_L \times U(1)_Y$ gauge symmetry and renormalizable Lagrangian, preserves accidentally global baryon (B) and lepton number (L). However, this is not the case in the MSSM and, a priori, terms that violate lepton and baryon number in one unit are allowed. The possible existence of such terms is very constraint since, up to date, the corresponding B and L violating processes have not been seen experimentally. The most obvious experimental constraint comes from the non-observation of proton decay, which would violate both B and L by 1 unit. The decay time of the proton into lepton+meson final states is known experimentally to be in excess of 10^{32} years. Nevertheless, squarks could mediate disastrously rapid proton decay

if $\Delta B = 1$ and $\Delta L = 1$ interactions were allowed, for instance in the decay $p \to e^+\pi^0$. The usual method to preserve these global symmetries is the, *ad hoc*, introduction of a discrete symmetry called R-parity. The R-parity is a multiplicative quantum number defined in terms of the Baryonic and Leptonic numbers, B and L, and the Spin, S, as R$= (-1)^{3(B-L)+2S}$. This leads to R $= 1$ for SM and Higgs particles and R$= -1$ for their SUSY partners. Besides, the fact that R-parity must be conserved implies that SUSY particles can only be produced in pairs from SM particles and also that the lightest SUSY particle must be stable. This stable particle is a suitable candidate for dark matter (DM) and gives SUSY the possibility of explaining the particle content of this non-baryonic DM.

1.2 Interactions and particle content of the MSSM

The following part of this MSSM section will be devoted to the description of the MSSM particle content and interactions, both the SUSY preserving and the soft SUSY breaking ones. For the later ones, we will assume a generic form without inquiring into its origins. Special interest will be devoted to parameters of the Higgs sector, both at tree level and at higher orders.

The SUSY preserving interactions, and in particular the Yukawa interactions between Higgs particles and fermions are described by the superpotencial W. The superpotential is an holomorphic function of the scalar fields and the SUSY preserving interaction Lagrangian is derived from it. Therefore, it contains all the information about the SUSY interactions. If one assumes that R symmetry is preserved the superpotential is given by

$$W = \epsilon_{ij}\left(Y_u^{ab}\,\hat{\mathcal{H}}_2^i\,\hat{Q}_j^a\,\hat{U}^b \;-\; Y_d^{ab}\,\hat{\mathcal{H}}_1^i\,\hat{Q}_j^a\,\hat{D}^b - Y_l^{ab}\,\hat{\mathcal{H}}_1^i\,\hat{L}_j^a\,\hat{R}^b \;+\mu\hat{\mathcal{H}}_1^i\hat{\mathcal{H}}_2^j\right), \qquad (1.8)$$

where Y_u, Y_d and Y_l are generically 3×3 Yukawa matrices in flavor space. The indices a, b represent generation indices and $\epsilon_{21} = -\epsilon_{12} = 1$. The superfield $\hat{Q}$ contains the $SU(2)$ quark doublet, (u_L, d_L) and its superpartner, the $SU(2)$ doublet of squarks, $(\tilde{u}_L, \tilde{d}_L)$. The superfield $\hat{L}$ represents the SU(2) lepton doublet, (ν_L, l_L), and the corresponding slepton doublet, $(\tilde{\nu}_L, \tilde{l}_L)$. On the other hand, the superfields $\hat{U}$, $\hat{D}$ and $\hat{R}$ contain the $SU(2)$ fermion singlets and sfermion singlets, $\{\tilde{u}_R^*, (u_R)^c\}$, $\{\tilde{d}_R^*, (d_R)^c\}$ and $\{\tilde{l}_R^*, (l_R)^c\}$, respectively. Here and in the following, f^c denotes the particle-antiparticle conjugate (c-conjugate in short) of a fermion f $\left(f^c = C\,\bar{f}^T\right)$ and $\tilde{f}^*$ denotes the complex conjugate of the sfermion $\tilde{f}$. $\hat{\mathcal{H}}_1$ and $\hat{\mathcal{H}}_2$ represent the two Higgs superfields that are needed to give

masses to both, down-type fermions/sfermions and up-type fermions/sfermions, respectively. The μ term is the supersymmetric version of the Higgs boson mass in the Standard Model. The scalar components of the doublet fields $\mathcal{H}_1$ and $\mathcal{H}_2$ are decomposed in the following way:

$$\begin{aligned} \mathcal{H}_1 &= \begin{pmatrix} H_1^0 \\ H_1^- \end{pmatrix} = \begin{pmatrix} v_1 + \frac{1}{\sqrt{2}}(\phi_1^0 - i\chi_1^0) \\ -\phi_1^- \end{pmatrix}, \\ \mathcal{H}_2 &= \begin{pmatrix} H_2^+ \\ H_2^0 \end{pmatrix} = \begin{pmatrix} \phi_2^+ \\ v_2 + \frac{1}{\sqrt{2}}(\phi_2^0 + i\chi_2^0) \end{pmatrix}. \end{aligned} \tag{1.9}$$

After the electroweak symmetry breaking, the Yukawa couplings are related to the physical masses. For instance, in the one generation case these relations are

$$\begin{aligned} Y_u &= \frac{g m_u}{\sqrt{2} M_W \sin\beta} = \frac{m_u}{v_2}, \\ Y_d &= \frac{g m_d}{\sqrt{2} M_W \cos\beta} = \frac{m_d}{v_1}, \\ Y_l &= \frac{g m_l}{\sqrt{2} M_W \cos\beta} = \frac{m_l}{v_1}, \end{aligned} \tag{1.10}$$

where

$$\tan\beta \equiv \frac{v_2}{v_1}, \tag{1.11}$$

$$\langle H_1^0 \rangle = v_1 = v\cos\beta, \quad \langle H_2^0 \rangle = v_2 = v\sin\beta, \tag{1.12}$$

and v is set by the M_W and M_Z values as in the SM

$$v^2 = \frac{2M_Z^2}{g^2 + g'^2} = \frac{2M_W^2}{g^2}. \tag{1.13}$$

The fact that there are two doublets, instead of one, introduces the extra parameter $\tan\beta$.

The SUSY preserving part of the scalar potential contains two terms, the F and the D terms:

$$V(\phi, \phi^*) = V_F + V_D. \tag{1.14}$$

The F-terms are fixed by the Yukawa interactions and by the fermion masses, and they are derived from the superpotential using:

$$V_F = F_i^* F_i = \sum_i \left(\frac{\partial W}{\partial \phi_i}\right)^* \left(\frac{\partial W}{\partial \phi_i}\right) = \sum_i \left|\frac{\partial W}{\partial \phi_i}\right|^2, \tag{1.15}$$

where ϕ are the scalar components of the corresponding superfield. On the other hand, the D-terms are fixed by the gauge interactions according to

$$V_D = \frac{1}{2}\sum_a D^a D^a = \frac{1}{2}\sum_a g_a^2 \left(\phi^* T^a \phi\right)^2 , \tag{1.16}$$

where g_a accounts for the different gauge couplings and T^a for the generator of the corresponding gauge group. Since $V(\phi, \phi^*)$ is a sum of squares, it is always greater than or equal to zero for every field configuration. It is an interesting and unique feature of supersymmetric theories that the scalar potential is completely determined by the other interactions in the theory.

By examining the Higgs boson contributions to the scalar potential we can check that $V_{\rm SUSY}^{\rm Higgs} \geq 0$ which implies that the minimum of the potential is at $\mathcal{H}_1 = \mathcal{H}_2 = 0$ and the SU(2)×U(1) gauge symmetry remains unbroken.

$$V_{\rm SUSY}^{\rm Higgs} = |\mu|^2 \left(|\mathcal{H}_1|^2 + |\mathcal{H}_2|^2\right) + \frac{1}{8}(g^2 + g'^2)\left(|\mathcal{H}_1|^2 - |\mathcal{H}_2|^2\right)^2 + \frac{1}{2}g^2|\mathcal{H}_1^*\mathcal{H}_2|^2 , \tag{1.17}$$

In order to complete the description of the MSSM model we have to add all possible explicit soft-supersymmetry breaking terms to the model. The allowable terms have been derived in [59]. The relevant terms for the scalar potential fall into two classes. The first class consists of all possible dimension-two terms consistent with gauge invariance. The second class consists of those gauge invariant dimension-three terms which do not mix the scalar fields with their complex conjugates. These terms correspond in form precisely to the cubic terms of the superpotential plus their hermitian conjugates. Following these rules, we enumerate all possible soft terms below that respect R-parity:

$$\begin{aligned}
V_{\rm soft} &= m_1^2|\mathcal{H}_1|^2 + m_2^2|\mathcal{H}_2|^2 - m_{12}^2\left(\epsilon_{ij}\mathcal{H}_1^i\mathcal{H}_2^j + \text{h.c.}\right) \\
&+ m_{\tilde{Q},q}^2\left[\tilde{q}_L^*\tilde{q}_L\right] + m_{\tilde{L},l}^2\left[\tilde{l}_L^*\tilde{l}_L\right] \\
&+ m_{\tilde{U},u}^2\tilde{u}_R^*\tilde{u}_R + m_{\tilde{U},c}^2\tilde{c}_R^*\tilde{c}_R + m_{\tilde{U},t}^2\tilde{t}_R^*\tilde{t}_R \\
&+ m_{\tilde{D},d}^2\tilde{d}_R^*\tilde{d}_R + m_{\tilde{D},s}^2\tilde{s}_R^*\tilde{s}_R + m_{\tilde{D},b}^2\tilde{b}_R^*\tilde{b}_R \\
&+ m_{\tilde{E},e}^2\tilde{e}_R^*\tilde{e}_R + m_{\tilde{E},\mu}^2\tilde{\mu}_R^*\tilde{\mu}_R + m_{\tilde{E},\tau}^2\tilde{\tau}_R^*\tilde{\tau}_R \\
&- \frac{g}{\sqrt{2}M_W}\epsilon_{ij}\left[\frac{m_e A_e}{\cos\beta}\mathcal{H}_1^i\tilde{l}_L^j\tilde{e}_R^* + \frac{m_\mu A_\mu}{\cos\beta}\mathcal{H}_1^i\tilde{l}_L^j\tilde{\mu}_R^* + \frac{m_\tau A_\tau}{\cos\beta}\mathcal{H}_1^i\tilde{l}_L^j\tilde{\tau}_R^*\right. \\
&+ \frac{m_d A_d}{\cos\beta}\mathcal{H}_1^i\tilde{q}_L^j\tilde{d}_R^* - \frac{m_u A_u}{\sin\beta}\mathcal{H}_2^i\tilde{q}_L^j\tilde{u}_R^* + \frac{m_s A_s}{\cos\beta}\mathcal{H}_1^i\tilde{q}_L^j\tilde{s}_R^* - \frac{m_c A_c}{\sin\beta}\mathcal{H}_2^i\tilde{q}_L^j\tilde{c}_R^* \\
&+ \left.\frac{m_b A_b}{\cos\beta}\mathcal{H}_1^i\tilde{q}_L^j\tilde{b}_R^* - \frac{m_t A_t}{\sin\beta}\mathcal{H}_2^i\tilde{q}_L^j\tilde{t}_R^* + h.c.\right]
\end{aligned}$$

$$+ \quad \frac{1}{2}\left[M_3\bar{\tilde{g}}^{\alpha}\tilde{g}^{\alpha} + M_2\bar{\tilde{W}}^{a}\tilde{W}^{a} + M_1\bar{\tilde{B}}\tilde{B}\right], \tag{1.18}$$

where,

$$\tilde{q}_L = \begin{pmatrix} \tilde{u}_L \\ \tilde{d}_L \end{pmatrix}, \begin{pmatrix} \tilde{c}_L \\ \tilde{s}_L \end{pmatrix}, \begin{pmatrix} \tilde{t}_L \\ \tilde{b}_L \end{pmatrix}, \tag{1.19}$$

and

$$\tilde{l}_L = \begin{pmatrix} \tilde{\nu}_{L,\,e} \\ \tilde{e}_L \end{pmatrix}, \begin{pmatrix} \tilde{\nu}_{L,\,\mu} \\ \tilde{\mu}_L \end{pmatrix}, \begin{pmatrix} \tilde{\nu}_{L,\,\tau} \\ \tilde{\tau}_L \end{pmatrix}, \tag{1.20}$$

for the first, second and third generation terms, respectively; $m^2_{\tilde{Q},u} = m^2_{\tilde{Q},d}$, $m^2_{\tilde{Q},c} = m^2_{\tilde{Q},s}$, $m^2_{\tilde{Q},t} = m^2_{\tilde{Q},b}$, $m^2_{\tilde{L},\nu_e} = m^2_{\tilde{L},e}$, $m^2_{\tilde{L},\nu_\mu} = m^2_{\tilde{L},\mu}$, $m^2_{\tilde{L},\nu_\tau} = m^2_{\tilde{L},\tau}$ due to $SU(2)_L$ invariance; m_f are the fermion masses, and, $\epsilon_{12} = -\epsilon_{21} = -1$, $\epsilon_{ii} = 0$. Notice that the trilinear terms for sneutrinos are absent since we are assuming in this section the generic MSSM without right-handed neutrinos and, therefore, vanishing neutrino Yukawa and trilinear couplings and neutrino masses. We will extend this simplest MSSM model to a modified version that includes three right-handed neutrinos, their corresponding superpartners and the associated interactions in the next section. To summarize the new terms introduced by the soft SUSY breaking potential:

- Soft masses for the scalar Higgs doublets, $m^2_{1,2}$, and a bilinear term, m^2_{12} between both Higgs doublets, $\mathcal{H}_1$ and $\mathcal{H}_2$.
- Soft masses for the squarks and sleptons, $m^2_{\tilde{Q}}$, $m^2_{\tilde{U}}$, $m^2_{\tilde{D}}$, $m^2_{\tilde{L}}$, $m^2_{\tilde{E}}$.
- Trilinear interactions between scalars respecting the gauge symmetries driven by the A_f couplings.
- Majorana mass terms for the gluino, M_3, wino, M_2, and bino, M_1 respectively.

With the complete set of SUSY preserving and soft SUSY breaking terms of the scalar potential we can analyze the Higgs potential to check if electroweak symmetry breaking can be achieved by the inclusion of these breaking terms:

$$\begin{aligned} V_{\text{Higgs}} &= m^2_{H_1}|\mathcal{H}_1|^2 + m^2_{H_2}|\mathcal{H}_2|^2 - m^2_{12}\left(\epsilon_{ij}\mathcal{H}^i_1\mathcal{H}^j_2 + \text{h.c.}\right) \\ &+ \frac{1}{8}(g^2 + g'^2)\left(|\mathcal{H}_1|^2 - |\mathcal{H}_2|^2\right)^2 + \frac{1}{2}g^2|\mathcal{H}^*_1\mathcal{H}_2|^2, \end{aligned} \tag{1.21}$$

where $m^2_{H_i} \equiv |\mu|^2 + m^2_i$ $(i = 1, 2)$, and m^2_i can be either positive or negative, thus allowing for a non-trivial minimum of the Higgs potential.

In order for the MSSM scalar potential to be viable, we must first make sure that the potential is bounded from below for arbitrarily large values of the scalar fields, so that V will really have a minimum. The scalar quartic interactions in $V_{\rm Higgs}$ will stabilize the potential for almost all arbitrarily large values of $\mathcal{H}_1$ and $\mathcal{H}_2$. However, for the special directions in field space $|\mathcal{H}_1| = |\mathcal{H}_2|$, the quartic contributions to $V_{\rm Higgs}$ are identically zero. In order for the potential to be bounded from below, we need the quadratic part of the scalar potential to be positive along those directions with the following requirement:

$$2|m_{12}^2| < 2|\mu|^2 + m_1^2 + m_2^2 \ . \tag{1.22}$$

On the other hand, by requiring that the potential has a non-trivial minimum the following condition is obtained

$$|m_{12}^2|^2 > (|\mu|^2 + m_1^2) \times (|\mu|^2 + m_2^2) \ . \tag{1.23}$$

Notice that if $m_1^2 = m_2^2$ both conditions cannot be satisfied simultaneously and, therefore, electroweak symmetry breaking would not be realized.

This issue is particularly problematic for models that impose universal conditions for the soft parameters. Actually, in these models electroweak symmetry breaking is driven by quantum corrections. The input condition, $m_1^2 = m_2^2$, is valid at a certain scale but the Renormalization Group Equations (RGEs) will correct m_1 and m_2 values at the electroweak scale, M_{EW}, such that $m_2^2(M_{EW}) < 0$. The mechanism is therefore known as radiative electroweak symmetry breaking (EWSB). The large negative contributions to m_2^2 from the RG equation are an important factor in ensuring that electroweak symmetry breaking can occur in models with universal boundary conditions for the soft terms. In fact, it was proven in Ref. [117] that the running of a large top Yukawa coupling generates negative contributions to m_2^2 in the required amount for being responsible of EWSB.

By imposing the minimization conditions, i.e. $\dfrac{\partial V}{\partial H_1^0} = \dfrac{\partial V}{\partial H_2^0} = 0$, and by requiring that the VEVs of H_1^0, H_2^0 are related to the known mass of the Z boson and the electroweak gauge couplings as shown in Eq. (1.13), Eq. (1.12), Eq. (1.11), Eq. (1.11) one obtains the conditions under which the Higgs potential Eq. (1.21) will have a minimum

$$\begin{aligned} |m_{12}^2| &= \frac{(m_1^2 - m_2^2)\tan 2\beta + M_Z^2 \sin 2\beta}{2} \ , \\ \frac{M_Z^2}{2} &= -|\mu|^2 + \frac{m_1^2 - m_2^2 \tan^2\beta}{\tan^2\beta - 1} \ . \end{aligned} \tag{1.24}$$

Notice that in the large $\tan\beta$ limit, this leads to the simple relation:

$$\frac{M_Z^2}{2} \approx -|\mu|^2 - m_2^2 \ . \tag{1.25}$$

As we can observe in Eq. (1.25) in order to obtain the correct measured mass of the Z gauge boson there will have to be a cancellation between the soft Higgs mass parameter m_2^2, which has to be negative, and the Higgsino mass parameter $|\mu|^2$. Therefore, parameters with very different origins have to be of the same order. There is no explanation for this puzzle and it is known as the μ problem. It is believed that there must be an underlying mechanism that relates the SUSY preserving parameter, that could have any value, to the SUSY breaking scale. The equations shown above establish a relation between the soft SUSY masses and B to μ, $\tan\beta$ and M_Z. This means that not all the parameters in the Higgs potential are independent because many of these parameters are fixed by supersymmetry and by imposing electroweak symmetry breaking.

We have now assembled all the pieces of the MSSM. The summary of the MSSM spectrum is collected in Table 1.1. It contains the SM particle content, extended with two Higgs doublets, and all their corresponding SUSY partners. There are the SUSY partners of the quarks, called squarks, the ones of the charged leptons and neutrinos, called charged sleptons and sneutrinos respectively, the gluinos being the superpartners of the gluons, and the SUSY partners of the electroweak gauge bosons, called gauginos, that after mixing with the SUSY partners of the Higgs bosons, called Higgsinos, give rise to the mass eigenstates named charginos and neutralinos. As a next step, we will proceed to the diagonalization of the mass matrices to obtain the mass eigenstates and their corresponding mass eigenvalues. We will study in detail only those sectors of the spectrum that are interesting for our work. Namely, the slepton sector, the squark sector, the chargino and neutralino sectors and the Higgs sector.

1.2.1 Squark sector

In this thesis we work under the hypothesis that there is not intergenerational mixing in the squark sector. Therefore, the tree-level 6×6 squark squared-mass matrices for the up and the down type squarks, referred to the $(\tilde{u}_L, \tilde{u}_R, \tilde{c}_L, \tilde{c}_R, \tilde{t}_L, \tilde{t}_R)$ and $(\tilde{d}_L, \tilde{d}_R, \tilde{s}_L, \tilde{s}_R, \tilde{b}_L, \tilde{b}_R)$

	SUSY particles			
Extended Standard Model spectrum	$SU(3)_C \times SU(2)_L \times U(1)_Y$ interaction eigenstates		Mass eigenstates	
	Notation	Name	Notation	Name
$q = u, d, s, c, b, t$ $l = e, \mu, \tau$ $\nu = \nu_e, \nu_\mu, \nu_\tau$	$\tilde{q}_L, \tilde{q}_R$ $\tilde{l}_L, \tilde{l}_R$ $\tilde{\nu}$	squarks sleptons sneutrino	$\tilde{q}_1, \tilde{q}_2$ $\tilde{l}_1, \tilde{l}_2$ $\tilde{\nu}$	squarks sleptons sneutrino
g	$\tilde{g}$	gluino	$\tilde{g}$	gluino
$W^\pm$ $H_1^+ \supset H^+$ $H_2^- \supset H^-$	$\tilde{W}^\pm$ $\tilde{H}_1^+$ $\tilde{H}_2^-$	wino higgsino higgsino	$\tilde{\chi}_i^\pm$ (i=1,2)	charginos
γ Z $H_1^o \supset h^0, H^0, A^0$ $H_2^o \supset h^0, H^0, A^0$ W^3 B	$\tilde{\gamma}$ $\tilde{Z}$ $\tilde{H}_1^o$ $\tilde{H}_2^o$ $\tilde{W}^3$ $\tilde{B}$	photino zino higgsino higgsino wino bino	$\tilde{\chi}_j^o$ (j=1,...,4)	neutralinos

Table 1.1: Summary of the MSSM spectrum.

basis respectively, can be written as

$$M_{\tilde{u}}^2 = \begin{pmatrix} M_{LL}^{uu\,2} & M_{LR}^{uu\,2} & 0 & 0 & 0 & 0 \\ M_{RL}^{uu\,2} & M_{RR}^{uu\,2} & 0 & 0 & 0 & 0 \\ 0 & 0 & M_{LL}^{cc\,2} & M_{LR}^{cc\,2} & 0 & 0 \\ 0 & 0 & M_{RL}^{cc\,2} & M_{RR}^{cc\,2} & 0 & 0 \\ 0 & 0 & 0 & 0 & M_{LL}^{tt\,2} & M_{LR}^{tt\,2} \\ 0 & 0 & 0 & 0 & M_{RL}^{tt\,2} & M_{RR}^{tt\,2} \end{pmatrix}, \tag{1.26}$$

$$M^2_{\tilde{d}} = \begin{pmatrix} M^{dd\,2}_{LL} & M^{dd\,2}_{LR} & 0 & 0 & 0 & 0 \\ M^{dd\,2}_{RL} & M^{dd\,2}_{RR} & 0 & 0 & 0 & 0 \\ 0 & 0 & M^{ss\,2}_{LL} & M^{ss\,2}_{LR} & 0 & 0 \\ 0 & 0 & M^{ss\,2}_{RL} & M^{ss\,2}_{RR} & 0 & 0 \\ 0 & 0 & 0 & 0 & M^{bb\,2}_{LL} & M^{bb\,2}_{LR} \\ 0 & 0 & 0 & 0 & M^{bb\,2}_{RL} & M^{bb\,2}_{RR} \end{pmatrix} , \tag{1.27}$$

where

$$M^{qq\,2}_{LL} = m^2_{\tilde{Q},q} + m^2_q + M^2_Z \cos 2\beta (T^q_3 - Q_q \sin^2\theta_W) , \tag{1.28}$$

$$M^{qq\,2}_{RR} = \begin{cases} m^2_{\tilde{U},q} + m^2_q + M^2_Z \cos 2\beta Q_q \sin^2\theta_W \text{ , if } q = u,\ c,\ t, \\ \\ m^2_{\tilde{D},q} + m^2_q + M^2_Z \cos 2\beta Q_q \sin^2\theta_W \text{ , if } q = d,\ s,\ b, \end{cases} \tag{1.29}$$

$$M^{qq\,2}_{LR} = M^{qq\,2*}_{RL} = \begin{cases} m_q(A_q - \mu \cot\beta) \text{ , } if\ q = u,\ c,\ t, \\ \\ m_q(A_q - \mu \tan\beta) \text{ , } if\ q = d,\ s,\ b\,. \end{cases} \tag{1.30}$$

Here, m_q, T^q_3 and Q_q are the mass, weak isospin and electric charge of the corresponding quark ($T^q_3 = \frac{1}{2}$, $Q_q = \frac{2}{3}$ for q=u, c, t and $T^q_3 = \frac{-1}{2}$, $Q_q = \frac{-1}{3}$ for q=d, s, b), M_Z is the Z gauge boson mass and θ_W is the weak mixing angle. The parameters $m_{\tilde{Q},q}$, $m_{\tilde{D},q}$ and $m_{\tilde{U},q}$ are the soft-SUSY-breaking masses for the squarks introduced in Eq. (1.18), A_q are the trilinear couplings, given also in Eq. (1.18). The rest of parameters are common with the slepton sector that will be introduced next. The diagonalization of the previous 6×6 squark squared-mass matrices is completely analog to the one of the slepton sector, so the corresponding mass eigenstates and physical masses have the corresponding analogous expresions to Eqs. (1.38) and (1.39), respectively.

1.2.2 Slepton sector

The tree-level 6×6 slepton squared-mass matrix can be written, for the case without intergenerational mixing in the slepton sector, in a three-box-submatrices form as follows

$$M_{\tilde{l}}^2 = \begin{pmatrix} M_{LL}^{ee\,2} & M_{LR}^{ee\,2} & 0 & 0 & 0 & 0 \\ M_{RL}^{ee\,2} & M_{RR}^{ee\,2} & 0 & 0 & 0 & 0 \\ 0 & 0 & M_{LL}^{\mu\mu\,2} & M_{LR}^{\mu\mu\,2} & 0 & 0 \\ 0 & 0 & M_{RL}^{\mu\mu\,2} & M_{RR}^{\mu\mu\,2} & 0 & 0 \\ 0 & 0 & 0 & 0 & M_{LL}^{\tau\tau\,2} & M_{LR}^{\tau\tau\,2} \\ 0 & 0 & 0 & 0 & M_{RL}^{\tau\tau\,2} & M_{RR}^{\tau\tau\,2} \end{pmatrix}, \tag{1.31}$$

where

$$\begin{aligned} M_{LL}^{ll\,2} &= m_{\tilde{L},l}^2 + m_l^2 + M_Z^2 \cos 2\beta \left(-\frac{1}{2} + \sin^2 \theta_W \right) , \\ M_{RR}^{ll\,2} &= m_{\tilde{E},l}^2 + m_l^2 - M_Z^2 \cos 2\beta \sin^2 \theta_W , \\ M_{LR}^{ll\,2} &= M_{RL}^{ll\,2*} = m_l (A_l - \mu \tan \beta) . \end{aligned} \tag{1.32}$$

Here, M_Z is again the Z boson mass, θ_W is the weak mixing angle, m_l is the charged lepton mass, the parameters $m_{\tilde{L},l}$, $m_{\tilde{E},l}$ are the soft-SUSY-breaking masses for the sleptons introduced in Eq. (1.18) and A_l is the corresponding trilinear coupling also given in Eq. (1.18). One can appreciate that the $\tilde{l}_L - \tilde{l}_R$ mixing is unimportant for $m_f << M_{\rm SUSY}$ where $M_{\rm SUSY}$ characterizes the scale of the SUSY breaking terms.

The diagonalization of this 6×6 mass matrices above gives the six slepton mass eigenstates, $\tilde{l}_\alpha$, $(\alpha = 1, .., 6)$, in terms of the interaction eigenstates $\tilde{l}'_\alpha$,

$$\tilde{l}'_\alpha = \begin{pmatrix} \tilde{e}_L \\ \tilde{e}_R \\ \tilde{\mu}_L \\ \tilde{\mu}_R \\ \tilde{\tau}_L \\ \tilde{\tau}_R \end{pmatrix} , \quad \tilde{l}_\alpha = \begin{pmatrix} \tilde{l}_1 \\ \tilde{l}_2 \\ \tilde{l}_3 \\ \tilde{l}_4 \\ \tilde{l}_5 \\ \tilde{l}_6 \end{pmatrix} . \tag{1.33}$$

The rotation matrix, $R^{(l)}$, between these two basis,

$$\tilde{l}'_\alpha = \sum R_{\alpha\beta}^{(l)} \tilde{l}_\beta , \tag{1.34}$$

therefore leads to the physical slepton masses:

$$M_{\tilde{l}_{\rm diag}}^2 = R^{(l)} M_{\tilde{l}}^2 R^{(l)\,\dagger} = {\rm diag}\,(m_{\tilde{l}_1}^2, .., m_{\tilde{l}_6}^2) . \tag{1.35}$$

The fact that there is not any intergenerational mixing yet allows us to diagonalize separately each box submatrix per flavor in Eqs. (1.31), via a 2×2 rotation matrix as follows

$$\begin{pmatrix} \tilde{l}_1 \\ \tilde{l}_2 \end{pmatrix} = (r^{(l)})^{-1} \begin{pmatrix} \tilde{l}_L \\ \tilde{l}_R \end{pmatrix} , \tag{1.36}$$

where l here can be any of the three charged leptons $l = e, \mu, \tau$ and the corresponding rotation matrix is

$$r^{(l)} = \begin{pmatrix} \cos\theta_{\tilde{l}} & -\sin\theta_{\tilde{l}} \\ \sin\theta_{\tilde{l}} & \cos\theta_{\tilde{l}} \end{pmatrix} . \tag{1.37}$$

Notice that this is the usual notation in the MSSM and these $\tilde{e}_1$, $\tilde{e}_2$, $\tilde{\mu}_1$, $\tilde{\mu}_2$ and $\tilde{\tau}_1$, $\tilde{\tau}_2$ correspond to $\tilde{l}_1$, $\tilde{l}_2$, $\tilde{l}_3$, $\tilde{l}_4$ and $\tilde{l}_5$, $\tilde{l}_6$ respectively of our alternative notation introduced in Eq. (1.33).

The mass eigenvalues in the usual notation are[1]

$$m^2_{\tilde{l}_{1,2}} = \frac{1}{2}\left[M^{ll\,2}_{LL} + M^{ll\,2}_{RR} \pm \sqrt{(M^{ll\,2}_{LL} - M^{ll\,2}_{RR})^2 + 4M^{ll\,4}_{LR}} \right] , \tag{1.38}$$

where $l = e, \mu, \tau$ and the corresponding mixing angle $\theta_{\tilde{l}}$ is given by

$$\cos 2\theta_{\tilde{l}} = \frac{M^{ll\,2}_{LL} - M^{ll\,2}_{RR}}{m^2_{\tilde{l}_1} - m^2_{\tilde{l}_2}} , \quad \sin 2\theta_{\tilde{l}} = \frac{2M^{ll\,2}_{LR}}{m^2_{\tilde{l}_1} - m^2_{\tilde{l}_2}} . \tag{1.39}$$

The sneutrino sector is an exception, since within the MSSM the neutrinos are massless, there are no right-handed neutrinos, ν_R, nor their corresponding SUSY partners $\tilde{\nu}_R$, and consequently there is not LR mixing. The physical sneutrino states, $\tilde{\nu}_L$, are the SUSY partners of the left handed neutrinos ν_L and their squared masses for the three generations are given by

$$m^2_{\tilde{\nu}_l} = m^2_{\tilde{L}\,l} + \frac{1}{2} M^2_Z \cos 2\beta , \tag{1.40}$$

where $l = e$, μ, τ, correspondingly.

1.2.3 Chargino sector

The charginos are four-components Dirac fermions that result from the mixture of charged gauginos, $\tilde{W}^{\pm}$, i.e., the SUSY partners of the charged gauge bosons $W^{\pm}$, and charged higgsinos, $\tilde{H}_1^-$ and $\tilde{H}_2^+$, i.e. the SUSY partners of the charged components of the two Higgs doublets, H_1 and H_2, respectively.

[1]Note that for the case without intergenerational mixing the convention is $m_{\tilde{l}_1} > m_{\tilde{l}_2}$

In the $\tilde{W}^+ - \tilde{H}^+$ basis, the chargino mass matrix at the tree-level is

$$X = \begin{pmatrix} M_2 & \sqrt{2}M_W \sin\beta \\ \sqrt{2}M_W \cos\beta & \mu \end{pmatrix} . \tag{1.41}$$

Due to the two independent mixings, $(\tilde{W}^-, \tilde{H}_1^-)$ and $(\tilde{W}^+, \tilde{H}_2^+)$, one needs to define two unitary mixing matrices, U and V, in order to obtain the mass eigenstates. The squared mass matrix of the charginos is diagonalised by

$$\mathcal{M}^2_{\tilde{\chi}^+} = \mathrm{diag}(m^2_{\tilde{\chi}_1^+}, m^2_{\tilde{\chi}_2^+}) = VX^\dagger XV^{-1} = U^* XX^\dagger (U^*)^{-1} , \tag{1.42}$$

where the two mass eigenstates are denoted by $\tilde{\chi}_1^+$ and $\tilde{\chi}_2^+$ and the corresponding eigenvalues are given by

$$\begin{aligned} m^2_{\tilde{\chi}^+_{1,2}} &= \frac{1}{2}\Big\{ M_2^2 + \mu^2 + 2m_W^2 \mp \big[(M_2^2 - \mu^2)^2 + 4m_W^4 \cos^2 2\beta \\ &+ 4m_W^2 (M_2^2 + \mu^2 + 2M_2 \mu \sin 2\beta) \big]^{1/2} \Big\} , \end{aligned} \tag{1.43}$$

where by convention, $m_{\tilde{\chi}_1^+} \leq m_{\tilde{\chi}_2^+}$.

1.2.4 Neutralino sector

Finally, the neutralinos, $\tilde{\chi}_j^0$ with $j = 1, ...4$, are mixtures among the photino, the zino and the SUSY partners of the neutral components of the two Higgs doublets, i.e. the neutral higgsinos. In the $\tilde{B} - \tilde{W}^3 - \tilde{H}_1^0 - \tilde{H}_2^0$ basis, the neutralino mass matrix is

$$Y = \begin{pmatrix} M_1 & 0 & -M_Z s_W \cos\beta & M_Z s_W \sin\beta \\ 0 & M_2 & M_Z c_W \cos\beta & -M_Z c_W \sin\beta \\ -M_Z s_W \cos\beta & M_Z c_W \cos\beta & 0 & -\mu \\ M_Z s_W \sin\beta & -M_Z c_W \sin\beta & -\mu & 0 \end{pmatrix} . \tag{1.44}$$

This is in general a complex symmetric matrix, and this symmetry is due to the Majorana nature of the neutralinos. As a consequence, only one unitary matrix, N, is required to diagonalise the neutralino sector, in contrast with the chargino one. The diagonal neutralino mass matrix is given by

$$\mathcal{M}_{\tilde{\chi}^0} = \mathrm{diag}(m_{\tilde{\chi}_1^0}, ..., m_{\tilde{\chi}_4^0}) = N^* Y N^{-1} . \tag{1.45}$$

The matrix N can be chosen in such a way that the elements of the diagonal matrix are real and non-negative. Our convention for the neutralino masses here is $m_{\tilde{\chi}_1^0} \leq ... \leq m_{\tilde{\chi}_4^0}$. The full expressions for $m_{\tilde{\chi}_1^0}, ..., m_{\tilde{\chi}_4^0}$ in terms of M_1, M_2, μ, M_Z, θ_W and $\tan\beta$ are lengthy and are omitted here for brevity.

1.2.5 The Higgs boson sector at tree-level

In this subsection we summarize the Higgs-boson sector of our model at tree-level. Contrary to the SM, in the MSSM two Higgs doublets are required. The two Higgs doublets $\mathcal{H}_1$ and $\mathcal{H}_2$ are given in Eq. (1.9) in terms of their components. The Higgs potential is given in Eq. (1.21). Notice that contrary to the SM, the quartic couplings of the MSSM Higgs potential are determined by the gauge couplings.

The potential of Eq. (1.21) can be described with the help of two independent parameters (besides g and g'):

$$\tan\beta = \frac{v_2}{v_1}\,, \qquad M_A^2 = -m_{12}^2(\tan\beta + \cot\beta)\,, \tag{1.46}$$

where M_A is the mass of the $\mathcal{CP}$-odd Higgs boson A.

The diagonalization of the bilinear part of the Higgs potential, i.e. of the Higgs mass matrices, is performed via the orthogonal transformations

$$\begin{pmatrix} H \\ h \end{pmatrix} = \begin{pmatrix} \cos\alpha & \sin\alpha \\ -\sin\alpha & \cos\alpha \end{pmatrix} \begin{pmatrix} \phi_1^0 \\ \phi_2^0 \end{pmatrix}\,, \tag{1.47}$$

$$\begin{pmatrix} G \\ A \end{pmatrix} = \begin{pmatrix} \cos\beta & \sin\beta \\ -\sin\beta & \cos\beta \end{pmatrix} \begin{pmatrix} \chi_1^0 \\ \chi_2^0 \end{pmatrix}\,, \tag{1.48}$$

$$\begin{pmatrix} G^\pm \\ H^\pm \end{pmatrix} = \begin{pmatrix} \cos\beta & \sin\beta \\ -\sin\beta & \cos\beta \end{pmatrix} \begin{pmatrix} \phi_1^\pm \\ \phi_2^\pm \end{pmatrix}\,. \tag{1.49}$$

The mixing angle α is determined through

$$\alpha = \arctan\left[\frac{-(M_A^2 + M_Z^2)\sin\beta\cos\beta}{M_Z^2\cos^2\beta + M_A^2\sin^2\beta - m_{h\ \mathrm{tree}}^2}\right]\,, \quad -\frac{\pi}{2} < \alpha < 0\,. \tag{1.50}$$

In the convention where $\tan\beta$ is positive, i.e. $0 \le \beta \le \pi/2$, the angle α lies in the range $-\pi/2 \le \alpha \le 0$.

One gets the following Higgs spectrum:

$$\begin{aligned} \text{2 neutral bosons, } \mathcal{CP} = +1 &: h, H \\ \text{1 neutral boson, } \mathcal{CP} = -1 &: A \\ \text{2 charged bosons} &: H^+, H^- \\ \text{3 unphysical Goldstone bosons} &: G, G^+, G^-. \end{aligned} \tag{1.51}$$

The 3 Goldstone bosons, which result from the spontaneous breaking of the electroweak symmetry, are absorbed and become the longitudinal components of the gauge bosons $W^{\pm}$ and Z, in analogy with the SM:

$$M_W^2 = \frac{1}{2}g^2(v_1^2+v_2^2); \qquad M_Z^2 = \frac{1}{2}(g^2+g'^2)(v_1^2+v_2^2); \qquad M_\gamma = 0\,. \tag{1.52}$$

Nevertheless, in the MSSM there are 5 physical Higgs bosons due to the extra degrees of freedom coming from the new Higgs doublet. At tree level the mass matrix of the neutral $\mathcal{CP}$-even Higgs bosons is given in the ϕ_1-ϕ_2-basis in terms of M_Z, M_A, and $\tan\beta$ by

$$\begin{aligned} M^2_{\text{Higgs}} &= \begin{pmatrix} m^2_{\phi_1} & m^2_{\phi_1\phi_2} \\ m^2_{\phi_1\phi_2} & m^2_{\phi_2} \end{pmatrix} \\ &= \begin{pmatrix} M_A^2\sin^2\beta + M_Z^2\cos^2\beta & -(M_A^2+M_Z^2)\sin\beta\cos\beta \\ -(M_A^2+M_Z^2)\sin\beta\cos\beta & M_A^2\cos^2\beta + M_Z^2\sin^2\beta \end{pmatrix}, \end{aligned} \tag{1.53}$$

which by diagonalization according to Eq. (1.47) yields the tree-level Higgs boson masses

$$m^2_{H,h} = \frac{1}{2}\left[M_A^2+M_Z^2 \pm \sqrt{(M_A^2+M_Z^2)^2 - 4M_Z^2M_A^2\cos^2 2\beta}\right]\,. \tag{1.54}$$

An important consequence of Eq. (1.54) is that the mass of the lightest $\mathcal{CP}$-even Higgs boson is bounded from above:

$$m_h \leq M_Z|\cos 2\beta| \leq M_Z \tag{1.55}$$

This contrasts sharply with the SM, where the Higgs boson mass is not constrained at tree level. In the SM the Higgs boson mass at tree level, $m_h^2 = \frac{1}{2}v^2\lambda^2$, is proportional to the Higgs self coupling λ, which is a free parameter of the model. However, in the MSSM all the Higgs self coupling parameters are determined by the electroweak gauge couplings.

The charged Higgs boson mass is given by

$$m^2_{H^\pm} = M_A^2 + M_W^2\,. \tag{1.56}$$

Notice that in the limit of large M_A, i.e. $M_A >> M_Z$, then $m_{H^\pm} \simeq m_H \simeq M_A$ and $\alpha \to \beta - \pi/2$, up to corrections of $\mathcal{O}(M_Z^2/M_A)$. This limit is known as the *decoupling* limit [118] because when M_A is large, there exists an effective low-energy theory below the scale of M_A in which the effective Higgs sector consists only of one CP-even Higgs boson, h, with precisely the same couplings as those of the Standard Model Higgs boson. There

is a significant region of the MSSM Higgs sector parameter space in which the decoupling limit applies, already for values of M_A larger than about 200 GeV. As a result, over a significant region of the MSSM parameter space, the search for the lightest $\mathcal{CP}$-even Higgs boson of the MSSM is equivalent to the search for the SM Higgs boson.

1.2.6 Radiative corrections to the lightest Higgs boson in the MSSM

The allowed range of the tree level lightest Higgs mass shown in Eq. (1.55) was already excluded by LEP [20], so, if the MSSM has not been ruled out yet is due to the importance of quantum corrections to the Higgs potential and, in particular, to m_h. The main corrections to m_h in the MSSM come from the tops/stops sector because the top mass is bigger than any of the other particles of the SM and, therefore, its coupling to the Higgs boson is stronger. The status of radiative corrections to m_h in the MSSM, can be summarized as follows. Full one-loop calculations [62] have been supplemented by the leading and subleading two-loop corrections, see [76] and references therein. Together with leading three-loop corrections [119] the current precision in the value of the Higgs corrected mass M_h is estimated to be $\sim 2-3$ GeV [76].

We show below the main one loop corrections $\sim \mathcal{O}(m_t^4)$ which take into account the important mixing $\theta_{\tilde{t}}$ in the stop sector [120–122]:

$$\begin{aligned} m^2_{H,h1-\text{loop}} &= \frac{1}{2}\left(M_A^2+M_Z^2+\omega_t+\sigma_t\right) \pm \left\{\frac{1}{4}\left((M_A^2+M_Z^2)^2+(\omega_t-\sigma_t)^2\right) - M_A^2 M_Z^2\cos^2 2\beta \right. \\ &\left. +\frac{1}{2}\left(\omega_t-\sigma_t\right)2\cos 2\beta\left(M_A^2-M_Z^2\right) - \lambda_t \sin 2\beta\left(M_A^2+M_Z^2\right)+\lambda_t^2\right\}^{1/2}, \quad (1.57) \end{aligned}$$

with

$$\begin{aligned} \omega_t &= \frac{3G_F m_t^4}{\sqrt{2}\pi^2\sin^2\beta}\left[\log\frac{m_{\tilde{t}_1}m_{\tilde{t}_2}}{m_t^2}+\frac{A_t\sin 2\theta_{\tilde{t}}}{2m_t}\log\frac{m^2_{\tilde{t}_1}}{m^2_{\tilde{t}_2}}+\frac{A_t^2\sin^2 2\theta_{\tilde{t}}}{2m_t}\left(1-\frac{m^2_{\tilde{t}_1}+m^2_{\tilde{t}_2}}{m^2_{\tilde{t}_1}-m^2_{\tilde{t}_2}}\log\frac{m^2_{\tilde{t}_1}}{m^2_{\tilde{t}_2}}\right)\right], \\ \lambda_t &= \frac{3G_F m_t^4}{\sqrt{2}\pi^2\sin^2\beta}\left[\frac{\mu\sin 2\theta_{\tilde{t}}}{2m_t}\log\frac{m^2_{\tilde{t}_1}}{m^2_{\tilde{t}_2}}+\frac{\mu A_t\sin^2 2\theta_{\tilde{t}}}{m_t}\left(1-\frac{m^2_{\tilde{t}_1}+m^2_{\tilde{t}_2}}{m^2_{\tilde{t}_1}-m^2_{\tilde{t}_2}}\log\frac{m^2_{\tilde{t}_1}}{m^2_{\tilde{t}_2}}\right)\right], \\ \sigma_t &= \frac{3G_F m_t^4}{\sqrt{2}\pi^2\sin^2\beta}\left[\frac{\mu^2\sin^2 2\theta_{\tilde{t}}}{2m_t}\left(1-\frac{m^2_{\tilde{t}_1}+m^2_{\tilde{t}_2}}{m^2_{\tilde{t}_1}-m^2_{\tilde{t}_2}}\log\frac{m^2_{\tilde{t}_1}}{m^2_{\tilde{t}_2}}\right)\right], \end{aligned} \quad (1.58)$$

where $m^2_{\tilde{t}_2}$ and $m^2_{\tilde{t}_1}$ are the eigenvalues of the stops squared mass matrix:

$$m^2_{\tilde{t}_{1,2}} = \frac{1}{2}\left[M^2_{LL} + M^2_{RR} \pm \sqrt{(M^2_{LL} - M^2_{RR})^2 + 4M^4_{LR}}\right], \tag{1.59}$$

with

$$M^2_{LL} = M^{tt^2}_{LL}, \qquad M^2_{RR} = M^{tt^2}_{RR}, \qquad M^2_{LR} = M^{tt^2}_{LR} = m_t X_t\,. \tag{1.60}$$

The corresponding expressions of $M^{tt^2}_{LL}, M^{tt^2}_{RR}$ and $M^{tt^2}_{LR}$ are given in Eq. (1.28), Eq. (1.29) and Eq. (1.30), respectively. Moreover, $\theta_{\tilde{t}}$ is the mixing angle that diagonalizes the stops squared mass matrix:

$$\sin 2\theta_{\tilde{t}} = \frac{2m_t(A_t - \mu\cot\beta)}{m^2_{\tilde{t}_1} - m^2_{\tilde{t}_2}}\,. \tag{1.61}$$

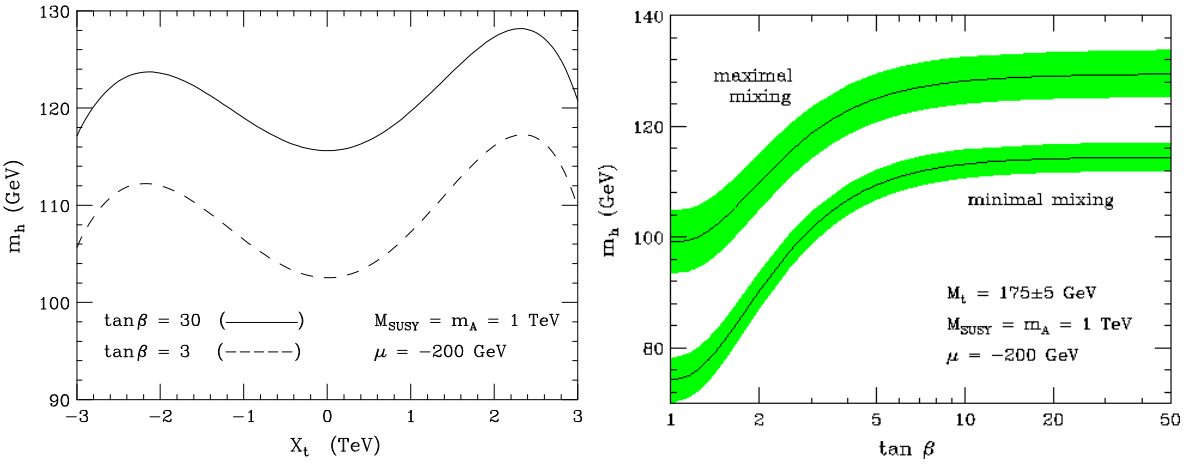

Figure 1.1: The radiatively corrected light $\mathcal{CP}$-even Higgs mass is plotted (a = left panel) as a function of X_t, where $X_t \equiv A_t - \mu\cot\beta$, for $M_t = 174.3$ GeV and two choices of $\tan\beta = 3$ and 30, and (b = right panel) as a function of $\tan\beta$, for the maximal mixing [upper band] and minimal mixing [lower band] benchmark cases. In (b), the central value of the shaded bands corresponds to $M_t = 175$ GeV, while the upper [lower] edge of the bands correspond to increasing [decreasing] M_t by 5 GeV. In both (a) and (b), $M_A = 1$ TeV and the diagonal soft squark squared-masses are assumed to be degenerate: $M_{\rm SUSY} \equiv m_{\tilde{Q}} = m_{\tilde{U}} = m_{\tilde{D}} = 1$ TeV.

As noted above, the largest contribution to the one-loop radiative corrections is enhanced by a factor of m_t^4 and grows logarithmically with the top squark mass. In fact, the precise upper bound on the light Higgs mass depends on the specific choice of the top-squark masses. The dependence of the light Higgs mass on the LR mixing parameter

$X_t = (A_t - \mu \cot\beta)$, implies that for a given value of M_S^2, being $M_S^2 = \frac{1}{2}(m_{\tilde{t}_1}^2 + m_{\tilde{t}_2}^2)$ the upper bound of the light Higgs mass initially increases with X_t and reaches its maximal value for $X_t^{OS} = 2M_S$, $X_t^{\bar{M}S} = \sqrt{6}M_S$. This point is referred to as the maximal mixing case, whereas $X_t^{OS} = X_t^{\bar{M}S} = 0$ corresponds to the minimal mixing case. One finds for $M_S \lesssim 2$ TeV, $M_A >> M_Z$, the following bounds in the light Higgs boson mass $m_h < m_h^{max} \equiv m_h^{max}(\tan\beta >> 1)$, [123]:

$$\begin{aligned} m_h^{max} &\simeq 122 \text{ GeV}, \quad \text{if top-squark mixing is minimal,} \\ m_h^{max} &\simeq 135 \text{ GeV}, \quad \text{if top-squark mixing is maximal.} \end{aligned} \tag{1.62}$$

Typical results for the radiatively corrected value of m_h as a function of the relevant

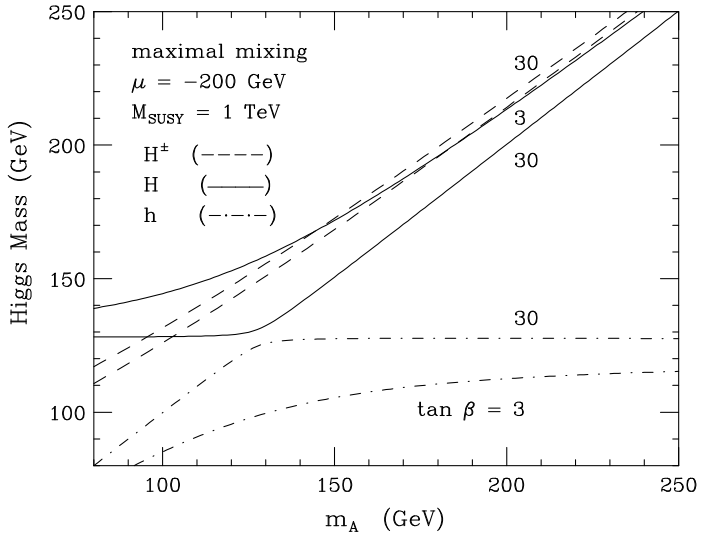

Figure 1.2: Lightest $\mathcal{CP}$-even Higgs mass (m_h), heaviest $\mathcal{CP}$-even Higgs mass (m_H) and charged Higgs mass ($m_{H^\pm}$) as a function of M_A for two choices of $\tan\beta = 3$ and $\tan\beta = 30$. Here, we have taken $M_t = 174.3$ GeV, and have assumed that the diagonal soft squark squared-masses are degenerate: $M_{SUSY} \equiv m_{\tilde{Q}} = m_{\tilde{U}} = m_{\tilde{D}} = 1$ TeV. In addition, we choose the other supersymmetric parameters corresponding to the maximal mixing scenario. The slight increase in the charged Higgs mass as $\tan\beta$ is increased from 3 to 30 is a consequence of the radiative corrections.

supersymmetric parameters are shown in Figures 1.1, 1.2 and 1.3, taken from Ref. [123]. The supersymmetric parameters in the maximal and minimal mixing cases have been chosen according to the first two benchmark scenarios of Ref. [60]. The numerical results

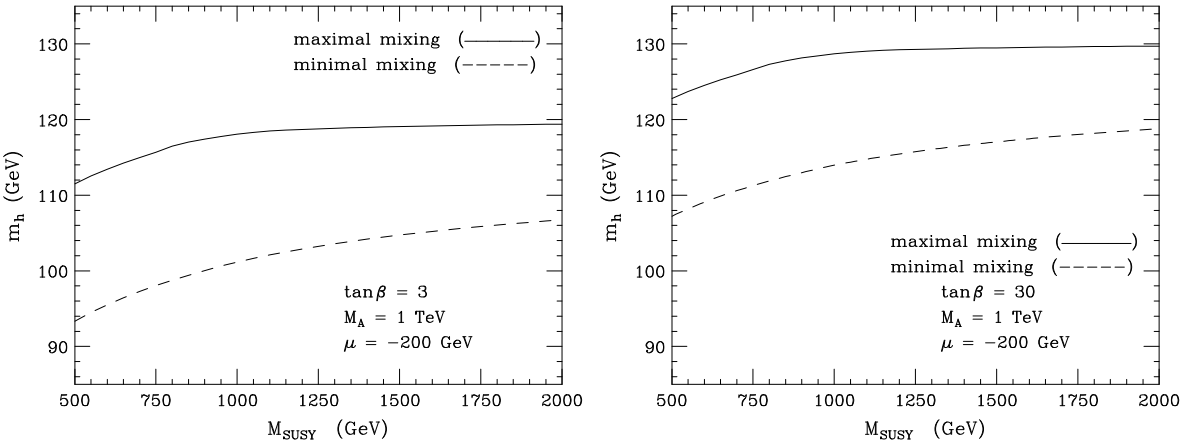

Figure 1.3: The radiatively corrected light $\mathcal{CP}$-even Higgs mass is plotted as a function of $M_{SUSY} \equiv m_{\tilde{Q}} = m_{\tilde{U}} = m_{\tilde{D}}$, for $M_t = 174.3$ GeV, $M_A = 1$ TeV and two choices of $\tan\beta = 3$ and $\tan\beta = 30$. Maximal mixing and minimal mixing are defined according to the value of X_t that yields the maximal and minimal Higgs mass as shown in Figure 1.1(a).

displayed in Figures 1.1, 1.2 and 1.3, are based on the calculations of Ref. [124] and Ref. [125], with improvements as described in Ref. [126] and Ref. [127].

In Figure 1.1(a) the dependence of the lightest Higgs boson mass is shown as a function of the mixing parameter X_t for two different values of $\tan\beta$, $\tan\beta = 3$ and $\tan\beta = 30$. We clearly see that the maximum value of m_h is obtained for $X_t = 2$ TeV $= 2M_{SUSY}$. It shows an asymmetry under $X_t \to -X_t$. Moreover, the Higgs mass prediction increases with $\tan\beta$ as we can appreciate in Figure 1.1(b). The green bands represent the dependence of the prediction of m_h on the top mass precision measurement. The value of m_t is varied from 169 to 179 GeV with a central value at 175 GeV. We can observe that a higher precision in the top mass measurement is extremely relevant to reduce the uncertainty in the prediction of m_h. At present, the mass of the top has been measured with the following uncertainty $m_t = 172.9 \pm 1.5$ [20].

In Figure 1.2 the masses of the neutral $\mathcal{CP}$ even Higgs bosons and the charged Higgs bosons are shown as a function of M_A for a common soft SUSY mass, $M_{SUSY} = 1$ TeV, in a maximal mixing scenario, and for two different values of $\tan\beta$, 3 and 30. We can appreciate from this plot, that the so-called decoupling limit ($M_A \gg M_Z$), where the lightest $\mathcal{CP}$ even MSSM Higgs is barely distinguishable from the SM Higgs and the rest of Higgs bosons become degenerate and heavy, applies already for values of $M_A \gtrsim 200$ GeV

as it was anticipated in Subsect. 1.2.5.

The dominant corrections to m_h have a logarithmic sensitivity to the top-squark masses as it was shown in Eq. (1.58). Therefore, the precise upper bound on the light Higgs mass depends on the specific choice for the upper limit of the top-squark masses. The dependence of the light Higgs mass obtained by a complete computation as a function of M_{SUSY} is shown in Figure 1.3. The flattening of the curves in Figure 1.3 as a function of M_{SUSY} in the maximal mixing scenario is due to the squark-mixing contributions at two-loops which partially cancel the contributions that grow logarithmically with M_{SUSY}. Higher order radiative corrections can be non-negligible for large top squark masses, in which case the large logarithms should be resumed.

1.3 Constrained MSSM scenarios and experimental bounds

1.3.1 Constrained SUSY models

Unlike the supersymmetry-preserving part of the Lagrangian, the soft breaking terms of the Lagrangian Eq. (1.18) introduce many new parameters that were not present in the ordinary Standard Model. In fact, there are 105 masses, phases and mixing angles in the MSSM Lagrangian that cannot be rotated away by redefining the phases and flavor basis for the quark and lepton supermultiplets, and that have no counterpart in the ordinary Standard Model. Thus, the MSSM has too many free parameters, making it very unpredictive.

On the other hand, the MSSM is not a phenomenologically-viable theory over most of its parameter space. This conclusion follows from the observation that a generic point in the MSSM parameter space exhibits:

- No conservation of the separate lepton numbers, L_e, L_μ and L_τ
- Flavour mixing in the squark and slepton sector give rise to unsuppressed flavor-changing neutral currents (FCNC's)
- New sources of CP violation that are inconsistent with the experimental bounds.

These phenomenological problems imply that the arbitrariness of the soft parameters

must be reduced. For example, the non-observation of FCNCs places strong constraints on the off-diagonal matrix elements of the squark and slepton soft supersymmetry- breaking squared masses and trilinear parameters. All of these potentially dangerous flavor-changing and CP-violating effects in the MSSM can be evaded if one assumes, adhoc, that supersymmetry breaking has universal soft parameters. One can consider, for instance, an idealized limit in which the squark and slepton squared-mass matrices are flavor-blind, each proportional to the 3×3 identity matrix in family space. More generically, it is usually assumed that the only source of flavor violation is coming from the Yukawa matrices and that the trilinear couplings do not introduce extra sources of flavor violation. Moreover, one assumes that the only source of flavour violation is coming from the Yukawa matrices and the trilinears don't introduced extra sources of flavour violation. Finally, one can avoid disastrously large CP-violating effects by assuming that the soft parameters do not introduce new complex phases so that the only CP-violating phase in the theory will be the usual CKM phase found in the ordinary Yukawa couplings.

These soft-breaking universality relations can be presumed to be the result of some specific model for the origin of supersymmetry breaking, although there is considerable disagreement among theorists as to what the specific model should actually be. In any case, they are indicative of an assumed underlying simplicity or symmetry of the Lagrangian at some very high energy scale Q. Therefore, the universal conditions should be interpreted as boundary conditions on the running soft parameters at the scale Q. We must then evolve with the RGEs all the soft parameters, the superpotential parameters, and the gauge couplings down to the electroweak scale. At the electroweak scale, these universal conditions will no longer hold, even if they were exactly true at the input scale Q. However, to a good approximation, key flavor- and CP-conserving properties remain because RGE corrections due to gauge interactions will respect the form in flavor space of the parameters imposed at the large scale, while RGE corrections due to Yukawa interactions are the only source of flavor violation.

The MSSM has the interesting property of unification of the gauge couplings at the GUT scale. Therefore the scale Q where the input soft parameters are universal is normally chosen at this scale $M_X = 2 \times 10^{16}$ GeV.

1.3.2 CMSSM/mSUGRA model

The well known constrained supersymmetric standard model (CMSSM/mSUGRA) [63] minimizes the number of universal parameters at the GUT scale, leaving only 5 free parameters, a soft mass for the scalar particles M_0, a common mass for the gauginos $M_{1/2}$, an universal trilinear coupling for all the scalars A_0 and the pure SUSY preserving parameters $\tan\beta$ and sign(μ) The universal conditions at the GUT scale are explicitly,

$$\begin{aligned}
&\left(m_{\tilde{Q}}\right)^2_{ij} = (m_{\tilde{U}})^2_{ij} = (m_{\tilde{D}})^2_{ij} = (m_{\tilde{L}})^2_{ij} = (m_{\tilde{E}})^2_{ij} = M_0^2\,\delta_{ij}\,,\\
&(A_u)_{ij} = A_0\,(Y_u)_{ij}\;,\;(A_d)_{ij} = A_0\,(Y_d)_{ij}\;,\;(A_l)_{ij} = A_0\,(Y_l)_{ij}\;,\\
&m^2_{H_1} = m^2_{H_2} = M_0^2\\
&M_1 = M_2 = M_3 = M_{1/2}\,,
\end{aligned} \tag{1.63}$$

In summary, the CMSSM scenarios are defined by the following (unknown) input parameters:

- SUSY parameters: M_0, $M_{1/2}$, A_0, sign (μ) and $\tan\beta$.

1.3.3 NUHM scenarios

An interesting departure from the previous CMSSM scenarios can be obtained by relaxing the universality hypothesis for the soft SUSY breaking masses of the Higgs sector. This partially constrained MSSM is commonly referred to as the Non Universal Higgs Mass (NUHM) scenario [64]. The universality conditions at the high energy scale M_X in these NUHM scenarios are,

$$\begin{aligned}
&\left(m_{\tilde{Q}}\right)^2_{ij} = (m_{\tilde{U}})^2_{ij} = (m_{\tilde{D}})^2_{ij} = (m_{\tilde{L}})^2_{ij} = (m_{\tilde{E}})^2_{ij} = M_0^2\,\delta_{ij}\,,\\
&(A_u)_{ij} = A_0\,(Y_u)_{ij}\;,\;(A_d)_{ij} = A_0\,(Y_d)_{ij}\;,\;(A_l)_{ij} = A_0\,(Y_l)_{ij}\;,\\
&M_1 = M_2 = M_3 = M_{1/2}\,,
\end{aligned} \tag{1.64}$$

Notice that now the soft Higgs mases m_{H_1} and m_{H_2} are not universal. The departure from universality in the soft Higgs masses of the NUHM scenarios is parametrised here in terms of two non-vanishing parameters, δ_1 and δ_2, defined as:

$$m^2_{H_1} = M_0^2(1+\delta_1),\; m^2_{H_2} = M_0^2(1+\delta_2)\,. \tag{1.65}$$

.

In summary, the NUHM are specified by the following (unknown) input parameters:

- SUSY parameters: M_0, $M_{1/2}$, A_0, sign (μ) and $\tan\beta$.
- NUHM parameters: δ_1 and δ_2.

1.3.4 Experimental status of the MSSM

Prior to the LHC, the lower experimental bounds (95% C.L.) from direct searches at LEP and Tevatron for the MSSM particle masses in GeV, were the following [20]:

$$m_{h^0} > 114.4,\ m_{A^0} > 93.4,\ m_{H^\pm} > 79.3,\ m_{\tilde{b}} > 89,\ m_{\tilde{t}} > 95.7,\ m_{\tilde{q}} > 379,\ m_{\tilde{g}} > 308,$$
$$m_{\tilde{e}} > 107,\ m_{\tilde{\mu}} > 94,\ m_{\tilde{\tau}} > 81.9,\ m_{\tilde{\nu}} > 94, m_{\tilde{\chi}_1^0} > 46,\ m_{\tilde{\chi}_1^\pm} > 94$$

The best direct information on the mass of the Standard Model Higgs boson was a lower limit of 114.4 GeV at the 95% confidence level, set using the combined results of the four LEP experiments [12] and an excluded band of 158 GeV to 173 GeV [13] from the combined Tevatron experiments [13, 14]. During the year 2011, the LHC has improved quite substantially the previous bounds. The ATLAS experiment has excluded at 95% CL a very wide range of Higgs boson mass in the two mass ranges from 155 GeV to 190 GeV and 295 GeV to 450 GeV. No significant evidence of a signal has yet been observed, although an excess corresponding to a 2.8σ fluctuation of the background occurs in the Higgs boson mass range between 130 GeV and 150 GeV [15]. The CMS experiment, has excluded the SM Higgs boson at 95% C.L. in the two mass ranges 149-206 and 300-440 GeV [16]. The Higgs boson mass limits are indeed improving very rapidly at the LHC. At the time this thesis is coming to an end, a very recent ATLAS and CMS combined analysis has been performed, where a Higgs boson like mass in the range from 144 to 476 GeV is excluded at at 95% C.L.. This analysis, combined with the LEP lower bound on the SM Higgs mass, leaves a quite narrow window left for the SM Higgs mass: $114 < m_h < 141$ GeV at 95% C.L. [17].

As an illustrive example, we show in Figs. 1.4 the exluded Higgs boson mass regions published by the ATLAS collaboration [15].

This limits apply only for the SM Higgs boson but as it was already mentioned in the decoupling limit, i.e. $M_A \gg M_Z$, there is only one light Higgs and the couplings of this light MSSM Higgs to the SM particles are approximately the same as the couplings of the SM Higss. Therefore the mentioned exclusion bounds apply also for the light MSSM Higgs, in the decoupling limit. However, in the MSSM the lightest Higgs boson

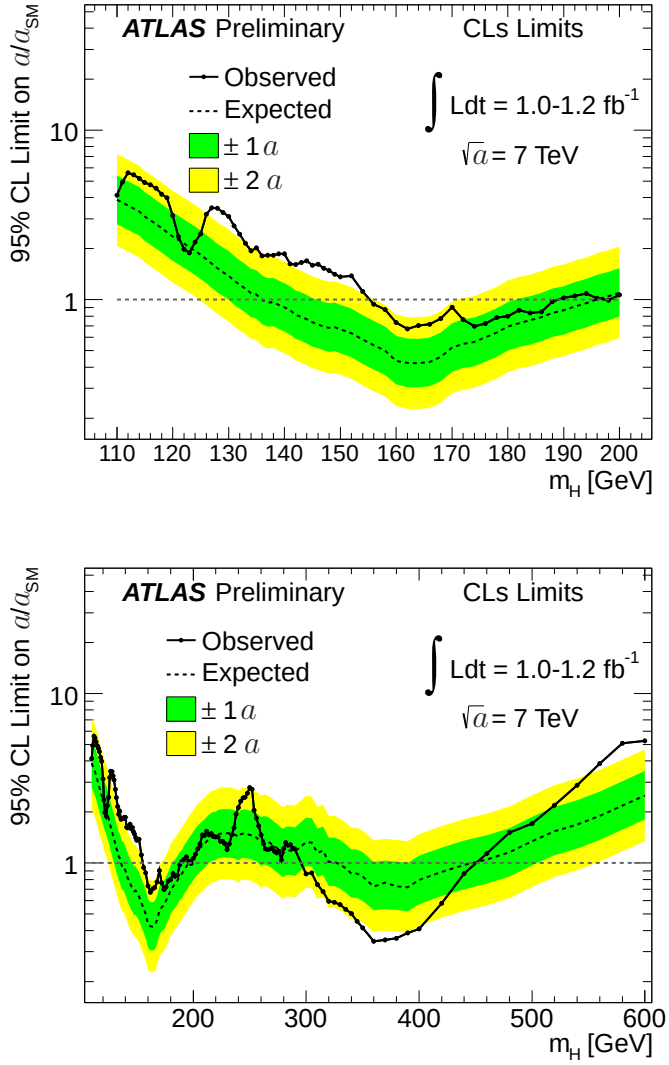

Figure 1.4: The combined upper limit on the Standard Model Higgs boson production cross section divided by the Standard Model expectation as a function of m_h is indicated by the solid line. This is a 95% CL limit using the CLs method in the lower mass range for the upper plot and in the entire mass range in the lower plot. The dotted line shows the median expected limit in the absence of a signal and the green and yellow bands reflect the corresponding 68% and 95% expected regions.

mass is predicted and from higher order corrections a bound of $\sim$ 135 GeV is obtained. Therefore, the information that we have gotten from the CDF, DO, ATLAS and CMS collaborations has not excluded any of the values of the lightest Higgs mass region allowed

by the theoretical upper bound and by the lower bound set by LEP:

$$114.4 \text{ GeV } < \mathrm{m}_{\mathrm{h}_{\mathrm{MSSM}}} \lesssim 135 \text{ GeV} \tag{1.66}$$

There are also bounds to the SUSY masses but mainly in contrained supersymmetric models. CMS has excluded squark and gluino masses below 1.1 TeV for a common value of the scalar mass at the GUT scale of $M_0 < 0.5$ TeV and for certain fixed values of the model parameters [65, 66]. The ATLAS detector has excluded squarks and gluinos of equal mass with masses below 950 GeV [128]. This analysis has been done in the CMSSM with $\tan\beta = 10$, $A_0 = 0$ and $\mathrm{sign}(\mu) > 0$. In Figure 1.5, we can see the combined exclusion limits in the $(M_0; M_{1/2})$ plane of mSUGRA for the choice of parameters $\tan\beta = 10$, $A_0 = 0$ and $\mu > 0$ [128].

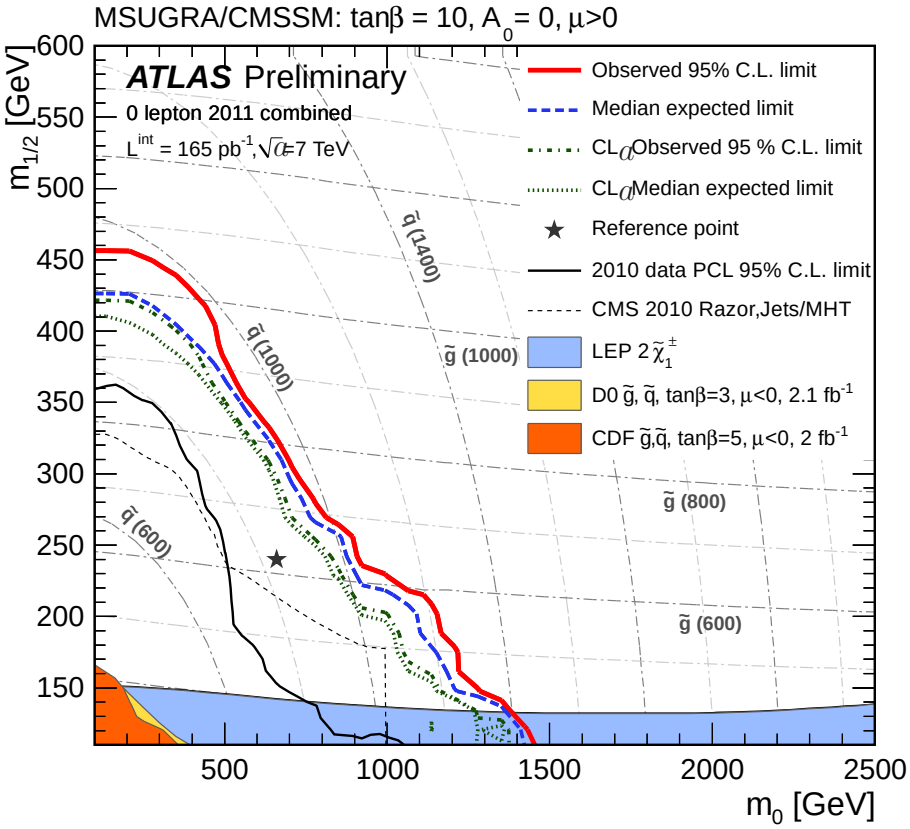

Figure 1.5: Combined exclusion limits in the $(M_0; M_{1/2})$ plane of mSUGRA/CMSSM for which $\tan\beta = 10$, $A_0 = 0$ and $\mu > 0$ taking the signal region with the best expected limit per point. The dashed-blue line corresponds to the expected $95\% C.L.$ limit and the red line is the equivalent observed limit. The dotted green line and the dash-dotted green line correspond respectively to the expected and observed limits calculated with the CLs method. Dot-dashed grey contours of constant gluino and squark mass are displayed at 200 GeV intervals. The observed ATLAS limit from 2010 is shown by the solid black line. The star indicates the position of the mSUGRA reference point with $M_0 = 660$ GeV, $M_{1/2} = 240$ GeV, $A_0 = 0$, $\tan\beta = 10$ and $\mu > 0$. Notice that ATLAS limits from 2010 are for $\tan\beta = 3$. Tevatron limits are taken from [129], [130], CMS limits are from [131], and LEP limits from [132].

Chapter 2

Majorana neutrinos, their SUSY partners and their interactions

In this chapter we will briefly review the need of enlarging the SM or any supersymmetric extension of it, such as the MSSM, to accomodate neutrino masses. The benefits of the the well-known seesaw mechanism [50] for generating neutrino mass will be pointed out. The new ingredients of the MSSM-seesaw with respect to the MSSM will be presented. In particular, the mass spectrum of neutrinos and sneutrinos and their interactions with the neutral Higgs bosons of the MSSM and the Z gauge boson will be derived, being the relevant ones for the calculation in the next chapter of the radiative effects of heavy Majorana neutrinos in the neutral CP even Higgs boson masses. The corresponding Feynman rules will also be presented. The complete set of new mass eigenvalues in the $\nu/\tilde{\nu}$ sector, new interactions with the Higgs and Z bosons and the new Feynman rules are original work of this thesis and have been published in Ref. [110]

2.1 Majorana neutrinos

The evidence of lepton flavour changing neutrino oscillations [24–36] in solar and atmospheric neutrinos, as well as in reactor experiments, implies that neutrinos are massive and that they mix in analogy with the quark sector. However, the absolute neutrino mass scale is so far not measured because only mass squared differences are relevant for neutrino oscillations. The direct limit on neutrino masses comes from the precise measurement of the end-point of the lepton energy spectrum in weak decays, which gets modified if neu-

trinos are massive. In particular the most stringent limit is obtained from tritium β-decay for the electron neutrino. The best limit to neutrino masses has been obtained by the Mainz and Troitsk experiments [133],

$$m_{\nu_e} < 2.2\,\text{eV (Mainz)} \qquad m_{\nu_e} < 2.1\,\text{eV (Troitsk)} \tag{2.1}$$

both at 95% C.L. The direct limits on the other two neutrino masses are much weaker.

The Standard Model in its simplest version does not allow neutrino masses for three independent reasons:

- There are no right handed neutrinos in its particle content.
- There are only Higgs doublets.
- It is a renormalizable theory.

Therefore, neutrino masses are a clear signal of physics beyond the SM and there is a need for a mechanism that explains neutrino masses and their small size.

The simplest way to generate neutrino masses consists in the introduction of right handed neutrinos. In this way, neutrinos can acquire their masses through their Yukawa interaction with the Higgs boson in parallelism with all the other fermions of the SM. However, due to the special properties of these right handed neutrinos, that are singlets under all the gauge groups of the SM, they can have explicit mass terms called Majorana mass terms. Moreover, these Majorana terms violate the global lepton number symmetry. There are two possibilities at this point:

- One can forbid those Majorana terms from the Lagrangian by imposing lepton number as a fundamental symmetry, although in the SM the conservation of lepton number and baryon number are accidental. In this case neutrinos would be Dirac particles and they would get their mass only through their Yukawa interaction with the Higgs. Due to the smallness of the neutrino masses one has to explain why neutrinos are much lighter than all the other particles in the SM, even those of the same family. The mass of the electron, the next to lightest particles of the SM, is 10^6 times bigger than the heaviest neutrino.
- One can allow for Majorana mass terms that are compatible with the gauge and Lorentz symmetries of the SM. Then, neutrinos would be their own antiparticles,

i.e they would be Majorana particles, in contrast with the other fermions of the SM, that are Dirac particles. Notice that only electrically neutral particles can be Majorana particles. If neutrinos are Majorana fermions it is very appealing the introduction of heavy Majorana mass terms for various reasons:

- One can explain naturally the smallness of neutrino masses through the well known seesaw mechanism [50]. In this model, the smallness of the light neutrino masses, $m_\nu \sim m_D^2/m_M$, appears naturally due to the induced large suppression by the ratio of the two very distant mass scales. Namely, the Majorana mass m_M, that represents the new physics scale, and the Dirac mass m_D, which is related to the electroweak scale via the neutrino Yukawa couplings.
- One can generate satisfactorily baryogenesis via leptogenesis [134].
- They can produce an interesting and singular phenomenology due to their potentially large Yukawa couplings to the Higgs sector of the theory.

However, the disadvantage of introducing these heavy neutrinos is that they can induce a huge hierarchy problem. An interesting solution to avoid this new hierarchy problem of the SM is considering the minimal supersymmetric version of the SM-seesaw. From now on we will focus on this SUSY model with the seesaw mechanism implemented and it will be referred to as the MSSM-seesaw. This model has the same particle content as the MSSM plus right handed neutrinos and their corresponding superpartners.

Among the most striking phenomenological implications of these MSSM-seesaw scenarios [135], it is worth mentioning: 1) the prediction of sizeable rates for lepton flavor violating (LFV) processes, indeed within the present experimental reach for specific areas of the model parameters [77–79, 82, 99], 2) non-negligible contributions to electric dipole moments of charged leptons [136–138], and 3) the occurrence of sneutrino-antisneutrino oscillations [139] and sneutrino flavor-oscillations [140].

In this thesis we will be mainly devoted to the implications of radiative corrections on the Higgs boson masses and on LFV processes.

2.2 The MSSM-seesaw: the three generations case

The MSSM-seesaw with three generation of neutrinos and its superpartners is described in terms of the well known MSSM superpotential of Eq. (1.8) and by new terms due to

the new superfields containing the right handed neutrinos. The new relevant terms are contained in [110, 139, 140]:

$$W \,=\, \epsilon_{ij}\left[Y_\nu^{ab}\hat{H}_2^i\,\hat{L}_a^j\hat{N}_b \,-\, Y_l^{ab}\hat{H}_1^i\,\hat{L}_a^j\,\hat{R}_b \,+\, \mu\hat{H}_1^i H_2^j\right] \,+\, \frac{1}{2}\,m_M^{ab}\,\hat{N}_a\,\hat{N}_b\,, \tag{2.2}$$

where Y_ν is a 3×3 complex matrices and m_M is a complex symmetric 3×3 mass matrix. Y_l and μ have already been introduced in Eq. (1.8). The a, b indexes refer to generations and i, j indexes refer to SU(2) doublets components and we use again the convention $\epsilon_{12} = -1$. The additional superfield with respect to the MSSM content, i.e $\hat{N} = \{\tilde{\nu}_R^*, (\nu_R)^c\}$, contains the right-handed neutrino ν_R and its scalar partner $\tilde{\nu}_R$. The other superfields, $\hat{L}$ containing the lepton (ν_L, e_L) and slepton $(\tilde{\nu}_L, \tilde{e}_L)$ $SU(2)$ doublets, $\hat{R}$ containing the lepton $(e_R)^c$ and slepton $\tilde{e}_R^*$ $SU(2)$ singlets, and $\hat{H}_{1,2}$ containing the Higgs boson $SU(2)$ doublets and their SUSY partners, are as in the MSSM. We follow here the notation of [141].

One can always redefine the superfields $\hat{L}, \hat{N}$ and $\hat{R}$ such that Y_l and m_M are real non-negative diagonal matrices and Y_ν is a general complex 3×3 matrix.

There are also new relevant terms in the soft SUSY breaking potential due to the additional sneutrinos $\tilde{\nu}_R$ [110, 139, 140]:

$$V_{\rm soft}^{\tilde{\nu}} = \left(m_{\tilde{L}}^2\right)^{ab}\tilde{\nu}_{aL}^*\tilde{\nu}_{bL} + \left(m_{\tilde{R}}^2\right)^{ab}\tilde{\nu}_{aR}\tilde{\nu}_{bR}^* + (A_\nu^{ab}H_2^2\tilde{\nu}_{La}\tilde{\nu}_{Rb}^* + \left(m_B^2\right)^{ab}\tilde{\nu}_{Ra}^*\tilde{\nu}_{Rb}^* + \text{h.c.})\,, \tag{2.3}$$

where $m_{\tilde{L}}^2$, $m_{\tilde{R}}^2$ are 3×3 hermitian matrices, m_B^2 is a complex symmetric matrix and A_ν is a 3×3 generic complex matrix. In the basis where Y_l and m_M are diagonal, the soft-SUSY masses and couplings, i.e $m_{\tilde{L}}^2$, $m_{\tilde{R}}^2$, m_B^2 and A_ν, do not present, in general, a simple diagonal form. After electro-weak (EW) symmetry breaking, the Higgs fields acquire a vacuum expectation value and the charged lepton and Dirac neutrino mass matrix elements can be written as:

$$m_l^{ab} \,=\, Y_l^{ab}\,v_1\,, \qquad m_D^{ab} \,=\, Y_\nu^{ab}\,v_2\,, \tag{2.4}$$

where v_i are the vacuum expectation values (vevs) of the neutral Higgs scalars, with $v_{1(2)} = v\,\cos(\sin)\beta$ and $v = 174$ GeV.

The scalar potential of our MSSM-seesaw contains the usual F-terms, D-terms and soft SUSY-breaking terms [116]

$$V = V_F + V_D + V_{\rm soft}\,, \tag{2.5}$$

where the F-terms are fixed by the Yukawa interactions and fermion masses and they are derived from the superpotential using:

$$V_F = F_i^* F_i = \sum_i \left(\frac{\partial W}{\partial\phi_i}\right)^* \left(\frac{\partial W}{\partial\phi_i}\right) = \sum_i \left|\frac{\partial W}{\partial\phi_i}\right|^2\,, \tag{2.6}$$

where ϕ are the scalar components of the corresponding superfield. On the other hand, the D-terms are fixed by the gauge interactions according to

$$V_D = \frac{1}{2}\sum_a D^a D^a = \frac{1}{2}\sum_a g_a^2 \left(\phi^* T^a \phi\right)^2 , \tag{2.7}$$

where g_a accounts for the different gauge couplings and T^a for the generator of the corresponding gauge group. The index a here runs over the adjoint representation of the gauge group ($a = 1, ..., 8$ for $SU(3)_C$ color gluons and gluinos; $a = 1, 2, 3$ for $SU(2)_L$ weak isospin; $a = 1$ for $U(1)_Y$ weak hypercharge) The generators satisfy the relation:

$$\left[T^a, T^b\right] = i f^{abc} T^c , \tag{2.8}$$

where f^{abc} are the totally antisymmetric structure constants that define the gauge group. For example, if the gauge group is $SU(2)_L \times U(1)_Y$ then the D-terms would be:

$$V_{D_{SU(2)\times U_1}} = \frac{1}{2} g_2^2 \left(\phi_i^* \sigma_{ij}^a \phi_j\right)^2 + \frac{1}{2} g_1^2 \left(Y_i \phi_i^* \phi_i\right)^2 . \tag{2.9}$$

The Yukawa couplings of the neutrinos and their corresponding mass terms can then be derived from the superpotential in Eq. (2.2):

$$-\mathcal{L}_{\text{mass}} - \mathcal{L}_{\text{Yukawa}} = \frac{1}{2}\sum_{ij}\left[\frac{\partial^2 W(\phi)}{\partial\phi_i \partial\phi_j}\psi_i\psi_j + \text{h.c.}\right] , \tag{2.10}$$

where the ψ_i are the two component fermion field superpartners of the corresponding ϕ_i and $W(\phi)$ is the superpotential of Eq. (2.2), where the superfields have been substituted by their scalar components.

We present the resulting mass and relevant interaction terms in the following.

2.2.1 The neutrino mass Lagrangian

After electroweak symmetry breaking the mass lagrangian of neutrinos in the MSSM-seesaw model with 3 generations of ν_L and ν_R is given by:

$$-L^{\nu}_{mass} = \overline{\nu_{R_i}}\; m^{\dagger}_{D_{ij}} \nu_{L_j} + \overline{\nu_{L_i}}\; m_{D_{ij}} \nu_{R_j} + \frac{1}{2}\overline{(\nu_{R_i})^c}\; m_{M_{ij}} \nu_{R_j} + \frac{1}{2}\overline{\nu_{R_i}}\, m^{\dagger}_{M_{ij}} \left(\nu_{R_j}\right)^c , \tag{2.11}$$

where $i, j = 1, 2, 3$ and m_D and m_M are the 3×3 Dirac and Majorana mass matrices, respectively. Notice that m_D is complex and is given in Eq. (2.4) in terms of the 3×3 neutrino Yukawa coupling matrix and the Higgs vev v_2. m_M is a real, non singular and symmetric matrix and, without loss of generality, can be considered diagonal and positive.

The electroweak eigenstates are the left and right components of the neutrino field, ν_L and ν_R. The c-conjugate fields are defined by:

$$\hat{C}: \ \nu \to \nu^c = C\overline{\nu}^T \,, \tag{2.12}$$

being $\hat{C}$ the particle-antiparticle conjugation operator and C the charge conjugation operator. The particle-antiparticle conjugation operator flips the chirality of a particle and changes all the quantum numbers of it. It converts a left handed neutrino into a right handed antineutrino and a right handed neutrino into a left handed antineutrino:

$$\begin{aligned} \hat{C}: \ \nu_L \to (\nu_L)^c = (\nu^c)_R \,, \\ \hat{C}: \ \nu_R \to (\nu_R)^c = (\nu^c)_L \,. \end{aligned} \tag{2.13}$$

In contrast, the charge conjugation operator changes all the charged-like (electric charge, baryon number...) quantum numbers of a field but preserves the others, such as chirality. Under charge conjugation a left handed neutrino transforms in a left-handed antineutrino. If a neutrino is a Dirac fermion then it has four degrees of freedom, two independent Weyl fields ν_L, ν_R plus their $\hat{C}$ conjugates $(\nu_L)^c$ and $(\nu_R)^c$. On the contrary, if a neutrino is a Majorana fermion it is invariant under $\hat{C}$, so that $\nu = \nu^c$, and it has only two independent degrees of freedom [142].

One can express L^{ν}_{mass} of Eq. (2.11) in a more compact form in terms of new Majorana fields, defined as:

$$\begin{aligned} f &= \nu_L + (\nu_L)^c \,, \\ F &= \nu_R + (\nu_R)^c \,, \end{aligned} \tag{2.14}$$

as follows:

$$-L^{\nu}_{mass} = \frac{1}{2}(\overline{f}_L, \overline{F}_L)_i M^{\nu}_{ij} \begin{pmatrix} f_R \\ F_R \end{pmatrix}_j + \ h.c. = \frac{1}{2}(\overline{\nu}_L, \overline{(\nu_R)^c}_i M^{\nu}_{ij} \begin{pmatrix} (\nu_L)^c \\ \nu_R \end{pmatrix}_j + \ h.c \,, \tag{2.15}$$

where

$$M^{\nu} = \begin{pmatrix} 0 & m_D \\ m_D^T & m_M \end{pmatrix} \tag{2.16}$$

is a 6×6 complex symmetric matrix. In order to diagonalize this symmetric matrix by an unitary transformation we will make use of the singular value decomposition of an arbitrary matrix $A \in \mathbb{C}^{n \times n}$:

$$V^{\dagger} A U = \mathrm{diag}(\lambda_1, ...\lambda_n) \,, \tag{2.17}$$

with V and U being two unitary matrices belonging to $\mathbb{C}^{n\times n}$ and $\lambda_i \geq 0$. If the complex A matrix is symmetric then $U = V^*$ and therefore :

$$U^T A\, U = \mathrm{diag}(\lambda_1, ...\lambda_n) \text{ with } \lambda_i \geq 0\,. \tag{2.18}$$

Notice that this is not the eigenvalue decomposition of matrix A, because $U^T \neq U^{-1}$ Therefore, one can diagonalize the neutrino mass matrix through the unitary matrix U:

$$U^T M^\nu U = \hat{M}^\nu = \mathrm{diag}(m_{n_1}, m_{n_2}, m_{n_3}, m_{n_4}, m_{n_5}, m_{n_6})\,, \tag{2.19}$$

where the diagonal elements of $\hat{M}^\nu$ are the non negative square roots of the eigenvalues of $M^\nu M^{\nu^\dagger}$.

The interaction eigenstates are related to the mass eigenstates in the following way:

$$\left(\begin{array}{c}(\nu_L)^c\\ \nu_R\end{array}\right)_i = \left(\begin{array}{c}U_{i,j}\\ U_{i+3,j}\end{array}\right) P_R\ n_j \quad , \quad \left(\begin{array}{c}\nu_L\\ (\nu_R)^c\end{array}\right)_i = \left(\begin{array}{c}U^*_{i,j}\\ U^*_{i+3,j}\end{array}\right) P_L\ n_j \ , \tag{2.20}$$

where $i, j = 1, 2, 3$.

In general, the diagonalization of the M^ν matrix, cannot be performed analytically, but if M^ν is of a seesaw type, i.e. if $||m_D|| << ||m_M||$ [1], then an analytic perturbative diagonalization in blocks can be performed in the dimensionless parameter $\xi = m_D m_M^{-1}$, that allows us to separate the light sector from the heavy sector by the introduction of a 6×6 (approximate) unitary matrix:

$$\hat{U}^\nu \ = \ \left(\begin{array}{cc}(1-\frac{1}{2}\xi^*\xi^T) & \xi^*(1-\frac{1}{2}\xi^T\xi^*)\\ -\xi^T(1-\frac{1}{2}\xi^*\xi^T) & (1-\frac{1}{2}\xi^T\xi^*)\end{array}\right) + \mathcal{O}(\xi^4)\,. \tag{2.21}$$

By inserting this $\hat{U}^\nu$ matrix in Eq. (2.19) one obtains two independent blocks of 3×3 neutrino mass matrices:

$$m_\nu \ = \ -m_D\xi^T + \mathcal{O}(m_D\xi^3) \simeq -m_D m_M^{-1} m_D^T\,, \tag{2.22}$$

$$m_N \ = \ m_M + \mathcal{O}(m_D\xi) \simeq m_M\,. \tag{2.23}$$

We can see that one of the matrices, m_N, is already diagonal and its elements are heavy, given by the Majorana masses, $m_{M_1}, m_{M_2}, m_{M_3}$. The other matrix, m_ν, is not yet diagonal,

[1] The euclidean matrix norm is defined by $||A|| = \left[tr\left(A^\dagger A\right)\right]^{1/2} = \left[\sum_{i,j}|a_{ij}|^2\right]^{1/2}$ for a matrix A whose elements are given by a_{ij}

but its elements are small since they are suppressed by the heavy Majorana masses. As we already pointed out, this is the characteristic of the seesaw mechanism, it gives rise to 3 light neutrinos and 3 heavy neutrinos as a consequence of the two distant scales m_M and m_D. Finally, the diagonalization of the m_ν matrix will be performed by the well-known Pontecorvo-Maki-Nakagawa-Sakata (PMNS) unitary matrix [37, 38], $U_{\rm PMNS}$ given by:

$$U_{\rm PMNS} = \begin{pmatrix} c_{12}\, c_{13} & s_{12}\, c_{13} & s_{13}\, e^{-i\delta} \\ -s_{12}\, c_{23} \,-\, c_{12}\, s_{23}\, s_{13}\, e^{i\delta} & c_{12}\, c_{23} \,-\, s_{12}\, s_{23}\, s_{13}\, e^{i\delta} & s_{23}\, c_{13} \\ s_{12}\, s_{23} \,-\, c_{12}\, c_{23}\, s_{13}\, e^{i\delta} & -c_{12}\, s_{23} \,-\, s_{12}\, c_{23}\, s_{13}\, e^{i\delta} & c_{23}\, c_{13} \end{pmatrix} \times V\,, \quad (2.24)$$

with

$$V \,=\, {\rm diag}\,(e^{-i\frac{\phi_1}{2}}, e^{-i\frac{\phi_2}{2}}, 1)\,, \quad (2.25)$$

and $c_{ij} \equiv \cos\theta_{ij}$, $s_{ij} \equiv \sin\theta_{ij}$. θ_{ij} are the light neutrino flavor mixing angles, δ is the Dirac phase and $\phi_{1,2}$ are the Majorana phases. In summary, the mass eigenvalues m_{n_j}, corresponding to light (ν) and heavy (N) Majorana neutrinos are given respectively by:

$$m_\nu^{\rm diag} \;=\; U_{\rm PMNS}^T m_\nu U_{\rm PMNS} = {\rm diag}\,(m_{\nu_1}, m_{\nu_2}, m_{\nu_3})\,, \quad (2.26)$$

$$m_N^{\rm diag} \;=\; m_N = {\rm diag}\,(m_{N_1}, m_{N_2}, m_{N_3})\,. \quad (2.27)$$

Parametrization of the seesaw and the contact with neutrino data

In order to make contact with the experimental data, we use the method proposed in [143]. It provides a simple way to reconstruct the Dirac mass matrix by using as inputs the physical light m_{ν_i} and heavy m_{N_i} neutrino masses, the $U_{\rm PMNS}$ matrix, and a general complex and orthogonal matrix R. To get this parametrization, valid in the seesaw limit, one simply solves Eq. (2.22) and Eq. (2.23) and express m_D in terms of m_{ν_i} and m_{N_i} using Eq. (2.26) and Eq. (2.27). Finally one gets:

$$m_D = i\sqrt{m_N^{\rm diag}}\, R\, \sqrt{m_\nu^{\rm diag}}\, U_{\rm PMNS}^\dagger\,, \quad (2.28)$$

where $R^T R = R R^T = \mathbb{1}$.

Thus, instead of proposing directly possible textures for m_D (i.e. for Y^ν), one proposes possible values for $m_{N_1}, m_{N_2}, m_{N_3}$ and R, and sets $m_{\nu_1}, m_{\nu_2}, m_{\nu_3}$ and $U_{\rm PMNS}$ to their suggested values from the experimental data. Notice that for $R = \mathbb{1}$, the lepton flavor mixing in $U_{\rm PMNS}$ is the unique source of lepton flavor mixing in m_D. Correspondingly, any hypothesis for R different from the unit matrix will lead to an additional lepton

flavor mixing in m_D. Notice also that the previous Eq. (2.28) is established at the right-handed neutrino mass scale m_M, so that the quantities appearing in it are indeed the renormalized ones, namely, $m_\nu^{\rm diag}\,(m_M)$ and $U_{\rm PMNS}\,(m_M)$. These latter are obtained here by means of the renormalization group equations (RGEs) and by starting the running from their corresponding renormalized values at M_Z, $m_\nu^{\rm diag}\,(M_Z)$ and $U_{\rm PMNS}\,(M_Z)$ which are identified respectively with the physical $m_\nu^{\rm diag}$ and $U_{\rm PMNS}$ from neutrino data. In this thesis we will consider the following plausible scenarios, for the neutrino sector, being all compatible with present data.

- Light neutrino sector:

  Hierarchical case (normal hierarchy) $\qquad m_{\nu_1} \ll m_{\nu_2}\,,\ m_{\nu_2} = \sqrt{\Delta m^2_{\rm sol}}\,,\ m_{\nu_3} = \sqrt{\Delta m^2_{\rm atm}}$

  . (2.29)

- Heavy neutrino sector:

$$\begin{aligned} &\text{Degenerate case:} && m_{N_1} = m_{N_2} = m_{N_3} = m_N\,, \\ &\text{Hierarchical case:} && m_{N_1} \ll m_{N_2} \ll m_{N_3}\,. \end{aligned} \tag{2.30}$$

This hierarchical case in the heavy neutrino sector is well known to provide a plausible scenario for the Baryon Asymmetry of the Universe (BAU) via leptogenesis.

For the numerical estimates in this thesis we will use the following input values for the light neutrino mass squared differences and the angles in the $U_{\rm PMNS}$ matrix:

$$\begin{aligned} &\Delta\, m^2_{\rm sol} \,=\, 8\,\times 10^{-5}\ {\rm eV}^2\,, \qquad \Delta\, m^2_{\rm atm} \,=\, 2.5\,\times 10^{-3}\ {\rm eV}^2\,, \\ &\theta_{12} \,=\, 30^\circ\,, \quad \theta_{23} \,=\, 45^\circ\,, \quad \theta_{13} \lesssim 10^\circ\,, \qquad \delta \,=\, \phi_1 \,=\, \phi_2 \,=\, 0\,, \end{aligned} \tag{2.31}$$

which are compatible with present experimental data [20]:

$$\begin{aligned} &\Delta\, m^2_{\rm sol} \,=\, (7.59 \pm 0.21)\times 10^{-5}\ {\rm eV}^2\,, \qquad |\Delta\, m^2_{\rm atm}| \,=\, (2.43 \pm 0.13)\times 10^{-3}\ {\rm eV}^2\,, \\ &\sin^2(2\theta_{12}) \,=\, 0.861^{+0.026}_{-0.022}\,, \quad \sin^2(2\theta_{23}) \,>\, 0.92\,, \quad \sin^2(2\theta_{13}) \,<\, 0.15\,. \end{aligned} \tag{2.32}$$

Regarding the R matrix, we will consider the following parameterization:

$$R = \begin{pmatrix} c_2 c_3 & -c_1 s_3 - s_1 s_2 c_3 & s_1 s_3 - c_1 s_2 c_3 \\ c_2 s_3 & c_1 c_3 - s_1 s_2 s_3 & -s_1 c_3 - c_1 s_2 s_3 \\ s_2 & s_1 c_2 & c_1 c_2 \end{pmatrix}\,, \tag{2.33}$$

where $c_i \equiv \cos\theta_i$, $s_i \equiv \sin\theta_i$ and θ_1, θ_2 and θ_3 are arbitrary complex angles. This parametrisation was proposed in [143] for the study of $\mu \to e\gamma$ decays and represents the most general parameterisation of an orthogonal complex matrix in terms of three complex angles.

2.2.2 The sneutrino mass Lagrangian

We present here our results for the mass terms of the sneutrinos first in the electroweak basis, $\{\tilde{\nu}_L, \tilde{\nu}_R\}$ and then in the physical basis $\{\tilde{n}_i\}$. For simplicity, we use matricial notation and omit the generation indexes. For instance, $(\tilde{\nu}_L)^T = (\tilde{\nu}_{L_1}, \tilde{\nu}_{L_2}, \tilde{\nu}_{L_3})$ etc.. For the mass terms coming from the F-terms we get the following:

$$\begin{aligned} -L_{mass\,\tilde{\nu}}^{F-terms} &= -\cot\beta\left[\mu^*\,\tilde{\nu}_L^T m_D \tilde{\nu}_R^* + \mu\,\tilde{\nu}_L^{*T} m_D^* \tilde{\nu}_R\right] + \tilde{\nu}_R^T m_D^\dagger m_D \tilde{\nu}_R^* \\ &\quad + \tilde{\nu}_L^T m_D m_D^\dagger \tilde{\nu}_L^* + \tilde{\nu}_R^T m_M^\dagger m_M \tilde{\nu}_R^* + \tilde{\nu}_L^{*T} m_D^* m_M \tilde{\nu}_R^* + \tilde{\nu}_L^T m_D m_M^* \tilde{\nu}_R\,. \end{aligned} \tag{2.34}$$

The D-terms give rise to the following sneutrinos mass terms:

$$-L_{mass\,\tilde{\nu}}^{D-terms} = \frac{1}{2} M_Z^2 \cos 2\beta\, \tilde{\nu}_L^{*T} \tilde{\nu}_L\,. \tag{2.35}$$

As we can see, the D-mass terms are 'pure gauge' terms and they do not depend at all on the neutrino mass matrices m_D or m_M. These terms are also present in the ordinary MSSM without neutrino masses.

Finally, the following mass terms come from the soft SUSY breaking terms in Eq. (2.3):

$$\begin{aligned} -L_{mass\,\tilde{\nu}}^{soft-terms} &= \tilde{\nu}_L^{*T} m_{\tilde{L}}^2 \tilde{\nu}_L + \tilde{\nu}_R^T m_{\tilde{R}}^2 \tilde{\nu}_R^* + \tilde{\nu}_R^{*T} m_B^2 \tilde{\nu}_R^* \\ &\quad + \tilde{\nu}_R^T m_B^{2*} \tilde{\nu}_R + \frac{\sqrt{2} M_W \sin\beta}{g}\left[\tilde{\nu}_L^T A_\nu \tilde{\nu}_R^* + \tilde{\nu}_L^{*T} A_\nu^* \tilde{\nu}_R\right], \end{aligned} \tag{2.36}$$

where, as already said, $m_{\tilde{L}}^2$ and $m_{\tilde{R}}^2$ are 3×3 hermitian matrices, m_B^2 is a 3×3 complex symmetric matrix (bilinear term) and A_ν is a 3×3 complex matrix. In principle, these four matrices are free parameters and they are not diagonal in general. Following [140], we will express the sneutrino mass terms in a more compact 6×6 matrix form. In order to do that we define the ϕ_L and ϕ_N six-dimensional vectors as $\phi_L = (\tilde{\nu}_L, \tilde{\nu}_L^*)^T$ and $\phi_N = (\tilde{N}, \tilde{N}^*)^T = (\tilde{\nu}_R^*, \tilde{\nu}_R)^T$. In this basis, the mass Lagrangian of the sneutrinos has the following expression:

$$-L_{mass} = \frac{1}{2}\begin{pmatrix} \phi_L^\dagger & \phi_N^\dagger \end{pmatrix}\begin{pmatrix} M_{LL}^2 & M_{LN}^2 \\ (M_{LN}^2)^\dagger & M_{NN}^2 \end{pmatrix}\begin{pmatrix} \phi_L \\ \phi_N \end{pmatrix}$$

$$= \frac{1}{2}\begin{pmatrix} \tilde{\nu}_L^{*T} & \tilde{\nu}_L^T & \tilde{\nu}_R^T & \tilde{\nu}_R^{*T} \end{pmatrix} M^2_{\tilde{\nu}_L\tilde{\nu}_R} \begin{pmatrix} \tilde{\nu}_L \\ \tilde{\nu}_L^* \\ \tilde{\nu}_R^* \\ \tilde{\nu}_R \end{pmatrix}, \tag{2.37}$$

where M^2_{LL} and M^2_{NN} are 6×6 hermitian matrices and M^2_{LN} is a 6×6 complex matrix. These, in turn, can be expressed in blocks of 3×3 matrices with the form:

$$M^2_{AB} = \begin{pmatrix} M^2_{A^\dagger B} & M^{2*}_{A^T B} \\ M^2_{A^T B} & M^{2*}_{A^\dagger B} \end{pmatrix}, \tag{2.38}$$

where the subscripts A, B stand for L or N. The $M^2_{A^\dagger A}$ are 3×3 hermitian matrices, whereas $M^2_{A^T A}$ are 3×3 complex symmetric matrices, for $A = L, N$. The matrices $M^2_{A^\dagger B}$ and $M^2_{A^T B}$ for $A \neq B$ are general complex matrices with no restrictions.

Finally, the expression of the different blocks of matrices that compose the complete 12×12 sneutrino mass matrix $M^2_{\tilde{\nu}_L,\tilde{\nu}_R}$is the following:

$$M^2_{LL} = \begin{pmatrix} M^2_{L^\dagger L} & M^{2*}_{L^T L} \\ M^2_{L^T L} & M^{2*}_{L^\dagger L} \end{pmatrix} = \begin{pmatrix} m^2_{\tilde{L}} + m_D^* m_D^T + \frac{1}{2}M_Z^2 \cos 2\beta & 0 \\ 0 & m^{2*}_{\tilde{L}} + m_D m_D^\dagger + \frac{1}{2}M_Z^2 \cos 2\beta \end{pmatrix}, \tag{2.39}$$

$$M^2_{NN} = \begin{pmatrix} M^2_{N^\dagger N} & M^{2*}_{N^T N} \\ M^2_{N^T N} & M^{2*}_{N^\dagger N} \end{pmatrix} = \begin{pmatrix} m^2_{\tilde{R}} + m_D^\dagger m_D + m_M^\dagger m_M & 2B_\nu^* m_M^* \\ 2B_\nu m_M & m^{2*}_{\tilde{R}} + m_D^T m_D^* + m_M^T m_M^* \end{pmatrix}, \tag{2.40}$$

$$M^2_{LN} = \begin{pmatrix} M^2_{L^\dagger N} & M^{2*}_{L^T N} \\ M^2_{L^T N} & M^{2*}_{L^\dagger N} \end{pmatrix} = \begin{pmatrix} m_D^* m_M & m_D^* \left(A_0^* - \mu^* \cot\beta\right) \\ m_D \left(A_0 - \mu \cot\beta\right) & m_D m_M^* \end{pmatrix}, \tag{2.41}$$

where we have used:

$$m_B^2 = B_\nu \, m_M \,, \tag{2.42}$$

$$A_\nu = A_0 Y_\nu \,, \tag{2.43}$$

$$\text{with} \quad Y_\nu = \frac{g m_D}{\sqrt{2} M_W s_\beta} \,. \tag{2.44}$$

In order to obtain the mass eigenstates we have to diagonalize the mass matrix in Eq. (2.37). As this matrix is hermitian, it can be diagonalized by an 12×12 unitary matrix $\tilde{U}$:

$$\tilde{U}^{\dagger} M^2_{\tilde{\nu}_L \tilde{\nu}_R} \tilde{U} = M^2_{\tilde{n}_i} = \mathrm{diag}(\tilde{n}^2_1, ..., \tilde{n}^2_{12}) \tag{2.45}$$

Finally, the relation between the interaction eigenstates and the mass eigenstates is the following:

$$\begin{pmatrix} \tilde{\nu}_L \\ \tilde{\nu}^*_L \\ \tilde{\nu}^*_R \\ \tilde{\nu}_R \end{pmatrix}_i = \begin{pmatrix} \tilde{U}_{i,j} \\ \tilde{U}_{i+3,j} \\ \tilde{U}_{i+6,j} \\ \tilde{U}_{i+9,j} \end{pmatrix} \tilde{n}_j \tag{2.46}$$

where i runs from 1 to 3 and j from 1 to 12. Notice that in Eq. (2.46) we have not made an 'a priori' distinction between light and heavy sneutrinos.

2.2.3 The neutrinos interaction Lagrangian

The interaction Lagrangian of the MSSM neutral Higgs bosons with the three ν_L and three ν_R neutrinos, introduced in Sect.2.2.1, reads:

$$\begin{aligned} -L^{\nu_L \nu_R h_i} &= \frac{g}{2M_W \sin\beta} \left(\overline{\nu_R} m^{\dagger}_D \nu_L + \overline{\nu_L} m_D \nu_R \right) (H \sin\alpha + h \cos\alpha) \\ &+ \frac{ig}{2M_W \sin\beta} \left(\overline{\nu_R} m^{\dagger}_D \nu_L - \overline{\nu_L} m_D \nu_R \right) A \cos\beta \,. \end{aligned} \tag{2.47}$$

Notice that m_M does not enter here because, contrary to m_D, the origin of m_M does not rely on electroweak symmetry breaking.

In order to express the Lagrangian in terms of the mass eigenstates n_i we use the following relations:

$$\begin{aligned} \overline{\nu_L} m_D \nu_R &= \overline{\nu_L}_i \left(m_D\right)_{im} \nu_{R_m} = \overline{U^*_{ij} P_L n_j} \left(m_D\right)_{im} U_{m+3,l} P_R n_l = \overline{n}_j U_{ij} \left(m_D\right)_{im} U_{m+3,l} P_R n_l \,, \\ \overline{\nu_R} m^{\dagger}_D \nu_L &= \overline{\nu_R}_i \left(m^{\dagger}_D\right)_{im} \nu_{L_m} = \overline{U_{i+3,j} P_R n_j} \left(m^{\dagger}_D\right)_{im} U^*_{ml} P_L n_l = \overline{n}_j U^*_{i+3,j} \left(m^{\dagger}_D\right)_{im} U^*_{ml} P_L n_l \,. \end{aligned}$$

Consequently, the interaction Lagrangian of the neutrinos with the MSSM neutral Higgs boson in the physical neutrino basis $n_i = (n_1, ..., n_6)$, where the neutrino mass matrix is diagonal reads:

$$\begin{aligned} -L^{n_j n_l h} &= \frac{g}{2M_W \sin\beta} \left[\overline{n}_j U^*_{i+3,j} \left(m^{\dagger}_D\right)_{im} U^*_{ml} P_L n_l + \overline{n}_j U_{ij} \left(m_D\right)_{im} U_{m+3,l} P_R n_l \right] (H \sin\alpha + h \cos\alpha) \\ &+ \frac{ig}{2M_W \sin\beta} \left[\overline{n}_j U^*_{i+3,j} \left(m^{\dagger}_D\right)_{im} U^*_{ml} P_L n_l - \overline{n}_j U_{ij} \left(m_D\right)_{im} U_{m+3,l} P_R n_l \right] A \cos\beta \,, \end{aligned} \tag{2.48}$$

where j and l indexes run from 1 to 6 and i and m indexes run from 1 to 3.

We are also interested in the gauge interactions of ν_L and ν_R with the neutral gauge boson Z. Since ν_R are not charged under $SU(2)_L \times U(1)_Y$ they do not interact with the Z gauge boson and only interactions with the ν_L appear:

$$L_{\nu_{L_i}\nu_{L_i}Z} = \frac{g}{2c_W}\left(\overline{\nu_{Li}}\,\gamma^\mu \nu_{L_i}\right) Z_\mu \,. \tag{2.49}$$

When expressed in terms of the physical neutrino basis it gives:

$$L_{n_j n_m Z} = \frac{g}{2c_W}\left(\overline{n}_j U_{ij} U^*_{im} \gamma^\mu P_L n_m\right) Z_\mu \tag{2.50}$$

where the indexes m and j run from 1 to 6 and i runs from 1 to 3.

2.2.4 The sneutrinos interaction Lagrangian

Finally, we will present here the interactions of the sneutrinos with the MSSM neutral Higgs bosons in the same way as we presented the sneutrino mass terms, i.e. separating the contributions from the F-terms, the D-terms and the soft SUSY breaking terms:

$$\begin{aligned}
-L^{F-terms}_{int-\tilde{\nu}-h} &= -\frac{g}{2M_W s_\beta}\left(H\cos\alpha - h\sin\alpha\right)\left[\mu^*\,\tilde{\nu}_L^T m_D \tilde{\nu}_R^* + \mu\,\tilde{\nu}_L^{*T} m_D^* \tilde{\nu}_R\right] \\
&+ i\frac{g}{2M_W} A\left[\mu^*\,\tilde{\nu}_L^T m_D \tilde{\nu}_R^* - \mu\,\tilde{\nu}_L^{*T} m_D^* \tilde{\nu}_R\right] \\
&+ \frac{g}{M_W s_\beta}\left(H\sin\alpha + h\cos\alpha\right)\left[\tilde{\nu}_R^T m_D^\dagger m_D \tilde{\nu}_R^* + \tilde{\nu}_L^T m_D m_D^\dagger \tilde{\nu}_L^*\right] \\
&+ \frac{g^2}{4M_W^2 s_\beta^2}\left(H^2\sin\alpha^2 + h^2\cos\alpha^2 + 2Hh\sin\alpha\cos\alpha + A^2 c_\beta^2\right)\times \\
&\left[\tilde{\nu}_R^T m_D^\dagger m_D \tilde{\nu}_R^* + \tilde{\nu}_L^T m_D m_D^\dagger \tilde{\nu}_L^*\right] \\
&+ \frac{g}{2M_W s_\beta}\left(H\sin\alpha + h\cos\alpha\right)\left[\tilde{\nu}_L^{*T} m_D^* m_M \tilde{\nu}_R^* + \tilde{\nu}_L^T m_D m_M^* \tilde{\nu}_R\right] \\
&- i\frac{g\cos\beta}{2M_W s_\beta} A\left[\tilde{\nu}_L^{*T} m_D^* m_M \tilde{\nu}_R^* - \tilde{\nu}_L^T m_D m_M^* \tilde{\nu}_R\right] \,,
\end{aligned} \tag{2.51}$$

$$\begin{aligned}
-L^{D-terms}_{int-\tilde{\nu}-h} &= \frac{gM_Z}{2c_{\rm w}}\left(H\cos(\alpha+\beta) - h\sin(\alpha+\beta)\right)\tilde{\nu}_L^{*T}\tilde{\nu}_L \\
&+ \frac{g^2}{8c_{\rm w}^2}\left(H^2\cos 2\alpha - h^2\cos 2\alpha - 2Hh\sin 2\alpha - A^2\cos 2\beta\right)\tilde{\nu}_L^{*T}\tilde{\nu}_L \,,
\end{aligned} \tag{2.52}$$

$$-L_{int-\tilde{\nu}-h}^{soft-terms} = \frac{1}{\sqrt{2}}\left(H\sin\alpha + h\cos\alpha\right)\left[\tilde{\nu}_L^T A_\nu \tilde{\nu}_R^* + \tilde{\nu}_L^{*T} A_\nu^* \tilde{\nu}_R\right] + i\frac{\cos\beta}{\sqrt{2}} A\left[\tilde{\nu}_L^T A_\nu \tilde{\nu}_R^* - \tilde{\nu}_L^{*T} A_\nu^* \tilde{\nu}_R\right]. \quad (2.53)$$

The final Lagrangian expressed in terms of the physical sneutrino basis $\tilde{n}_j$, $(j = 1, .., 12)$ is obtained by using Eq. (2.46) in the previous Eqs. (2.51), (2.52) and (2.53). We omit to write the final formula here for brevity.

All the corresponding Feynman rules, for the previously reported couplings between the physical neutrinos $n_i, (i = 1, ..., 6)$, and sneutrinos $\tilde{n}_j, (j = 1, ..., 12)$ with the neutral Higgs bosons, h, H, A and the Z gauge boson are collected in the Appendix A and have been implemented into a new *FeynArts* [144] model file which is available upon request.

2.3 The MSSM-seesaw: the one generation case

In this subsection we will particularize our previous study of masses, Yukawa and gauge interactions of neutrinos and sneutrinos, to the one generation case. A systematic and detailed study of the one generation case is very convenient to fully understand the role played by the new Majorana scale introduced into the model. We will obtain here simple and compact analytical formulas for the mass eigenvalues of the neutrinos/sneutrinos, which will be used in our posterior calculation of the radiative corrections to the Higgs boson masses of the MSSM.

The superpotential and soft Lagrangian in the one generation case are the same ones as in the three generation case, given in Eq. (2.2) and Eq. (2.3), but obviously without generation indexes.

In the one generation case the mass matrix of neutrinos is a 2×2 given in terms of m_D and m_M by:

$$M^\nu = \begin{pmatrix} 0 & m_D \\ m_D & m_M \end{pmatrix}. \quad (2.54)$$

Diagonalization of M^ν leads to two mass eigenstates, $n_i\,(i = 1, 2)$, which are Majorana fermions:

$$n_1 \equiv \nu = \cos\theta(\nu_L + (\nu_L)^c) - \sin\theta(\nu_R + (\nu_R)^c)\,,$$
$$n_2 \equiv N = \sin\theta(\nu_L + (\nu_L)^c) + \cos\theta(\nu_R + (\nu_R)^c) \quad (2.55)$$

with the respective mass eigenvalues given by:

$$m_{\nu,\,N} = \frac{1}{2}\left(m_M \mp \sqrt{m_M^2 + 4m_D^2}\right) \ . \tag{2.56}$$

It should be noticed that we have introduced an alternative notation that makes it easier to identify the specific neutrino by its mass: ν is the lighter one and N is the heavier one. It should also be kept in mind that with this convention $m_\nu < 0$ and $m_N > 0$, but the physical Majorana neutrino states have the proper positive masses. These physical neutrinos can be reached by an additional rotation, $\nu \to \nu' = e^{i\gamma_5\pi/2}\nu = -i\gamma_5\nu$, leading to $m_{\nu'} = |m_\nu|$. However, we prefer to work instead with the mass eigenstates in Eq. (2.55) to avoid extra i and γ_5 factors in the computation. Of course the final results for the predictions of any observable in which they are involved are not sensitive to this choice.

The mixing angle that defines the mass eigenstates is given by,

$$\tan\theta = -\frac{m_\nu}{m_D} = \frac{m_D}{m_N} \ . \tag{2.57}$$

Other useful relations between the model parameters m_D, m_M and the physical neutrino parameters, m_ν, m_N and θ are the following:

$$\sin^2\theta = \frac{-m_\nu}{m_N - m_\nu} = \frac{1}{2}\left(1 - \frac{m_M}{\sqrt{m_M^2 + 4m_D^2}}\right) \ , \tag{2.58}$$

$$\cos^2\theta = \frac{m_N}{m_N - m_\nu} = \frac{1}{2}\left(1 + \frac{m_M}{\sqrt{m_M^2 + 4m_D^2}}\right) \ , \tag{2.59}$$

$$m_D = \frac{1}{2}\sqrt{(m_N - m_\nu)^2 - (m_N + m_\nu)^2} \ , \tag{2.60}$$

$$m_D^2 = -m_\nu m_N \ , \tag{2.61}$$

$$m_M = m_\nu + m_N \tag{2.62}$$

It is worth mentioning that in the present MSSM-seesaw model with Majorana neutrinos m_D^2 is obtained singularly from the product of two quantities, one very small m_ν and one very large m_N. This is in contrast with the case of Dirac neutrinos where m_D is directly the tiny neutrino mass.

Regarding the sneutrino sector, the sneutrino mass matrices for the $\mathcal{CP}$-even, $\tilde{M}_+$, and the $\mathcal{CP}$-odd, $\tilde{M}_-$, subsectors are given respectively by [139]:

$$\tilde{M}_\pm^2 = \begin{pmatrix} m_{\tilde{L}}^2 + m_D^2 + \frac{1}{2}M_Z^2\cos 2\beta & m_D(A_\nu - \mu\cot\beta \pm m_M) \\ m_D(A_\nu - \mu\cot\beta \pm m_M) & m_{\tilde{R}}^2 + m_D^2 + m_M^2 \pm 2B_\nu m_M \end{pmatrix} \ . \tag{2.63}$$

The diagonalization of these two matrices, $\tilde{M}^2_{\pm}$, leads to four sneutrino mass eigenstates, $\tilde{n}_i\,(i=1,2,3,4)$ with respective $\mathcal{CP}$ parities $\mathcal{CP}(\tilde{n}_{1,2})=+1$ and $\mathcal{CP}(\tilde{n}_{3,4})=-1$:

$$\begin{aligned}
\tilde{n}_1 &\equiv \tilde{\nu}_+ = \sqrt{2}(\cos\theta_+ \,\mathrm{Re}\,\tilde{\nu}_L - \sin\theta_+ \,\mathrm{Re}\,\tilde{\nu}_R)\ ,\\
\tilde{n}_2 &\equiv \tilde{N}_+ = \sqrt{2}(\sin\theta_+ \,\mathrm{Re}\,\tilde{\nu}_L + \cos\theta_+ \,\mathrm{Re}\,\tilde{\nu}_R)\ ,\\
\tilde{n}_3 &\equiv \tilde{\nu}_- = \sqrt{2}(\cos\theta_- \,\mathrm{Im}\,\tilde{\nu}_L - \sin\theta_- \,\mathrm{Im}\,\tilde{\nu}_R)\ ,\\
\tilde{n}_4 &\equiv \tilde{N}_- = \sqrt{2}(\sin\theta_- \,\mathrm{Im}\,\tilde{\nu}_L + \cos\theta_- \,\mathrm{Im}\,\tilde{\nu}_R)\ .
\end{aligned} \tag{2.64}$$

It should again be noted that we have introduced an alternative notation that makes it easier to identify the specific sneutrino by its parity and mass: $\tilde{\nu}_+$, $\tilde{N}_+$ are respectively the lighter and the heavier ones with $\mathcal{CP}=+1$, and $\tilde{\nu}_-$, $\tilde{N}_-$ are the lighter and the heavier ones with $\mathcal{CP}=-1$. The corresponding mass eigenvalues are:

$$\begin{aligned}
m^2_{\tilde{\nu}_+,\tilde{N}_+} &= \frac{1}{2}(m_M^2 + m_{\tilde{L}}^2 + m_{\tilde{R}}^2 + 2m_D^2 + \frac{1}{2}M_Z^2\cos 2\beta + 2B_\nu m_M) \qquad (2.65)\\
&\mp \frac{1}{2}\sqrt{4m_D^2(A_\nu - \mu\cot\beta + m_M)^2 + (m_M^2 + m_{\tilde{R}}^2 - m_{\tilde{L}}^2 - \frac{1}{2}M_Z^2\cos 2\beta + 2B_\nu m_M)^2}\ ,\\
m^2_{\tilde{\nu}_-,\tilde{N}_-} &= \frac{1}{2}(m_M^2 + m_{\tilde{L}}^2 + m_{\tilde{R}}^2 + 2m_D^2 + \frac{1}{2}M_Z^2\cos 2\beta - 2B_\nu m_M) \qquad (2.66)\\
&\mp \frac{1}{2}\sqrt{4m_D^2(A_\nu - \mu\cot\beta - m_M)^2 + (m_M^2 + m_{\tilde{R}}^2 - m_{\tilde{L}}^2 - \frac{1}{2}M_Z^2\cos 2\beta - 2B_\nu m_M)^2}\ .
\end{aligned}$$

The mixing angles in the two subsectors are given respectively by:

$$\sin 2\theta_\pm = \frac{2m_D(A_\nu - \mu\cot\beta \pm m_M)}{\sqrt{4m_D^2(A_\nu - \mu\cot\beta \pm m_M)^2 + (m_M^2 + m_{\tilde{R}}^2 - m_{\tilde{L}}^2 - \frac{1}{2}M_Z^2\cos 2\beta \pm 2B_\nu m_M)^2}}\ . \tag{2.67}$$

2.3.1 The neutrinos and sneutrinos interaction Lagrangian

Finally the interaction Lagrangian that is relevant for the present work, expressed in the (ν_L,ν_R), $(\tilde{\nu}_L,\tilde{\nu}_R)$ electroweak interaction basis, is given by:

$$\mathcal{L}_{\mathrm{int}} = \mathcal{L}_{\nu H} + \mathcal{L}_{\nu Z} + \mathcal{L}_{\tilde{\nu} H} + \mathcal{L}_{\tilde{\nu} Z}\ . \tag{2.68}$$

Here $\mathcal{L}_{\nu H}$ and $\mathcal{L}_{\tilde{\nu} H}$ contain the interactions of the neutrinos and sneutrinos with the Higgs bosons respectively; and $\mathcal{L}_{\nu Z}$ and $\mathcal{L}_{\tilde{\nu} Z}$ those of the neutrinos and sneutrinos with the Z boson respectively.

For the various terms in Eq. (2.68) we find the following expressions:

$$\mathcal{L}_{\nu H} = -\frac{gm_D}{2M_W \sin\beta}((\overline{\nu_L}\nu_R + \overline{\nu_R}\nu_L)(H\sin\alpha + h\cos\alpha) - i(\overline{\nu_L}\nu_R - \overline{\nu_R}\nu_L)A\cos\beta) \ , \tag{2.69}$$

$$\mathcal{L}_{\nu Z} = \frac{g}{2\cos\theta_W}\left[(\overline{\nu_L}\gamma^\mu\nu_L)Z_\mu\right] \ , \tag{2.70}$$

$$\begin{aligned}
\mathcal{L}_{\tilde{\nu} H} = &-\frac{gm_D}{2M_W\sin\beta}\mu\left[(\tilde{\nu}_L^*\tilde{\nu}_R + \tilde{\nu}_L\tilde{\nu}_R^*)(-H\cos\alpha + h\sin\alpha)\right] \\
&- \frac{gm_D^2}{M_W\sin\beta}\left[(\tilde{\nu}_R^*\tilde{\nu}_R + \tilde{\nu}_L^*\tilde{\nu}_L)(H\sin\alpha + h\cos\alpha)\right] \\
&+ \frac{igm_D}{2M_W}\mu\left[(\tilde{\nu}_L^*\tilde{\nu}_R - \tilde{\nu}_L\tilde{\nu}_R^*)A\right] \\
&- \frac{gM_Z}{2cos\theta_W}\left[(\tilde{\nu}_L^*\tilde{\nu}_L)(H\cos(\alpha+\beta) - h\sin(\alpha+\beta))\right] \\
&- \frac{gm_D}{2M_W\sin\beta}A_\nu\left[(\tilde{\nu}_L^*\tilde{\nu}_R + \tilde{\nu}_L\tilde{\nu}_R^*)(H\sin\alpha + h\cos\alpha)\right] \\
&+ \frac{igm_D}{2M_W\sin\beta}A_\nu\left[(\tilde{\nu}_L^*\tilde{\nu}_R - \tilde{\nu}_L\tilde{\nu}_R^*)A\cos\beta\right] \\
&- \frac{gm_Dm_M}{2M_W\sin\beta}\left[(\tilde{\nu}_L\tilde{\nu}_R + \tilde{\nu}_L^*\tilde{\nu}_R^*)(H\sin\alpha + h\cos\alpha)\right] \\
&- i\frac{gm_Dm_M}{2M_W\sin\beta}\left[(\tilde{\nu}_L\tilde{\nu}_R - \tilde{\nu}_L^*\tilde{\nu}_R^*)A\cos\beta\right] \\
&- \frac{g^2m_D^2}{4M_W^2\sin^2\beta}\left[(\tilde{\nu}_L^*\tilde{\nu}_L)(H^2\sin^2\alpha + h^2\cos^2\alpha + A^2\cos^2\beta + hH\sin 2\alpha)\right] \\
&- \frac{g^2}{8\cos^2\theta_W}\left[(\tilde{\nu}_L^*\tilde{\nu}_L)(H^2\cos 2\alpha - h^2\cos 2\alpha - A^2\cos 2\beta - 2hH\sin 2\alpha)\right] \\
&- \frac{g^2m_D^2}{4M_W^2\sin^2\beta}\left[(\tilde{\nu}_R^*\tilde{\nu}_R)(H^2\sin^2\alpha + h^2\cos^2\alpha + A^2\cos^2\beta + hH\sin 2\alpha)\right] \ ,
\end{aligned} \tag{2.71}$$

$$\mathcal{L}_{\tilde{\nu} Z} = -\frac{ig}{2\cos\theta_W}\left[(\tilde{\nu}_L^*\bar{\partial}^\mu\tilde{\nu}_L)Z_\mu\right] + \frac{g^2}{4\cos^2\theta_W}\left[(\tilde{\nu}_L^*\tilde{\nu}_L)(Z_\mu Z^\mu)\right] \ . \tag{2.72}$$

The corresponding Feynman rules, expressed in the mass eigenstate basis, are collected in the Appendix A. Notice that this complete set of Feynman rules is, to our knowledge, not available in the literature so far.

Some comments are in order. In the previous interaction Lagrangian, and consequently in the Feynman rules, there are terms already present in the MSSM. These are the pure gauge interactions between the left-handed neutrinos and the Z boson, given in Eq. (2.70), those between the 'left-handed' sneutrinos and the Higgs bosons, given in Eq. (2.71), and those between the 'left-handed' sneutrinos and the Z bosons, given in

Eq. (2.72). In addition, in this MSSM-seesaw scenario, there are interactions driven by the neutrino Yukawa couplings (or equivalently m_D since $Y_\nu = (g m_D)/(\sqrt{2} M_W \sin\beta)$), and new interactions due to the Majorana nature driven by m_M. These genuine Majorana terms are those in the seventh and eight lines of Eq. (2.71) and are not present in the case of Dirac fermions.

2.3.2 Relevant parameters and limits

Regarding the size of the new parameters that have been introduced in this model, in addition to those of the MSSM, i.e., m_M, m_D, $m_{\tilde{R}}$, A_ν and B_ν, there are no significant constraints. In the literature it is often assumed that m_M has a very large value, $m_M \sim \mathcal{O}(10^{14-15})$ GeV, in order to get small physical neutrino masses $|m_\nu| \sim 0.1$ - 1 eV with large Yukawa couplings $Y_\nu \sim \mathcal{O}(1)$. This is an interesting possibility since it can lead to important phenomenological implications due to the large size of the radiative corrections driven by these large Yukawa couplings. In this paper we will explore, however, not only these extreme values but the full range for m_M from the electroweak scale $\sim 10^2$ GeV up to $\sim 10^{15}$ GeV.

On the other hand, the new soft SUSY-breaking parameters introduced in the sneutrino sector could be unrelated to those of the MSSM, or could be related, for instance, in the case one imposes (by hand) some kind of universality conditions. Whereas the non-singlet soft mass parameter $m_{\tilde{L}}$, being common to the charged 'left handed' slepton, is constrained by the solution to the hierarchy problem to lie below a few TeV, the singlet soft mass $m_{\tilde{R}}$ is not, because it is not connected to the electroweak symmetry breaking at tree level. The other sneutrino soft mass parameters, B_ν and A_ν are not connected either. However, they can generate a mass-splitting between sneutrinos and antisneutrinos which in turn and via loop corrections can generate neutrino mass splittings [140] that are experimentally constrained. Then, if $m_{\rm SUSY}$ represents a generic low SUSY breaking scale, with $m_{\rm SUSY} \lesssim \mathcal{O}(10^3)$ GeV one expects that $|A_\nu|, |B_\nu| \lesssim m_{\rm SUSY}$ [145]. According to these constraints, we will explore in this work values of these soft parameters ranging from the electroweak scale up to a few TeV. Besides, and due to the peculiarity of the behavior with $m_{\tilde{R}}$ and B_ν, as will be shown later, we will explore in addition the less conservative but interesting possibility where $m_{\tilde{R}}$ or B_ν are close to m_M.

For illustrative purposes and a clear understanding of our full one-loop results, three interesting limiting cases will also be considered in this work.

(1) The seesaw limit:
This assumes a large separation between the two neutrino mass scales involved, the Majorana mass and the Dirac mass, $m_M \gg m_D$. Notice that both masses are different from zero, $m_M \neq 0$ and $m_D \neq 0$, in this seesaw limit and, as we have said above, Y_ν can be large. The predictions are then given in power series of a dimensionless parameter defined as,

$$\xi \equiv \frac{m_D}{m_M} \ll 1 \ . \tag{2.73}$$

The light and heavy neutrino masses, as well as the mixing angle, are given in this limit by:

$$m_\nu = -m_D\xi + \mathcal{O}(m_D\xi^3) \simeq -\frac{m_D^2}{m_M} \ , \tag{2.74}$$

$$\begin{aligned} m_N &= m_M + \mathcal{O}(m_D\xi) \simeq m_M \ , \\ \sin\theta &= \xi + \mathcal{O}(\xi^3) \simeq \frac{m_D}{m_M} \\ \cos\theta &= 1 - \mathcal{O}(\xi^2) \simeq 1 \end{aligned} \tag{2.75}$$

Consequently, the neutrino mass eigenstates are given by:

$$\begin{aligned} n_1 \equiv \nu &\simeq (\nu_L + (\nu_L)^c) - \frac{m_D}{m_M}(\nu_R + (\nu_R)^c) \ , \\ n_2 \equiv N &\simeq \frac{m_D}{m_M}(\nu_L + (\nu_L)^c) + (\nu_R + (\nu_R)^c) \end{aligned} \tag{2.76}$$

Therefore, in the seesaw limit ν is made predominantly of ν_L and its c-conjugate, $(\nu_L)^c$, whereas N is made predominantly of ν_R and its c-conjugate, $(\nu_R)^c$.

In the sneutrino sector several mass scales are involved. Consequently, one has to set as an extra input their relative size to m_M. The simplest assumption is to set the value of m_M to be much larger than all the other mass scales involved, i.e., $m_M \gg m_D, M_Z, \mu, m_{\tilde{L}}, m_{\tilde{R}}, B_\nu, A_\nu$. In this limit the sneutrino masses are given by:

$$\begin{aligned} m^2_{\tilde{\nu}_+,\tilde{\nu}_-} &= m^2_{\tilde{L}} + \frac{1}{2}M_Z^2\cos 2\beta \mp 2m_D(A_\nu - \mu\cot\beta - B_\nu)\xi \ , \\ m^2_{\tilde{N}_+,\tilde{N}_-} &= m^2_M \pm 2B_\nu m_M + m^2_{\tilde{R}} + 2m_D^2 \ . \end{aligned} \tag{2.77}$$

Moreover, the mixing angles in this limit are given by:

$$\sin 2\theta_\pm = \pm\frac{2m_D}{m_M} \tag{2.78}$$

As we can appreciate in Eq. (2.78) the mixing angles $\theta_\pm$ are small in this limit and, therefore, $\tilde{\nu}_+$ and $\tilde{\nu}_-$ are made predominantly of $\tilde{\nu}_L$ and its c-conjugate, $\tilde{\nu}_L^*$, whereas $\tilde{N}_+$ and $\tilde{N}_-$ are made predominantly of $\tilde{\nu}_R$ and its c-conjugate, $\tilde{\nu}_R^*$.

(2) The Dirac limit:
In this limit one sets $m_M = 0$ (and $m_D \neq 0$) and one recovers the neutrinos as any other fermion of the MSSM, i.e., as Dirac fermions. In the basis that we have used in Eq. (2.55) this is manifested by the fact that when $m_M = 0$, the two Majorana neutrinos ν and N are degenerate with $m_\nu = -m_D$ and $m_N = +m_D$, and they combine maximally, i.e. with $\theta = \pi/4$, to form a four component Dirac neutrino with mass m_D. On the other hand, the sneutrino sector in this Dirac limit simplifies as well. When $m_M = 0$, the real scalar fields get degenerate in pairs,

$$m^2_{\tilde{\nu}_+} = m^2_{\tilde{\nu}_-} = \frac{1}{2}(m^2_{\tilde{L}} + m^2_{\tilde{R}} + 2m^2_D + \frac{1}{2}M_Z^2\cos 2\beta) \qquad (2.79)$$
$$- \frac{1}{2}\sqrt{4m_D^2(A_\nu - \mu\cot\beta)^2 + (m^2_{\tilde{R}} - m^2_{\tilde{L}} - \frac{1}{2}M_Z^2\cos 2\beta)^2}\ ,$$
$$m^2_{\tilde{N}_+} = m^2_{\tilde{N}_-} = \frac{1}{2}(m^2_{\tilde{L}} + m^2_{\tilde{R}} + 2m^2_D + \frac{1}{2}M_Z^2\cos 2\beta) \qquad (2.80)$$
$$+ \frac{1}{2}\sqrt{4m_D^2(A_\nu - \mu\cot\beta)^2 + (m^2_{\tilde{R}} - m^2_{\tilde{L}} - \frac{1}{2}M_Z^2\cos 2\beta)^2}\ ,$$

and they combine to form two complex scalar fields,

$$\tilde{\nu}_1 = \frac{1}{\sqrt{2}}(\tilde{\nu}_+ + i\tilde{\nu}_-) = \cos\tilde{\theta}\ \tilde{\nu}_L - \sin\tilde{\theta}\ \tilde{\nu}_R\ , \qquad (2.81)$$
$$\tilde{\nu}_2 = \frac{1}{\sqrt{2}}(\tilde{N}_+ + i\tilde{N}_-) = \sin\tilde{\theta}\ \tilde{\nu}_L + \cos\tilde{\theta}\ \tilde{\nu}_R \qquad (2.82)$$

with $m_{\tilde{\nu}_1} = m_{\tilde{\nu}_\pm}$, $m_{\tilde{\nu}_2} = m_{\tilde{N}_\pm}$, $\tilde{\theta} = \theta_+ = \theta_-$, and

$$\sin 2\tilde{\theta} = \frac{2m_D(A_\nu - \mu\cot\beta)}{\sqrt{4m_D^2(A_\nu - \mu\cot\beta)^2 + (m^2_{\tilde{R}} - m^2_{\tilde{L}} - \frac{1}{2}M_Z^2\cos 2\beta)^2}}\ . \qquad (2.83)$$

Notice that these two sneutrino states, $\tilde{\nu}_{1,2}$, are equivalent to the usual sfermion mass eigenstates within the MSSM.

In this Dirac limit it is interesting to study the similarities in the analytical behavior of the neutrino/sneutrino radiative corrections and the other MSSM fermion/sfermion radiative corrections. In particular we are interested in the comparison with the top/stop radiative corrections. As for the phenomenological implications, this limit

is not expected to lead to relevant numerical results, since to get compatibility with the experimentally tested small neutrino masses, $|m_\nu| \sim 0.1 - 1$ eV one needs Yukawa couplings extremely small, $Y_\nu \sim 10^{-12} - 10^{-13}$.

(3) The MSSM limit:
This limit is reached when one sets $m_D = 0$ (the value of m_M is not relevant since once the Yukawa couplings are set to zero the predictions are absolutely independent of this mass scale) and one is left with a neutrino/sneutrino sector with just pure gauge couplings. Concretely, there are just interactions of the left-handed neutrinos and the 'left-handed' sneutrinos to the Z boson, exactly as in the MSSM. We are interested in this limit, because we want to compare the radiative corrections from the neutrino/sneutrino sector within the MSSM-seesaw with those within the MSSM and to find the interesting regions in the new parameters of the MSSM-seesaw where the deviation from the MSSM result could be sizeable.

Chapter 3

Radiative corrections to m_h in the MSSM-seesaw model

In this chapter we study the indirect effects of Majorana neutrinos via their radiative corrections to the MSSM Higgs boson masses. Concretely, we present a calculation of the 1-loop radiative corrections to the lightest $\mathcal{CP}$ even Higgs boson mass from the neutrino/sneutrino sector within the MSSM-seesaw framework. We work here in general MSSM-seesaw scenarios with no universality conditions imposed, and explore the full parameter space of the neutrino/sneutrino sector. We restrict our computation to the one generation case of neutrinos/sneutrinos for simplicity and to fully understand the effect of just a single Majorana scale. The complete set of one-loop neutrino/sneutrino contributing diagrams will be taken into account, with both Yukawa and gauge couplings switched on. We also analyze the results in different renormalization schemes, which will be shown to provide remarkable differences. In addition to the exact results, we present some analytical and numerical results in the interesting limit of very large m_M as compared to all other scales involved, which will help us in the understanding of the important issue of the decoupling/non-decoupling of the heavy Majorana scale. Finally, we will discuss to what extent the radiative corrections computed here enter into the measurable range. The results presented in this chapter are original work of this thesis and have been published in [110, 114].

3.1 Higher-order corrections to m_h

3.1.1 Regularization and renormalization

Higher order corrections to an n point Green function are related to loop diagrams, which involve integrals over momentum that are in general divergent for large momentum (UV Divergent). For this reason a regularization procedure is needed to redefine the integrals in such a way that they become finite and mathematically well defined obejects. The broadly used regularization procedure for gauge theories is dimensional regularization (DREG), that conserves Lorentz and gauge invariance. In this method integrals in four dimensions are substituted by integrals in lower D dimensions where the integrals are convergent :

$$\int \frac{d^4k}{(2\pi)^4} \to \mu^{D-4} \int \frac{d^Dk}{2\pi^D} \tag{3.1}$$

An arbitrary mass parameter μ is introduced to mantain the couplings independent of D. After renormalization the result for physical quantities is finite in the limit $D \to 4$.

However, in SUSY, dimensional regularization cannot be used, because although it respects the gauge and Lorentz symmetry it breaks supersymmetry, due to the fact that by going to D dimensions the number of bosonic and fermionic degrees of freedom change. In order to avoid this problem the Dimensional Reduction procedure was proposed [146]. In this method all the fields and the corresponding γ_μ matrices are defined in 4 dimensions and only the integrals and the momentum are treated in D dimensions. Therefore, as regularization scheme for our calculation of 1-loop corrections to the Higgs 2 point function we will use dimensional reduction [146], thus preserving SUSY [147, 148].

The tree-level Higgs potential of the MSSM-seesaw shown in Eq. (1.21) contains a set of free parameters that are not fixed by theory. The definition of these parameters and their dependence on physical observables changes in higher orders of perturbation theory with respect to the definitions at tree level. In fact, the definitions of these parameters depend on the renormalization scheme. Here we have used a multiplicative renormalization to replace the bare parameters and fields of the initial Higgs potential by the renormalized ones. Generically:

$$\begin{aligned} g_0 &\to Z_g g = g + \delta g \\ m_0^2 &\to Z_m m^2 = m^2 + \delta m^2 \\ \phi_0 &\to Z_\phi^{1/2} \phi = \left(1 + \frac{1}{2}\delta Z_\phi\right) \phi \end{aligned} \tag{3.2}$$

After expanding $Z_i = 1 + \delta Z_i$, the bare couplings, masses and fields are replaced by the renormalized ones plus the corresponding counterterms δg, δm and δZ_ϕ . These counterterms absorb the infinites, but unobservable shifts, between the bare parameters and the renormalized ones. With these substitutions the bare Higgs potential is splited into two pieces, the renormalized one plus the counterterm part:

$$V(g_0, m_0, \phi_0) = V(g, m, \phi) + \delta V(g, m, \phi, \delta g, \delta m, \delta Z_\phi) \tag{3.3}$$

The decomposition in Eq. (3.2) is to a large extent arbitrary. Only the divergent parts of the counterterms are determined directly by the structure of the divergences of the one-loop amplitudes. The finite parts depend on the choice of the explicit renormalization conditions [149].

In our work, of the radiative corrections to the lightest Higgs mass of the MSSM we have used the Feynman Diagrammatic approach.

3.1.2 The concept of higher order corrections in the Feynman-diagrammatic approach

Among the three main approaches to calculate 1-loop corrections to the MSSM Higgs boson masses, i.e the Effective Potential Approach (EPA) [121, 150], the method of Renormalization Group Equations (RGE) [151–153], the Feynman Diagrammatic calculation [154–157], we have made use of the diagrammatic method. Although this method is technically involved, it is the most accurate one at the 1-loop level and can be used as a reference frame for simpler approximations.

In the Feynman diagrammatic (FD) approach the higher-order corrected $\mathcal{CP}$-even Higgs boson masses in the MSSM are derived by finding the poles of the (h, H)-propagator matrix. The inverse of this matrix is given by

$$(\Delta_{\rm Higgs})^{-1} = -i \begin{pmatrix} p^2 - m^2_{H,\rm tree} + \hat{\Sigma}_{HH}(p^2) & \hat{\Sigma}_{hH}(p^2) \\ \hat{\Sigma}_{hH}(p^2) & p^2 - m^2_{h,\rm tree} + \hat{\Sigma}_{hh}(p^2) \end{pmatrix} . \tag{3.4}$$

Determining the poles of the matrix $\Delta_{\rm Higgs}$ in Eq. (3.4) is equivalent to solving the equation

$$\left[p^2 - m^2_{h\ \rm tree} + \hat{\Sigma}_{hh}(p^2)\right] \left[p^2 - m^2_{H\ \rm tree} + \hat{\Sigma}_{HH}(p^2)\right] - \left[\hat{\Sigma}_{hH}(p^2)\right]^2 = 0\,. \tag{3.5}$$

In perturbation theory, a (renormalized) self-energy is expanded as follows

$$\hat{\Sigma}(p^2) = \hat{\Sigma}^{(1)}(p^2) + \hat{\Sigma}^{(2)}(p^2) + \dots\ ,$$

$$\Sigma(p^2) = \Sigma^{(1)}(p^2) + \Sigma^{(2)}(p^2) + \dots \ , \tag{3.6}$$

in terms of the ith-order contributions $\hat{\Sigma}^{(i)}, \Sigma^{(i)}$. In the following sections we concentrate on the one-loop corrections and drop the order index, i.e. $\hat{\Sigma} \equiv \hat{\Sigma}^{(1)}$ in the following.

3.1.3 One-loop renormalization

In order to calculate one-loop corrections to the Higgs boson masses, the renormalized Higgs boson self-energies are needed. Following the procedure used in [62, 160], the parameters appearing in the Higgs potential, (1.21), are renormalized as follows:

$$\begin{aligned} M_Z^2 &\to M_Z^2 + \delta M_Z^2, & T_h &\to T_h + \delta T_h, \\ M_W^2 &\to M_W^2 + \delta M_W^2, & T_H &\to T_H + \delta T_H, \\ M^2_{\text{Higgs}} &\to M^2_{\text{Higgs}} + \delta M^2_{\text{Higgs}}, & \tan\beta &\to \tan\beta\,(1 + \delta\tan\beta\,). \end{aligned} \tag{3.7}$$

M^2_{Higgs} denotes the tree-level Higgs boson mass matrix given in Eq. (1.53). T_h and T_H are the tree-level tadpoles, i.e. the terms linear in h and H in the Higgs potential.

The field renormalization matrices of both Higgs multiplets can be set up symmetrically,

$$\begin{pmatrix} h \\ H \end{pmatrix} \to \begin{pmatrix} 1 + \frac{1}{2}\delta Z_{hh} & \frac{1}{2}\delta Z_{hH} \\ \frac{1}{2}\delta Z_{hH} & 1 + \frac{1}{2}\delta Z_{HH} \end{pmatrix} \cdot \begin{pmatrix} h \\ H \end{pmatrix} \ . \tag{3.8}$$

For the mass counter term matrices we use the definitions

$$\delta M^2_{\text{Higgs}} = \begin{pmatrix} \delta m_h^2 & \delta m_{hH}^2 \\ \delta m_{hH}^2 & \delta m_H^2 \end{pmatrix} \ . \tag{3.9}$$

The renormalized self-energies, $\hat{\Sigma}(p^2)$, can now be expressed through the unrenormalized self-energies, $\Sigma(p^2)$, the field renormalization constants and the mass counter terms. This reads for the $\mathcal{CP}$-even part,

$$\hat{\Sigma}_{hh}(p^2) = \Sigma_{hh}(p^2) + \delta Z_{hh}(p^2 - m^2_{h,\text{tree}}) - \delta m_h^2, \tag{3.10a}$$

$$\hat{\Sigma}_{hH}(p^2) = \Sigma_{hH}(p^2) + \delta Z_{hH}(p^2 - \tfrac{1}{2}(m^2_{h,\text{tree}} + m^2_{H,\text{tree}})) - \delta m_{hH}^2, \tag{3.10b}$$

$$\hat{\Sigma}_{HH}(p^2) = \Sigma_{HH}(p^2) + \delta Z_{HH}(p^2 - m^2_{H,\text{tree}}) - \delta m_H^2 \ . \tag{3.10c}$$

Inserting the renormalization transformation into the Higgs mass terms leads to expressions for their counter terms which consequently depend on the other counter terms introduced in Eq. (3.7).

For the $\mathcal{CP}$-even part of the Higgs sectors, these counter terms are:

$$\begin{aligned}
\delta m_h^2 &= \delta M_A^2 \cos^2(\alpha-\beta) + \delta M_Z^2 \sin^2(\alpha+\beta) \\
&\quad + \tfrac{e}{2M_Z s_\mathrm{w} c_\mathrm{w}}(\delta T_H \cos(\alpha-\beta)\sin^2(\alpha-\beta) + \delta T_h \sin(\alpha-\beta)(1+\cos^2(\alpha-\beta))) \\
&\quad + \delta\tan\beta\, \sin\beta\, \cos\beta\, (M_A^2 \sin 2(\alpha-\beta) + M_Z^2 \sin 2(\alpha+\beta)), \qquad (3.11a)\\
\delta m_{hH}^2 &= \tfrac{1}{2}(\delta M_A^2 \sin 2(\alpha-\beta) - \delta M_Z^2 \sin 2(\alpha+\beta)) \\
&\quad + \tfrac{e}{2M_Z s_\mathrm{w} c_\mathrm{w}}(\delta T_H \sin^3(\alpha-\beta) - \delta T_h \cos^3(\alpha-\beta)) \\
&\quad - \delta\tan\beta\, \sin\beta\, \cos\beta\, (M_A^2 \cos 2(\alpha-\beta) + M_Z^2 \cos 2(\alpha+\beta)), \qquad (3.11b)\\
\delta m_H^2 &= \delta M_A^2 \sin^2(\alpha-\beta) + \delta M_Z^2 \cos^2(\alpha+\beta) \\
&\quad - \tfrac{e}{2M_Z s_\mathrm{w} c_\mathrm{w}}(\delta T_H \cos(\alpha-\beta)(1+\sin^2(\alpha-\beta)) + \delta T_h \sin(\alpha-\beta)\cos^2(\alpha-\beta)) \\
&\quad - \delta\tan\beta\, \sin\beta\, \cos\beta\, (M_A^2 \sin 2(\alpha-\beta) + M_Z^2 \sin 2(\alpha+\beta))\ . \qquad (3.11c)
\end{aligned}$$

For the field renormalization we choose to give each Higgs doublet one renormalization constant,

$$\mathcal{H}_1 \to (1+\tfrac{1}{2}\delta Z_{\mathcal{H}_1})\mathcal{H}_1, \quad \mathcal{H}_2 \to (1+\tfrac{1}{2}\delta Z_{\mathcal{H}_2})\mathcal{H}_2\ . \qquad (3.12)$$

This leads to the following expressions for the various field renormalization constants in Eq. (3.8):

$$\begin{aligned}
\delta Z_{hh} &= \sin^2\alpha\, \delta Z_{\mathcal{H}_1} + \cos^2\alpha\, \delta Z_{\mathcal{H}_2}, \qquad (3.13a)\\
\delta Z_{hH} &= \sin\alpha\, \cos\alpha\, (\delta Z_{\mathcal{H}_2} - \delta Z_{\mathcal{H}_1}), \qquad (3.13b)\\
\delta Z_{HH} &= \cos^2\alpha\, \delta Z_{\mathcal{H}_1} + \sin^2\alpha\, \delta Z_{\mathcal{H}_2}\ . \qquad (3.13c)
\end{aligned}$$

The counter term for $\tan\beta$ can be expressed in terms of the vacuum expectation values as

$$\delta\tan\beta = \frac{1}{2}(\delta Z_{\mathcal{H}_2} - \delta Z_{\mathcal{H}_1}) + \frac{\delta v_2}{v_2} - \frac{\delta v_1}{v_1}\ , \qquad (3.14)$$

where the δv_i are the renormalization constants of the v_i:

$$v_1 \to (1+\delta Z_{\mathcal{H}_1})(v_1+\delta v_1), \quad v_2 \to (1+\delta Z_{\mathcal{H}_2})(v_2+\delta v_2)\ . \qquad (3.15)$$

It can be shown that the divergent parts of $\delta v_1/v_1$ and $\delta v_2/v_2$ are equal [62]. Consequently, one can set $\delta v_2/v_2 - \delta v_1/v_1$ to zero.

By setting $\delta v_2/v_2 - \delta v_1/v_1$ to zero, $\delta \tan\beta$ is just a combination of field counterterms:

$$\delta \tan\beta = \frac{1}{2}\left(\delta Z_{\mathcal{H}_2} - \delta Z_{\mathcal{H}_1}\right) \tag{3.16}$$

3.1.4 Renormalization schemes

With respect to the renormalization scheme, the on-shell (OS) is particularly appropriate when the parameters of the theory can be determined through precise experiments because in this scheme the renormalized masses and coupling constants are identified with the physical masses and coupling constants (cross sections and decay widths). Two conditions characterize the usual OS scheme:

- The mass that appears in the ϕ propagator represents the ϕ physical mass.

$$\mathrm{Re}\,\hat{\Sigma}_{\phi\phi}(p^2 = m_\phi^2) = 0 \qquad \Rightarrow \qquad \mathrm{Re}\,\Sigma_{\phi\phi}(p^2 = m_\phi^2) = \mathrm{Re}\,\delta m_\phi^2 \tag{3.17}$$

- The residue of the ϕ renormalized propagator at the ϕ pole mass is fixed to one.

$$\hat{\Sigma}'_{\phi\phi}(p^2 = m_\phi^2) = 0 \qquad \Rightarrow \qquad \delta Z_{\phi\phi} = -\Sigma'_{\phi\phi}(p^2 = m_\phi^2) \tag{3.18}$$

1) Renormalization scheme for the boson masses

In our work we will use on-shell renormalization conditions for the mass counterterms of the pseudoscalar A boson, the Z and the W gauge bosons, because they are physical observables, leading to:

$$\delta M_Z^2 = \mathrm{Re}\,\Sigma_{ZZ}(M_Z^2), \quad \delta M_W^2 = \mathrm{Re}\,\Sigma_{WW}(M_W^2), \quad \delta M_A^2 = \mathrm{Re}\,\Sigma_{AA}(M_A^2). \tag{3.19}$$

Here $\Sigma_{ZZ,WW}$ denotes the transverse part of the self-energies. Since the tadpole coefficients are chosen to vanish in all orders, their counter terms follow from $T_{\{h,H\}} + \delta T_{\{h,H\}} = 0$:

$$\delta T_h = -T_h, \quad \delta T_H = -T_H \ . \tag{3.20}$$

2) Renormalization schemes for the Higgs boson wave function

On the other hand, $\tan\beta$ is just a Lagrangian parameter, and it is not a directly measurable quantity. There is no obvious and unique way to relate $\tan\beta$ to an observable. The actual definition of $\tan\beta$, its physical meaning and its relation to observables is given by the choice of a renormalization scheme. This ambiguity in the definition of $\tan\beta$ is similar to the ambiguity in the definition of the weak mixing angle θ_W.

Therefore, for the remaining renormalization constants, $\delta\tan\beta$, $\delta Z_{\mathcal{H}_1}$ and $\delta Z_{\mathcal{H}_2}$ various renormalization schemes are possible [158–160]. The different renormalization schemes for $\delta\tan\beta$, $\delta Z_{\mathcal{H}_1}$ and $\delta Z_{\mathcal{H}_2}$ that we have used for our calculation are the following:

On-shell renormalization

One possible choice is an on-shell (OS) renormalization. There is not an unique way of renormalizing OS $\delta\tan\beta$, $\delta Z_{\mathcal{H}_1}$ and $\delta Z_{\mathcal{H}_2}$ [161]. Among the various possibilities we have chosen the following renormalization conditions for the renormalized Higgs-boson self-energies:

$$\hat{\Sigma}'_{hh}(m^2_{h,\mathrm{tree}}) = 0 \ , \tag{3.21}$$

$$\hat{\Sigma}'_{HH}(m^2_{H,\mathrm{tree}}) = 0 \ . \tag{3.22}$$

This yields

$$\delta Z^{\mathrm{OS}}_{hh} = -\,\mathrm{Re}\,\Sigma'_{hh}(m^2_{h,\mathrm{tree}}) \ , \tag{3.23}$$

$$\delta Z^{\mathrm{OS}}_{HH} = -\,\mathrm{Re}\,\Sigma'_{HH}(m^2_{H,\mathrm{tree}}) \ , \tag{3.24}$$

equivalently to

$$\delta Z^{\mathrm{OS}}_{\mathcal{H}_1} = \frac{1}{\cos 2\alpha}\left(\sin^2\alpha\ \mathrm{Re}\,\Sigma'_{hh}(m^2_{h,\mathrm{tree}}) - \cos^2\alpha\ \mathrm{Re}\,\Sigma'_{HH}(m^2_{H,\mathrm{tree}})\right) \ , \tag{3.25}$$

$$\delta Z^{\mathrm{OS}}_{\mathcal{H}_2} = \frac{1}{\cos 2\alpha}\left(-\cos^2\alpha\ \mathrm{Re}\,\Sigma'_{hh}(m^2_{h,\mathrm{tree}}) + \sin^2\alpha\ \mathrm{Re}\,\Sigma'_{HH}(m^2_{H,\mathrm{tree}})\right) \ . \tag{3.26}$$

For $\delta\tan\beta^{\mathrm{OS}}$ a convenient choice is

$$\begin{aligned}\delta\tan\beta^{\mathrm{OS}} &= \frac{1}{2}\left(\delta Z^{\mathrm{OS}}_{\mathcal{H}_2} - \delta Z^{\mathrm{OS}}_{\mathcal{H}_1}\right) \\ &= \frac{-1}{2\cos 2\alpha}\left(\mathrm{Re}\,\Sigma'_{hh}(m^2_{h,\mathrm{tree}}) - \mathrm{Re}\,\Sigma'_{HH}(m^2_{H,\mathrm{tree}})\right) \ .\end{aligned} \tag{3.27}$$

It should be kept in mind that this scheme can lead to large corrections to m_h in the MSSM [158, 161], hence worsening the convergence of the perturbative expansion. Furthermore, it is known to provide gauge dependent corrections at the one-loop level [159].

$\overline{\text{DR}}$ renormalization

A convenient choice which avoids the previously commented large corrections to m_h in the MSSM and is (linear) gauge independent at the one-loop level is a $\overline{\text{DR}}$ renormalization of $\delta \tan\beta$, $\delta Z_{\mathcal{H}_1}$ and $\delta Z_{\mathcal{H}_2}$,

$$\delta Z_{\mathcal{H}_1}^{\overline{\text{DR}}} = -\left[\text{Re}\,\Sigma'_{HH\,|\alpha=0}\right]^{\text{div}}, \tag{3.28a}$$

$$\delta Z_{\mathcal{H}_2}^{\overline{\text{DR}}} = -\left[\text{Re}\,\Sigma'_{hh\,|\alpha=0}\right]^{\text{div}}, \tag{3.28b}$$

$$\delta\tan\beta^{\,\overline{\text{DR}}} = \frac{1}{2}\left(\delta Z_{\mathcal{H}_2}^{\overline{\text{DR}}} - \delta Z_{\mathcal{H}_1}^{\overline{\text{DR}}}\right) . \tag{3.28c}$$

The $[\,]^{\text{div}}$ terms are the ones proportional to $\Delta = 2/\varepsilon - \gamma_{\text{E}} + \log(4\pi)$, when using dimensional regularization/reduction in $d = 4 - \varepsilon$ dimensions; γ_{E} is the Euler constant. The corresponding renormalization scale, $\mu_{\overline{\text{DR}}}$, has to be fixed to a certain mass scale that will be discussed below.

Modified $\overline{\text{DR}}$ renormalization (m$\overline{\text{DR}}$)

The $\mu_{\overline{\text{DR}}}$ dependence introduced in the $\overline{\text{DR}}$ scheme can lead in the present context to large logarithmic corrections $\propto \log(m_M^2/\mu_{\overline{\text{DR}}}^2)$ for large values of the Majorana mass m_M (as will be discussed below). These large corrections could again worsen the convergence of the perturbative expansion. One possible way out is to replace $[\,]^{\text{div}}$ by $[\,]^{\text{mdiv}}$, where the latter means to select not only the terms $\propto \Delta$ as in Eqs. 3.28, but the terms $\propto \Delta_m \equiv \Delta - \log(m_M^2/\mu_{\overline{\text{DR}}}^2)$. This prescription for the counterterms defines the modified $\overline{\text{DR}}$ renormalization scheme, which will be named in this work in short as m$\overline{\text{DR}}$,

$$\delta Z_{\mathcal{H}_1}^{m\overline{\text{DR}}} = -\left[\text{Re}\,\Sigma'_{HH\,|\alpha=0}\right]^{\text{mdiv}}, \tag{3.29a}$$

$$\delta Z_{\mathcal{H}_2}^{m\overline{\text{DR}}} = -\left[\text{Re}\,\Sigma'_{hh\,|\alpha=0}\right]^{\text{mdiv}}, \tag{3.29b}$$

$$\delta\tan\beta^{\,m\overline{\text{DR}}} = \frac{1}{2}\left(\delta Z_{\mathcal{H}_2}^{m\overline{\text{DR}}} - \delta Z_{\mathcal{H}_1}^{m\overline{\text{DR}}}\right) . \tag{3.29c}$$

As will be shown below, effectively this corresponds to the particular choice of $\mu_{\overline{\text{DR}}} = m_M$. In this way the potentially large logarithms vanish, what makes it a convenient choice. Usually this choice is referred to in the literature as 'decoupling the large mass scale by hand' (see e.g. [162, 163] and references therein).

It should be kept in mind that in the m$\overline{\rm DR}$ scheme the parameter $\tan\beta = \tan\beta^{\rm m\overline{DR}}$ has a different meaning than the "conventional" parameter $\tan\beta = \tan\beta^{\overline{\rm DR}}$. However, we have checked that this shift is numerically insignificant.

3.2 Results

In this section we first present the results of the one-loop corrections from neutrino/sneutrino contributions to the neutral Higgs boson renormalized self-energies within the MSSM-seesaw and then we discuss the derived results for the Higgs mass corrections.

3.2.1 One-loop calculation of the renormalized self-energies

The full one-loop neutrino/sneutrino corrections to the self-energies, $\hat{\Sigma}^{\nu/\tilde{\nu}}_{hh}$, $\hat{\Sigma}^{\nu/\tilde{\nu}}_{HH}$ and $\hat{\Sigma}^{\nu/\tilde{\nu}}_{hH}$, entering Eq. (3.5) have been evaluated with the help of *FeynArts* [144] and *FormCalc* [164]. For shortness, in this and the next subsection these self-energies will be named simply as $\hat{\Sigma}_{hh}$, $\hat{\Sigma}_{HH}$, and $\hat{\Sigma}_{hH}$, respectively. The new Feynman rules for the neutrino/sneutrino sector, derived in this work and collected in the Appendix A, have been inserted into a new model file[1].

The generic one-loop Feynman-diagrams contributing to the renormalized self-energies are depicted in Figure 3.1. They include the two-point and one-point diagrams in the Higgs self-energies, tadpole diagrams, and the two-point and one-point diagrams in the Z boson self-energy. Here the notation is: ϕ refers generically to all neutral Higgs bosons, h, H, A; F refers to all neutrinos n_i $(i = 1, 2)$; S refers to all sneutrinos $\tilde{n}_i$ $(i = 1, ..4)$, and Z refers to the Z boson.

The analytical results for the unrenormalized self-energies and tadpoles are collected in the Appendix B. The final analytical results for the renormalized self-energies are easily obtained by inserting these results into Eq. (3.10).

We have checked that all the divergences involved in the computation cancel and the renormalized self-energies, $\hat{\Sigma}_{hh}(p^2)$, $\hat{\Sigma}_{HH}(p^2)$ and $\hat{\Sigma}_{hH}(p^2)$ in the three schemes OS, $\overline{\rm DR}$, and m$\overline{\rm DR}$ are all finite, as expected. We have also checked that the renormalized self-energies in the OS scheme, are independent of the regularization scale $\mu_{\overline{\rm DR}}$, as they must be. The renormalized self-energies in the $\overline{\rm DR}$ are $\mu_{\overline{\rm DR}}$ dependent whereas the ones in

[1]This model file is available upon request.

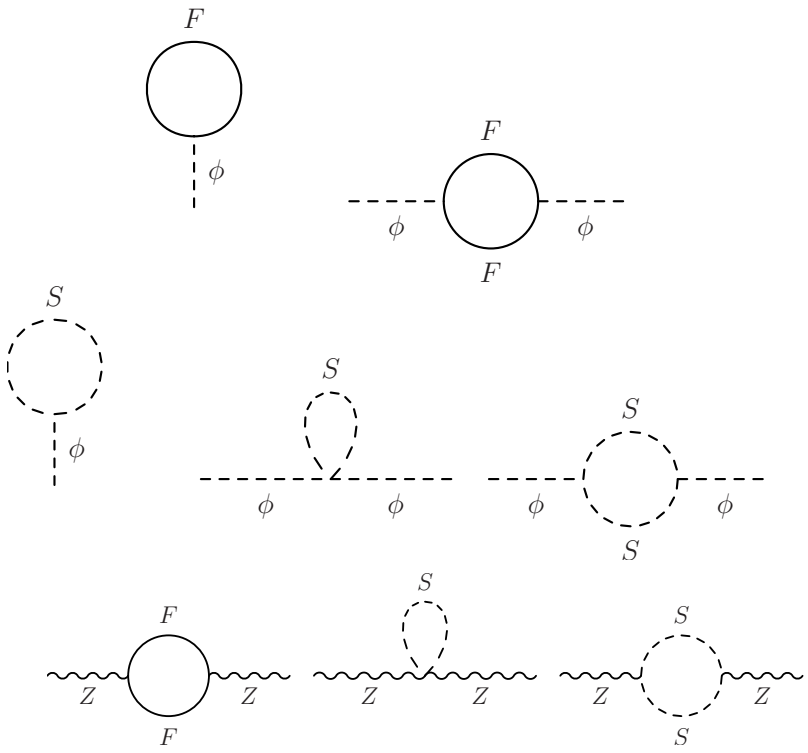

Figure 3.1: Generic one-loop Feynman-diagrams contributing to the neutral Higgs bosons renormalized self-energies (see text)

the m$\overline{\text{DR}}$ scheme are $\mu_{\overline{\text{DR}}}$ independent by construction. Analytically they are related by $\hat{\Sigma}^{\text{m}\overline{\text{DR}}}(p^2) = \hat{\Sigma}^{\overline{\text{DR}}}(p^2)|_{\mu_{\overline{\text{DR}}}=m_M}$.

3.2.2 Analysis of the renormalized self-energies

In the following we discuss the numerical results for the renormalized self-energies. They are collected in Figs. 3.2 through 3.10. First we compare the predictions of the one-loop renormalized self-energies in the three schemes for the full interval 10^3 GeV $\lesssim m_M \lesssim 10^{15}$ GeV, and next we analyze these exact results at large m_M with the help of the simple analytical formulas that are obtained in the seesaw limit. Then we choose the m$\overline{\text{DR}}$ scheme and show the exact numerical results of the renormalized self-energies as functions of all the neutrino/sneutrino parameters involved. Finally we conclude on the subset of most relevant parameters (specifically, m_M, $m_{\tilde{R}}$, B_ν and m_ν) which will be the selected ones to study the corrections to M_h in the next subsection. For the final estimate of these cor-

rections, and to localize the regions of the parameter space where they can reach sizeable values, we will vary these relevant parameters within some selected plausible intervals. For the parameters which do not exhibit a relevant numerical effect on M_h (specifically, $\tan\beta$, M_A, μ, $m_{\tilde{L}}$ and A_ν) we choose representative values. For completeness, we will also comment shortly at the end of this subsection on the Dirac case.

In order to compare systematically our predictions of the neutrino/sneutrino sector in the MSSM-seesaw with those in the MSSM, we have split the full one-loop neutrino/sneutrino result into two parts:

$$\hat{\Sigma}(p^2)|_{\rm full} = \hat{\Sigma}(p^2)|_{\rm gauge} + \hat{\Sigma}(p^2)|_{\rm Yukawa} \ , \tag{3.30}$$

where $\hat{\Sigma}(p^2)|_{\rm gauge}$ means the contributions from pure gauge interactions and they are obtained by switching off the Yukawa interactions, i.e. by setting $Y_\nu = 0$ (or equivalently $m_D = 0$). The remaining part is named here $\hat{\Sigma}(p^2)|_{\rm Yukawa}$ and refers to the contributions that are only present if $Y_\nu \neq 0$. In other words, this separation splits the full result into the common part with the MSSM, given by $\hat{\Sigma}(p^2)|_{\rm gauge}$, and the new contributions due to the presence of Majorana neutrinos with non vanishing Yukawa interactions, given by $\hat{\Sigma}(p^2)|_{\rm Yukawa}$. Thus, by comparing the size of these two parts, within the allowed parameter space region, we will localize the areas where $\hat{\Sigma}(p^2)|_{\rm Yukawa} \gg \hat{\Sigma}(p^2)|_{\rm gauge}$, which will therefore indicate a significant departure from the MSSM result.

Dependence on m_M

We show in Figure 3.2 the predictions for $\hat{\Sigma}_{hh}(p^2)$ as a function of m_M in the three schemes: $\overline{\rm DR}$ (upper left plot), OS (upper right plot), and m$\overline{\rm DR}$ (lower left plot). In these plots we have considered an extremely wide range for the m_M values, from 10^3 GeV up to 10^{15} GeV, and fixed the physical light neutrino mass to $|m_\nu| = 0.5$ eV. Consequently, m_D is derived from m_M and m_ν by using Eq. (2.61) and Eq. (2.62). The other parameters are fixed as indicated in the figure. In this and in the following figures we have fixed p^2 in the self-energies to a particular value, corresponding to an approximation of the higher-order corrected value of M_h for the input MSSM parameters set in each figure, see below. The numerical values used here and in the following for the SUSY parameters are representative values (as will also be shown below). Therefore, despite choosing only a few values for the parameters, the results obtained can be considered as more general.

In the three mentioned plots in Figure 3.2 one can see that the numerical value of the full result is nearly constant with m_M in the three schemes from $m_M = 10^3$ GeV

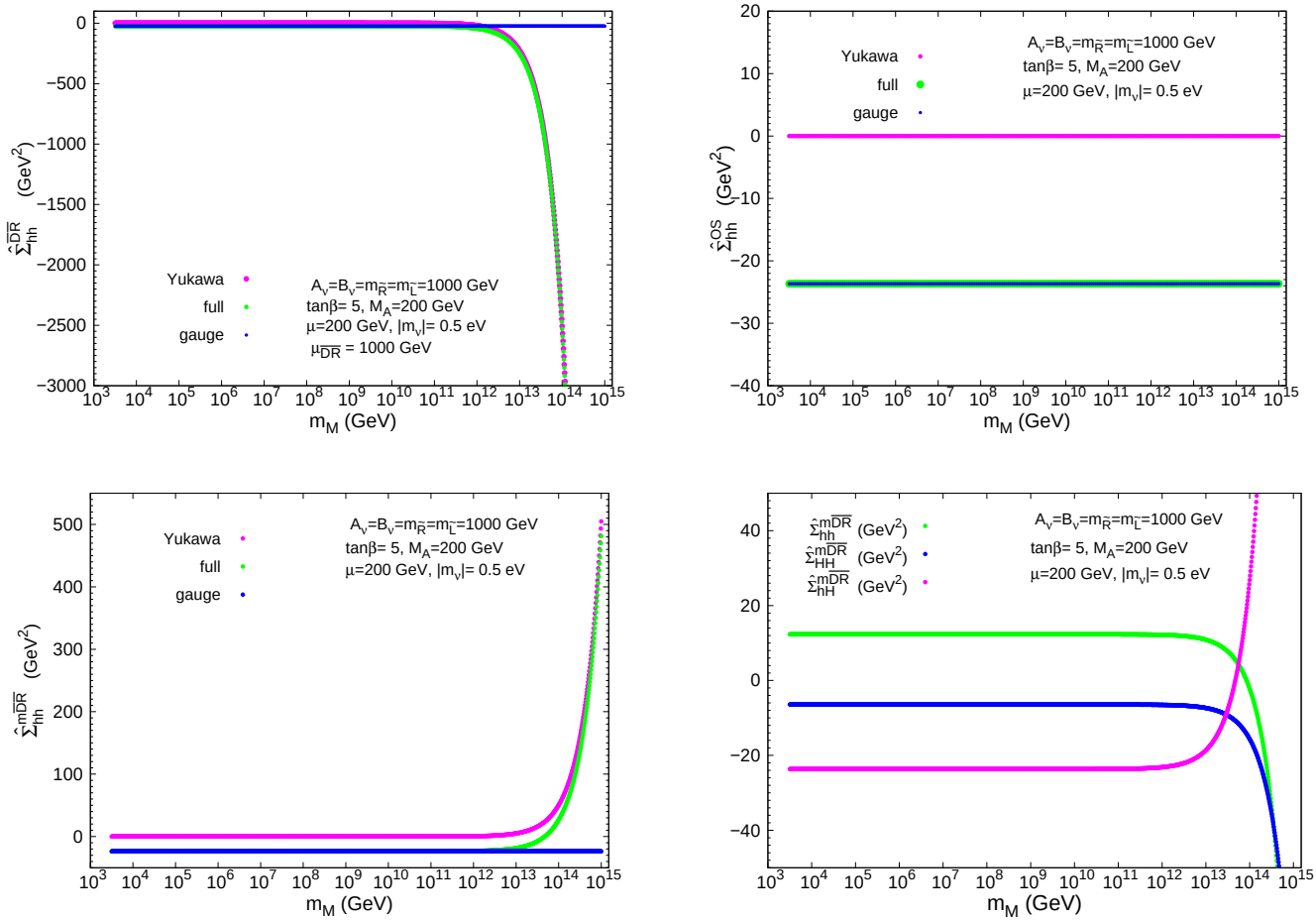

Figure 3.2: Renormalized Higgs boson self-energies as a function of m_M and comparison between the three considered schemes. Upper left panel: $\hat{\Sigma}^{\overline{\rm DR}}_{hh}(p^2)$. Upper right panel: $\hat{\Sigma}^{\rm OS}_{hh}(p^2)$. Lower left panel: $\hat{\Sigma}^{\rm m\overline{DR}}_{hh}(p^2)$. Lower right panel: $\hat{\Sigma}^{\rm m\overline{DR}}_{hh}(p^2)$, $\hat{\Sigma}^{\rm m\overline{DR}}_{HH}(p^2)$ and $\hat{\Sigma}^{\rm m\overline{DR}}_{hH}(p^2)$. All self-energies are evaluated at $p^2 = (116\ \text{GeV})^2$.

up to $m_M \sim 10^{12}$ GeV. Furthermore, this constant value is approximately the same in the three schemes (the differences are below $\sim 10^{-2}$ GeV^2), and is totally dominated by the 'pure gauge contributions'. Thus, for 10^3 GeV $\lesssim m_M \lesssim 10^{12}$ GeV the result in the MSSM-seesaw nearly coincides with the result in the MSSM, irrespectively of the scheme. For the choice of input parameters in this plot, we get $\hat{\Sigma}_{hh}|_{\rm full} \simeq \hat{\Sigma}_{hh}|_{\rm gauge} \simeq -23.67$ GeV^2.

For larger values of m_M in the range 10^{12} GeV $< m_M < 10^{15}$ GeV, there are, however, remarkable differences between the three considered schemes, and the main

differences come clearly from the 'Yukawa contributions'. Whereas $\hat{\Sigma}^{\rm OS}_{hh}|_{\rm full}$ is apparently constant with m_M, also for $m_M > 10^{12}$ GeV, $|\hat{\Sigma}^{\overline{\rm DR}}_{hh}|_{\rm full}|$ and $|\hat{\Sigma}^{m\overline{\rm DR}}_{hh}|_{\rm full}|$ grow noticeably with m_M at these large m_M values. The numerical value of $\hat{\Sigma}^{\overline{\rm DR}}_{hh}|_{\rm full}$ is negative for $m_M > 10^{12}$ GeV and gets large values in this range, where they are totally dominated by the 'Yukawa contributions'. For instance, for $m_M = 10^{13}$ GeV, we get $\hat{\Sigma}^{\overline{\rm DR}}_{hh}|_{\rm full} \simeq \hat{\Sigma}^{\overline{\rm DR}}_{hh}|_{\rm Yukawa} \simeq -250$ GeV^2, and for $m_M = 10^{14}$ GeV, we get $\hat{\Sigma}^{\overline{\rm DR}}_{hh}|_{\rm full} \simeq \hat{\Sigma}^{\overline{\rm DR}}_{hh}|_{\rm Yukawa} \simeq -3000$ GeV^2. In the m$\overline{\rm DR}$ scheme, the result is negative up to 5×10^{13} GeV and then becomes positive and large for $m_M > 5 \times 10^{13}$ GeV. Notice that, the absolute value in the m$\overline{\rm DR}$ scheme at large m_M is always smaller than in the $\overline{\rm DR}$ scheme, due to the commented cancellation of the large logarithms $\log(m_M/\mu_{\overline{\rm DR}})$ corresponding to the choice $\mu_{\overline{\rm DR}} = m_M$. Notice also that, in spite of this cancellation, the size of the corrections in m$\overline{\rm DR}$, are still large for large enough m_M values. For instance, for $m_M = 10^{15}$ GeV, we get dominance of the 'Yukawa contributions' $\hat{\Sigma}^{m\overline{\rm DR}}_{hh}|_{\rm full} \simeq \hat{\Sigma}^{m\overline{\rm DR}}_{hh}|_{\rm Yukawa} \simeq 500$ GeV^2. In contrast, for $m_M = 10^{14}$ GeV, the 'Yukawa contributions' and the 'pure gauge contributions', compete since $\hat{\Sigma}^{m\overline{\rm DR}}_{hh}|_{\rm Yukawa} \simeq 60$ GeV^2 and $\hat{\Sigma}^{m\overline{\rm DR}}_{hh}|_{\rm gauge} \simeq -24$ GeV^2 leading to $\hat{\Sigma}^{m\overline{\rm DR}}_{hh}|_{\rm full} \simeq 36$ GeV^2.

In the lower right plot of Figure 3.2 we compare $\hat{\Sigma}^{m\overline{\rm DR}}_{hh}|_{\rm full}$ to the other two renormalized self-energies, $\hat{\Sigma}^{m\overline{\rm DR}}_{HH}|_{\rm full}$ and $\hat{\Sigma}^{m\overline{\rm DR}}_{hH}|_{\rm full}$. One can observe that the three self-energies behave qualitatively very similarly with m_M, being approximately constant for $m_M < 10^{12}$ GeV and growing (in modulus) with m_M for 10^{12} GeV $< m_M < 10^{15}$ GeV. For the choice of parameters in this plot, $|\hat{\Sigma}^{m\overline{\rm DR}}_{hh}|_{\rm full}|$ is larger than the others in the full explored m_M range. This will be relevant for the forthcoming estimate of the one-loop radiative corrections to M_h.

The previously commented growing behavior of the renormalized self-energies with m_M is a consequence of the corresponding growing behavior of the neutrino Yukawa interactions with m_M, see Eq. (2.61) and Eq. (2.62). This is a well known feature of the seesaw models that, in order to get the light neutrino masses m_ν in agreement with data, one must impose for each input m_M value the proper Y_ν (and therefore m_D) to precisely match the experimentally inspired input m_ν. Y_ν is therefore not an input but an output in this approach, and according to Eq. (2.61) and Eq. (2.62) Y_ν grows with m_M as $Y_\nu \propto \sqrt{m_M}$. The behavior of the renormalized self-energies with m_M is, consequently, the result of the two competing facts, the increase of Y_ν with m_M and the decreasing with m_M from the neutrino and sneutrino propagators in the loops.

Dependence on m_M in the seesaw limit

In order to illustrate more clearly the behavior with m_M, we have analyzed in more detail the renormalized self-energies in the seesaw limit, as defined in chapter 2. As the increase with m_M starts at very large $m_M > 10^{12}$ GeV values (i.e. much larger than the other scales, $m_M \gg m_D, M_Z, M_A, \mu, m_{\tilde{L}}, m_{\tilde{R}}, B_\nu, A_\nu$), one expects that this limit should approximate pretty well the full result and show its same main features.

For the computation of the renormalized self-energies in this seesaw limit, we have performed a systematic expansion of the exact result in powers of the seesaw parameter $\xi = m_D/m_M$. In order to reduce the number of parameters, and for a clearer interpretation of the results, we have set in this expansion, $A_\nu = \mu = B_\nu = 0$ (which is justified, see below) and we have assumed universal soft SUSY breaking masses, i.e., $m_{\tilde{L}} = m_{\tilde{R}} = m_{\rm SUSY}$.

The analytical expressions for these expanded renormalized self-energies are of the generic form:

$$\hat{\Sigma}(p^2) = \left(\hat{\Sigma}(p^2)\right)_{m_D^0} + \left(\hat{\Sigma}(p^2)\right)_{m_D^2} + \left(\hat{\Sigma}(p^2)\right)_{m_D^4} + \dots \ . \tag{3.31}$$

where, $\left(\hat{\Sigma}(p^2)\right)_{m_D^0}$ is the first term in the expansion, i.e. $\mathcal{O}(\xi^0)$, $\left(\hat{\Sigma}(p^2)\right)_{m_D^2}$ is the next term, i.e.$\mathcal{O}(\xi^2)$, $\left(\hat{\Sigma}(p^2)\right)_{m_D^4}$ is the term of $\mathcal{O}(\xi^4)$, etc. It should be noticed that there are no terms with odd powers of ξ. The first term in this expansion is precisely the pure gauge contribution, $\left(\hat{\Sigma}(p^2)\right)_{m_D^0} = \hat{\Sigma}(p^2)|_{\rm gauge}$. Therefore, it approximates the result in the MSSM and the rest approximates the Yukawa part,

$$\begin{aligned} \left(\hat{\Sigma}(p^2)\right)_{\rm MSSM} &\simeq \left(\hat{\Sigma}(p^2)\right)_{m_D^0} \ , \\ \left(\hat{\Sigma}(p^2)\right)_{\rm Yukawa} &\simeq \left(\hat{\Sigma}(p^2)\right)_{m_D^2} + \left(\hat{\Sigma}(p^2)\right)_{m_D^4} + \dots \ . \end{aligned} \tag{3.32}$$

In order to get simple formulas, we have expanded in addition each term in the series in Eq. (3.31) in powers of the other small dimensionless parameters, namely, M_Z/m_M, M_A/m_M, p/m_M and $m_{\rm SUSY}/m_M$.

The result of the previous seesaw expansion (we just show the leading terms; terms suppressed by factors $1/m_M^2$ respect to these leading ones are not relevant and, therefore, are not included) for each of the three considered renormalization schemes is as follows.

$\mathcal{O}(m_D^0)$

$$\left(\hat{\Sigma}_{hh}^{\overline{\rm DR}}(p^2)\right)_{m_D^0} = \frac{g^2 M_Z^2 \sin^2(\alpha+\beta)}{1152 c_{\rm w}^2 m_{\rm SUSY}^2 \pi^2}\Big[-20m_{\rm SUSY}^2 + 3p^2 + 12m_{\rm SUSY}^2 \log\frac{M_Z^2}{m_{\rm SUSY}^2}\Big] \tag{3.33a}$$

$$\left(\hat{\Sigma}_{hh}^{\rm m\overline{DR}}(p^2)\right)_{m_D^0} = \left(\hat{\Sigma}_{hh}^{\overline{\rm DR}}(p^2)\right)_{m_D^0} \tag{3.33b}$$

$$\begin{aligned}\left(\hat{\Sigma}_{hh}^{\rm OS}(p^2)\right)_{m_D^0} &= \left(\hat{\Sigma}_{hh}^{\overline{\rm DR}}(p^2)\right)_{m_D^0} + \frac{g^2 M_Z^2}{3072 c_{\rm w}^2 m_{\rm SUSY}^2 \pi^2}\Big[4\left(p^2 - m_h^2\right)(\cos 2\alpha \cos 2\beta - 1) \\ &\quad + \sec 2\alpha \sin 2\beta \left(M_A^2(\sin 4\beta - \sin 4\alpha) - M_Z^2 \sin 4(\alpha+\beta)\right)\Big]\end{aligned} \tag{3.33c}$$

$\mathcal{O}(m_D^2)$

$$\begin{aligned}\left(\hat{\Sigma}_{hh}^{\overline{\rm DR}}(p^2)\right)_{m_D^2} &= \frac{g^2 m_D^2}{64\pi^2 M_W^2 \sin^2\beta}\left[1 - \log\frac{m_M^2}{\mu_{\overline{\rm DR}}^2}\right]\big[-2M_A^2 \cos^2(\alpha-\beta)\cos^2\beta \\ &\quad + 2p^2\cos^2\alpha - M_Z^2 \sin\beta \sin(\alpha+\beta)\left(2\left(1+\cos^2\beta\right)\cos\alpha - \sin 2\beta \sin\alpha\right)\big]\end{aligned} \tag{3.34a}$$

$$\left(\hat{\Sigma}_{hh}^{\rm m\overline{DR}}(p^2)\right)_{m_D^2} = \left(\hat{\Sigma}_{hh}^{\overline{\rm DR}}(p^2)\right)_{m_D^2}\Big|_{\mu_{\overline{\rm DR}}=m_M} \tag{3.34b}$$

$$\begin{aligned}\left(\hat{\Sigma}_{hh}^{\rm OS}(p^2)\right)_{m_D^2} &= \frac{g m_D^2}{768\pi^2 M_W^2 p^2 m_M^2}\Big[12m_{\rm SUSY}^2\Big[M_A^2 p^2\left(2\cos^2(\alpha-\beta)\cot^2\beta - \cot\beta\sin 2(\alpha-\beta)\right) \\ &\quad - 2m_h^2 p^2\cos^2\alpha\csc^2\beta - 4M_Z^2 p^2\cos\alpha\csc\beta\sin(\alpha+\beta) + 4M_Z^4\sin^2(\alpha+\beta) \\ &\quad + 2M_Z^2 p^2\sin^2(\alpha+\beta) - M_Z^2 p^2\cot\beta\sin 2(\alpha+\beta) - 4M_Z^2 p^2\sin^2(\alpha+\beta)\log\frac{M_Z^2}{m_M^2} \\ &\quad + 4M_Z^4\sin^2(\alpha+\beta)\log\frac{p^2}{m_M^2} - \log\frac{m_{\rm SUSY}^2}{m_M^2}\Big[2m_h^2 p^2\cos^2\alpha\csc^2\beta + 4M_Z^4\sin^2(\alpha+\beta) \\ &\quad - M_Z^2 p^2\left(2\sin^2(\alpha+\beta) - \cot\beta\sin 2(\alpha+\beta) + 4\cos\alpha\csc\beta\sin(\alpha+\beta)\right) \\ &\quad + M_A^2 p^2\left(\cot\beta\sin 2(\alpha-\beta) - 2\cot^2\beta\cos^2(\alpha-\beta)\right)\Big]\Big] \\ &\quad + p^2\Big[8M_A^4\cos^2(\alpha-\beta)\cot^2\beta + 8\cos^2\alpha\left(3M_Z^2\left(m_h^2 - p^2\right) + p^2\csc^2\beta\left(3m_h^2 - p^2\right)\right) \\ &\quad + 24M_Z^2 p^2\cos\alpha\csc\beta\sin(\alpha+\beta) + 12M_A^2 M_Z^2\cos^2\beta\cos 2\beta\sec 2\alpha \\ &\quad + 12M_Z^4\sin^2(\alpha+\beta)(-1 + 2\log\frac{M_Z^2}{p^2}) + 3\cot\beta\Big[-2M_A^2 M_Z^2\sin 2\alpha \\ &\quad + 2\sec 2\alpha\Big[-M_A^2\sin 2(\alpha-\beta)\left(-M_A^2 + 2m_h^2 - M_Z^2 + M_A^2\cos 2\alpha\right)\end{aligned}$$

$$+ M_Z^2 \sin 2(\alpha+\beta)\left(M_A^2 - 2m_h^2 + M_Z^2 - M_A^2\cos 2\alpha - M_Z^2\cos 2(\alpha+\beta)\right)\Big]\Big]\Big] \tag{3.34c}$$

$\mathcal{O}(m_D^4)$

$$\begin{aligned}
\left(\hat{\Sigma}_{hh}^{\overline{\rm DR}}(p^2)\right)_{m_D^4} &= \frac{g^2 m_D^4}{128\pi^2 M_W^2 m_M^2 p^4}\Big[4M_Z^2p^2\left(p^2-M_Z^2\right)\log\frac{m_{\rm SUSY}^2}{m_M^2}\sin^2(\alpha+\beta) \\
&+ 8M_A^2p^4\cos^2(\alpha-\beta)\cot^2\beta\log\frac{M_A^2}{m_M^2} + 4\left(2m_{\rm SUSY}^2-3M_Z^2\right)p^4\sin^2(\alpha+\beta)\log\frac{M_Z^2}{m_M^2} \\
&+ 8p^4\csc^2\beta\big[M_A^2\cos^2\beta\cos^2(\alpha-\beta) - p^2\cos^2\alpha\big] \\
&+ 8M_Z^2\sin(\alpha+\beta)p^4\big[2\cos\alpha\csc\beta - \sin(\alpha+\beta)\big] \\
&+ 4m_{\rm SUSY}^2\log\frac{m_{\rm SUSY}^2}{m_M^2}\big[p^4\left(-1+\cos 2(\alpha+\beta) - 4\cos^2\alpha\csc^2\beta\right) \\
&+ 8M_Z^2p^2\cos\alpha\csc\beta\sin(\alpha+\beta) - 2M_Z^4\sin^2(\alpha+\beta)\big] \\
&- 4\log\frac{p^2}{m_M^2}\big[2p^6\cos^2\alpha\csc^2\beta + 4M_Z^2p^2\left(2m_{\rm SUSY}^2-p^2\right)\cos\alpha\csc\beta\sin(\alpha+\beta) \\
&- M_Z^4\sin^2(\alpha+\beta)\left(2m_{\rm SUSY}^2+p^2\right)\big] - 8m_{\rm SUSY}^2\big[2p^4\cos^2\alpha\csc^2\beta \\
&+ 4M_Z^2p^2\cos\alpha\csc\beta\sin(\alpha+\beta) + \sin^2(\alpha+\beta)\left(M_Z^4-p^4\right)\big]\Big] \qquad (3.35a)
\end{aligned}$$

$$\left(\hat{\Sigma}_{hh}^{\rm m\overline{DR}}(p^2)\right)_{m_D^4} = \left(\hat{\Sigma}_{hh}^{\overline{\rm DR}}(p^2)\right)_{m_D^4} \tag{3.35b}$$

$$\begin{aligned}
\left(\hat{\Sigma}_{hh}^{\rm OS}(p^2)\right)_{m_D^4} &= \left(\hat{\Sigma}_{hh}^{\overline{\rm DR}}(p^2)\right)_{m_D^4} + \frac{g^2m_D^4}{32\pi^2M_W^2m_M^2}\Big[\cot\beta\sec 2\alpha\sin^2\alpha\big[M_A^2\sin 2(\alpha-\beta) \\
&+ M_Z^2\sin 2(\alpha+\beta)\big]\Big[2+\log\frac{m_H^2}{m_M^2}\Big] - \cos^2\alpha\Big[2+\log\frac{m_h^2}{m_M^2}\Big]\big[2(m_h^2-p^2)\csc^2\beta \\
&+ \cot\beta\sec 2\alpha\big[M_A^2\sin 2(\alpha-\beta) + M_Z^2\sin 2(\alpha+\beta)\big]\big]\Big] \qquad (3.35c)
\end{aligned}$$

From these formulas the qualitatively different behavior of the renormalized Higgs-boson self-energies on the Majorana mass scale m_M can be understood. The main difference between the OS scheme and the $\overline{\rm DR}$/m$\overline{\rm DR}$ schemes appears in the Yukawa part, especially in the term of $\mathcal{O}(m_D^2)$. At the various orders the comparison of the three schemes is given as follows.

At the leading order in the seesaw expansion, $\mathcal{O}(m_D^0)$ in Eq. (3.33), the results in the $\overline{\rm DR}$ and m$\overline{\rm DR}$ schemes coincide. This is indeed a consequence of the fact that, at this order, $\hat{\Sigma}_{hh}^{\overline{\rm DR}}(p^2)$ turns out to be $\mu_{\overline{\rm DR}}$ independent. The result in the OS scheme differs from these

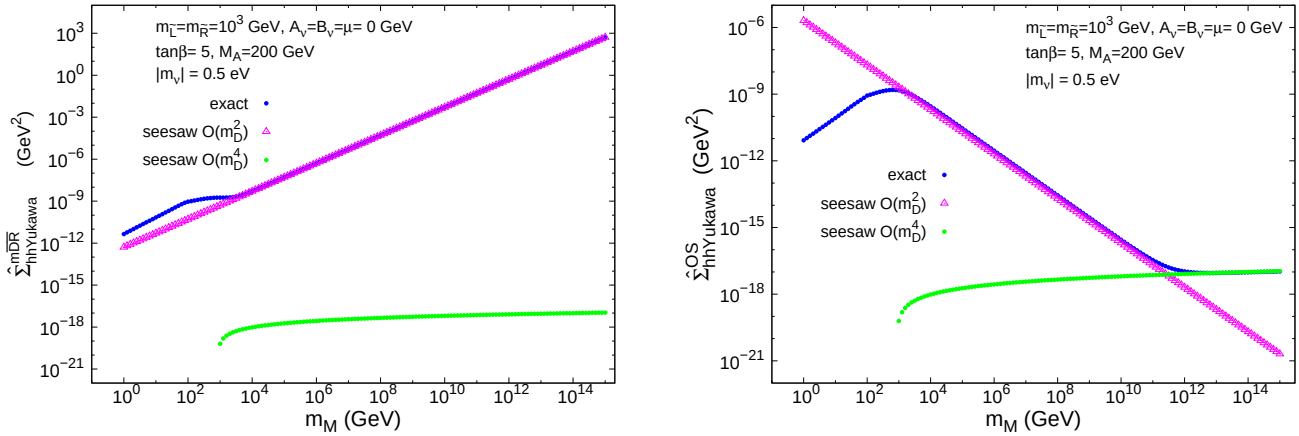

Figure 3.3: Comparison between the predictions from the seesaw expansion and the exact results for the Yukawa part. Left panel: m$\overline{\text{DR}}$ scheme. Right panel: OS scheme. In both panels, $p^2 = (116\ \text{GeV})^2$.

later by a term of order $g^2 M_Z^2 M_{\text{EW}}^2/m_{\text{SUSY}}^2$, where M_{EW}^2 refers generically to the involved masses of the order of the electroweak scale, i.e., M_A^2, p^2, M_Z^2, $m_{h\,\text{tree}}^2$. Furthermore, this difference turns out to be numerically extremely small. This explains why, for low values of the Majorana scale, where the $\mathcal{O}(m_D^0)$ term of the expansion dominates, the predictions from the three schemes are nearly indistinguishable.

At the next order in the seesaw expansion, $\mathcal{O}(m_D^2)$ in Eq. (3.34), the OS result differs substantially from the $\overline{\text{DR}}$ and m$\overline{\text{DR}}$ schemes. First, the OS result is extremely suppressed with respect to the $\overline{\text{DR}}$ and m$\overline{\text{DR}}$ results at large m_M. This is due to the fact that the leading contribution, i.e. of the order of $g^2 m_D^2 M_{\text{EW}}^2/M_Z^2$, vanishes in the OS whereas it is present in the other schemes. As can be seen in Eq. (3.34), the first non vanishing contribution contains an extra factor $\sim m_{\text{SUSY}}^2/m_M^2$ which can be extremely small for $m_M \gg m_{\text{SUSY}}$. This remarkable difference of the OS result has its origin in the different values of the δZ_{hh} and $\delta \tan\beta$ counterterms. More specifically, by computing their finite parts in the OS scheme and in the seesaw limit, we get

$$\delta^{\text{OS}} Z_{hh}|_{\text{finite}} = -\frac{g^2 m_D^2 \cos^2\alpha}{32 c_{\text{w}}^2 M_Z^2 \pi^2 \sin^2\beta}\left[1 - \log\frac{m_M^2}{\mu_{\overline{\text{DR}}}^2}\right] + \mathcal{O}\left(\frac{M_{\text{EW}}^2, m_{\text{SUSY}}^2}{m_M^2}\right), \tag{3.36}$$

$$\delta^{\text{OS}} \tan\beta|_{\text{finite}} = -\frac{g^2 m_D^2}{64 c_{\text{w}}^2 M_Z^2 \pi^2 \sin^2\beta}\left[1 - \log\frac{m_M^2}{\mu_{\overline{\text{DR}}}^2}\right] + \mathcal{O}\left(\frac{M_{\text{EW}}^2, m_{\text{SUSY}}^2}{m_M^2}\right). \tag{3.37}$$

These finite contributions lead to the cancellation of the above commented leading contributions.

In the $\overline{\rm DR}$ scheme, we get an explicit logarithmic dependence on m_M, concretely as $-\log(m_M^2/\mu^2_{\overline{\rm DR}})$. By construction this term is absent in the m$\overline{\rm DR}$ result. Therefore, the main difference between these two schemes $\overline{\rm DR}$ and m$\overline{\rm DR}$ is this logarithmic contribution that can be sizeable for $m_M \gg \mu_{\overline{\rm DR}}$.

The results at the next to next order in the seesaw expansion, $\mathcal{O}(m_D^4)$ in Eq. (3.35), show that they all go (leaving apart the logarithms) as $g^2 m_D^4 (M^2_{\rm EW}, m^2_{\rm SUSY})/(M_Z^2 m_M^2)$. Therefore the $\mathcal{O}(m_D^4)$ terms are extremely suppressed in the three schemes, and consequently they are not relevant in the large m_M regime.

All the above commented analytical features of the seesaw expansion have also been checked numerically, as it is illustrated in Figure 3.3. In this figure we show separately the $\mathcal{O}(m_D^2)$ and $\mathcal{O}(m_D^4)$ contributions and the exact Yukawa prediction in both the m$\overline{\rm DR}$ (left plot) and OS scheme (right plot).[2] One clearly observes the dominance of the $\mathcal{O}(m_D^2)$ over the $\mathcal{O}(m_D^4)$ in the m$\overline{\rm DR}$ scheme by many orders of magnitude in the full explored m_M range. One also sees that the $\mathcal{O}(m_D^2)$ result approximates extremely well the exact Yukawa result for $m_M \gtrsim 10^4$ GeV. In contrast, in the OS scheme, the $\mathcal{O}(m_D^2)$ term dominates just up to about $m_M = 10^{10}$ GeV, but then for larger values the $\mathcal{O}(m_D^4)$ dominates. In this plot it is also manifested that the exact Yukawa result in the OS is well approximated by the $\mathcal{O}(m_D^2)$ term in the interval 10^3 GeV $< m_M < 10^{11}$ GeV and by the $\mathcal{O}(m_D^4)$ term for $m_M > 10^{12}$ GeV. At this large values, however, the size of the correction is extremely small (below 10^{-17} GeV^2), hence, irrelevant. It is also clear from this plot that the numerical results for the $\mathcal{O}(m_D^4)$ contributions are similar in the three schemes.

From the definition of the three renormalization schemes, see Sect. 3.1.3, and our analytical and numerical analysis in this section we conclude that the m$\overline{\rm DR}$ scheme is best suited for higher-order calculations in MSSM-seesaw model. The other two schemes can lead to unphysically large corrections at the one-loop level. We will focus in the following on this scheme, and the numerical evaluation of $M_h^{\nu/\tilde{\nu}}$, see Sect. 3.2.3, will be performed solely in this "preferred" scheme.

Finally, in this context, we discuss the decoupling or non-decoupling behavior of the

[2]It should be kept in mind that due to the different renormalization of $\tan\beta$ the meaning of this input parameter is different in OS and in the m$\overline{\rm DR}$ scheme. In order to perform a real numerical comparison a transition from $\tan\beta \equiv \tan\beta^{\rm m\overline{DR}} \to \tan\beta^{\rm OS}$ would have to be performed. However, here we are interested in the qualitative behavior and we do not consider this shift.

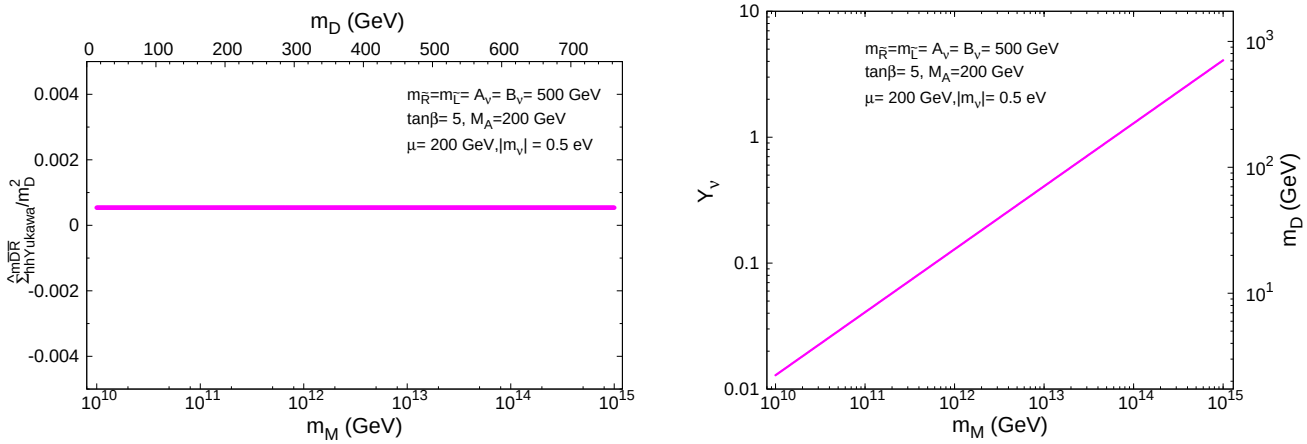

Figure 3.4: Left panel: Decoupling/Non-decoupling behavior of the one-loop neutrino/sneutrino corrections to the renormalized lightest Higgs boson self-energy at large m_M in the m$\overline{\text{DR}}$ scheme. Right panel: Dependence of the neutrino Yukawa coupling (and m_D) with m_M.

neutrino/sneutrino one-loop radiative corrections with the Majorana scale. According to Figs. 3.2 and 3.3, the Yukawa part of the renormalized self-energy in the m$\overline{\text{DR}}$ scheme grows with m_M. However, this does not constitute by itself a proof of non-decoupling of m_M in the radiative corrections to $\hat{\Sigma}_{hh}^{\text{m}\overline{\text{DR}}}$ for asymptotically large m_M. To analyze this question, we have to investigate separately the behaviors of $\hat{\Sigma}_{hh}^{\text{m}\overline{\text{DR}}}$ and m_D with m_M, since in the way the seesaw mechanism is implemented here, as we have mentioned before, m_D (or equivalently Y_ν) is not an input but an output and it grows proportional to $\sqrt{m_M}$. To analyze these two behaviors separately we show in the left plot of Figure 3.4 the ratio $(\hat{\Sigma}_{hh}^{\text{m}\overline{\text{DR}}})_{\text{Yukawa}}/m_D^2$ versus m_M (and m_D), and in the right plot we show the predictions of the Yukawa coupling (and m_D) as a function of m_M. The latter one exhibits the (trivial) result of $Y_\nu \propto \sqrt{m_M}$ as expected. In the left plot a constant behavior of the ratio $(\hat{\Sigma}_{hh}^{\text{m}\overline{\text{DR}}})_{\text{Yukawa}}/m_D^2$ is clearly manifested, which means that the growing of $(\hat{\Sigma}_{hh}^{\text{m}\overline{\text{DR}}})_{\text{Yukawa}}$ with m_M is exclusively due to the growing of Y_ν (or m_D) with m_M. However, still this ratio turns out to be non-vanishing for asymptotically large m_M, and constant with m_D, as can be seen in Figure 3.4. Therefore, a non-decoupling constant behavior must be concluded in the Majorana case from all this discussion. This constant, on the other hand, is very well approximated by the coefficient multiplying the factor m_D^2 in the $\hat{\Sigma}_{hh}^{\text{m}\overline{\text{DR}}}(p^2)_{m_D^2}$ result of Eq. (3.34).

In order to understand this issue better, we compare this analytical result, showing a constant behaviour of the renormalized Higgs boson self-energy in the $m_M \to \infty$ limit when Y_ν is kept fixed, with the corresponding result in the Dirac case. For simplification in this analytical comparison we focus just on the $\mathcal{O}(p^2 m_D^2)$ terms and use the electroweak basis for neutrinos and sneutrinos[3]. The results at $\mathcal{O}(p^2 m_D^2)$ for the renormalized self-energies in the $\overline{\rm DR}$ scheme for the Majorana and Dirac cases are:

$$\begin{aligned}\hat{\Sigma}_{hh}^{\rm Majorana,\overline{DR}}(p^2) &= \frac{g^2 m_D^2 p^2 \cos^2\alpha}{32\pi^2 M_W^2 \sin^2\beta}\left(\frac{1}{2} - \log\frac{m_M^2}{\mu^2_{\overline{\rm DR}}}\right) \\ &\quad + \frac{g^2 m_D^2 p^2 \cos^2\alpha}{64\pi^2 M_W^2 \sin^2\beta} \qquad (3.38)\\ \hat{\Sigma}_{hh}^{\rm Dirac,\overline{DR}}(p^2) &= \frac{g^2 m_D^2 p^2 \cos^2\alpha}{32\pi^2 M_W^2 \sin^2\beta}\left(2 - \log\frac{p^2}{\mu^2_{\overline{\rm DR}}}\right) \qquad (3.39)\end{aligned}$$

where the first and second lines in $\hat{\Sigma}_{hh}^{\rm Majorana,\overline{DR}}(p^2)$ are the contributions from neutrinos and sneutrinos respectively. It should be noticed that the $\mathcal{O}(p^2 m_D^2)$ sneutrino contributions come exclussively from the new couplings $g'_{h\tilde{\nu}_L\tilde{\nu}_R} = -\frac{igm_D m_M \cos\alpha}{2M_W \sin\beta}$, which are not present in the Dirac case. It should also be noticed that this result in the Majorana case translates into our $\mathcal{O}(p^2 m_D^2)$ term in (3.34a). The comparison of the two formulas shows that the result of the Majorana case for low momenta, $p^2 \ll m_M^2$, does not coincide with the result of the Dirac case.

From the right plot in Figure 3.4 we can also conclude on the range of m_M values where the neutrino Yukawa couplings get too large and potential non-perturbative. The concrete crossing line to set the perturbativity region is not uniquely defined, but it should be considered around $Y_\nu \sim \mathcal{O}(1)$. For instance, by setting the crossing at $Y_\nu^2/(4\pi) = 1.5$ ($Y_\nu = 4.34$) we get perturbativity for $m_M < 10^{15}$ GeV, and by setting it at $Y_\nu = 1.5$ it is got for $m_M < 10^{14}$ GeV. In the following of this subsection we set $m_M = 10^{14}$ GeV as our reference value.

Dependence on $\tan\beta$, M_A, μ, $m_{\tilde{L}}$, $m_{\tilde{R}}$, A_ν, m_ν, B_ν and p

The behavior of the renormalized self-energy in the m$\overline{\rm DR}$ scheme with the other parameters entering in this computation are shown in Figs. 3.5 - 3.10. In all these plots we have included separately the gauge, Yukawa and total results for comparison.

[3]The computation in this case reduces to just the evaluation of one type of loop diagrams, the sunset diagrams, 2nd and 5th in Figure 3.1.

First, the behavior with $\tan\beta$ is analyzed in the left plot of Figure 3.5. It exhibits basically the expected features that can be inferred from the loop corrections of an up-type fermion/sfermion. The neutrino/sneutrino one-loop radiative corrections reach their maximum value at the lowest considered value of $\tan\beta$, $\tan\beta = 2$ in this plot. For $\tan\beta > 5$ the dependence is nearly flat. There are no relevant differences between the behaviors with $\tan\beta$ of the Yukawa and the gauge parts. From now on, we will set $\tan\beta = 5$ as our reference value.

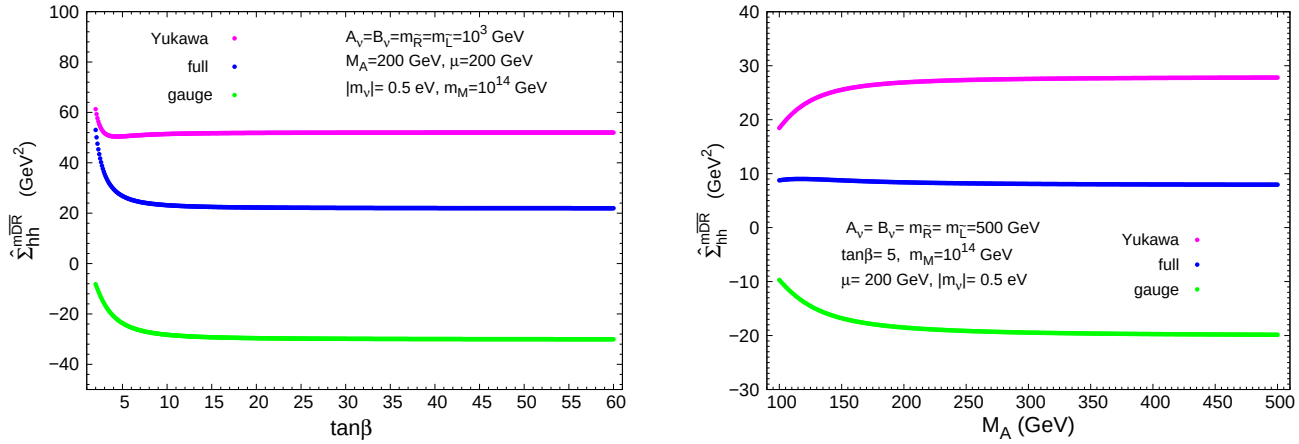

Figure 3.5: Left panel: $\hat{\Sigma}_{hh}^{\mathrm{m}\overline{\mathrm{DR}}}(p^2)$ as a function of $\tan\beta$. Right panel: $\hat{\Sigma}_{hh}^{\mathrm{m}\overline{\mathrm{DR}}}(p^2)$ as a function of M_A. In the left (right) panel, $p^2 = (116\ \mathrm{GeV})^2$ ($p^2 = (105\ \mathrm{GeV})^2$).

The behavior with M_A is displayed in the right panel of Fig.3.5. Again we see no relevant differences with respect to the well known behavior in the MSSM. For M_A larger that 150 GeV the total contribution from the neutrino/sneutrino sector to the renormalized self-energy is nearly flat with M_A. In the following we will take $M_A = 200$ GeV as our reference value.

The dependence with the soft SUSY breaking mass of the 'left handed' $SU(2)$ doublet, $m_{\tilde{L}}$, is shown in Figure 3.6. We see that the gauge contribution is negative and increases in modulus with increasing $m_{\tilde{L}}$, whereas the Yukawa contribution is positive and nearly insensitive to changes of $m_{\tilde{L}}$ in the investigated interval, $10^2\ \mathrm{GeV} < m_{\tilde{L}} < 10^4\ \mathrm{GeV}$. The total neutrino/sneutrino corrections, at these selected values of the model parameters, are positive and decreasing with $m_{\tilde{L}}$ for $10^2\ \mathrm{GeV} < m_{\tilde{L}} < 2\times 10^3\ \mathrm{GeV}$ and then become negative and increasing in modulus with $m_{\tilde{L}}$ for $2\times 10^3\ \mathrm{GeV} < m_{\tilde{L}} < 10^4\ \mathrm{GeV}$.

The behavior with the soft SUSY breaking parameter of the 'right handed' sector $m_{\tilde{R}}$

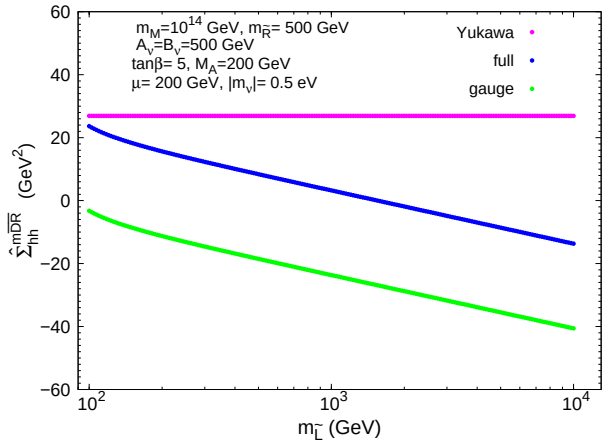

Figure 3.6: $\hat{\Sigma}_{hh}^{\mathrm{m}\overline{\mathrm{DR}}}(p^2)$ as a function of $m_{\tilde{L}}$; we have set $p^2 = (105\ \mathrm{GeV})^2$.

is shown in Figure 3.7. In the left plot a mass scale similar to the other soft SUSY-breaking parameters is investigated, whereas in the right plot values of $m_{\tilde{R}}$ closer to m_M are explored. It should be reminded that these values are not constrained by data. An interesting feature can be observed at large values of $m_{\tilde{R}}$. The contributions to the renormalized self-energy stay flat up to about $m_{\tilde{R}} \sim 10^{13}$ GeV. Above this mass scale the Yukawa part grows rapidly, reaching very large values at $m_{\tilde{R}} \sim 10^{14}$ GeV of around $\hat{\Sigma}_{hh}^{\mathrm{m}\overline{\mathrm{DR}}} \sim 7000\ \mathrm{GeV}^2$.

The behavior with the new soft SUSY-breaking trilinear coupling A_ν is shown in the left plot of Figure 3.8. The full result, the gauge, and Yukawa parts are nearly independent on this parameter in the studied interval, $-1000\ \mathrm{GeV} < A_\nu < 1000\ \mathrm{GeV}$. Although not shown explicitly, we have also studied the behavior with μ and got the same 'flat' behavior for $-1000\ \mathrm{GeV} < \mu < 1000\ \mathrm{GeV}$. This justifies our choice $A_\nu = \mu = 0$ in our seesaw expansion above.

The behavior with the lightest neutrino mass, m_ν, is demonstrated in the right plot of Figure 3.8. One can see that the Yukawa part is quite sensitive to this mass that we have varied in a plausible and compatible with data range. The growing of the result with $|m_\nu|$, for fixed m_M, is the consequence of the growing of Y_ν (or m_D) with $|m_\nu|$ since in this model they are correlated, as shown in (2.61) and (2.62).

The behavior with B_ν is analyzed in Figure 3.9. We have found a flat result with this new soft parameter for most of the explored range, except at very large values,

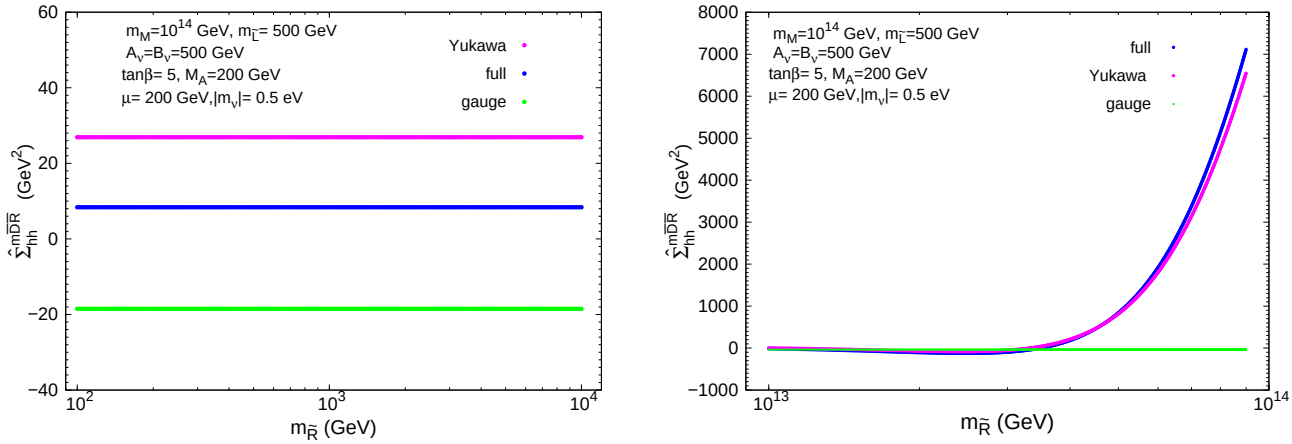

Figure 3.7: $\hat{\Sigma}^{\mathrm{m}\overline{\mathrm{DR}}}_{hh}(p^2)$ as a function of $m_{\tilde{R}}$. Left panel: low mass values 10^2 GeV $< m_{\tilde{R}} < 10^4$ GeV. Right panel: high mass values 10^{13} GeV $< m_{\tilde{R}} < 10^{14}$ GeV. In both panels we have set $p^2 = (105 \text{ GeV})^2$.

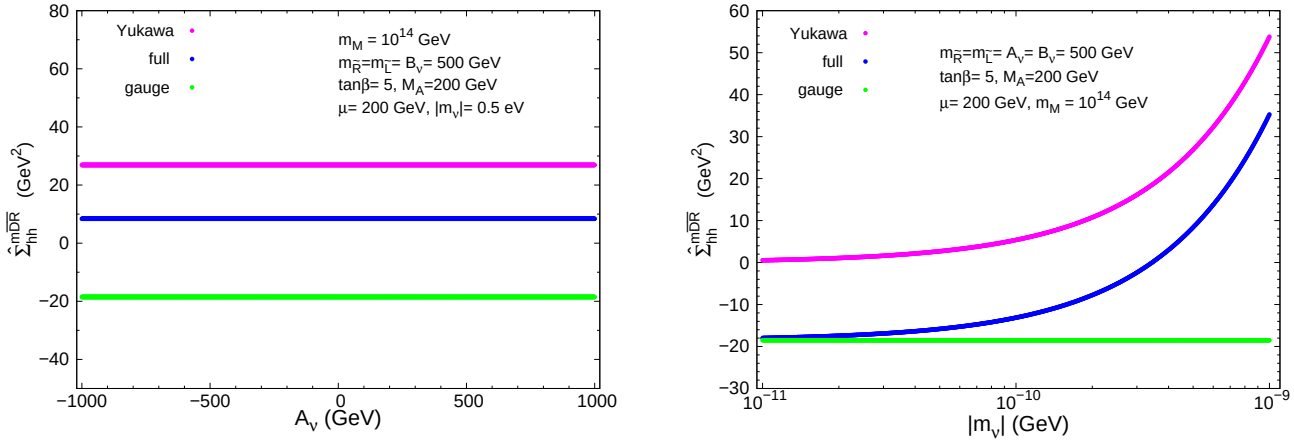

Figure 3.8: Left panel: $\hat{\Sigma}^{\mathrm{m}\overline{\mathrm{DR}}}_{hh}(p^2)$ as a function of A_ν. Right panel: $\hat{\Sigma}^{\mathrm{m}\overline{\mathrm{DR}}}_{hh}(p^2)$ as a function of $|m_\nu|$. In both panels we have set $p^2 = (105 \text{ GeV})^2$.

$B_\nu > 10^{12}$ GeV, as shown in the right plot. For these large values the Yukawa part grows noticeably with B_ν and dominates largely the total result, leading to large radiative corrections. For instance, for the parameters chosen in this figure and $B_\nu = 10^{13}$ GeV, we found $\hat{\Sigma}^{\mathrm{m}\overline{\mathrm{DR}}}_{hh} \sim 2400$ GeV^2. The question whether such large values of B_ν are realistic depends on the particular models and universality conditions. However, such an analysis

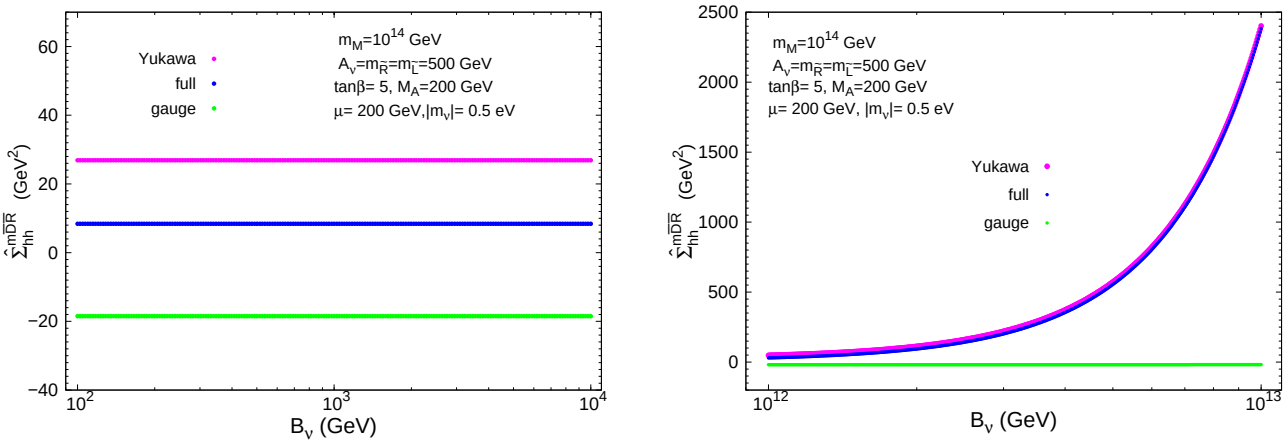

Figure 3.9: $\hat{\Sigma}_{hh}^{\mathrm{mDR}}(p^2)$ as a function of B_ν. Left panel: low B_ν values, 10^2 GeV $< B_\nu <$ 10^4 GeV. Right panel: high B_ν values, 10^{12} GeV $< B_\nu < 10^{13}$ GeV. In both panels we have set $p^2 = (105\ \mathrm{GeV})^2$.

is beyond the scope of our work. On the other hand, if we apply the bounds that are imposed in order to avoid destabilizing the electroweak symmetry breaking [145], leading to $B_\nu Y_\nu^2/(8\pi^2) < m_{\mathrm{SUSY}}/\tan\beta$, one gets an upper limit on B_ν. For $Y_\nu \sim 1$, $m_{\mathrm{SUSY}} \sim$ 1000 GeV and $\tan\beta \sim 5$ one finds $B_\nu < 1.6 \times 10^4$ GeV. For this range the renormalized Higgs-boson self-energy is nearly independent of B_ν. From now on, we will choose $B_\nu =$ 500 GeV as our reference value.

Finally, we show in Figure 3.10 the behavior with p^2, the square of the external momentum of the Higgs boson self-energies, which is a relevant issue for the discussion of the radiative corrections to the Higgs-boson masses (see the next subsection). The three renormalized self-energies, $\hat{\Sigma}_{hh}$, $\hat{\Sigma}_{HH}$ and $\hat{\Sigma}_{hH}$, are clearly dependent on p^2, but the most sensitive one is $\hat{\Sigma}_{hh}$. It is clear from this figure that setting $p^2 = 0$ in the renormalized self-energies does not provide a good approximation for the estimate of the radiative corrections to the Higgs boson mass from the neutrino/sneutrino sector in the present case of Majorana neutrinos. One can also see that mainly the Yukawa part is responsible for this sensitivity to p^2. Setting the proper p^2 in order to estimate realistically the Higgs mass corrections will be discussed in the next subsection.

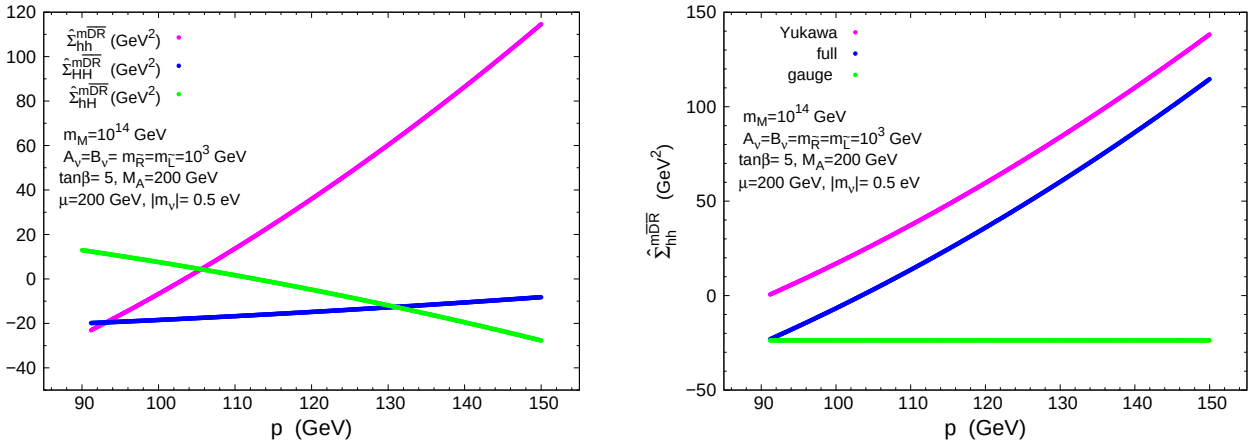

Figure 3.10: Left panel: $\hat{\Sigma}^{\overline{\rm mDR}}_{hh}(p^2)$, $\hat{\Sigma}^{\overline{\rm mDR}}_{hh}(p^2)$ and $\hat{\Sigma}^{\overline{\rm mDR}}_{hh}(p^2)$ as a function of the external momentum p. Right panel: the two contributions $\hat{\Sigma}^{\overline{\rm DR}}_{hh}(p^2)_{\rm gauge}$ $\hat{\Sigma}^{\overline{\rm DR}}_{hh}(p^2)_{\rm Yukawa}$ and the full result are shown separately.

The Dirac case

Finally, we perform a comparison between the case of massive Majorana neutrinos (as analyzed so far) and the case of Dirac neutrinos. In order to analyze the Dirac case, we have computed the one-loop neutrino/sneutrino contributions to the renormalized lightest Higgs boson self-energy for $m_M = 0$. The analytical results for this Dirac case are collected in Appendix C. We have chosen here the $\overline{\rm DR}$ scheme, since due to the absence of m_M no large logarithmic corrections are expected, and a comparison to existing calculations can readily be performed. First, we have checked the finiteness of the result. Second, we have also checked that the obtained formulas agree with the well known result of the one-loop radiative corrections from other massive fermion/sfermion sectors of the MSSM, with the obvious corresponding changes of fermion/sfermion parameters and quantum numbers. In particular, it can be seen that the formulas in Appendix C coincide with the one-loop corrections from the MSSM top/stop sector by replacing, correspondingly, the neutrino $SU(2) \times U(1)$ quantum numbers by the top quark ones, m_D by m_t, $m_{\tilde{\nu}_\pm}$ $(= m_{\tilde{\nu}_1})$ by $m_{\tilde{t}_1}$, $m_{\tilde{N}_\pm}$ $(= m_{\tilde{\nu}_2})$ by $m_{\tilde{t}_2}$, $\theta_\pm$ $(= \tilde{\theta})$ by $\tilde{\theta}_t$ and by adding the proper color factor, $N_C = 3$.

As for the numerical estimate, we present in Fig.3.11 the result of the Yukawa contributions from the one-loop neutrino/sneutrino radiative corrections to the renormalized self-energy, $(\hat{\Sigma}^{\rm Yukawa}_{hh})_{\rm Dirac}$, as a function of the physical neutrino mass, $|m_\nu| = m_D$. The

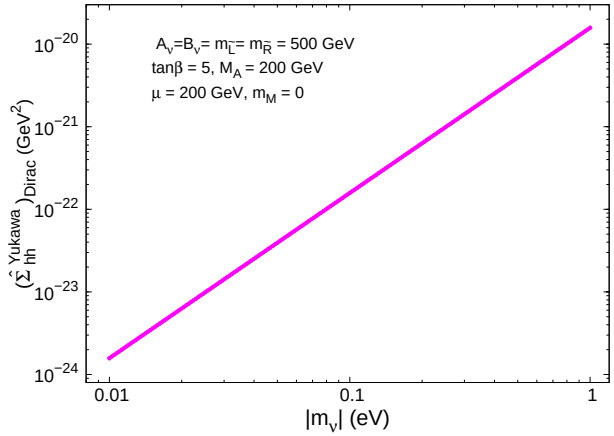

Figure 3.11: One-loop corrections to the Yukawa part of the lightest Higgs boson renormalized self-energy from the neutrino/sneutrino sector in the case of massive Dirac neutrinos

regularization scale has been fixed here to $\mu_{\overline{\rm DR}} = 100$ GeV and the external momentum to $p = 116$ GeV. As in the Majorana case, we consider an interval for the neutrino mass inspired by experimental data, 0.01 eV $\lesssim |m_\nu| \lesssim$ 1 eV. In this plot we see clearly that, as expected, these Yukawa contributions are extremely small (below 10^{-20} GeV^2) and are fully dominated by the gauge part which we have also estimated, for the chosen parameters in this plot, leading to $(\hat{\Sigma}^{\rm gauge}_{hh})_{\rm Dirac} = -18.5\,{\rm GeV}^2$. Notice that this gauge part is similar in both Majorana and Dirac cases, as can be seen in the right plot of Fig.3.8. In summary, the radiative corrections from the massive neutrinos/sneutrinos in the Dirac case are phenomenologically irrelevant and therefore this case is totally indistinguishable from the MSSM with massless neutrinos.

3.2.3 Estimate of the one-loop corrections from neutrino/sneutrino sector to M_h within the MSSM-seesaw

Our final aim is to find out to what extent the radiative corrections computed here enter into the measurable range. The experimental perspectives for the Higgs mass measurements with precision enough to be sensitive to such sizeable radiative corrections, as the ones found here, are indeed quite promising. The LHC has good prospects to discover at least one neutral Higgs boson over the full MSSM parameter space and a precision on the mass of a Standard Model (SM)-like Higgs boson of ~ 200 MeV are expected [68–71]

(see e.g. [165, 166] for reviews). At the ILC a determination of the Higgs boson properties (within the kinematic reach) will be possible, and an accuracy on the mass could reach the 50 MeV level [72–75]. The interplay of the LHC and the ILC in the neutral MSSM Higgs sector will improve certainly these measurements [167, 168].These experimental precisions set the goal for the theoretical accuracies. For the estimates of the total corrections to M_h in the MSSM-seesaw, obviously, the one-loop corrections from the neutrino/sneutrino sector that we have calculated have to be added to the existing MSSM corrections.

As outlined in Sect. 3.1.2 the higher-order corrected light MSSM Higgs-boson mass is obtained as a pole from Eq. (3.5), i.e. where $p^2 = M_h^2$. A realistic evaluation requires to take into account all known higher-order corrections to the renormalized Higgs-boson self-energies [169]. In order to simplify our analysis, but to maintain the high accuracy we follow a slightly different strategy. For a given set of SUSY parameters we first calculate M_h and M_H in the MSSM with the help of `FeynHiggs` [76, 160, 170, 171]. In this way all relevant known higher-order corrections are included, but no $\nu/\tilde{\nu}$ contributions are taken into account yet. This corresponds to a 'diagonalization' of the $\mathcal{CP}$-even Higgs sector in the MSSM without heavy Majorana (s)neutrinos. In a second step we search for the poles of

$$\left[p^2 - M_h^2 + \hat{\Sigma}_{hh}^{\nu/\tilde{\nu}}(M_h^2)\right]\left[p^2 - M_H^2 + \hat{\Sigma}_{HH}^{\nu/\tilde{\nu}}(M_h^2)\right] - \left[\hat{\Sigma}_{hH}^{\nu/\tilde{\nu}}(M_h^2)\right]^2 = 0 \ , \tag{3.40}$$

where, $\hat{\Sigma}_{hh,HH,hH}^{\nu/\tilde{\nu}}$ denote the full corrections to the renormalized Higgs-boson self-energies from the $\nu/\tilde{\nu}$ sector, obtained in the m$\overline{\rm DR}$ scheme as described in the present work. The pole, the light Higgs mass including the $\nu/\tilde{\nu}$ corrections (i.e. in the MSSM-seesaw model), is denoted by $M_h^{\nu/\tilde{\nu}}$. This 're-diagonalization' now effectively takes into account the full result of the MSSM-seesaw. The momentum in the self-energies is fixed to the value M_h as obtained with `FeynHiggs`, since it is expected that the new contributions only give a relatively small correction to this M_h. In a more elaborate analysis the renormalized self-energies should be evaluated with free p^2. However, we expect only a very minor effect from fixing the external momentum to this value. In the near future the results of the new neutrino/sneutrino corrections will be implemented into the code `FeynHiggs`.

The numerical results for $\Delta m_h^{\rm m\overline{DR}} := M_h^{\nu/\tilde{\nu}} - M_h$ are summarized in Figs. 3.12 through 3.15. We have chosen here to explore the Higgs mass predictions as a function of just the most relevant model parameters which, according to our previous exhaustive analysis of the renormalized Higgs-boson self-energies, are going to provide the most interesting/sizeable corrections. These are: the Majorana mass m_M (or, equivalently, the heaviest physical Majorana neutrino mass m_N), the soft SUSY breaking parameters $m_{\tilde{R}}$ and B_ν and the

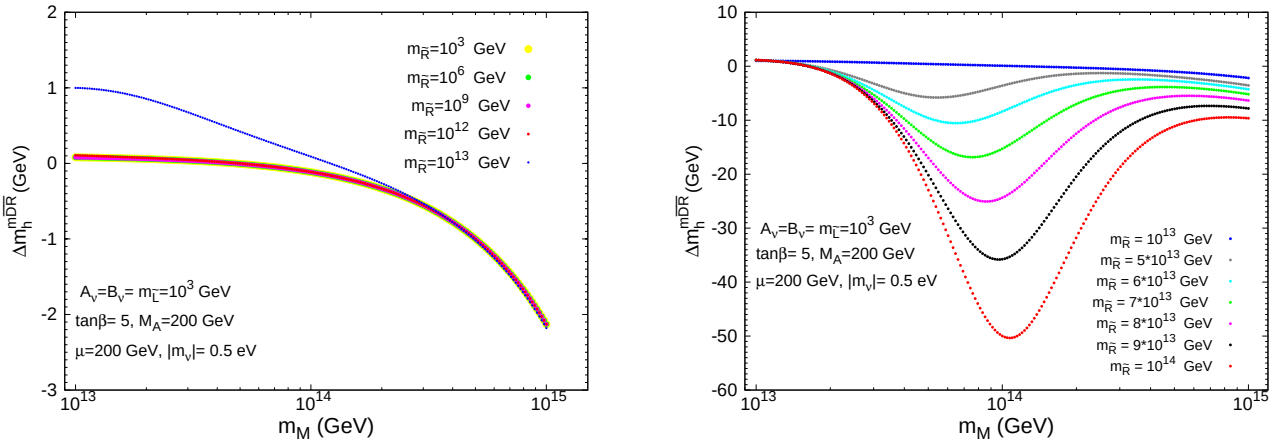

Figure 3.12: One-loop corrections to the lightest Higgs boson mass from the neutrino/sneutrino sector as a function of the heavy Majorana mass for various choices of the soft mass $m_{\tilde{R}}$. Left panel: $m_{\tilde{R}} < 10^{13}$ GeV. Right panel:10^{13} GeV $< m_{\tilde{R}} < 10^{14}$ GeV.

lightest physical Majorana neutrino mass m_ν. As for the numerical values of these relevant parameters, we focus here in the following intervals: 10^{13} GeV $\leq m_M \leq 10^{15}$ GeV, 0.1 eV $\leq |m_\nu| \leq 1$ eV, 10^3 GeV $\leq m_{\tilde{R}} \leq m_M$ and 10^3 GeV $\leq B_\nu \leq 4\times 10^{12}$ GeV. For the remaining model parameters, $\tan\beta$, M_A, μ, $m_{\tilde{L}}$ and A_ν, we choose here the same reference values as in the previous subsection. The corresponding predictions for other choices of the parameters can be easily inferred from our previous results of the renormalized self-energies.

In Fig. 3.12 we show the predictions for $\Delta m_h^{\overline{\rm mDR}}$ as a function of the Majorana mass m_M, for several input $m_{\tilde{R}}$ values. As a general feature, the Higgs mass corrections for the reference parameter values in the left plot are positive and below 0.1 GeV if $m_M \lesssim 5 \times 10^{13}$ GeV and $m_{\tilde{R}} < 10^{12}$ GeV. For larger Majorana mass values, the corrections get negative and grow up to a few GeV. For instance, $\Delta m_h^{\overline{\rm mDR}} = -2.15$ GeV for $m_M = 10^{15}$ GeV. The results in the right plot show that for larger values of the soft mass, $m_{\tilde{R}} \gtrsim 10^{13}$ GeV the Higgs mass corrections are negative and can be sizeable, a few tens of GeV, reaching their maximum values at $m_{\tilde{R}} \simeq m_M$. For instance, for $m_{\tilde{R}} = m_M = 10^{14}$ GeV we get a very large correction, $\Delta m_h^{\overline{\rm mDR}} = -50$ GeV. This last large negative value is in agreement with the prediction in Ref. [67] for the same corresponding input values of the parameters in their split SUSY scenario. It should be noticed that, in the case of such large corrections our approximation of Eq. (3.40) is not accurate enough to

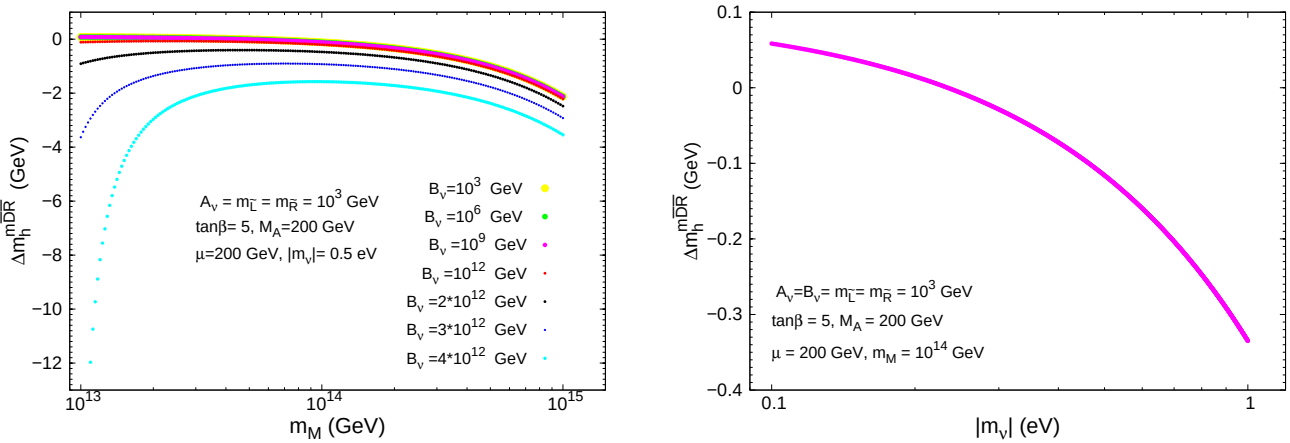

Figure 3.13: Left panel: One-loop corrections to the lightest Higgs boson mass from the neutrino/sneutrino sector as a function of the heavy Majorana mass, m_M, for various choices of the soft B-parameter, 10^3 GeV $< B_\nu < 4 \times 10^{12}$ GeV. Right panel: Dependence of the Higgs mass corrections with the lightest neutrino mass, $|m_\nu|$.

obtain a precise result for $M_h^{\nu/\tilde{\nu}}$. However, our method still yields an indication of the size of the corrections from the $\nu/\tilde{\nu}$ sector to M_h.

The behavior of the Higgs mass corrections as a function of the B_ν parameter is displayed in the left plot of Fig. 3.13. Again, $\Delta m_h^{\overline{\rm mDR}}$ gets negative and large for large B_ν, reaching the maximum size at $B_\nu \simeq m_M$. For instance, for the input model parameters in this plot, and $B_\nu = 4 \times 10^{12}$ GeV, $m_M = 10^{13}$ GeV, we find $\Delta m_h^{\overline{\rm mDR}} = -21$ GeV.

The dependence of the mass corrections with the light Majorana neutrino mass is illustrated in the right panel of Fig. 3.13. The size of the corrections grow with $|m_\nu|$, as expected, and can be either positive in the low region, close to $|m_\nu| \sim 0.1$ eV, or negative in the high region, close to $|m_\nu| \sim 1$ eV.

These same interesting features of the Higgs mass corrections in terms of the two relevant physical Majorana neutrino masses, m_N and m_ν, are summarized in the contour-plot in Figure 3.14. Here we have fixed all the soft parameters, including $m_{\tilde{R}}$, to be at 1 TeV. The contour-lines for fixed $\Delta m_h^{\overline{\rm mDR}}$ range from positive values around 0.1 GeV in the left lower corner of the plot, corresponding to neutrino mass values of $|m_\nu| = 0.1 - 0.3$ eV and $m_N = 3 \times 10^{13}$ GeV, up to negative values around -5 GeV in the right upper corner of the plot, corresponding to, for instance, $|m_\nu| = 1$ eV and $m_N = 10^{15}$ GeV. It should

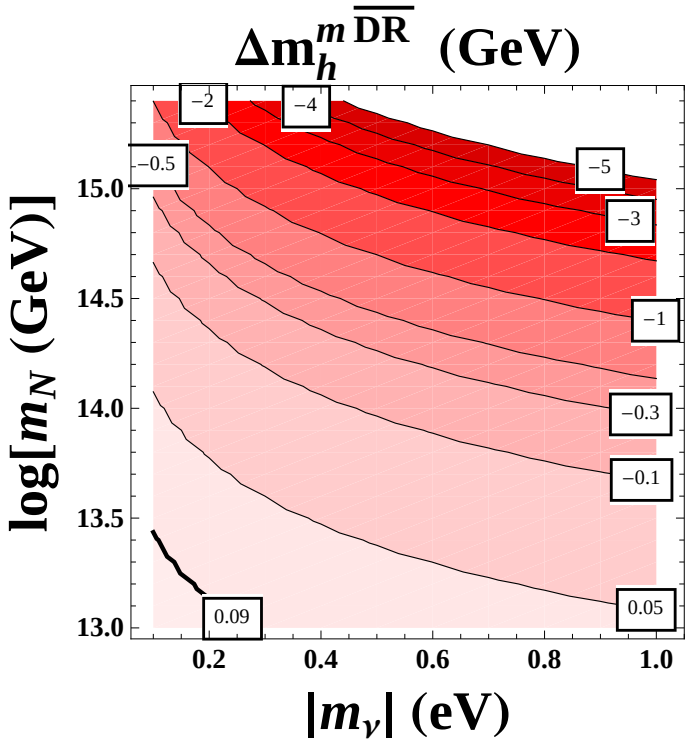

Figure 3.14: Contour-lines for the Higgs mass corrections from the neutrino/sneutrino sector as a function of the physical Majorana neutrino masses, light $|m_\nu|$ and heavy m_N. The other parameters are fixed to: $A_\nu = B_\nu = m_{\tilde{L}} = m_{\tilde{R}} = 10^3$ GeV, $\tan\beta = 5$, $M_A = 200$ GeV and $\mu = 200$ GeV.

be noticed that the contour-line with fixed $\Delta m_h^{\mathrm{m}\overline{\mathrm{DR}}} = 0.09$ (drawn with a wider black line in this plot) coincides with the prediction for the case where just the gauge part in the self-energies have been included. This means that 'the distance' of any other contour-line respect to this line represents the difference in the radiative corrections respect to the MSSM prediction.

We plot in Fig. 3.15, the contour-lines for fixed $\Delta m_h^{\mathrm{m}\overline{\mathrm{DR}}}$ in the less conservative case where $m_{\tilde{R}}$ is close to m_M. These are displayed as a function of $|m_\nu|$ and the ratio $m_{\tilde{R}}/m_M$. m_M is fixed here to the reference value, $m_M = 10^{14}$ GeV. For the interval studied here, we see again that the radiative corrections can be negative and as large as tens of GeV in the upper right corner of the plot. For instance, $\Delta m_h^{\mathrm{m}\overline{\mathrm{DR}}} = -30$ GeV for $m_M = 10^{14}$ GeV, $|m_\nu| = 0.6$ eV and $m_{\tilde{R}}/m_M = 0.7$.

Finally, given our previous simple analytical results of the renormalized self-energies

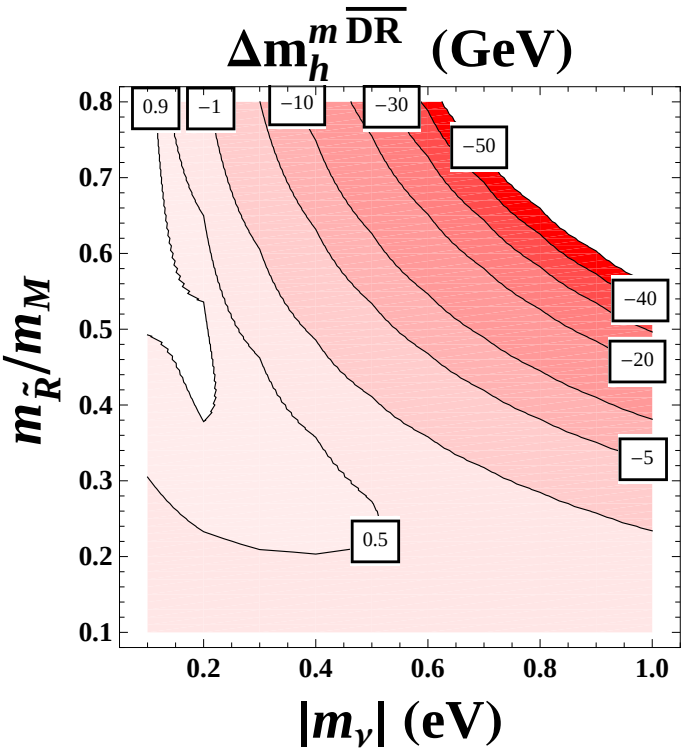

Figure 3.15: Contour-lines for the Higgs mass corrections from the neutrino/sneutrino sector as a function of the ratio $m_{\tilde{R}}/m_M$ and the lightest Majorana neutrino mass $|m_\nu|$. The other parameters are fixed to: $m_M = 10^{14}$ GeV, $A_\nu = B_\nu = m_{\tilde{L}} = 10^3$ GeV, $\tan\beta = 5$, $M_A = 200$ GeV and $\mu = 200$ GeV

in the seesaw limit, see Eqs. 3.33, (3.34), it is interesting to derive a simple analytical expression for the contribution of the heavy neutrino-sneutrino sector to the one-loop radiatively corrected Higgs mass in the limit of large m_M. Neglecting in Eq. (3.40) the contributions from $\hat{\Sigma}^{\nu/\tilde{\nu}}_{HH}$ and $\hat{\Sigma}^{\nu/\tilde{\nu}}_{hH}$ one finds,

$$\Delta m_h^{\rm m\overline{DR}} \simeq -\frac{\hat{\Sigma}^{\nu/\tilde{\nu}}_{hh}(M_h^2)}{2M_h} \tag{3.41}$$

where $\hat{\Sigma}^{\nu/\tilde{\nu}}_{hh}$ denotes the full corrections to the renormalized Higgs-boson self-energy from the $\nu/\tilde{\nu}$ sector and obtained in the m$\overline{\rm DR}$ scheme as described in the present work. We have found that this yields a very good approximation to the full result, i.e. the pole obtained from Eq. (3.40). In a next step in the above expression $\hat{\Sigma}^{\nu/\tilde{\nu}}_{hh}$ has to be replaced by our simplified results in the large m_M limit, namely, those in Eqs. 3.33b and (3.34b), providing the leading $\mathcal{O}(m_D^0)$ and $\mathcal{O}(m_D^2)$ contributions. We have compared numerically

this approximate $\Delta m_h^{\mathrm{m}\overline{\mathrm{DR}}}$ with our full numerical results for large m_M in Figure 3.12, and found very good agreement, whenever the soft SUSY masses are well below m_M. In fact, the behaviour with m_M of this approximate formula is indistinguisible from the lower line in the left plot of Figure 3.12.

We therefore conclude that the use of the previous Eq. (3.41) with

$$\hat{\Sigma}_{hh}^{\nu/\tilde{\nu}}(M_h^2) \simeq \left(\hat{\Sigma}_{hh}^{\mathrm{m}\overline{\mathrm{DR}}}(M_h^2)\right)_{m_D^0} + \left(\hat{\Sigma}_{hh}^{\mathrm{m}\overline{\mathrm{DR}}}(M_h^2)\right)_{m_D^2} \tag{3.42}$$

as given in Eqs. 3.33b and (3.34b), respectively, provides an excellent approximation to the full result for large Majorana mass values, 10^{13} GeV $< m_M < 10^{15}$ GeV and soft masses well below m_M, $m_{\mathrm{SUSY}} \lesssim 10^4$ GeV. Furthermore, the above simple approximation can also be used for estimates of the differences in the mass correction when applied to the $\overline{\mathrm{DR}}$ scheme versus the m$\overline{\mathrm{DR}}$ scheme for different choices of the $\mu_{\overline{\mathrm{DR}}}$ scale. For instance, for $m_M = 10^{14}$ GeV and the other parameters set to our reference values as defined in section 3.2.2, we got small differences of $|(\Delta m_h^{\overline{\mathrm{DR}}} - \Delta m_h^{\mathrm{m}\overline{\mathrm{DR}}})/M_h| < 1\%$ for $0.1 < \mu_{\overline{\mathrm{DR}}}/m_M < 1$.

Finally, we shortly comment about the similarities or differences of our work with earlier works in the literature where the effects of the neu/sneu sector in the Higgs mass parameters were also studied. In fact, previous studies in particular SUSY scenarios and under specific assumptions on the model parameters [67, 97, 109, 145, 172–174] already indicated that the size of these radiative corrections to the Higgs mass parameters in the case of extremely heavy Majorana neutrinos can be sizeable due to the large size of Y_ν.

In Ref. [67] the one-loop corrections to M_h were estimated within a split SUSY scenario where the soft-SUSY-breaking mass associated to the right handed neutrino, $m_{\tilde{R}}$, was chosen to be very large, of the order of the Majorana scale m_M. They made several approximations that we did not make in our calculation. They worked in the zero external momentum approximation and switching off the $SU(2) \times U(1)$ gauge interactions. Besides, they used the mass insertion approximation for the other soft-breaking sneutrino parameters, A_ν and B_ν, associated to the trilinear coupling and neutrino B-term respectively. Moreover, in their calculations of m_h 1-loop corrections they have not taken into account the well known relevant MSSM contribution but only the loops of neutrinos/sneutrinos. They obtain a large and negative correction from the neutrino/sneutrino sector of the order of a few tens of GeV for $m_M = 10^{14}$ GeV and $m_{\tilde{R}} \sim \mathcal{O}(m_M)$. Our results in the same limit, shown in Figure 3.15, are in agreement with their result for a similar choice of parameters.

In appendix B of Ref. [140] they calculate the corrections to the Higgs mass in the

MSSM-seesaw type I in the limit where $m_{\tilde{R}} \sim m_M$ using the effective potential approach. Therefore, their result is not comparable to ours because in the effective potential approach one neglects the external momentum and with this approximation one would never recover our result as one could appreciate in Figure 3.10, where the dependence of the renormalized energies with the momentum were shown and we have seen that this fact plays a relevant role in the estimate of the size of the mass corrections.

In Ref. [140, 145, 173–176], the impact of a big B_ν parameter, via a RGEs analysis, was shown to be relevant in different contexts, increasing the LFV rates, generating EDM, inducing a large oscillation in the sneutrino sector that contributes to the 1-loop neutrino masses, modifying the Higgs mass parameters and affecting the relic abundance of neutralino dark matter. In this thesis, we also observed relevant effects of a large B_ν parameter to the lightest MSSM Higgs mass as shown in left panel of Figure 3.13 but we did not pay much attention to the effects in this limit $B_\nu \sim \mathcal{O}(m_M)$ because B_ν contributes to observables that are highly constrained, as mentioned before. In particular, in Ref. [145] they concluded with an upper bound in an mSUGRA framework of $B_\nu Y_\nu^2/(8\pi^2) < m_{\rm SUSY}/\tan\beta$, from the requirement that electroweak symmetry breaking occurs. Large corrections to the Higgs soft mass parameters within a SUSY-seesaw framework with total or partial universality conditions have also been found by a similar RGEs analysis in [97, 109, 172–174]. In [97, 109, 172] it was concluded that these corrections induce a considerable decrease in the physical Higgs boson masses which in turn enhance the rates of the Higgs-mediated LFV processes. However it should be noticed that an analysis with RGE's is not comparable to our full 1-loop diagrammatic computation. The RGE's only provide a good truck to the logarithmic dependence on the Majorana mass but they do not provide the full result, which contains, as we have said, the most relevant $\mathcal{O}(m_D^2)$ contributions in Eq. (3.34a) and Eq. (3.34b).

Chapter 4

LFV processes mediated by Higgs bosons within constrained MSSM-seesaw scenarios

The SM in its simplest version does not allow for Lepton Flavor Violating processes. When one extends the SM in order to include the neutrino masses and mixings observed in atmospheric and solar neutrino experiments, the lepton flavor violation in the neutrino sector can be transmitted to the charged lepton sector, giving rise to charged lepton flavor violating processes. However, with the inclusion of Dirac neutrino masses and mixings, these processes are allowed but are extremely suppressed due to the small masses of the neutrinos (leptonic version of the GIM suppression mechanism). For instance, the decay rate of the radiative LFV decay $\mu \to e\gamma$ for massive Dirac neutrinos is given by [177–179]:

$$BR(\mu \to e\gamma) = \frac{3\alpha}{32\pi} \left| \sum_k \left(U^*_{MNS}\right)_{ek} \left(U_{MNS}\right)_{\mu k} \times \frac{m^2_{\nu_k}}{M^2_W} \right|^2 BR(\mu \to e\bar{\nu}_e\nu_\mu) \qquad (4.1)$$

Even if a 1 eV neutrino mass with maximal mixing is considered, Eq. (4.1) only gives a branching ratio of the order of 10^{-47} [81], far below the present sensitivities shown in Table 4.1.

When Dirac plus Majorana mass terms are introduced in the SM, generating neutrino masses and mixings via a seesaw type I mechanism, the suppression factor of $\frac{m^2_{\nu_k}}{M^2_W}$ is substituted by $\mathcal{O}\left(\frac{m_{\nu_k}}{m_M}\right)$ [178], where m_M is the Majorana mass scale. Then the branching

ratio is still $\mathcal{O}(10^{-40})$ or less for $m_\nu = 1$ eV and $m_M = 10^{10}$ GeV [81]. We conclude that it is therefore difficult to expect observable LFV effects from the ordinary neutrino masses and mixing indicated by the atmospheric and solar neutrinos.

In a MSSM seesaw framework the situation is completely different. Besides the previous contributions, supersymmetry provides new direct sources of flavor violation, namely the possible presence of off-diagonal soft terms in the slepton mass matrices and in the trilinear couplings at low energies. In practice, flavor violation originates from the misalignment between fermion and sfermion mass matrices, that cannot be diagonalized simultaneously. Even if the scalar masses are universal at high energy, flavor changing entries in the neutrino Yukawa coupling matrices induce, through renormalization effects, flavor mixing in the slepton masses at low energies, and these sleptons, in turn, when propagating in loops can, therefore, generate large rates in LFV processes, like $l_j \to l_i \gamma$ $(i, j = 1, 2, 3)$, and others.

We are interested here, mainly in the LFV processes that can be mediated by the MSSM Higgs bosons, since these ones can provide interesting information on all the sectors involved, namely: SUSY, the Higgs sector and our main subject: the Majorana neutrinos. We will first shortly review the basic ingredients and status of LFV within SUSY-seesaw models and then present our results for the specific channels considered in this thesis, $\tau \to \mu\eta$ and $\tau \to \mu f_0$. The results presented in this chapter have been published in [100], [109] and [111].

4.1 Flavor mixing in the slepton sector within the MSSM-seesaw

The most general squared mass matrix for the case of charged sleptons is given by a 6×6 matrix, with all entries being now non-vanishing. Therefore, the corresponding matrix, referred to the $(\tilde{e}_L, \tilde{e}_R, \tilde{\mu}_L, \tilde{\mu}_R, \tilde{\tau}_L, \tilde{\tau}_R)$ basis, can be written as follows

$$M_{\tilde{l}}^2 = \begin{pmatrix} M_{LL}^{ee\,2} & M_{LR}^{ee\,2} & M_{LL}^{e\mu\,2} & M_{LR}^{e\mu\,2} & M_{LL}^{e\tau\,2} & M_{LR}^{e\tau\,2} \\ M_{RL}^{ee\,2} & M_{RR}^{ee\,2} & M_{RL}^{e\mu\,2} & M_{RR}^{e\mu\,2} & M_{RL}^{e\tau\,2} & M_{RR}^{e\tau\,2} \\ M_{LL}^{\mu e\,2} & M_{LR}^{\mu e\,2} & M_{LL}^{\mu\mu\,2} & M_{LR}^{\mu\mu\,2} & M_{LL}^{\mu\tau\,2} & M_{LR}^{\mu\tau\,2} \\ M_{LR}^{\mu e\,2} & M_{RR}^{\mu e\,2} & M_{RL}^{\mu\mu\,2} & M_{RR}^{\mu\mu\,2} & M_{RL}^{\mu\tau\,2} & M_{RR}^{\mu\tau\,2} \\ M_{LL}^{\tau e\,2} & M_{LR}^{\tau e\,2} & M_{LL}^{\tau\mu\,2} & M_{LR}^{\tau\mu\,2} & M_{LL}^{\tau\tau\,2} & M_{LR}^{\tau\tau\,2} \\ M_{RL}^{\tau e\,2} & M_{RR}^{\tau e\,2} & M_{RL}^{\tau\mu\,2} & M_{RR}^{\tau\mu\,2} & M_{RL}^{\tau\tau\,2} & M_{RR}^{\tau\tau\,2} \end{pmatrix}, \tag{4.2}$$

where

$$
\begin{aligned}
M_{LL}^{ij\,2} &= m_{\tilde{L},ij}^2 + v_1^2 \left(Y_l^\dagger Y_l\right)_{ij} + m_Z^2 \cos 2\beta \left(-\frac{1}{2} + \sin^2\theta_W\right) \delta_{ij}\,, \\
M_{RR}^{ij\,2} &= m_{\tilde{E},ij}^2 + v_1^2 \left(Y_l^\dagger Y_l\right)_{ij} - m_Z^2 \cos 2\beta \sin^2\theta_W \,\delta_{ij}\,, \\
M_{LR}^{ij\,2} &= v_1 \left(A_l^{ij}\right)^* - \mu\, Y_l^{ij}\, v_2\,, \\
M_{RL}^{ij\,2} &= \left(M_{LR}^{ji\,2}\right)^*\,.
\end{aligned}
\tag{4.3}
$$

The off-diagonal entries in flavor space are originated from the soft-SUSY breaking masses and trilinear couplings, i.e. $m_{\tilde{L},ij}$, $m_{\tilde{E},ij}$ and A_l^{ij}, with $i,j = e\,,\,\mu\,,\,\tau$, which here refer to their corresponding values at the electroweak scale. The key point is that Majorana neutrinos (and sneutrinos) quantum effects in the LFV rates do appear when the running effects from the high energy M_X to the EW scale are included. Namely, the heavy ν_{R_i}, $\tilde{\nu}_{R_i}$ effects are induced via the running in the soft SUSY breaking parameters and by means of the Yukawa neutrino couplings.

Regarding the sneutrino sector, there is a 12×12 squared mass matrix, already given in Eq. (2.37). But for the purpose of computing LFV rates, it is a very good approximation to keep in the mass matrix at low energies, i.e. at the EW scale, just the light sneutrino states which are made mainly of $\tilde{\nu}_L$'s. Thus, the diagonalization procedure becomes simpler than in the charged slepton case since the sneutrino squared mass matrix is 3×3 type. This 3×3 matrix, referred to the $\tilde{\nu}' = (\tilde{\nu}_{e,\,L},\, \tilde{\nu}_{\mu,\,L},\, \tilde{\nu}_{\tau,\,L})$ basis can be written as follows

$$
M_{\tilde{\nu}}^2 \;=\; \begin{pmatrix}
m_{\tilde{L},e}^2 + \frac{1}{2} m_Z^2 \cos 2\beta & m_{\tilde{L},e\mu}^2 & m_{\tilde{L},e\tau}^2 \\
m_{\tilde{L},\mu e}^2 & m_{\tilde{L},\mu}^2 + \frac{1}{2} m_Z^2 \cos 2\beta & m_{\tilde{L},\mu\tau}^2 \\
m_{\tilde{L},\tau e}^2 & m_{\tilde{L},\tau\mu}^2 & m_{\tilde{L},\tau}^2 + \frac{1}{2} m_Z^2 \cos 2\beta
\end{pmatrix}\,,
\tag{4.4}
$$

where $m_{\tilde{L},ij}^2$ are the same as in the previous charged slepton and sneutrino squared mass matrix.

The physical masses and states are obtained by diagonalizing the previous squared mass matrices, leading to

$$
\begin{aligned}
M_{\tilde{l}}^{2\,\mathrm{diag}} &= R^l\, M_{\tilde{l}}^2\, R^{l\,\dagger} = \mathrm{diag}\,(m_{\tilde{l}_1}^2, .., m_{\tilde{l}_6}^2)\,, \\
M_{\tilde{\nu}}^{2\,\mathrm{diag}} &= R^\nu\, M_{\tilde{\nu}}^2\, R^{\nu\,\dagger} = \mathrm{diag}\,(m_{\tilde{\nu}_1}^2,\, m_{\tilde{\nu}_2}^2,\, m_{\tilde{\nu}_3}^2)\,,
\end{aligned}
\tag{4.5}
$$

where R^l and R^ν are unitary rotation matrices.

Notice that when working in the physical mass eigenstate basis, all the information of flavor mixing is encoded in the previous values of the physical masses $m_{\tilde{l}_i}$ and $m_{\tilde{\nu}_i}$ and the rotation matrices R^l and R^ν. In particular, these physical parameters will transmit the flavor mixing to the relevant couplings for the forthcoming computation of LFV rates.

For illustration, we show here the 1-loop renormalization group equation for $m^2_{\tilde{L}}$ that is given by [79]:

$$\begin{aligned}\frac{dm^2_{\tilde{L}_{ij}}}{d\log\mu} &= \left(\frac{dm^2_{\tilde{L}_{ij}}}{d\log\mu}\right)_{MSSM} + \frac{1}{16\pi^2}\left(\left(m^2_{\tilde{L}}Y^\dagger_\nu Y_\nu\right)_{ij} + \left(Y^\dagger_\nu Y_\nu m^2_{\tilde{L}}\right)_{ij}\right. \\ &\left. +2\left(m^2_{H_2}Y^\dagger_\nu Y_\nu\right)_{ij} + 2\left(Y^\dagger_\nu m^2_{\tilde{R}} Y_\nu\right)_{ij} + 2\left(A^\dagger_\nu A_\nu\right)_{ij}\right) \end{aligned} \tag{4.6}$$

where $\left(\frac{dm^2_{\tilde{L}}}{d\log\mu}\right)_{MSSM}$ is the corresponding RGE in the MSSM and the terms explicitly written are additional contributions by the right-handed neutrino Yukawa couplings. Since we will work in constrained SUSY-seesaw scenarios with universal conditions on the mass matrices at M_X and where the unique possible source of flavor mixing at M_X is the Yukawa matrix, all slepton flavor mixing at low energies will solely come from the RGE generated radiative corrections involving Y_ν, as we can appreciate in Eq. (4.6).

In order to obtain the slepton mass matrix at the EW scale the running of the RGE is performed in two steps. The first step is running the parameters from M_X to m_M using the full one-loop RGE's with extended neutrino and sneutrino sectors [79]. In the second step, from m_M to the EW scale, the Majorana neutrinos are assumed to decouple in the RGE's and the running is performed using the RGE's of the MSSM. The most important flavor mixing in the slepton and sneutrino soft terms is produced in the first step of this running.

The clearest way to illustrate this RGE-induced intergenerational mixing is by working in the one loop leading-log approximation where the approximate solution for the off-diagonal terms ($i \neq j$, $i,j = 1,2,3$) can be written as [79]:

$$(\Delta m^2_{\tilde{L}})_{ij} \;=\; -\frac{1}{8\,\pi^2}\,(3\,M_0^2 + A_0^2)\,(Y^\dagger_\nu\,L\,Y_\nu)_{ij}\,, \tag{4.7a}$$

$$(\Delta A_l)_{ij} \;=\; -\frac{3}{16\,\pi^2}\,A_0\,Y_{l_i}\,(Y^\dagger_\nu\,L\,Y_\nu)_{ij}\,, \tag{4.7b}$$

$$(\Delta m^2_{\tilde{E}})_{ij} \;=\; 0\;;\; L_{kl} \;\equiv\; \log\left(\frac{M_X}{m_{M_k}}\right)\,\delta_{kl}\,. \tag{4.7c}$$

We can see that within the LLog approximation, the dominant flavor off-diagonal matrix elements are those of the LL sector since they become enhanced with factors given by

squared soft-breaking parameters. The next dominant elements are those of the LR sector (which are suppressed by the small lepton mass) and the smallest ones are those of the RR sector. For the present thesis we will not use this Llog approximation, but we will solve, instead, the full one-loop RGE's.

In practice, LFV processes, like $l_i \to l_j\gamma$ $(i \neq j)$, arise at one loop level through the exchange of sleptons and sneutrinos that carry in their propagation the off-diagonal flavor entries. The expected magnitudes of the LFV effects depend on the strength of the neutrino Yukawa coupling and the flavor mixing in the neutrino sector. The neutrino Yukawa couplings which can be $Y_\nu \sim \mathcal{O}(1)$ or even larger for heavy $m_M \sim 10^{14} - 10^{15}$ GeV give rise to sizable LFV rates that are in some cases [77–81, 95–100, 143, 172, 180–188], at the reach of the present experimental sensitivity [20].

In order to illustrate the size of the flavor mixing in slepton and sneutrino sectors, the following flavor changing dimensionless parameters are usually defined:

$$\begin{aligned}
\delta^{ij}_{LL} &= \frac{M^{ij2}_{LL}}{M^2_{\rm SUSY}}\,, \\
\delta^{ij}_{LR} &= \frac{M^{ij2}_{LR}}{M^2_{\rm SUSY}}\,, \\
\delta^{ij}_{RR} &= \frac{M^{ij2}_{RR}}{M^2_{\rm SUSY}}\,,
\end{aligned} \tag{4.8}$$

where $i, j = 1, 2, 3$, $i \neq j$ and $M_{\rm SUSY}$ is an average slepton squared mass, which is usually set in terms of the physical sleptons masses.

One can estimate the previous dimensionless parameters of Eq. (4.8) by using the LLog approximation which leads to the following simple results:

$$\delta^{ij}_{LL}\big|_{\rm LLog} = \frac{(\Delta m^2_{\tilde{L}})_{ij}}{M^2_{\rm SUSY}}\,, \tag{4.9a}$$

$$\delta^{ij}_{LR}\big|_{\rm LLog} = \frac{v_1(\Delta A_l)_{ij}}{M^2_{\rm SUSY}}\,, \tag{4.9b}$$

$$\delta^{ij}_{RR}\big|_{\rm LLog} = \frac{(\Delta m^2_{\tilde{E}})_{ij}}{M^2_{\rm SUSY}}\,, \tag{4.9c}$$

where $(\Delta m^2_{\tilde{L}})_{ij}$, $(\Delta A_l)_{ij}$ and $(\Delta m^2_{\tilde{E}})_{ij}$ are given in Eq. (4.7). Notice that the results in Eq (4.7) imply the following hierarchy in the size of these parameters:

$$\delta^{ij}_{LL}\big|_{\rm LLog} \gg \delta^{ij}_{LR}\big|_{\rm LLog} \gg \delta^{ij}_{RR}\big|_{\rm LLog}\,. \tag{4.10}$$

For the present work we have not used the Llog approximation nor the MIA [189]. We have instead solved the full one-loop RGE's with the extended neutrino and sneutrino sectors, in two steps, as explained above, and for that we have used the public code SPheno [190]. The code is also used for the exact diagonalization of the slepton mass matrices.

4.2 LFV in Higgs mediated processes

It is well known that Higgs bosons within MSSM-seesaw scenarios, can mediate, at the one-loop level, interesting LFV processes, like $\tau \to 3\mu$ [99] and μ-e conversion in nuclei [172]. In addition, some semileptonic decays like $\tau \to \mu\eta$ have been proven to be sensitive to the Higgs sector within this same context [97].

The different LFV decays are classified in pure leptonic decays and semileptonic ones. The first ones include the following type of decays, $l_i \to l_j\gamma$ and $l_i \to l_j l_k \bar{l_k}$, where i, j, k are family indices. In Table 4.1 the present experimental bounds on the branching ratios of relevant leptonic processes are shown. The semileptonic decays contain, among others, $l_i \to l_j P$ and $l_i \to l_j S$ where P and S refer to a pseudoscalar and a scalar meson, respectively.In Table 4.2 the present experimental bounds on the branching ratios of few semileptonic processes are shown. We are interested here, in particular, in $\tau \to \mu\eta$ and $\tau \to \mu f_0$ because they turn out to be the most sensitive to the Higgs sector.

By comparing both tables, it is clear that the channel with the strongest experimental bound is $\mu \to e\gamma$ with an upper bound of 2.4×10^{-12}, given by the MEG collaboration this year. The rest of the channels have bounds much less restrictive than $\mu \to e\gamma$, at $\mathcal{O}(10^{-8})$, but it is worth mentioning that semileptonic decays have as stringent bounds as the rest of the leptonic decays, being also able to set strong constraints in the parameter space of the new physics responsible of these flavor violating decays.

In order to roughly compare the predicted LFV decay rates of different channels in the $\tau-\mu$ sector, within SUSY-seesaw scenarios, it is more convenient to use here the simplified expressions of some of the decays rates in the Llog and mass insertion approximations and work in the large $\tan\beta$ regime. These simple formulas are written in terms of $\tan\beta$, the largest insertion $\delta^{32}_{LL} = \delta_{32}$ and the relevant mass.

The approximate formula for the $\tau \to \mu\gamma$ decay is given by [80, 185]:

$$\mathrm{BR}(\tau \to \mu\gamma)_{\mathrm{approx}} = 1.5 \times 10^{-2} \, |\delta_{32}|^2 \left(\frac{100}{M_{\mathrm{SUSY}}(\mathrm{GeV})}\right)^4 \left(\frac{\tan\beta}{60}\right)^2 , \tag{4.11}$$

where M_{SUSY} represents generically the relevant SUSY particle mass in the loop. The amplitude of the decay $\tau \to 3\mu$ is the sum of various contributions [99],

$$T(\tau \to 3\,\mu) = T_{\gamma-\mathrm{penguin}} + T_{Z-\mathrm{penguin}} + T_{H-\mathrm{penguin}} + T_{\mathrm{boxes}} \, . \tag{4.12}$$

In particular, the branching ratio coming just from the Higgs mediated amplitude (neglecting interferences between the channels) reads [99, 180]:

$$\mathrm{BR}(\tau \to 3\mu)_{H_{\mathrm{approx}}} = 1.2 \times 10^{-7} \, |\delta_{32}|^2 \left(\frac{100}{m_{A^0}(\mathrm{GeV})}\right)^4 \left(\frac{\tan\beta}{60}\right)^6 .$$

However, this channel is known to be dominated, within the present constrained SUSY-seesaw scenarios, by the photon contribution. The approximate formula for this contribution is [99]:

$$\mathrm{BR}(\tau \to 3\mu)_{\gamma_{\mathrm{approx}}} = 3.4 \times 10^{-5} \, |\delta_{32}|^2 \left(\frac{100}{M_{\mathrm{SUSY}}(\mathrm{GeV})}\right)^4 \left(\frac{\tan\beta}{60}\right)^2 ,$$

For low $M_{\mathrm{SUSY}} \sim 100$ GeV, it is clear from the above expresions that $\tau \to \mu\gamma$ is by far the dominant channel. However, the latest LHC results point to larger SUSY masses, $\gtrsim \mathcal{O}(1\mathrm{TeV})$ and, in that case, the other channels not suppressed by $1/M^4_{\mathrm{SUSY}}$ may be competitive.

We can also observe from the previous formulas that the photon mediated channels, besides being suppressed by $1/M^4_{\mathrm{SUSY}}$ they grow just quadratically with $\tan\beta$, in contrast with H^0 and A^0 mediated channels that are suppressed by the mass of the Higgs that mediates the decay as $1/M^4_H$ and grow with $\tan\beta$ as $(\tan\beta)^6$. Therefore, the Higgs mediated channels will be particularly interesting in the large $\tan\beta$ and M_{SUSY} regime with light m_{H^0} and/or m_{A^0}. However, in constrained SUSY-seesaw models, such as the CMSSM-seesaw, these Higgs boson masses are highly correlated with the universal soft masses and, therefore, with M_{SUSY}, so that it is not possible to get light m_{H^0}, m_{A^0} for large SUSY masses, say $M_{\mathrm{SUSY}} \gtrsim 1$ TeV. This situation can be improved by relaxing the universality conditions of the CMSSM, in such a way that the soft Higgs masses are not universal, as it happens in the NUHM-seesaw. In the NUHM-seesaw light Higgs masses can be obtained ever for large SUSY masses, for specific choices of δ_1 and δ_2 parameters.

Regarding the LFV semileptonic τ decays [97], some particular channels have also been proven to offer new windows for Higgs boson searches. For instance, the channels $\tau \to \mu\pi\pi$ and $\tau \to \mu K\bar{K}$ can be mediated by a Higgs boson, similarly to $\tau \to 3\mu$. However, these $\tau \to \mu PP$ semileptonic channels are also dominated by the photon contribution, as it happens in $\tau \to 3\mu$. The most interesting channel that manifests a clear sensitivity to the Higgs sector considered so far in the literature, is the semileptonic channel $\tau \to \mu\eta$ [95, 97]. This channel can be mediated by a Z boson and an A^0 Higgs boson, but at large $\tan\beta$, the later dominates. In this case the predicted branching ratio is also proportional to $(\tan\beta)^6$ and $1/M_{A^0}^4$ and is relevant for sufficiently large $\tan\beta$ and light m_{A^0}.

Here we will study, in addition, a new LFV semileptonic τ decay that is also sensitive to the Higgs sector, concretely the channel $\tau \to \mu f_0$. This channel offers an unique window for searches of the $\mathcal{CP}$-even Higgs bosons, h^0 and H^0, and it is expected to be dominated at large $\tan\beta$ by the interchange of the H^0 boson. We will present here, the study of this $\tau \to \mu f_0$ channel, together with $\tau \to \mu\eta$, because they can be complementary in that the first one has access to the $\mathcal{CP}$-even Higgs sector, h^0 and H^0, whereas the second one has access to the $\mathcal{CP}$-odd A^0. Besides, as will be shown in the following, these two channels have important branching ratios because the exchanged Higgs bosons interact with sizeable couplings to the strange quark components of both η and f_0. The inherited couplings of the A^0 and H^0 to the η and f_0, respectively, will be consequently also sizeable. The corresponding branching ratios estimates will be performed here by means of Chiral Perturbation Theory χPT and Resonance Chiral Theory RχT.

To sum up, we have seen that some semileptonic channels have the advantage of being sensitive to the Higgs, while in leptonic decays the Higgs contribution is, in general, not the dominant one. As we are interested in the interplay between LFV and Higgs physics, from now on, we will focus our attention in the two semileptonic decays $\tau \to \mu f_0(980)$ and $\tau \to \mu\eta$.

4.3 Framework for the LFV decays

For the present study of the $\tau \to \mu f_0(980)$ and $\tau \to \mu\eta$ decays, we choose a SUSY-seesaw framework where the SUSY spectrum is enlarged by three right-handed neutrinos, ν_{R_i} $(i = 1, 2, 3)$, and their SUSY partners, $\tilde{\nu}_{R_i}$ $(i = 1, 2, 3)$. We assume again a seesaw mechanism for neutrino mass generation and, in order to make contact with neutrino data, we use the parametrization of Eq. (2.28) that was already introduced at the end of

decay mode	Experiment	References	Upper limit 90% C.L
$\mu^+ \to e^+\gamma$	MEG	[85]	2.4×10^{-12}
$\tau^- \to \mu^-\gamma$	Babar	[89]	4.4×10^{-8}
$\tau^- \to e^-\gamma$	Babar	[89]	3.3×10^{-8}
$\tau^- \to \mu^-\gamma$	Babar	[89]	4.4×10^{-8}
$\tau^- \to e^-e^+e^-$	Belle	[90]	2.7×10^{-8}
$\tau^- \to \mu^-e^+e^-$	Belle	[90]	1.8×10^{-8}
$\tau^- \to e^-\mu^+\mu^-$	Belle	[90]	2.7×10^{-8}
$\tau^- \to \mu^-\mu^+\mu^-$	Belle	[90]	2.1×10^{-8}
$\tau^- \to e^-\mu^+e-$	Belle	[90]	1.5×10^{-8}
$\tau^- \to \mu^-e^+\mu^-$	Belle	[90]	1.7×10^{-8}

Table 4.1: Present bounds on LFV leptonic decays

decay mode	Experiment	References	Upper limit 90% C.L
$\tau^- \to e^-\eta$	Belle	[93]	4.4×10^{-8}
$\tau^- \to \mu^-\eta$	Belle	[93]	2.3×10^{-8}
$\tau^- \to e^- f^0(980)$	Belle	[94]	$3.2 \times 10^{-8}(incl.Br(f^0 \to \pi^+\pi^-))$
$\tau^- \to \mu^- f^0(980)$	Belle	[94]	$3.4 \times 10^{-8}(incl.Br(f^0 \to \pi^+\pi^-))$

Table 4.2: Present bounds for the LFV semileptonic decays of interest here

Sect. 2.2.1 .

For the light and heavy neutrino sector different plausible scenarios, shown in Eq. (2.29) and Eq. (2.30), have been considered. For the numerical predictions in this chapter we will use the input values for the light neutrino mass squared differences and the angles in the $U_{\rm PMNS}$ matrix given by Eq. (2.31) which are compatible with present neutrino data [20]. Finally, the free neutrino input parameters, not constrained by data, are the heavy neutrino masses m_{N_1}, m_{N_2}, m_{N_3} and the complex angles θ_1, θ_2, θ_3 of the R matrix defined in Eq. (2.33).

Regarding the SUSY parameters we will work within two different constrained MSSM-seesaw scenarios, the CMSSM with universal soft SUSY breaking parameters, defined in Sect. 1.3.2, and the NUHM model with non-universal Higgs soft masses, defined in Subsect. 1.3.3. Thus, in addition to the previous neutrino parameters, m_{N_i} and θ_i, the input parameters of these two models are, as already introduced in Subsect. 1.3, respectively,

$$\begin{aligned} &\text{CMSSM}: M_0\,, M_{1/2}\,, A_0\,, \tan\beta\,, \text{sign}(\mu)\,. \\ &\text{NUHM}: M_0\,, M_{1/2}\,, A_0\,, \tan\beta\,, \text{sign}(\mu)\,, M_{H_1}^2 \,=\, M_0^2\,(1+\delta_1), M_{H_2}^2 \,=\, M_0^2\,(1+\delta_2). \end{aligned} \tag{4.13}$$

Notice, that the departure from universality in the soft Higgs masses of the NUHM is parameterized here in terms of the two dimensionless parameters δ_1 and δ_2. Consequently, by taking $\delta_1 = \delta_2 = 0$ in the NUHM one recovers the CMSSM case. Finally, in order to evaluate the previous SUSY parameters and the physical masses at low energies (taken here as the Z gauge boson mass m_Z), we solve the full one-loop Renormalization Group Equations (RGEs) including the extended neutrino and sneutrino sectors. For this and the computation of the full spectra at the low energy we use here the public FORTRAN code SPheno [190]. In the numerical estimates of the LFV rates, we will set $M_0 = M_{1/2}$, $A_0 = 0$ and $\text{sign}(\mu) = +1$, for simplicity.

For the purpose of the present analysis the most relevant difference between the two previous constrained SUSY-seesaw scenarios is the spectrum of the Higgs sector as it was announced in the previous section. In particular, we want to explore the possibility of having light neutral Higgs bosons mediating the $\tau \to \mu f_0(980)$ and $\tau \to \mu\eta$ channels, while keeping the SUSY spectra heavy enough so that other relevant LFV $\tau - \mu$ decays are suppressed. This is clearly possible within the NUHM-seesaw scenario, as illustrated in Figure 4.1. We see in this figure that, by properly adjusting the input δ_1 and δ_2 parameters, the heavy Higgs boson H^0 can get masses as low as 100-250 GeV even for a

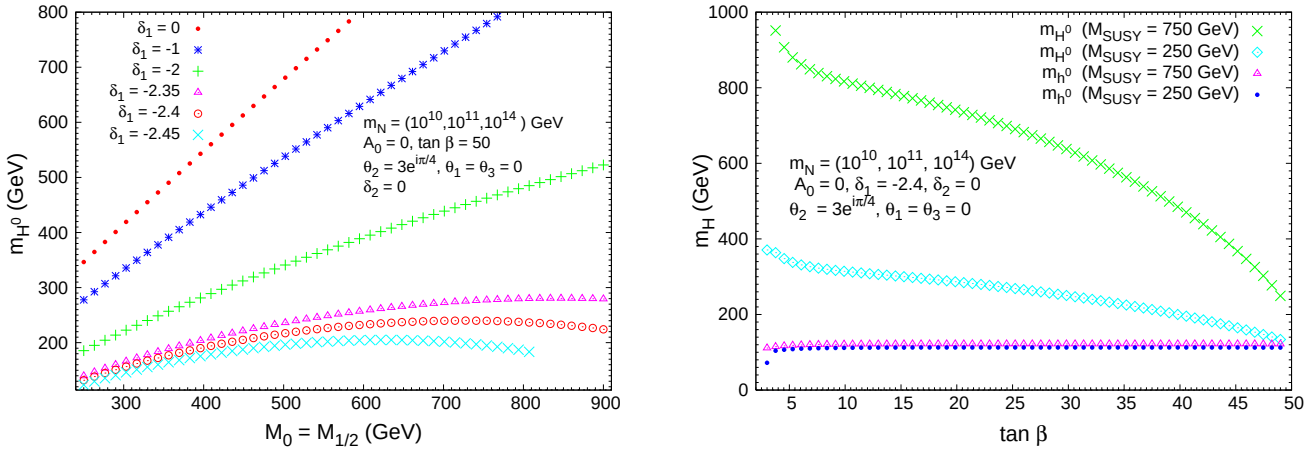

Figure 4.1: CP-even Higgs boson masses in the NUHM-Seesaw scenario: 1) m_{H^0} as a function of $M_{\rm SUSY} = M_0 = M_{1/2}$ for several input $\delta_{1,2}$ (left panel). The predictions in the CMSSM-Seesaw scenario ($\delta_1 = \delta_2 = 0$) are included for comparison; 2) m_{H^0} and m_{h^0} as functions of $\tan\beta$ for $M_{\rm SUSY} = 250$ GeV and 750 GeV (right panel).

very heavy SUSY spectrum. For instance, for $\delta_1 = -2.4$, $\delta_2 = 0$, $\tan\beta = 50$, $M_{\rm SUSY} = M_0 = M_{1/2} = 750$ GeV and the other input parameter values as specified in this figure, we get $m_{H^0} = 249$ GeV and $m_{h^0} = 122$ GeV, to be compared with $m_{H^0} = 998$ GeV and $m_{h^0} = 122$ GeV of the CMSSM-Seesaw case. With choices for $\delta_2 \neq 0$ one gets even lower values of m_{H^0}. For the following numerical analysis and, for simplicity, we will set, however, $\delta_2 = 0$ and play just with δ_1. It is worth also mentioning that the predictions for m_{A^0} (not shown in this figure) are practically indistinguishable from those of m_{H^0}.

Although for the forthcoming evaluation of the LFV branching ratios we will perform a full one-loop computation with an exact diagonalization of the 6×6 slepton mass matrix, it is however, very illustrative to estimate previously the size of the relevant flavor changing deltas δ^{ij}_{XY} within the simple Llog approximation. The flavor violation in the $\tau - \mu$ sector is encoded in the flavor mixing parameter δ^{32}_{XY} ($XY = LL, LR, RR$), with δ^{32}_{LL} being the dominant one in the constrained scenarios that we are considering. The expression of $\delta^{32}_{LL} \equiv \delta_{32}$ in the LLog approximation is given by (see Eq. (4.7a) and Eq. (4.9a)):

$$\delta_{32} \;=\; -\frac{1}{8\,\pi^2}\,\frac{(3\,M_0^2 + A_0^2)}{M^2_{\rm SUSY}}\,(Y_\nu^\dagger\,L\,Y_\nu)_{32}\;, \qquad L_{kl} \;\equiv\; \log\left(\frac{M_X}{m_{N_k}}\right)\,\delta_{kl}\,,\; k,l = 1,2,3, \tag{4.14}$$

where again $M_{\rm SUSY}$ is an average SUSY mass. The connection of δ_{32} , with the low energy

neutrino parameters is given in the following expression:

$$
\begin{aligned}
& v_2^2 \, \left(Y_\nu^\dagger \, L \, Y_\nu\right)_{32} \, = \\
& L_{33} \, m_{N_3} \, \Big[\Big(\sqrt{m_{\nu_3}} \, c_1 \, c_2 \, c_{13} \, s_{23} \, + \, \sqrt{m_{\nu_2}} \, s_1 \, c_2 \, (c_{12} \, c_{23} \, - \, s_{12} \, s_{13} \, s_{23}) \, - \, \sqrt{m_{\nu_1}} \, s_2 \, (s_{12} \, c_{23} \, + \, c_{12} \, s_{13} \, s_{23})\Big) \\
& \quad \Big(\sqrt{m_{\nu_3}} \, c_1^* \, c_2^* \, c_{13} \, c_{23} \, - \, \sqrt{m_{\nu_2}} \, s_1^* \, c_2^* \, (c_{12} \, s_{23} \, + \, s_{12} \, s_{13} \, c_{23}) \, + \, \sqrt{m_{\nu_1}} \, s_2^* \, (s_{12} \, s_{23} \, - \, c_{12} \, s_{13} \, c_{23})\Big)\Big] \\
& L_{22} \, m_{N_2} \, \Big[\Big(-\sqrt{m_{\nu_3}} \, c_{13} \, s_{23} \, (s_1 \, c_3 \, + \, c_1 \, s_2 \, s_3) \, - \, \sqrt{m_{\nu_1}} \, c_2 \, s_3 \, (s_{12} \, c_{23} \, + \, c_{12} \, s_{13} \, s_{23}) \, + \\
& \quad \sqrt{m_{\nu_2}} \, (c_{12} \, c_{13} \, - \, s_{12} \, s_{13} \, s_{23}) \, (c_1 \, c_3 \, - \, s_1 \, s_2 \, s_3)\Big) \\
& \quad \Big(-\sqrt{m_{\nu_3}} \, c_{13} \, c_{23} \, (s_1^* \, c_3^* \, + \, c_1^* \, s_2^* \, s_3^*) \, + \, \sqrt{m_{\nu_1}} \, c_2^* \, s_3^* \, (s_{12} \, s_{23} \, - \, c_{12} \, s_{13} \, c_{23}) \, - \\
& \quad \sqrt{m_{\nu_2}} \, (c_{12} \, s_{23} \, + \, s_{12} \, s_{13} \, c_{23}) \, (c_1^* \, c_3^* \, - \, s_1^* \, s_2^* \, s_3^*)\Big)\Big] \\
& L_{11} \, m_{N_1} \, \Big[\Big(\sqrt{m_{\nu_3}} \, c_{13} \, s_{23} \, (s_1 \, s_3 \, - \, c_1 \, s_2 \, c_3) \, - \, \sqrt{m_{\nu_1}} \, c_2 \, c_3 \, (s_{12} \, c_{23} \, + \, c_{12} \, s_{13} \, s_{23}) \, - \\
& \quad \sqrt{m_{\nu_2}} \, (c_{12} \, c_{23} \, - \, s_{12} \, s_{13} \, s_{23}) \, (s_1 \, s_2 \, c_3 \, + \, c_1 \, s_3)\Big) \\
& \quad \Big(\sqrt{m_{\nu_3}} \, c_{13} \, c_{23} \, (s_1^* \, s_3^* \, - \, c_1^* \, s_2^* \, c_3^*) \, + \, \sqrt{m_{\nu_1}} \, c_2^* \, c_3^* \, (s_{12} \, s_{23} \, - \, c_{12} \, s_{13} \, c_{23}) \, + \\
& \quad \sqrt{m_{\nu_2}} \, (c_{12} \, s_{23} \, + \, s_{12} \, s_{13} \, c_{23}) \, (c_1^* \, s_3^* \, + \, s_1^* \, s_2^* \, c_3^*)\Big)\Big] \, . \qquad (4.15)
\end{aligned}
$$

where the parametrization of Eq. (2.28) for the Y_ν matrix elements has been used and we have used a short notation for the cosines and sines: $s_{ij} \equiv \sin\theta_{ij}$, $c_{ij} \equiv \cos\theta_{ij}$, where θ_{ij} are the light neutrino flavor mixing angles of the $U_{\rm PMNS}$ matrix defined in Eq. (2.24) and $s_i \equiv \sin\theta_i$, $c_i \equiv \cos\theta_i$, where θ_i are the arbitrary complex angles of the orthogonal matrix R defined in Eq. (2.33).

Notice that the most relevant parameters to get large intergenerational mixings are m_{N_3} in the case of hierarchical neutrinos (m_N in the degenerate case) and the complex angles θ_1 and θ_2 (all θ_i for the degenerate case). The size of $|\delta_{32}|$ can be indeed quite large. For instance, for mass values of the heavy neutrinos m_{N_3} (or m_N) in the range $10^{14} - 10^{15}$ GeV and θ_i (i= 1 or/and 2) with large modulus in the range $3-5$ or/and large argument in the range $[\pm\pi/4, \pm\pi/2]$ one can get values of $|\delta_{32}|$ as large as 0.5-10. This is clearly illustrated in the contour plots of Figure 4.2, where we have considered both scenarios with either degenerate or hierarchical heavy neutrinos and we have explored in the (m_{N_i}, θ_i) parameter space. In the hierarchical case the relevant mass is the heaviest one m_{N_3} and the predictions for $|\delta_{32}|$ do not vary appreciably with $m_{N_{1,2}}$. In addition, we have checked that $|\delta_{32}|$ is nearly constant with θ_3. The contour plots for θ_1 (not shown) are very similar to those of θ_2. We have also found that the largest values of $|\delta_{32}|$ are obtained for the degenerate case with both θ_1 and θ_2 being large. This is also clearly illustrated in the lower right panel of Fig. 4.2. For instance, we get $|\delta_{32}| \simeq 5$ for

$m_N = 10^{14}$ GeV and $\theta_1 = \theta_2 = 3\exp(i\pi/4)$. Notice also that values of $|\delta_{32}|$ larger than ~ 0.5 correspond in our parameterization of the Yukawa coupling matrices in Eq. (2.28) to values of $|Y_\nu|^2/(4\pi)$ that are above the threshold where the SPheno code [190], that will be used later, sets the limit of perturbativity, which is at $|Y_\nu|^2/(4\pi) \sim 1.5$. It means that, in the following, we will be able to provide full predictions for the decay rates with the SPheno code only for those model parameters producing Y_ν values that are within the perturbativity region or, equivalently, leading to $|\delta_{32}| < 0.5$. The implications for the $\tau \to \mu f_0(980)$ and $\tau \to \mu\eta$ decays of values $|\delta_{32}| \geq 0.5$ will be explored later, not with our full computation implemented by us in SPheno, but using approximate formulas that will also be presented here and that turn out to work reasonably well.

Finally, one more comment is in order here regarding the use of the parametrization of Eq. (2.28) for the neutrino Yukawa couplings. Whenever we use this parametrization in this chapter, for the numerical evaluation of the full one-loop LFV rates, the input values that we use in this formula for the light neutrino masses m_{ν_i} $(i = 1, 2, 3)$ are not their experimental values at the low energies, but their corresponding values, after the one-loop running from these low energies to the high energy, given by the Majorana scale. This is the scale at which the parametrization of the seesaw formula of Eq. (2.28) really holds.

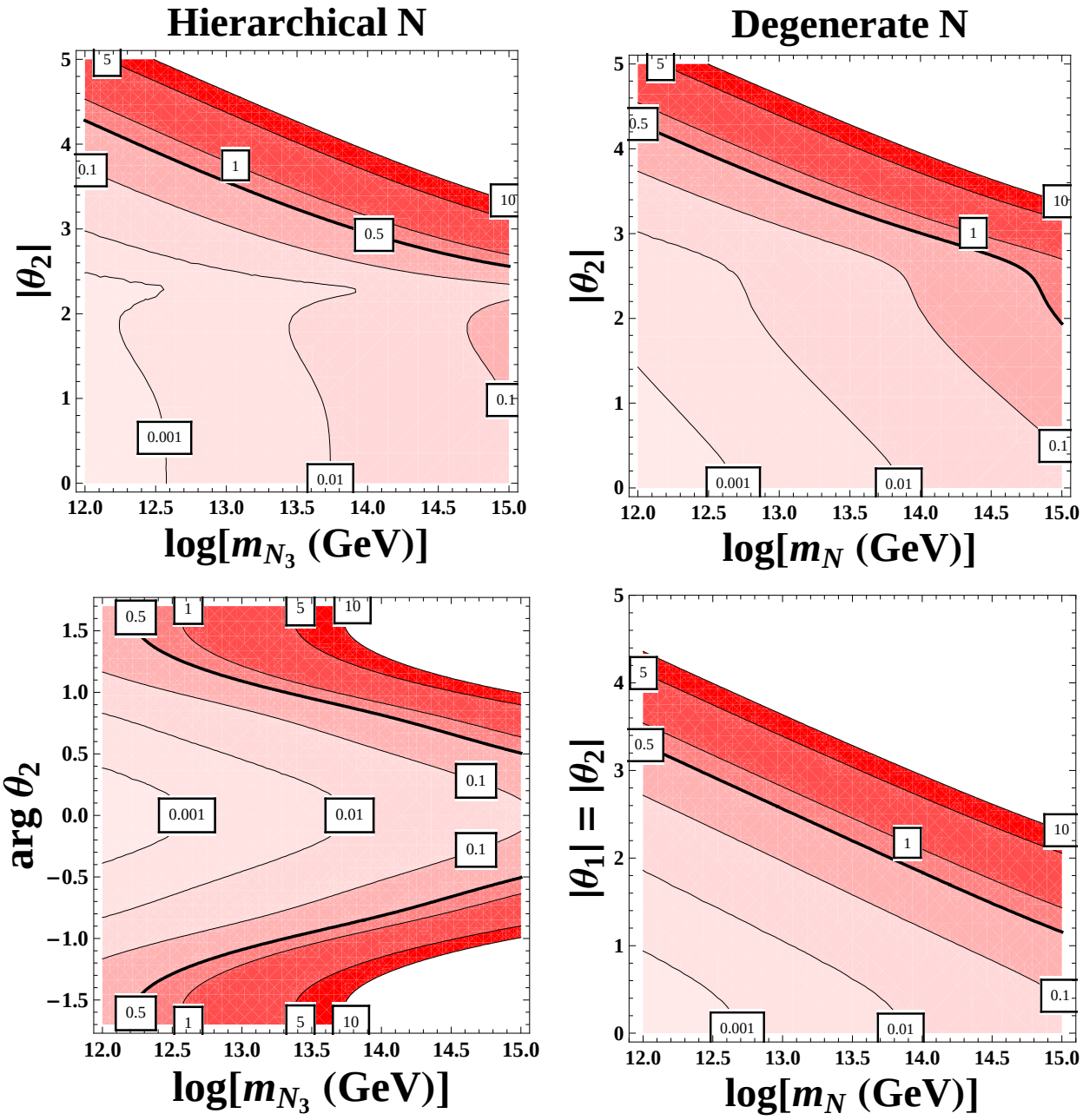

Figure 4.2: Contours of $|\delta_{32}|$ in the CMSSM-seesaw scenario: 1) For hierarchical heavy neutrinos. Upper left panel: in the $(|\theta_2|,m_{N_3})$ plane for $\arg\theta_2 = \pi/4$. Lower left panel: in the $(\arg\theta_2,m_{N_3})$ plane for $|\theta_2| = 3$. The other heavy neutrino parameters are set to $\theta_1 = \theta_3 = 0$, $m_{N_1} = 10^{10}$ GeV, $m_{N_2} = 10^{11}$ GeV; 2) For degenerate heavy neutrinos. Upper right panel: in the $(|\theta_2|,m_N)$ plane for $\arg\theta_2 = \pi/4$ and $\theta_1 = \theta_3 = 0$. Lower right panel: in the $(|\theta_1| = |\theta_2|,m_N)$ plane for $\arg\theta_1 = \arg\theta_2 = \pi/4$, and $\theta_3 = 0$. In all plots we have set: $M_{\rm SUSY} = M_0 = M_{1/2}$, $A_0 = 0$, $\tan\beta = 50$, and the θ_i are expressed in radians.

4.4 Hadronisation of quark bilinears

Semileptonic decays of the tau lepton, like the ones we are studying here, are a relatively clean scenario from the strong interaction point of view. Hadrons in the final state result from the hadronization of quark bilinears, namely $\overline{\psi}\,\Gamma\psi$, where ψ is a vector in the $SU(3)_F$ flavor space and Γ is, in general, a matrix both in the spinor and the flavor space.

A suitable framework to handle the procedure of hadronization is provided by the large-N_C expansion of $SU(N_C)$ QCD [191], with N_C being the number of colors. In short it states that in the $N_C \to \infty$ limit any Green function is given by meromorphic functions provided by the tree level diagrams of a Lagrangian theory with an infinite spectrum of zero-width states. Though we do not know how to implement fully this limit, an useful [192] although debatable [193] approach lies in cutting the spectrum, keeping only the lightest multiplets of resonances. We will attach to this tenet as a guiding principle.

A suitable tool to realize the $1/N_C$ expansion is provided by chiral Lagrangians. More specifically we consider Lagrangians that are invariant under the $SU(3)_L \times SU(3)_R$ chiral symmetry. In those processes where hadron resonances do not play a dynamical role, Chiral Perturbation Theory (χPT) [101–103] is the appropriate scheme to describe the strong interaction of Goldstone bosons (π, K and η). This is the case, for instance, of $\tau \to \mu P$ (being P short for a pseudoscalar meson). However, when resonances participate in the dynamics of the process it is necessary to include them as active degrees of freedom in the Lagrangian as it is properly done in the Resonance Chiral Theory (RχT) frame [105]. Hence we will make use of both RχT and χPT, to hadronise the relevant currents that appear in the processes under study here.

We consider bilinear light quark operators coupled to external sources and added to the massless QCD Lagrangian:

$$\mathcal{L}_{\rm QCD} \;=\; \mathcal{L}^0_{\rm QCD} + \overline{q}\,[\gamma_\mu\,(v^\mu \,+\, \gamma_5\, a^\mu) \,-\, (\,s \,-\, i\,p\,\gamma_5)]\,q\,, \tag{4.16}$$

where the vector ($v^\mu = v^\mu_i \lambda^i/2$), axial-vector ($a^\mu = a^\mu_i \lambda^i/2$), scalar ($s = s_i \lambda^i$) and pseudoscalar ($p = p_i \lambda^i$) external fields are 3×3 hermitian matrices in flavor space, and $\mathcal{L}^0_{\rm QCD}$ is the massless QCD Lagrangian[1]. The Lagrangian in Eq. (4.16) exhibits a $SU(3)_L \times SU(3)_R$ chiral symmetry, remaining invariant under the following transformations:

$$q \;\;\to\;\; g_R\, P_R\, q + g_L\, P_L\, q\,,$$

[1]The Gell-Mann matrices λ^i are normalized as $\langle \lambda_i \lambda_j \rangle = 2\delta_{ij}$ and the gluons are denoted here by G_μ.

$$
\begin{aligned}
(v_\mu \pm a_\mu) &\rightarrow g_{R,L}\,(v_\mu \pm a_\mu)\,g_{R,L}^\dagger + i g_{R,L}\,\partial_\mu\, g_{R,L}^\dagger\,, \\
(s + i\,p) &\rightarrow g_R\,(s + i\,p)\,g_L^\dagger\,,
\end{aligned}
\tag{4.17}
$$

with $g_{R,L} \,\epsilon\, SU(3)_{L,R}$.

This Lagrangian density gives the QCD generating functional $\mathcal{Z}_{\rm QCD}\,[v,a,s,p]$ as follows,

$$
e^{i\,\mathcal{Z}_{\rm QCD}[v,a,s,p]} \,=\, \int [\,DG_\mu\,][\,Dq\,][\,D\overline{q}\,]\, e^{i\,\int d^4x\,\mathcal{L}_{\rm QCD}[q,\overline{q},G,v,a,s,p]}\,. \tag{4.18}
$$

This generating functional admits an expression in powers of the external momenta and of the quark masses. Approximating it by a given order in this expansion defines the usual χPT.

In order to construct the corresponding Lagrangian theory in terms of the lightest hadron modes we need first to specify them. The lightest $U(3)$ nonet of pseudoscalar mesons is given by,

$$
\begin{aligned}
\Phi(x) &= \sum_{a=0}^{8} \frac{\lambda_a}{\sqrt{2}}\,\varphi_a \qquad (4.19)\\
&= \begin{pmatrix}
\dfrac{1}{\sqrt{2}}\,\pi^0 + \dfrac{1}{\sqrt{6}}\,\eta_8 + \dfrac{1}{\sqrt{3}}\eta_0 & \pi^+ & K^+ \\
\pi^- & -\dfrac{1}{\sqrt{2}}\,\pi^0 + \dfrac{1}{\sqrt{6}}\,\eta_8 + \dfrac{1}{\sqrt{3}}\eta_0 & K^0 \\
K^- & \bar{K}^0 & -\dfrac{2}{\sqrt{6}}\,\eta_8 + \dfrac{1}{\sqrt{3}}\eta_0
\end{pmatrix},
\end{aligned}
$$

and it is realized nonlinearly into the unitary matrix in the flavor space,

$$
u(\varphi) = \exp\left[i\,\frac{\Phi}{\sqrt{2}F}\right]. \tag{4.20}
$$

As a consequence of $SU(3)_L \times SU(3)_R$ chiral symmetry and its spontaneous breakdown, the generating functional $\mathcal{Z}_{QCD}$ coincides in the meson sector at leading order in χPT, $\mathcal{O}(p^2)$, with the classical action:

$$
\mathcal{Z}_{QCD} = \int d^4x\; \mathcal{L}_2^{\chi\rm PT} \tag{4.21}
$$

where

$$
\mathcal{L}_2^{\chi\rm PT} \,=\, \frac{F^2}{4}\,\langle u_\mu\,u^\mu \,+\, \chi_+\rangle\,, \tag{4.22}
$$

with

$$
u_\mu \;=\; i[u^\dagger(\partial_\mu - i r_\mu)u - u(\partial_\mu - i\ell_\mu)u^\dagger]\,,
$$

$$\chi_+ \;=\; u^\dagger \chi u^\dagger + u \chi^\dagger u \quad , \quad \chi = 2B_0(s+ip) \;\; , \tag{4.23}$$

and $\langle \ldots \rangle$ stands for the trace in the flavor space. Interactions with electroweak bosons can be accommodated as usual in χPT through the vector $v_\mu = (r_\mu + \ell_\mu)/2$ and axial-vector $a_\mu = (r_\mu - \ell_\mu)/2$ external fields. The scalar field s incorporates explicit chiral symmetry breaking through the quark masses $s = \mathcal{M} + ...$, where $\mathcal{M} = \mathrm{diag}(m_u, m_d, m_s)$ and finally, $F \simeq F_\pi \simeq 92.4$ MeV is the pion decay constant and $B_0 F^2 = -\langle 0|\overline{\psi}\psi|0\rangle_0$ is the chiral condensate in the chiral limit. The chiral tensor χ provides masses to the Goldstone bosons through the external scalar field s, as can be seen in Eq. (4.23). Indeed in the isospin limit we have

$$\chi \;=\; 2\,B_0\,\mathcal{M} \,+ ... \,=\, \begin{pmatrix} m_\pi^2 & & \\ & m_\pi^2 & \\ & & 2m_K^2 - m_\pi^2 \end{pmatrix} + \,.... \tag{4.24}$$

Hence we identify (in the isospin limit)

$$\begin{aligned} B_0\, m_u \;&=\; B_0\, m_d \;=\; \frac{1}{2}\, m_\pi^2 \,, \\ B_0\, m_s \;&=\; m_K^2 - \frac{1}{2}\, m_\pi^2 \,, \end{aligned} \tag{4.25}$$

that will be used when considering the Higgs contributions to the LFV decays.

The mass eigenstates η and η' are defined from the octet η_8 and singlet η_0 states through the rotation

$$\begin{pmatrix} \eta \\ \eta' \end{pmatrix} = \begin{pmatrix} \cos\theta & -\sin\theta \\ \sin\theta & \cos\theta \end{pmatrix} \begin{pmatrix} \eta_8 \\ \eta_0 \end{pmatrix} , \tag{4.26}$$

and we input[2] a value of $\theta \simeq -18^\circ$.

Next, we specify our framework for the hadronization of the quark bilinears into the $f_0(980)$ meson. We use here the chiral Lagrangian of RχT that is a suitable tool to realise the $1/N_C$ expansion of $SU(N_C)$ QCD and includes both the Goldstone bosons $\Phi(\pi,\, K$ and $\eta)$ and the resonances as active degrees of freedom, and their interactions. For the present work, it is sufficient to consider the lightest nonet of scalar resonances $R(0^+)$ in RχT. By demanding the chiral symmetry invariance this resonance Lagrangian reads [105, 108, **?**]

$$\mathcal{L}_{\mathrm{R}\chi\mathrm{T}} \;=\; \mathcal{L}_2^{\chi\mathrm{PT}} \,+\, \mathcal{L}_{\mathrm{kin}}^R \,+\, \mathcal{L}_{(2)}^R \;, \tag{4.27}$$

[2]The values of θ in the literature range between $\theta \sim -12^\circ$ up to $\theta \sim -20^\circ$ [194].

where $\mathcal{L}_2^{\chi\rm PT}$ is the chiral Lagrangian given in Eq. (4.22) and

$$\begin{aligned}\mathcal{L}^R_{\rm kin} &= \frac{1}{2}\langle \nabla^\mu R \nabla_\mu R - M_R^2 R^2\rangle \,, \\ \mathcal{L}^R_{(2)} &= c_d \,\langle\, R\, u_\mu u^\mu \,\rangle \,+\, c_m \,\langle\, R\,\chi_+ \,\rangle \,,\end{aligned} \tag{4.28}$$

with:

$$\nabla_\mu R \;=\; \partial_\mu R + [\Gamma_\mu, R] \,, \qquad\qquad \Gamma_\mu = \frac{1}{2}\,[\, u^\dagger(\partial_\mu - i r_\mu) u + u(\partial_\mu - i\ell_\mu)u^\dagger\,], \tag{4.29}$$

and M_R is the resonance mass. Short-distance dynamics [106] constrains the couplings of RχT by imposing the QCD ruled behaviour of Green functions and associated form factors. For the couplings in $\mathcal{L}^R_{(2)}$ one gets[3] :

$$2\,c_m \;=\; 2\,c_d \;=\; F \,. \tag{4.30}$$

The connection between the low energy lagrangian $\mathcal{L}_{\rm R\chi T}$ and QCD comes via the contribution of the low energy modes to the QCD functional which is formally given by:

$$e^{i\,\mathcal{Z}_{\rm QCD}[v,a,s,p]}\Big|_{\rm low\ modes} = \int [Du][DR]\, e^{i\int d^4x\,\mathcal{L}_{\rm R\chi T}[u,R,v,a,s,p]} \,. \tag{4.31}$$

With this identification we can already carry out the hadronization of the bilinear quark currents included in Eq. (4.16) by taking the appropriate partial derivatives, with respect to the external auxiliary fields, of the functional action,

$$\begin{aligned} V^i_\mu \,=\, \overline{q}\,\gamma_\mu\,\frac{\lambda^i}{2}\,q \;&=\; \frac{\partial\,\mathcal{L}_{\rm R\chi T}}{\partial\, v^\mu_i}\Bigg|_{j=0}\,, \qquad & A^i_\mu \,=\, \overline{q}\,\gamma_\mu\,\gamma_5\,\frac{\lambda^i}{2}\,q \;&=\; \frac{\partial\,\mathcal{L}_{\rm R\chi T}}{\partial\, a^\mu_i}\Bigg|_{j=0}\,, \\ S^i \,=\, -\,\overline{q}\,\lambda^i\,q \;&=\; \frac{\partial\,\mathcal{L}_{\rm R\chi T}}{\partial\, s_i}\Bigg|_{j=0}\,, \qquad & P^i \,=\, \overline{q}\,i\gamma_5\lambda^i\,q \;&=\; \frac{\partial\,\mathcal{L}_{\rm R\chi T}}{\partial\, p_i}\Bigg|_{j=0}\,, \end{aligned} \tag{4.32}$$

where $j=0$ indicates that all external currents are set to zero. This gives

$$V^i_\mu \;=\; \frac{F^2}{4}\,\langle\,\lambda^i\,\left(u\,u_\mu\,u^\dagger \,-\, u^\dagger\,u_\mu\,u\right)\rangle \,-\, \frac{F_V}{2\sqrt{2}}\,\langle\,\lambda^i\,\partial^\nu\left(u^\dagger\,V_{\nu\mu}\,u \,+\, u\,V_{\nu\mu}\,u^\dagger\right)\rangle\,,$$

[3]Short-distance constraints on the RχT couplings depend on the operators included. The result in Eq. (4.30) is obtained when only linear operators in the resonances are considered [105]. A weaker constraint, though compatible with that result, arises if non-linear couplings in the resonances are included [108].

$$
\begin{aligned}
A^i_\mu &= \frac{F^2}{4}\,\langle\,\lambda^i\,\left(u\,u_\mu\,u^\dagger\,+\,u^\dagger\,u_\mu\,u\right)\rangle\,, \\
S^i &= \frac{1}{2}\,B_0F^2\,\langle\,\lambda^i\,\left(u^\dagger u^\dagger\,+\,uu\right)\rangle\,, \\
P^i &= \frac{i}{2}\,B_0F^2\,\langle\,\lambda^i\,\left(u^\dagger u^\dagger\,-\,uu\right)\rangle\,.
\end{aligned}
\tag{4.33}
$$

In particular, using Eq. (4.33), Eq. (4.32) and Eq. (4.26) we can find a compact expression of the hadronization of the the pseudo-Goldstone boson η in terms of quark bilinears:

$$
\eta(548) = \frac{-i}{2B_0F}\left\{\left(\frac{-1}{\sqrt{3}}\cos\theta + \frac{\sqrt{2}}{\sqrt{3}}\sin\theta\right)\left(\bar{u}\gamma_5 u + \bar{d}\gamma_5 d\right) + \left(\frac{2}{\sqrt{3}}\cos\theta + \frac{\sqrt{2}}{\sqrt{3}}\sin\theta\right)\bar{s}\gamma_5 s\right\} \tag{4.34}
$$

From this expression we can already expect a relevant contribution to the decay $\tau \to \mu\eta$ coming from the A^0 mediated channel due to the contribution of bilinears of strange quarks in the hadronization of the η meson. The strength of the coupling of the A^0 to the strange quarks is given by $g_{A^0\bar{s}s} = \dfrac{g}{2M_W} m_s \tan\beta$, and as we could appreciate in Eq. (4.25) in the isospin limit $m_s \propto m_K^2$. Therefore, the coupling of A^0 to the η meson is proportional to m_K^2 and to $\tan\beta$ and it is expected to be large in the large $\tan\beta$ regime.

The QCD spectrum of scalar resonance states is far from being settled and constitutes, at present, a highly debated issue. It is not our goal in this thesis to enter in the details of the discussion and, therefore, we will attach to the scheme put forward in [107] for the description of the isosinglet $f_0(980)$ state. The later is defined as a rotation of the octet R_8 and the singlet R_0 components of the $R(0^+)$ nonet,

$$
\begin{pmatrix} f_0(1500) \\ f_0(980) \end{pmatrix} = \begin{pmatrix} \cos\theta_S & -\sin\theta_S \\ \sin\theta_S & \cos\theta_S \end{pmatrix} \begin{pmatrix} R_8 \\ R_0 \end{pmatrix}\,. \tag{4.35}
$$

The value of the θ_S mixing angle is uncertain. In the analysis carried out in [107] considering nonet breaking (i.e. subleading effects in the large-N_C expansion) a possible dual scenario is favored :

A) The candidates for the nonet are: $f_0(980)$, $K_0^*(1430)$, $a_0(1450)$ and $f_0(1500)$. In this framework the $a_0(980)$ is dynamically generated (through loops). The mixing angle, around $\theta_S \simeq 30^\circ$, provides a dominant non-strange component for the lightest $I = 0$ state and, consequently, justifies their dominant decay into two pions.

B) The nonet would be composed by: $f_0(980)$, $a_0(980)$, $K_0^*(1430)$ and $f_0(1500)$. Hence $a_0(980)$ is a pre-existing state in the $N_C \to \infty$ limit. The mixing angle in this case is around $\theta_S \simeq 7^\circ$, that gives a noticeable strange component.

Given the uncertainty provided by the large corrections due to $1/N_C$ subleading effects we will consider the two previous scenarios for the $f_0(980)$ as plausible and will present estimates of the $\tau \to \mu f_0(980)$ decay rates for the two mixing angles, $\theta_S \simeq 7^\circ$ and $\theta_S \simeq 30^\circ$. The dispersion between these two results can be considered as part of the theoretical error in our estimates.

Finally, the hadronization of the relevant scalar quark bilinears into the $f_0(980)$ is implemented by replacing the following expressions in the results for the decay rates at the quark level,

$$\begin{aligned}
\overline{u}\,u &= -\left[\frac{1}{2}S_3 + \frac{1}{2\sqrt{3}}S_8 + \frac{1}{\sqrt{6}}S_0\right], \\
\overline{d}\,d &= -\left[-\frac{1}{2}S_3 + \frac{1}{2\sqrt{3}}S_8 + \frac{1}{\sqrt{6}}S_0\right], \\
\overline{s}\,s &= -\left[-\frac{1}{\sqrt{3}}S_8 + \frac{1}{\sqrt{6}}S_0\right],
\end{aligned} \tag{4.36}$$

with

$$S_i = \frac{8}{\sqrt{2}}\,B_0\,c_m\,R_i\,, \quad i = 0, 3, 8\,, \tag{4.37}$$

and, according to Eq. (4.30), $c_m = F/2$. As R_3 does not contain information on $f_0(980)$ (in the isospin limit) we will discard the S_3 contribution.

Using Eq. (4.35), Eq. (4.36) and Eq. (4.37) one gets the following expression of the $f_0(980)$ scalar mesons in terms of quark bilinears:

$$f_0(980) = \frac{-1}{2\sqrt{2}B_0F}\left\{\left(\frac{\sqrt{2}}{\sqrt{3}}\cos\theta_S + \frac{1}{\sqrt{3}}\sin\theta_S\right)\left(\bar{u}u + \bar{d}d\right) + \left(\frac{\sqrt{2}}{\sqrt{3}}\cos\theta_S - \frac{2}{\sqrt{3}}\sin\theta_S\right)\bar{s}s\right\} \tag{4.38}$$

As we can observe the scalar $f_0(980)$ meson has also an important contribution of strange quark bilinears. Since the strength of the coupling of H^0 to the strange quarks is given by $g_{H^0\bar{s}s} = \dfrac{g m_s \cos\alpha}{2M_W \cos\beta}$, and since $m_s \propto m_K^2$, one expects large couplings of H_0 to the f_0 meson, mainly at large $\tan\beta$. In contrast, the coupling of h^0 to the f_0 meson, given

by $g_{h^0\bar{s}s} = \dfrac{g m_s \sin\alpha}{2 M_W \cos\beta}$, is not enhanced at large $\tan\beta$. Hence, $\tau \to \mu f_0(980)$ is expected to be dominated by the exchange of a H^0, rather than a h^0, at large $\tan\beta$.

Before proceeding, a word of caution is necessary when dealing with processes with resonances as initial or final states. A resonance is not an asymptotic state as it decays strongly. Hence from a quantum field theory point of view RχT only describes the creation, propagation and destruction of resonances and the later should not appear as "in" or "out" states. For instance, in our case the physical process should be $\tau \to \mu\pi\pi$ mediated by a $f_0(980)$ state, and not $\tau \to \mu f_0(980)$. However the description of scalars, as has been pointed out, is far from clear and therefore considering the $f_0(980)$ as an asymptotic state should not increase effectively the already rather large uncertainty.

4.5 Results for BR($\tau \to \mu\eta$)

The semileptonic $\tau \to \mu\eta$ decay can be mediated by the $\mathcal{CP}$ odd A^0 Higgs boson and by the Z gauge boson. The contributing diagrams are shown in Figure 4.3. In these diagrams the LFV vertex is represented by a black circle and the hadronic vertex by a white box. The one loop diagrams contributing to the LFV vertex, $\tau\mu A^0$, are those shown in Figure 4.7 with $H_p = A^0$. The full calculation of the ratio of this semileptonic decay was performed in [97]. For the numerical evaluation of BR($\tau \to \mu\eta$) we follow closely the procedure and formulas of Ref. [97] and use their implementation into the SPheno code as well. Our main interest here is to evaluate separately the Z and the A^0 contributions to the decay rate of $\tau \to \mu\eta$ for further comparison with the decay rates of the channel $\tau \to \mu f_0(980)$. This separation is studied here for the first time.

In Figure 4.6 we have plotted the branching ratio of $\tau \to \mu\eta$ as a function of $\tan\beta$, in a NUHM-seesaw model with the following choice of SUSY parameters $\delta_1 = -2.4, \delta_2 = 0, M_0 = M_{1/2} = 250$ GeV and a spectrum of hierarchical heavy Majorana neutrinos, being the only non vanishing angle from the R matrix $\theta_2 = 2.9e^{i\pi/4}$. These values of $\delta_{1,2}$ and M_{SUSY} have been chosen so that the wanted light A^0 boson, $m_{A^0} \lesssim 200$ GeV, and heavy SUSY spectra are produced (see Figure 4.1). The values of θ_2 and m_{N_i} are set to produce a sizeable τ-μ LFV transition (see Figure 4.2). Different predictions have been shown, the full result, where both the Z and A^0 contributions have been taken into account, the separated contributions coming from the A^0 mediated channel and the Z mediated channel and, finally, the approximate result of the Higgs mediated channel.

This approximate result was found in [97] and it is only valid in the Llog and mass insertion approximation and in the large $\tan\beta$ regime. We include here their estimate for completeness and further comparison:

$$\mathrm{BR}(\tau \to \mu\eta)_{H_{\mathrm{approx}}} = 1.2 \times 10^{-7}\,(\theta = 18^\circ)\,|\delta_{32}|^2 \left(\frac{100}{m_{A^0}(\mathrm{GeV})}\right)^4 \left(\frac{\tan\beta}{60}\right)^6 . \qquad (4.39)$$

The main feature of Figure 4.4 is the increase of the $\mathrm{BR}(\tau \to \mu\eta)$ with $\tan\beta$. In fact, $\mathrm{BR}(\tau \to \mu\eta)_{\tan\beta=50} \sim 10^{-9}$ close to the present experimental bound shown in Table 4.2. For $\tan\beta \geq 20$, the Higgs contribution dominates the decay and the full result can be reproduced neglecting the Z boson contribution and using the simplified formula of Eq. (4.39). Thanks to this formula, one can easily understand the behaviour of the decay rate with $\tan\beta$. The reason for this Higgs dominance is because of the large A^0 coupling to the strange components of the η meson, which results in a large $A^0\eta$ coupling proportional to m_K^2.

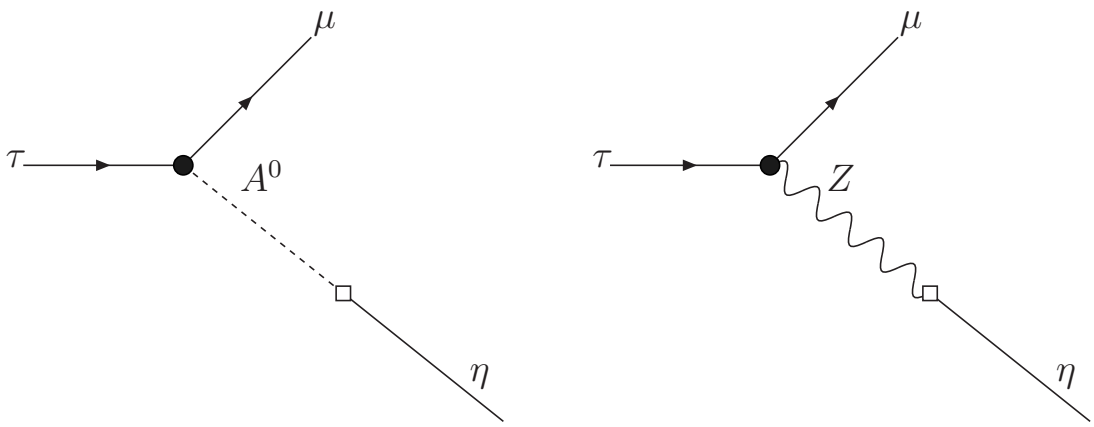

Figure 4.3: A^0 and Z contribution to the LFV semileptonic $\tau \to \mu\eta$ decay

In Figure 4.5 we show the excluded regions in the $(m_{A^0}, \tan\beta)$ plane for fixed values of $|\delta_{32}| = 0.1, 0.5, 1, 5, 10$, which are easily reachable in our scenarios (see Figure 4.2). For completeness, we have included the present experimental bound for the SM Higgs mass at 114.4 GeV. For each $|\delta_{32}|$ the excluded areas are the ones above the corresponding contour line. For generating this contour plot, we have made use of the approximate formula of the branching ratio of $\tau \to \mu\eta$ shown in Eq. (4.39). By comparing the corresponding

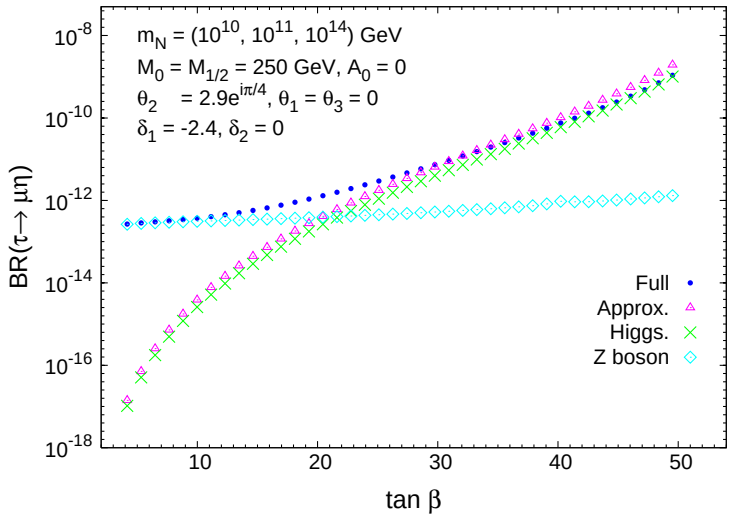

Figure 4.4: BR($\tau \to \mu\eta$) as a function of $\tan\beta$. The blue points correspond to the predicted rate of the full result, the green crosses (light blue diamonds) show the contribution coming from the A^0 (Z) mediated channel and the magenta triangles correspond to the approximate result for the Higgs mediated contribution

predicted BR($\tau \to \mu\eta$) for fixed values of the LFV mixing parameter $|\delta_{32}|$ with the present upper experimental bound on the decay, i.e. BR($\tau \to \mu\eta$) $< 2.3 \times 10^{-8}$, one gets regions of the (m_{A^0}, $\tan\beta$) plane that fulfill the bound constraints and are allowed (below the corresponding $|\delta_{32}|$ contour line) and other regions that are excluded (above the corresponding $|\delta_{32}|$ contour line), because they lead to too large BR($\tau \to \mu\eta$) not compatible with present data. As one can appreciate, for large values of $|\delta_{32}|$ one can already exclude large regions, for example for $|\delta_{32}| = 10$, one can exclude $\tan\beta \geq 30$ and $m_{A^0} \leq 200$. However, one should keep in mind that the wider black contour line $|\delta_{32}| \sim 0.5$ sets the limit of perturbativity in the neutrino Yukawa couplings, as already said in Sect. 4.3. Therefore, for larger values of $|\delta_{32}|$, the predicted decay rates with Eq. (4.39) are not so reliable because we are beyond the perturbative regime and the MI approximation is no longer valid.

4.6 Results for BR($\tau \to \mu f_0(980)$)

Analytical results

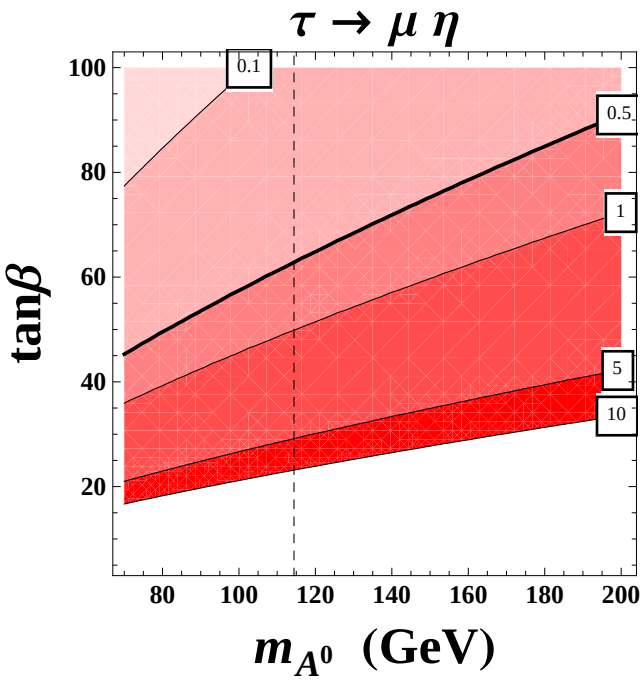

Figure 4.5: The excluded regions in the $(m_{A^0}, \tan\beta)$ plane are the areas above the contour lines corresponding to fixed $|\delta_{32}| = 0.1, 0.5, 1, 5, 10$.

The semileptonic $\tau \to \mu f_0(980)$ decay can be mediated by h^0 and H^0 Higgs bosons, as shown in Fig. 4.6. In this figure the LFV vertex is represented by a black circle and the hadronic vertex by a grey box. The total amplitude for this decay, $T_H = T_{h^0} + T_{H^0}$, is first evaluated at the quark level, that is for $\tau \to \mu\overline{q}q$, and then at the hadron level by substituting the quark bilinears by the corresponding scalar currents containing the $f_0(980)$ meson as evaluated from $\mathcal{L}_{R\chi T}$ in Eq. (4.27). The amplitude at the quark level can be computed in terms of the corresponding $\tau\mu H_p$ one-loop vertex functions, $H^{(p)}_{L,R}$, with $H_p = h^0, H^0$, resulting from the evaluation of the diagrams in Fig. 4.7 with sleptons, $\tilde{l}_X$, sneutrinos, $\tilde{\nu}_X$, charginos, $\tilde{\chi}^-_A$, and neutralinos, $\tilde{\chi}^0_A$, in the loops. The resulting amplitude at the quark level is given by:

$$T_H(\tau \to \mu\overline{q}q) = \sum_{h^0,H^0} \frac{1}{m^2_{H_p}} \Big\{ H^{(p)}_L S^{(p)}_{L,q} \left[\overline{\mu}P_L\tau\right]\left[\overline{q}P_Lq\right] + H^{(p)}_R S^{(p)}_{R,q} \left[\overline{\mu}P_R\tau\right]\left[\overline{q}P_Rq\right] + H^{(p)}_L S^{(p)}_{R,q} \left[\overline{\mu}P_L\tau\right]\left[\overline{q}P_Rq\right] + H^{(p)}_R S^{(p)}_{L,q} \left[\overline{\mu}P_R\tau\right]\left[\overline{q}P_Lq\right] \Big\} \,. \quad (4.40)$$

where $P_{L,R} = (1 \mp \gamma_5)/2$, and

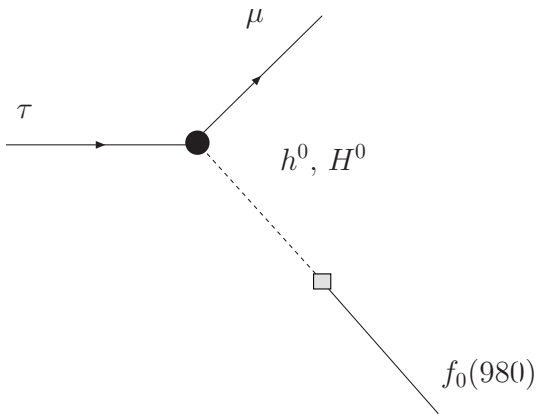

Figure 4.6: Higgs-mediated contributions to the LFV semileptonic $\tau \to \mu f_0(980)$ decay

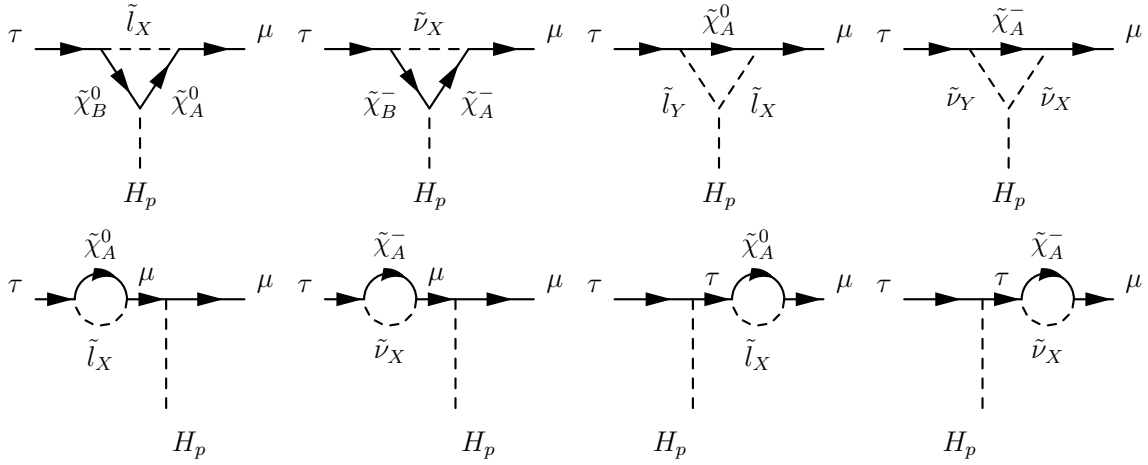

Figure 4.7: Relevant SUSY one-loop diagrams for the Higgs-mediated contributions to the $\tau \to \mu f_0(980)$ decay. Here $H_p = h^0, H^0$.

$$
\begin{aligned}
S^{(p)}_{L,q} &= \frac{g}{2M_W}\left(\frac{-\sigma_2^{(p)*}}{\sin\beta}\right) m_q\,, \quad q = u\,; \\
S^{(p)}_{L,q} &= \frac{g}{2M_W}\left(\frac{\sigma_1^{(p)*}}{\cos\beta}\right) m_q\,, \quad q = d, s\,; \\
S^{(p)}_{R,q} &= S^{(p)*}_{L,q}
\end{aligned}
\tag{4.41}
$$

with

$$\sigma_1^{(p)} = \begin{pmatrix} \sin\alpha \\ -\cos\alpha \\ i\sin\beta \end{pmatrix}, \quad \sigma_2^{(p)} = \begin{pmatrix} \cos\alpha \\ \sin\alpha \\ -i\cos\beta \end{pmatrix}. \tag{4.42}$$

Here again M_W is the W gauge boson mass, m_q the q-quark mas, α the mixing angle in the $\mathcal{CP}$-even Higgs sector, $\tan\beta$ the ratio of the two Higgs vevs and g the $SU(2)$ gauge coupling. The three entries in $\sigma_{1,2}^{(p)}$ are, in order from top to bottom, for $H_p = h^0, H^0, A^0$, respectively.

The results of the LFV vertex functions are taken from [184], and are not written here explicitely for shortness. Just to mention that it is a full one-loop computation, including all the contributions with charginos in the loops, $H_{L(R),c}^{(p)}$, and those with neutralinos, $H_{L(R),n}^{(p)}$. Besides, all these contributions are written in terms of the physical particle masses. As we have mentioned before, these physical masses are computed here in the SUSY-seesaw scenario by solving the one-loop RGEs with SPheno and for a given set of universal (in the CMSSM) or non-universal conditions (for the NUHM) at the unification scale. Since the three right-handed neutrinos and their SUSY partners are included in the RGEs, they will affect as well in the predicted physical masses at the low energies.

To get the amplitude for the process $\tau \to \mu f_0(980)$ we substitute the quark bilinears of Eq. (4.36) in Eq. (4.40) and use Eq. (4.35) and Eq. (4.37) (or equivalently, Eq. (4.38)). Notice that it is just the scalar part in $[\overline{q}P_{L,R}q]$, and not the pseudoscalar, the one that contributes in the present case. We obtain:

$$T_H(\tau \to \mu f_0(980)) = \sum_{p=h^0,H^0} c_p\, \overline{\mu}\, \tau\,, \tag{4.43}$$

where

$$c_p = \frac{g}{2M_W}\frac{1}{2m_{H_p}^2}\left(J_L^{(p)} + J_R^{(p)}\right)\left(H_R^{(p)} + H_L^{(p)}\right), \tag{4.44}$$

and

$$\begin{aligned} J_L^{(p)} &= \frac{c_m}{\sqrt{3}}\left\{\frac{\sigma_2^{(p)*}}{\sin\beta}\left[\frac{1}{\sqrt{2}}\sin\theta_S + \cos\theta_S\right] m_\pi^2 \right. \\ &\quad \left. - \frac{\sigma_1^{(p)*}}{\cos\beta}\left[\frac{3}{\sqrt{2}}\sin\theta_S\, m_\pi^2 + \left(\cos\theta_S - \sqrt{2}\sin\theta_S\right) 2\, m_K^2\right]\right\}, \\ J_R^{(p)} &= J_L^{(p)*}. \end{aligned} \tag{4.45}$$

Notice that due to the mass relations in Eq. (4.25), the couplings of the Higgs bosons, h^0 and H^0, to the quarks ($q = u, d, s$), $S^{(p)}_{L,q}$ and $S^{(p)}_{L,q}$ in Eq. (4.41), being proportional to the quark masses, lead to Higgs-f_0 couplings that are proportional to m_P^2 ($P = \pi, K$). This is seen clearly in the predicted functions $J^{(p)}_{L,R}$ of Eq. (4.45). In consequence, the dominant contributions to BR($\tau \to \mu f_0(980)$) will come clearly from the terms in the amplitude that are proportional to m_K^2.

Finally, the result of the branching ratio for the $\tau \to \mu f_0(980)$ decay is given by,

$$\mathrm{BR}(\tau \to \mu f_0(980)) \;=\; \frac{1}{4\pi}\,\frac{\lambda^{1/2}(m_\tau^2, m_\mu^2, m_{f_0}^2)}{m_\tau^2 \Gamma_\tau}\,\frac{1}{2}\sum_{i,f}|T_H|^2\,, \tag{4.46}$$

where

$$\frac{1}{2}\sum_{i,f}|T_H|^2 \;=\; \frac{(m_\mu + m_\tau)^2 - m_{f_0}^2}{4\,m_\tau}\,|c_{h^0} + c_{H^0}|^2\,, \tag{4.47}$$

being Γ_τ is the total τ width and $\lambda(x, y, z) = (x + y - z)^2 - 4xy$.

Approximate formula

Next we derive a simple formula which approximates reasonably well our full one-loop prediction in Eq. (4.46) and Eq. (4.47). For this, we work within the approximation of large $\tan\beta$ that is appropriate for LFV tau decays, whose rates grow quite fast with this parameter. This is especially relevant for channels where the LFV rates are dominated by the Higgs mediated diagrams, as it is the present case, and where the growth with $\tan\beta$ is extremely pronounced.

The other approximation which is used frequently in the literature, due to its simplicity, is the use of the mass insertion (MI) method, where the tau-muon LFV is encoded in the dimensionless parameters δ^{32}_{XY} ($XY = LL, RR, LR$). In the SUSY models the dominant one is δ^{32}_{LL} and its expression in the LLog approximation, $(\delta^{32}_{LL})_{\mathrm{LLog}} \equiv \delta_{32}$, is that given in Eq. (4.14).

It is known [184] [99] that at large $\tan\beta$ the vertex function H_L dominates H_R by about a factor m_τ/m_μ. In addition $H_L^{H^0}$ is by far larger than $H_L^{h^0}$ in this limit, and one can safely neglect the later one. More specifically, by using the MI approximation, its chargino and neutralino contributions in the large $\tan\beta$ and heavy M_{SUSY} limits give, correspondingly, the following expressions :

$$H^{(H^0)}_{L,c} \;\;=\;\; \frac{g^3}{16\pi^2}\,\frac{m_\tau}{12 M_W}\,\delta_{32}\,\tan^2\beta\,,$$

$$H_{L,n}^{(H^0)} \;=\; \frac{g^3}{16\pi^2}\,\frac{m_\tau}{24 M_W}\,(1-3\tan^2\theta_W)\,\delta_{32}\,\tan^2\beta\,. \qquad (4.48)$$

One can further verify that H_c dominates H_n by about a factor 20, so that we will simplify $H_L \simeq H_{L,c}$.

On the other hand, we also consider the large $\tan\beta$ limit of the functions that define the H^0 couplings to $f_0(980)$, J_L and J_R in Eq. (4.45). We obtain :

$$J_L^{(H^0)} \;=\; J_R^{(H^0)} \;=\; \frac{F}{2\sqrt{3}}\tan\beta\left[\frac{3}{\sqrt{2}}\sin\theta_S\, m_\pi^2 + (\cos\theta_S - \sqrt{2}\sin\theta_S) 2 m_K^2\right]. \quad (4.49)$$

By using the above sequence of approximations and by neglecting the muon mass, we finally get the following simple result:

$$\begin{aligned}\mathrm{BR}(\tau\to\mu f_0(980))_{\rm approx} &= \frac{1}{16\pi m_\tau^3}\left(m_\tau^2 - m_{f_0}^2\right)^2 \left|\frac{g}{2M_W}\,\frac{1}{m_{H^0}^2}\,J_L^{(H^0)}\,H_{L,c}^{(H^0)}\right|^2 \frac{1}{\Gamma_\tau} \qquad (4.50)\\ &= \begin{pmatrix} 7.3\times 10^{-8}\ (\theta_S = 7^\circ) \\ 4.2\times 10^{-9}\ (\theta_S = 30^\circ)\end{pmatrix} |\delta_{32}|^2 \left(\frac{100}{m_{H^0}(\mathrm{GeV})}\right)^4 \left(\frac{\tan\beta}{60}\right)^6.\end{aligned}$$

In the last line we see explicitly the fast growth with $\tan\beta$, as $(\tan\beta)^6$, the expected dependence with the relevant Higgs mass, as $(m_{H^0})^{-4}$, and also with the LFV parameter, as $|\delta_{32}|^2$. The two numerical factors correspond to the two assumed values for the mixing angle that defines the $f_0(980)$ state, $\theta_S = 7^\circ$ and $\theta_S = 30^\circ$. These two numbers differ by a factor 17, meaning that the predicted rates will carry a theoretical uncertainty of about this number, due to the uncertainty in the definition of the $f_0(980)$ state.

Numerical results

In the following we present the numerical predictions for $\mathrm{BR}(\tau\to\mu f_0(980))$. We first show the results from the full computation in Eq. (4.46) and Eq. (4.47) and then compare with the approximate results in Eq. (4.50) and also with the rates of other LFV tau decay channels.

In Fig. 4.8 it is shown the $\mathrm{BR}(\tau\to\mu f_0(980))$ versus the heavy neutrino masses, in both scenarios with hierarchical and degenerate heavy neutrinos. In the hierarchical case we display just the dependence with the relevant mass, m_{N_3}. As expected, from the previously manifested behaviour of $|\delta_{32}|$ with m_{N_3} (or with m_N, in the degenerate case) in Fig. 4.2, we find a fast growing of $\mathrm{BR}(\tau\to\mu f_0(980))$ with this mass. Although not explicitely shown here, we have also checked in the hierarchical case, the near independence on the

other masses, m_{N_1} and m_{N_2}. From this figure it is also evident that by choosing properly the δ_1 and δ_2 parameters of the NUHM scenario, such that the relevant Higgs boson mass m_{H^0} gets lower than for $\delta_1 = \delta_2 = 0$, the branching ratios get larger than in the CMSSM scenario. Finally, by comparing the rates of the two neutrino scenarios, and for the same input model parameter values, including the same m_N and m_{N_3}, we find rates in the degenerate case that are generally larger than in the hierarchical case. For instance, for the choice of input parameters in Fig. 4.8 we find larger rates by a factor of about 3. In the following we will focus more on the hierarchical case since it has the appealing feature of providing successful baryogenesis, via leptogenesis, for some regions of the heavy neutrino parameter space.

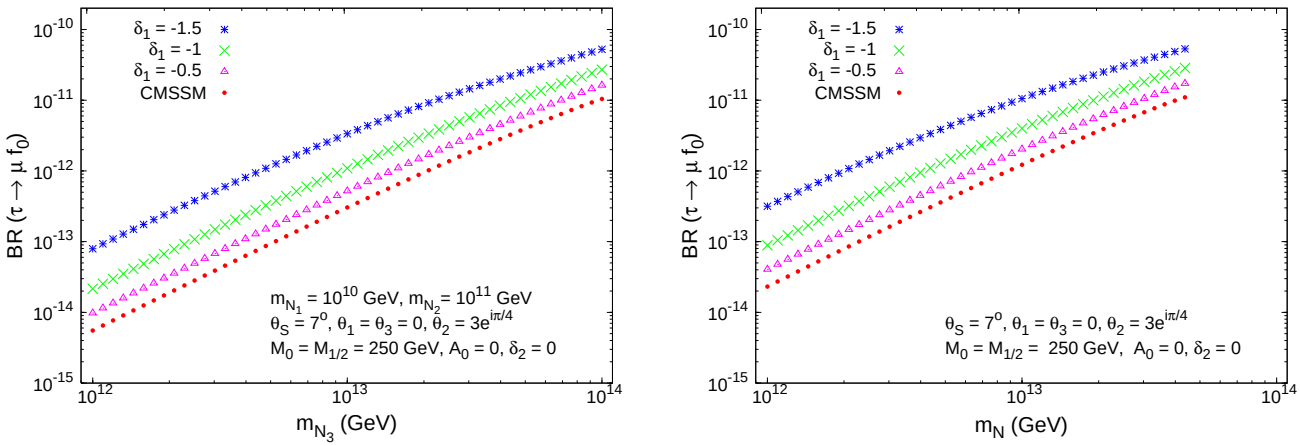

Figure 4.8: BR($\tau \to \mu f_0(980)$) in the NUHM-seesaw, for several δ_1 values, and in the CMSSM-seesaw versus the relevant heavy neutrino mass, 1) for hierarchical heavy neutrinos (left panel), and 2) degenerate heavy neutrinos (right panel).

We present the predictions of the BR($\tau \to \mu f_0(980)$) versus the soft SUSY masses M_0 and $M_{1/2}$ in Fig. 4.9. Here we take again $M_0 = M_{1/2} \equiv M_{\rm SUSY}$ and compare the results in both scenarios, the NUHM with $\delta_1 = -2.4$ and $\delta_2 = 0$, where the predicted Higgs boson masses for large $\tan\beta \sim 50$ lay within the interval 100-250 GeV, and the CMSSM. The most evident feature in this plot is the different behavior of the BR($\tau \to \mu f_0(980)$) with $M_{\rm SUSY}$ in these two scenarios. Whereas in the CMSSM the rates are found to decrease with increasing $M_{\rm SUSY}$, as expected, it clearly does not happen in the NUHM. In fact, the rates are practically constant for $M_{\rm SUSY} > 400$ GeV. The reason for this behavior is that the SUSY particles do not decouple at large $M_{\rm SUSY}$ in this decay. The non-decoupling

behavior can be checked analytically in that the LFV vertex, described by the dominant form factor H_L, tends to a constant value at asymptotically large $M_{\rm SUSY}$, as indicated in Eq. (4.48). Since, on the other hand, m_{H^0} is kept at the low region even for large $M_{\rm SUSY}$, then a constant H_L with $M_{\rm SUSY}$ implies approximately constant BR($\tau \to \mu f_0(980)$) as well.

Another interesting feature of the predicted rates in the NUHM scenario, that is manifested in Fig. 4.9 as well, is the clear dominance by many orders of magnitude of the H^0 contribution over the h^0 one in the whole $M_{\rm SUSY}$ considered interval. This is due to the fact that at large $\tan\beta$ the H^0 contribution is enhanced by a $\tan^6\beta$ factor, whereas the h^0 one is suppressed in this limit. In fact, we also see in this plot that the total rates are nearly indistinguishable from the H^0 contributions. Thus, to neglect the h^0 contribution is an extremely good approximation.

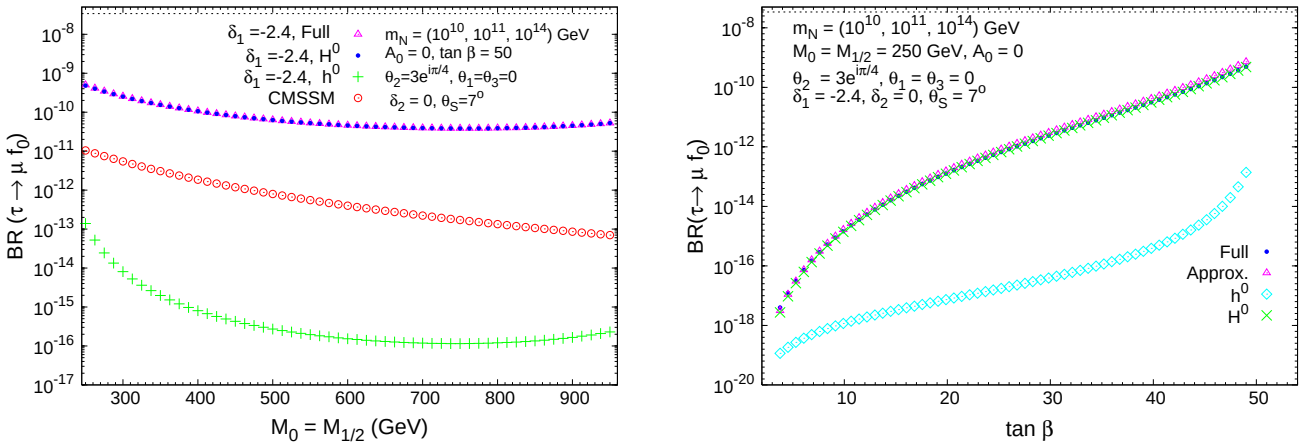

Figure 4.9: BR($\tau \to \mu f_0(980)$) in the NUHM-Seesaw scenario: 1) As a function of $M_0 = M_{1/2} = M_{\rm SUSY}$ (left panel). We show separately the H_0 and h_0 contributions as well as the total. The predictions for the total rates within the CMSSM-Seesaw scenario are also included for comparison; 2) As a function of $\tan\beta$ (right panel). Again, the dominant H^0, the subdominant h^0 and the total rates are displayed. We also include here the approximate predictions given by Eq. (4.50) for comparison with the full rates.

Concerning the Higgs sector parameters, the BR($\tau \to \mu f_0(980)$) is mainly sensitive to $\tan\beta$ and m_{H^0} since, as said before, the H^0-mediated LFV semileptonic decays grow very fast with both $\tan\beta$ and $1/m_{H^0}$. In fact, in the approximation given in Eq. (4.50), as already said, BR($\tau \to \mu f_0(980)$) goes as $(\tan\beta)^6$ and $(1/m_{H^0})^4$, respectively.

The predictions of BR($\tau \to \mu f_0(980)$) as a function of $\tan\beta$ are shown in the right panel of Fig.4.9. We show again separately the h^0 and H^0 contributions and the total rates which are clearly dominated by the H^0 in the full studied interval of $\tan\beta$. Besides, it also displays the fast growing of the total rates with $\tan\beta$, reaching values at the $\sim 10^{-9}$ level for $\tan\beta \sim 50$ which are close but still below the present experimental bound. We also see that the particular shape of the curve for the total rates is a consequence as well of the m_{H^0} dependence with $\tan\beta$ in these SUSY scenarios, as illustrated in Fig. 4.1.

The comparison between our predictions for the full result in Eq. (4.46)) and Eq. (4.47)) and the approximate results in Eq. (4.50), which include just the H^0 boson contribution, can be seen as well in Fig. 4.9. The agreement between the full and the approximate results is quite remarkable, for all the studied values in the $5 \lesssim \tan\beta \lesssim 50$ range. Therefore, we conclude that our simple formula Eq. (4.50) provides a very good approximation to BR($\tau \to \mu f_0(980)$) for all $\tan\beta$.

It is interesting to compare $\tau \to \mu f_0(980)$ to other Higgs-mediated LFV tau decay channels like $\tau \to \mu\eta$ and $\tau \to 3\mu$. First, notice that our previous result of the H^0 dominance in the $\tau \to \mu f_0(980)$ channel over the full $\tan\beta$ interval, is not true for the correlated channel $\tau \to \mu\eta$, nor the leptonic $\tau \to 3\mu$ decay. The semileptonic LFV $\tau \to \mu\eta$ decay can be mediated by a CP-odd A^0 Higgs boson and a Z boson, but the contribution from A^0 dominates the full rates only in the large $\tan\beta \gtrsim 20$ region [97, 100]. The $\tau \to 3\mu$ channel can be mediated (apart from the box diagrams, which are negligible) by a photon, a Z boson and the three neutral Higgs bosons, h^0, H^0 and A^0 [99]. The photon dominates largely this decay, except at the extreme high values of $\tan\beta \geq 60$ and $M_{\rm SUSY} \geq 1$ TeV, where the two type of contributions from the photon and the Higgs bosons, H^0 and A^0 compete. These features can be seen clearly by comparing the corresponding approximate formulas, valid at large $\tan\beta$, for their respective Higgs boson contributions. That is, one should compare our result in Eq. (4.50) to the previous results of BR($\tau \to \mu\eta$) [96, 97] and BR($\tau \to 3\mu$) [99, 180, 181, 183] for the same input parameters. These are [97],

$$\begin{aligned} \mathrm{BR}(\tau \to \mu\eta)_{H_{\rm approx}} &= \frac{1}{8\pi m_\tau^3}\left(m_\tau^2 - m_\eta^2\right)^2 \left| \frac{g}{2M_W}\,\frac{F}{m_{A^0}^2}\, B_L^{(A^0)}(\eta)\, H_{L,c}^{(A^0)} \right|^2 \frac{1}{\Gamma_\tau} \\ &= 1.2\times 10^{-7}(\theta = -18^o)\,|\delta_{32}|^2 \left(\frac{100}{m_{A^0}(\mathrm{GeV})}\right)^4 \left(\frac{\tan\beta}{60}\right)^6 , \end{aligned} \quad (4.51)$$

where,

$$B_L^{(A^0)}(\eta) \;=\; -i\frac{1}{4\sqrt{3}}\tan\beta\left[(3m_\pi^2 - 4m_K^2)\cos\theta - 2\sqrt{2}m_K^2\sin\theta\right] ,\; H_{L,c}^{(A^0)} = iH_{L,c}^{(H^0)} , \quad (4.52)$$

and:

$$\mathrm{BR}(\tau \to 3\mu)_{H_{\rm approx}} = \frac{G_F^2}{2048\pi^3}\frac{m_\tau^7 m_\mu^2}{\Gamma_\tau}\left(\frac{1}{m_{H^0}^4}+\frac{1}{m_{A^0}^4}+\frac{2}{3m_{H^0}^2 m_{A^0}^2}\right)\left|\frac{g^2\delta_{32}}{96\pi^2}\right|^2 (\tan\beta)^6 \quad (4.53)$$

$$= 1.2\times 10^{-7}\,|\delta_{32}|^2\left(\frac{100}{m_{A^0}(\mathrm{GeV})}\right)^4\left(\frac{\tan\beta}{60}\right)^6. \quad (4.54)$$

From this comparison, we conclude that, for the same choice of the model parameters, and for $\theta_S = 7°$, the three rates $\mathrm{BR}(\tau \to \mu f_0(980))$, $\mathrm{BR}(\tau \to \mu\eta)$ and $\mathrm{BR}(\tau \to 3\mu)$ are very similar if $\tan\beta \gtrsim 60$ and $M_{\rm SUSY} \gtrsim 1$ TeV. Concretely, we predict $\mathrm{BR}(\tau \to \mu f_0(980)):\mathrm{BR}(\tau \to 3\mu):\mathrm{BR}(\tau \to \mu\eta) \sim 0.6 : 1 : 1$, and they are all at the $\sim \mathcal{O}(10^{-7})$ level for $|\delta_{32}| \sim 1$, $m_H \sim 100$ GeV and $\tan\beta \sim 60$. Therefore, the three are closely competitive channels at these very large large $\tan\beta$ values.

It should also be mentioned that our estimate of $\mathrm{BR}(\tau \to \mu f_0(980))$ for $\theta_S \simeq 7^o$ and for the same input parameters, m_H, $\tan\beta$ and $|\delta_{32}|$, is about one order of magnitud smaller than the prediction in [98]. They also predict a different ratio among the three LFV channels of $\sim 1.3 : 0.5 : 1$. We believe that the main differences come from our different approaches for hadronization which produce, as we have already said, a dispersion in the results of about this factor.

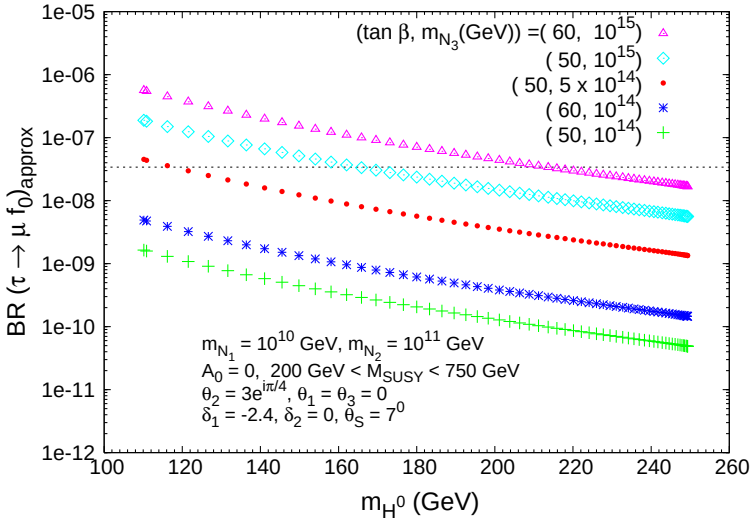

Figure 4.10: Sensitivity to the Higgs Sector in $\tau \to \mu f_0(980)$ within the NUHM-seesaw scenario. The predicted rates are within the approximation of Eq. (4.50) and are displayed as a function of m_{H^0}, for various choices of large m_{N_3} and $\tan\beta$.

Finally, we summarize the sensitivity to the Higgs sector in the NUHM-seesaw scenario in Fig.4.10. In this plot we are using the approximate formula in Eq. (4.50) and we are setting $\theta_2 = 3\, e^{i\frac{\pi}{4}}$ and $\delta_1 = -2.4$, $\delta_2 = 0$. The soft masses are varied in the range $200\,\text{GeV} \leq M_0 = M_{1/2} \equiv M_{\text{SUSY}} \leq 750\,\text{GeV}$. The explored m_{H^0} values in this plot correspond precisely to the output Higgs masses for this later M_{SUSY} interval. The main conclusion from this plot is that for large $m_{N_3} \sim 5\times 10^{14} - 10^{15}$ GeV and large $\tan\beta \sim 50-60$ the predicted rates are already at the present experimental reach and, therefore, there is indeed Higgs sensitivity in this channel. In this concern, we find interesting to further explore if with the present experimental bound of $\text{BR}(\tau \to \mu f_0(980)) \times \text{BR}(f_0(980) \to \pi^+\pi^-) < 3.4 \times 10^{-8}$ one may already exclude some region of the model parameter space. Our conclusion is that indeed it is possible to exclude the regions in the (m_{H^0}, $\tan\beta$) plane as summarized in Fig. 4.11. In this plot we assume, for simplicity, $\text{BR}(f_0(980) \to \pi^+\pi^-) \sim 1$ and choose the specific input values, $|\delta_{32}| = 0.1, 0.5, 1, 5, 10$. For each fixed $|\delta_{32}|$ the excluded region is the area above the corresponding contour line. For completeness, we have also included in this plot the present experimental lower bound for the SM Higgs mass at 114.4 GeV. Some words of caution should be said, anyway, about the conclusions from this plot since there are large uncertainties involved in the theoretical estimate of $\text{BR}(\tau \to \mu f_0(980))$. There are two main ones: 1) the uncertainty in the definition of $f_0(980)$ that, as evaluated in Eq. (4.50), can produce a dispersion of more than one order of magnitude in the predicted rates, and 2) the use of the approximate formula for values of $|\delta_{32}| > 0.5$ which are out of the region that is allowed by a perturbative approach. The use of the MI approximation for such large values of $|\delta_{32}|$ is also questionable.

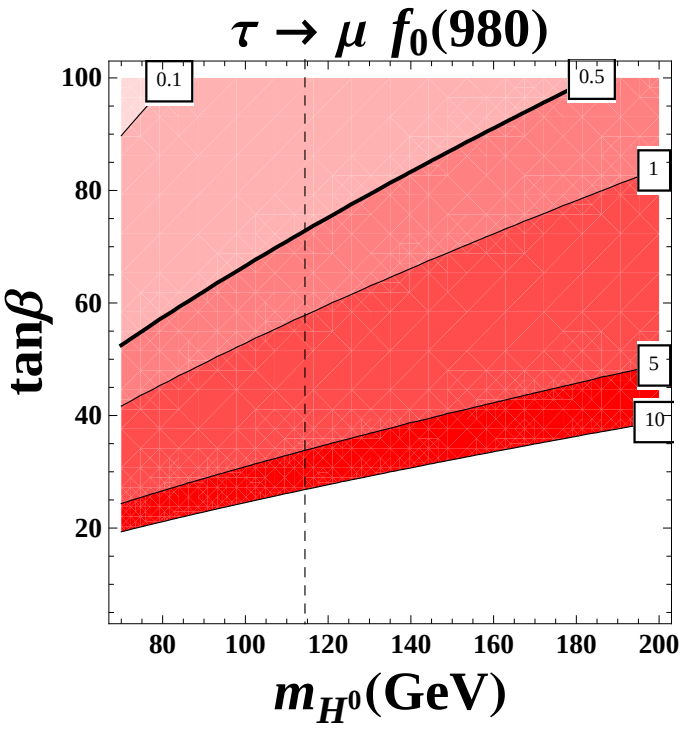

Figure 4.11: The excluded regions in the $(m_{H^0}, \tan\beta)$ plane are the areas above the contour lines corresponding to fixed $|\delta_{32}| = 0.1, 0.5, 1, 5, 10$.

Conclusions

The so far established Standard Model of Particle Physics has to be extended to explain some phenomena that cannot be understood within this model. First of all, the mechanism that generates the masses of all the gauge bosons and fermions in the SM, namely, the Higgs mechanism, has not been proven yet. It predicts the existence of a scalar particle, the well-known Higgs boson which has not yet been detected in any of the past or present colliders. The LHC is actually excluding some significant region for the SM Higgs mass values and it results are improving very rapidly. Concretely, a very recent ATLAS and CMS combined analysis has been performed, where a Higgs boson like mass in the range from 144 to 476 GeV is excluded at at 95% C.L.. This analysis, combined with the LEP lower bound on the SM Higgs mass, leaves a quite narrow window left for the SM Higgs mass: $114 < m_h < 141$ GeV at 95% C.L. [17]. On the other hand, a light Higgs mass is preferred by electroweak precision data $m_h \sim \mathcal{O}(100)$ GeV but the Higgs boson, being a scalar particle, is quadratically sensitive to the scale of new physics where the SM is no longer valid, known as the hierarchy problem. If no fine tuning is desired between the tree level Higgs mass and higher order corrections, then the scale of new physics should be at or below $\mathcal{O}(1)$ TeV. This can be interpreted as a theoretical hint of new physics at or below the TeV.

Moreover, the SM needs clearly to be enlarged to accommodate neutrino masses because the SM contains just three left handed neutrinos, which are massless. The simplest possibility is the introduction of right handed neutrinos, but depending on whether neutrinos are Dirac particles, as any of the other fermions, or Majorana particles, being their own antiparticles, their unique interactions with the Higgs will be either negligible or might be relevant, respectively. In the later case, the seesaw mechanism is a simple way of explaining the smallness of neutrino masses, by the ratio of two very different scales, the Dirac scale, $m_D \sim \mathcal{O}(100)$ GeV, and the Majorana scale, $m_M \sim \mathcal{O}(10^{13} - 10^{15})$ GeV. Nevertheless, the appearance of new physics at such large scale would worsen the hier-

archy problem and a huge fine tuning would be needed in order to obtain a light Higgs boson mass of $m_h \sim \mathcal{O}(100)$ GeV.

Furthermore, the existence of neutrino oscillations caused by nonzero neutrino masses and neutrino mixing implies that lepton flavor violation manifestly occurs in the neutrino sector. As a consequence, lepton flavor in the charged sector is not conserved either due to quantum corrections involving neutrinos. However, the decay rate of any charged LFV process is extremely suppressed in the SM enlarged with 3 right-handed Dirac neutrinos, due to the smallness of neutrino masses and Yukawa neutrino couplings. Furthermore, in the SM-seesaw with three right-handed Majorana neutrinos, the charged LFV branching ratios are also very suppressed, far below the present sensitivities. Therefore, any potential future measurement of LFV in the charged lepton sector would be a clear signal not only of physics beyond the SM but also of physics beyond the SM enlarged with three right handed neutrinos.

A supersymmetric extension of the SM-seesaw, like the MSSM-seesaw, comprises neutrino masses and mixing angles and at the same time solves the hierarchy problem of the SM-seesaw. Moreover, in SUSY-seesaw models a new source of LFV appears in the off-diagonal elements of the slepton and sneutrino mass matrices, which can be radiatively generated from the neutrino Yukawa interactions with large $Y_\nu \sim \mathcal{O}(1)$, and, therefore, the LFV rates in the charged lepton sector may lay within the present experimental sensitivities.

This thesis has been been devoted to the study of some of the indirect effects of Majorana neutrinos and their SUSY partners, the sneutrinos, via loop corrections, to observables that have a potential sensitivity to the Higgs sector. In particular, we have focused on two main effects: 1) one-loop radiative corrections to the lightest Higgs boson mass of the MSSM-seesaw and, 2) one-loop contributions to lepton flavor violating processes that are mediated by Higgs bosons within constrained SUSY-seesaw models. In the following we will sum up the main results and conclusions that can be extracted from our works.

- A full one-loop computation of the renormalized self energies of the neutral Higgs bosons of the MSSM-seesaw has been performed using the Feynman diagrammatic approach. Only the new contributions coming from the neutrino and sneutrino sector have been considered, because the pure MSSM corrections are well-known in the literature. We have focused our calculation on the one generation case for simplicity. The three generations case has been worked out at the Lagrangian level

and will be continued at the one-loop level in a forthcoming work. Both Yukawa interactions and gauge interactions have been taken into account. The relevant interactions have been derived and presented in terms of all the physical masses and mixing angles of the particles involved, namely, the $\mathcal{CP}$-even Higgs bosons h and H, the $\mathcal{CP}$-odd Higgs boson A, the light and heavy Majorana neutrinos ν and N, their SUSY partners $\tilde{\nu}_{\pm}$, $\tilde{N}_{\pm}$ and the neutral gauge boson Z. Three renormalization schemes, namely, $\overline{\rm DR}$, m$\overline{\rm DR}$ and OS, have been used and compared. We have fully analyzed the behavior of the neutrino/sneutrino corrections to the renormalized $\mathcal{CP}$-even Higgs self-energies with all the involved masses and parameters: m_M, $\tan\beta$, M_A, $m_{\tilde{L}}$, $m_{\tilde{R}}$, A_ν, m_ν, p and B_ν and concluded from an exhaustive numerical analysis that m_M, M_A, $m_{\tilde{R}}$, m_ν, p and B_ν are by far the most important ones. However, the soft SUSY breaking parameters $m_{\tilde{R}}$, B_ν start being relevant for large values, close to the Majorana mass scale.

In order to obtain a simple analytical formula of the renormalized self energies we have performed an expansion valid when m_M is much larger than all the other mass scales involved, and where we have set $A_\nu = B_\nu = \mu = 0$ and $m_{\tilde{R}} = m_{\tilde{L}} = m_{SUSY}$, for simplicity. The first term of this expansion is the $\mathcal{O}\left(m_D^0\right)$ which corresponds to the pure gauge contribution and it approximates the MSSM result with massless neutrinos. The other terms of the expansion correspond to the pure Yukawa contribution. The main conclusion from this Yukawa part is that in the m$\overline{\rm DR}$ scheme and in the $\overline{\rm DR}$ scheme the $\mathcal{O}\left(m_D^2\right)$ is the leading term, in contrast to the OS scheme which is dominated by the $\mathcal{O}\left(m_D^4/m_M^2\right)$.

The differences among those schemes have been explained in terms of the finite part of $\tan\beta$ and Higgs fields counterterms. We have chosen the m$\overline{\rm DR}$ as the most suitable scheme for our calculation because it is a gauge independent scheme at one loop and it minimizes higher order corrections improving, therefore, the convergence of the perturbative expansion. In the m$\overline{\rm DR}$ scheme there is no explicit dependence on the Majorana scale in the dominant $\mathcal{O}(m_D^2)$ contribution and the implicit dependence comes via m_D^2 from imposing the seesaw equation such that $m_D^2 = |m_\nu| m_N$, with $m_N \approx m_M$. Therefore, the renormalized self energies increase linearly with the Majorana scale and the light neutrino mass. The other relevant parameters in this leading Yukawa term are the external momentum and the pseudoscalar Higgs mass M_A. Consequently, our results can not be reproduced by using the effective potential approach because in this method the external momentum is neglected.

Regarding the numerical computation, we have estimated the extra corrections coming from the neu/sneu sector to the lightest MSSM Higgs boson mass Δm_h to check if they enter into the measurable range. When m_M is much larger than all the other scales involved, in particular, much larger that any of the soft breaking parameters, the corrections to the lightest Higgs boson mass depend mainly on Y_ν, thus on m_ν and m_M. For 10^{13} GeV $< m_M < 10^{14}$ GeV and 0.1 eV $< |m_\nu| <$ 0.5 eV the corrections are positive and smaller than 0.1 GeV, because in this region the gauge corrections still dominate the small Yukawa contributions. But for larger values of any of the neutrino masses, m_ν and/or m_M, the corrections change to negative sign and grow in size with these two masses up to values of around -5 GeV for $m_M = 10^{15}$ GeV and $|m_\nu| = 1$ eV. It is worth mentioning that for $m_M = 10^{14}$ GeV and $|m_\nu| = 0.5$ eV, $Y_\nu \approx 1$. Consequently, the perturbativity in the neutrino Yukawa coupling Y_ν is the constraining condition for not exploring much larger values of m_M and/or m_ν. Furthermore, when the soft mass associated to the right handed neutrino sector, $m_{\tilde{R}}$, is of the order of the Majorana mass scale we find very large negative corrections that can lower the lightest Higgs boson mass by a few tens of GeV. For instance, the corrections are around -30 GeV , for $m_M = 10^{14}$ GeV, $m_{\tilde{R}}/m_M = 0.7$ and $|m_\nu| = 0.6$ eV. We have shown that the neutrino/sneutrino effects have, in general, an opposite sign to the top/stop effects and thus lighten the lightest Higgs boson. Consequently, the present upper bound within the MSSM of $m_h \lesssim 135$ GeV will be diminished if neutrino/sneutrino loop effects are taken into account.

In view of the anticipated experimental precisions at the LHC and the ILC we believe that these new contributions from the Majorana neu/sneu sector should be taken into account whenever one wants to calculate precisely the Higgs spectrum within MSSM-seesaw scenarios. If in the future months/years a very light Higgs boson mass, close to the present experimental lower bound, is detected at the LHC and, on the other hand, no SUSY particle has yet been detected, with the corresponding increase of the lower bounds on the SUSY mass spectrum, in particular the stop and sbottom masses, that might be a hint of some new physics beyond the MSSM responsible of generating such a light Higgs. In that case, the MSSM-seesaw with heavy Majorana neutrinos/sneutrinos would be a good candidate for explaining such a light Higgs.

In summary, we conclude that the one-loop corrections from heavy Majorana neutrinos and their SUSY partners to the Higgs boson masses are important in this

MSSM-seesaw scenario, and overwhelm by many orders of magnitude the corresponding corrections in the case of Dirac massive neutrinos. These have also been estimated here and are extremely tiny, smaller than 10^{-22} GeV.

- A comparative study of the LFV semileptonic decays $\tau \to \mu f_0(980)$ and $\tau \to \mu\eta$ has been performed within the context of two constrained SUSY-seesaw models, the CMSSM-seesaw and the NUHM-seesaw which have a very different Higgs sector spectra. The potential sensitivity to the Higgs sector of these decays has been explored with special interest. Through all this analysis, we have required compatibility with both the present experimental upper bound for these decays and with neutrino data for masses and oscillations. The present upper bounds for both decays are $\mathrm{BR}(\tau \to \mu f_0(980)) < 3.4 \times 10^{-8}$(incl. $\mathrm{Br}(f^0 \to \pi^+\pi^-)$) and $\mathrm{BR}(\tau \to \mu\eta) < 2.3\times10^{-8}$ at the 90% C.L. given by the BELLE collaboration [93, 94]. These decays bounds are very competitive with respect to other LFV channels in the $\tau - \mu$ sector such as the well-known $\tau \to \mu\gamma$ decay, with an upper bound of $\mathrm{BR}(\tau \to \mu\gamma) < 4.4 \times 10^{-8}$ at the 90% C.L. given by the BABAR collaboration [89].

  We have presented a full computation of $\mathrm{BR}(\tau \to \mu f_0(980))$ that takes into account the full set of one-loop SUSY diagrams in the LFV vertex $\tau\mu H$, where H stands for any of the neutral CP-even Higgs bosons h^0 and H^0. The hadronization of the quark bilinears has been performed by means of the standard techniques in χPT and RχT. Within this chiral approach, the Higgs couplings to the $f_0(980)$ and to the η are dominated by their strange quark components. On the other hand, the $H^0 - f_0$ coupling is dominant over the $h^0 - f_0$ coupling since the first one goes as $\tan\beta$ in the large $\tan\beta$ limit, similarly to the $A^0 - \eta$ coupling, whereas the second one is suppressed in this limit.

  In the $\tau \to \mu\eta$ decay we have shown that the Z mediated contribution is the dominant one for values of $\tan\beta < 20$. Only for values of $\tan\beta > 20$ the A^0 mediated contribution dominates, in contrast with the $\tau \to \mu f_0(980)$ decay which is sensitive to the Higgs sector in the full $\tan\beta$ interval. Much larger rates have been found in the NUHM-Seesaw than in the CMSSM-Seesaw scenario, due mainly to the lighter Higgs masses m_{H^0}/m_{A^0} found in the first scheme even for large soft SUSY masses at $\sim \mathcal{O}(1\,\mathrm{TeV})$. This is precisely the main interest of the Higgs mediated channels such as $\tau \to \mu\eta$ and $\tau \to \mu f_0(980)$, namely, the fact that the decay rates can be sizeable even for large SUSY masses, $M_{\mathrm{SUSY}} \sim \mathcal{O}(1\,\mathrm{TeV})$, in clear contrast with other competitive tau flavor violating channels like $\tau \to \mu\gamma$,

whose rates decrease as $1/M^2_{\rm SUSY}$ and lay below the present experimental bound for such a heavy SUSY spectrum. Indeed, it is just in the NUHM-Seesaw case where the predictions for BR($\tau \to \mu f_0(980)$) can reach the present experimental sensitivity. We have shown, that in order to get values of BR($\tau \to \mu f_0(980)$) at the $10^{-8} - 10^{-7}$ level one needs large values for the relevant parameters, namely, $m_{N_3} \sim 10^{14} - 10^{15}$ GeV, $|\theta_{1,2}| \sim 2 - 3$, $\pm \arg(\theta_{1,2}) \sim \pi/4 - 3\pi/4$, $\tan\beta \sim 50 - 60$ and $m_{H^0} \sim 100 - 200$ GeV. In addition to the full results, we have provided an approximate simple formula for BR($\tau \to \mu f_0(980)$) which has been obtained in the large $M_{\rm SUSY}$ and large $\tan\beta$ limit, and with the MI approximation for the relevant LFV parameter δ_{32}. Furthermore, we have shown in this work that this approximate result agrees pretty well with the full result in practically all the explored parameter space. The main basic features of the full predicted rates are very well reproduced by the approximate formula, which summarizes the fast growing with $\tan\beta$, going as $(\tan\beta)^6$, with $1/m_{H^0}$, going as $(1/m_{H^0})^4$, and being approximately constant with $M_{\rm SUSY}$. The dependences with m_{N_3} and $\theta_{1,2}$ go via the δ_{32} parameter, and the large m_{N_3} values are what enhance dominantly the rates, growing approximately as BR $\sim |m_{N_3} \log m_{N_3}|^2$. The approximate formula for BR($\tau \to \mu\eta$) in the same limit, shows the same dependence on $\tan\beta$, the mixing parameter δ_{32} and on the Higgs boson mass, but exchanging m_{H^0} by m_{A^0}.

The most important conclusion from this work is that both LFV tau decays $\tau \to \mu\eta$ $\tau \to \mu f_0(980)$ are, indeed, sensitive to the Higgs sector of the NUHM-seesaw models. Concretely, the $\tau \to \mu\eta$ decay is sensitive to the CP-odd Higgs boson A^0 while the $\tau \to \mu f_0(980)$ channel is mostly sensitive to the CP-even Higgs boson H^0, and, therefore, these two channels complement nicely each other. These two channels are undoubtedly the most competitive LFV tau decays where to look for indirect Higgs signals. As a final product of our analysis we have extracted some excluded areas in the parameter space of these models by using the corresponding approximate formulas. The sensitivity found here to the Higgs sector will presumably improve in the future if the experimental reach increases up to $10^{-9} - 10^{-10}$, as it seems to be the case in the future SuperB and flavor factories [195].

All in all, I hope it became clear from this thesis that heavy Majorana neutrinos and sneutrinos can leave remarkable imprints in low energy observables sensitive to the Higgs sector.

Conclusiones

El consolidado Modelo Estándar de Física de Partículas (SM), tiene que ser extendido para poder explicar algunas observaciones experimentales que no tienen cabida dentro de este modelo. En primer lugar, el mecanismo que genera las masas de todos los bosones gauge y fermiones del SM, a saber, el mecanismo de Higgs, no ha sido corroborado todavía experimentalmente. Este mecanismo predice la existencia de una partícula escalar, el famoso bosón de Higgs, que no ha sido detectado todavía en ninguno de los aceleradores pasados o presentes. De hecho, hasta la fecha, el Gran Colisionador de Hadrones (LHC) ha excluído una región muy amplia de valores posibles de masas del bosón de Higgs del SM. Concretamente, un reciente análisis conjunto de CMS y ATLAS ha excluído al 95% de nivel de confianza el intervalo 141 GeV $< m_h <$ 476 GeV , dejando una estrecha ventana donde pueda encontrarse el Higgs del SM, 114.4 GeV $< m_h <$ 141 GeV [17]. Por un lado, los datos de precisión electrodébiles prefieren un Higgs ligero $m_h \sim \mathcal{O}(100)$ GeV, pero, por otro lado, el bosón de Higgs, al ser una partícula escalar, es cuadráticamente sensible a la escala de nueva física donde el SM ya no tiene validez, conociéndose esta inestabilidad frente a nuevas escalas como el problema de las jerarquías. Si no queremos que haya un ajuste fino entre la masa del Higgs a nivel árbol y correcciones radiativas de órdenes superiores, entonces la escala de nueva física debe ser $\lesssim \mathcal{O}(1)$ TeV. Esto puede ser interpretado como un indicio teórico de nueva física a la escala del TeV o, incluso, por debajo del TeV.

Por otra parte, es necesario ampliar el SM para acomodar las masas de los neutrinos porque el SM contiene sólo tres neutrinos de levógiros (*left-handed*), que no tienen masa. La opción más sencilla es la introducción de neutrinos dextrógiros (*right-handed*), pero dependiendo de si son neutrinos de Dirac, como el resto de los fermiones del SM, o neutrinos de Majorana, en cuyo caso serían sus propias antipartículas, su interacción con el Higgs será despreciable o podrá ser relevante, respectivamente. En caso de tratarse de neutrinos de Majorana, el mecanismo de seesaw da una explicación sencilla sobre las

masas tan pequeñas de los neutrinos, a traves del cociente de dos escalas muy dispares, la escala de Dirac, $m_D \sim \mathcal{O}(100)$ GeV, y la escala de Majorana, $m_M \sim \mathcal{O}(10^{13} - 10^{15})$ GeV. Sin embargo, la existencia de nueva física a esa escala tan grande empeoraría el problema de las jerarquías y sería necesario un ajuste muy fino para obtener una masa del bosón de Higgs ligero de $m_h \sim \mathcal{O}(100)$ GeV.

Adicionalmente, la existencia de oscilaciones de neutrinos originadas por las masas de los neutrinos y sus ángulos de mezcla, implica que hay violación de sabor leptónico (LFV) en el sector de los neutrinos. Consecuentemente, el sabor leptónico en el sector de leptones cargados no se conserva tampoco debido a correcciones cuánticas en las que intervienen los neutrinos. Sin embargo, la tasa de desintegración de cualquier proceso de LFV en el sector cargado está extremadamente suprimida en la versión extendida del SM con tres neutrinos de Dirac dextrógiros, debido a la pequeñez de las masas de los neutrinos y de los acoplamientos de Yukawa de los neutrinos. Por otra parte, en el SM-seesaw con tres neutrinos de Majorana dextrógiros, las tasas de desintegración de leptones cargados con violación de sabor están también muy suprimidas, muy lejos de poder ser contrastadas experimentalmente. Por lo tanto, cualquier medida futura que implique violación de sabor en el sector cargado, sería una clara señal, no sólo de nueva física más allá del SM (BSM) sino también de física más allá del SM extendido con tres neutrinos dextrógiro.

Una extensión supersimétrica del SM-seesaw, por ejemplo el MSSM-seesaw, incluye las masas y ángulos de mezcla de los neutrinos y, al mismo tiempo, resuelve el gran problema de las jerarquías que tiene el SM-seesaw. Además, en modelos SUSY-seesaw una nueva fuente de LFV aparece en los elementos no diagonales de las matrices de masa de los sleptones y los sneutrinos, que puede ser generada radiativamente a través de las interacciones de Yukawa de los neutrinos cuando estas interacciones son fuertes ,i.e. $Y_\nu \sim \mathcal{O}(1)$. Es por esta razón, que las tasas de desintegración de leptones cargados con violación de sabor leptónico pueden hallarse dentro de la precisión experimental actual.

Esta tesis se ha centrado en el estudio de algunos de los efectos indirectos de los neutrinos de Majorana y de sus compañeros supersimétricos, los sneutrinos, a través de correcciones radiativas, a observables que son potencialmente sensibles al sector Higgs. En particular, nos hemos centrado en dos efectos importantes: 1) correcciones radiativas a un lazo (one-loop) a la masa del bosón de Higgs más ligero del MSSM-seesaw y, 2) correcciones radiativas a un loop a los procesos LFV que están mediados por bosónes de Higgs en modelos SUSY-seesaw restringidos. A continuación resumiremos los resultados más relevantes y las conclusiones que pueden extraerse de nuestro trabajo.

- Hemos realizado un cálculo diagramático completo a un loop de las autoenergías renormalizadas de los bosones de Higgs neutros del MSSM-seesaw. Solamente hemos tenido en cuenta las nuevas contribuciones provenientes del sector de neutrinos y sneutrinos, porque las correcciones del MSSM ya han sido estudiadas en profundidad por diversos autores. Hemos restringido nuestro cálculo al caso de una generación por una cuestión de sencillez. El caso de tres generaciones ha sido desarrollado a nivel de Lagrangiano y será completado el cálculo a un loop en un trabajo próximo. En nuestro trabajo, hemos tenido en cuenta tanto las interacciones de Yukawa como las interacciones gauge. Se han derivado las interacciones relevantes y han sido presentadas en términos de las masas físicas y de los ángulos de mezcla de las partículas involucradas, a saber, los bosones de Higgs pares bajo $\mathcal{CP}$, h y H, el bosón de Higgs impar bajo $\mathcal{CP}$, A, los neutrinos de Majorana ν y N, ligero y pesado respectivamente, sus companẽros supersimétricos $\tilde{\nu}_{\pm}$ y $\tilde{N}_{\pm}$ y el bosón gauge neutro Z. Se han utilizado tres esquemas de renormalización y comparado los resultados obtenidos en cada uno de ellos. Hemos analizado en profundidad el comportamiento de las correcciones radiativas de los neutrinos/sneutrinos a las autoenergías renormalizadas de los bosones de Higgs con $\mathcal{CP}$-par, con todos los parámetros y masas involucradas, i.e. m_M, $\tan\beta$, M_A, $m_{\tilde{L}}$, $m_{\tilde{R}}$, A_ν, m_ν, p y B_ν. Tras un análisis numérico exahustivo, hemos concluido que m_M, M_A, $m_{\tilde{R}}$, m_ν, p y B_ν son los parámetros más importantes. No obstante, los parámetros de ruptura *suave* de SUSY, $m_{\tilde{R}}$, y B_ν, empiezan a ser relevantes cuando tienen valores muy grandes, cerca de la escala de Majorana.

  Con el fin de obtener una fórmula analítica sencilla de las autoenergías renormalizadas, hemos llevado a cabo una expansión válida sólo en el límite en que m_M es mucho más grande que cualquiera de las otras masas involucradas, y donde además, hemos impuesto $A_\nu = B_\nu = \mu = 0$ y $m_{\tilde{R}} = m_{\tilde{L}} = m_{SUSY}$ por simplicidad. El primer término de esta expansión es el de $\mathcal{O}\left(m_D^0\right)$, que corresponde a la contribución gauge pura y se asemeja a la contribución de los neutrinos sin masa del MSSM. Los otros términos de la expansión corresponden a la contribución Yukawa pura. La conclusión principal de los términos de Yukawa es que, tanto en el esquema de renormalización m$\overline{\text{DR}}$ como en el $\overline{\text{DR}}$, el término dominante es el $\mathcal{O}\left(m_D^2\right)$, a diferencia del esquema de renormalización OS, donde el término dominante es el $\mathcal{O}\left(m_D^4/m_M^2\right)$.

  Las diferencias entre los distintos esquemas han sido explicadas en términos de la parte finita de los contratérminos de $\tan\beta$ y de los campos de Higgs. Hemos elegido el esquema m$\overline{\text{DR}}$ como el esquema más apropiado para nuestro cálculo, porque es un esquema con independencia gauge a un loop y porque minimiza las

correcciones radiativas de órdenes superiores, mejorando, por tanto, la convergencia de la serie perturbativa. En el esquema m$\overline{\text{DR}}$, no hay una dependencia explícita en la escala de Majorana en la contribución dominante $\mathcal{O}(m_D^2)$ y la dependencia implícita aparece a través de m_D^2 cuando imponemos la ecuación del seesaw, de forma que $m_D^2 = |m_\nu| m_N$, con $m_N \approx m_M$. Por lo tanto, las autoenergías renormalizadas crecen linealmente con la escala de Majorana y con la masa del neutrino ligero. Los otros parámetros relevantes en este término de Yukawa dominante, son el momento externo y la masa del Higgs pseudoscalar M_A. En consecuencia, nuestros resultados no pueden ser obtenidos utilizando el método del potencial efectivo porque en este método el momento externo se desprecia.

En lo que respecta a la computación numérica, hemos estimado las correcciones adicionales, provenientes del sector neu/sneu, al bosón de Higgs más ligero del MSSM, Δm_h, para comprobar si son comparables con la precisión experimental y por tanto susceptibles de ser medidas experimentalmente. Cuando m_M es mucho más grande que el resto de escalas involucradas, en concreto, mucho más grande que cualquiera de los parámetros de ruptura *suave* de SUSY, las correcciones a la masa del bosón de Higgs ligero dependen fundamentalmente de Y_ν, y por tanto, de m_ν y m_M. Cuando 10^{13} GeV $< m_M < 10^{14}$ GeV y 0.1 eV $< |m_\nu| <$ 0.5 eV, las correcciones son positivas y más pequeñas que 0.1 GeV, porque en esta región las correcciones gauge todavía dominan las pequeñas contribuciones de Yukawa. Sin embargo, para valores más grandes de cualquiera de las masas de los neutrinos, m_ν y/o m_M, las correcciones cambian de signo y crecen en valor absoluto con estas dos masas hasta valores alrededor de -5 GeV para $m_M = 10^{14}$ GeV y $|m_\nu| = 0.5$ eV. Es importante resaltar que $m_M = 10^{14}$ GeV y $|m_\nu| = 0.5$ eV, $Y_\nu \approx 1$. Por tanto, si no se han explorado valores mucho más grandes de m_M y/o m_ν, se debe a las restricciones impuestas por la condición de perturbatividad en el acoplamiento de Yukawa del neutrino Y_ν.

Adicionalmente, cuando la masa *suave* asociada al sector del neutrino dextrógiro, $m_{\tilde{R}}$, es del orden de la escala de masas de Majorana, encontramos correcciones negativas muy grandes que pueden disminuir la masa del bosón de Higgs más ligero en unas pocas decenas de GeV. Por ejemplo, se obtienen correcciones alrededor de -30 GeV, cuando $m_M = 10^{14}$ GeV, $m_{\tilde{R}}/m_M = 0.7$ y $|m_\nu| = 0.6$ eV. Hemos mostrado que los efectos de los neutrinos/sneutrinos tienen, generalmente, signo opuesto a los efectos de los tops/stops y, por tanto, reducen la masa del Higgs más ligero. Consecuentemente, la cota superior de este Higgs en el MSSM, que es $m_h \lesssim 135$ GeV, disminuirá si se tienen en cuenta los efectos de loops de neutrinos

y sneutrinos.

En vista de la precisión experimental prevista en el LHC y en el ILC, consideramos que estas nuevas contribuciones, provenientes del sector de neutrinos y sneutrinos de Majorana, deberían tenerse en cuenta siempre que alguien quiera calcular con precisión el espectro del Higgs en escenarios MSSM-seesaw. Si en los próximos meses/años detectan en el LHC un bosón de Higgs muy ligero, cerca de la cota experimental inferior y, por otro lado, no detectan ninguna partícula supersimétrica con el correspondiente aumento de las cotas inferiores del espectro de masas supersimétrico, en particular, las masas del stop y del sbottom, eso podría ser una señal de nueva física más allá del MSSM responsable de la existencia que un Higgs tan ligero. En ese caso, el MSSM-seesaw con neutrinos y sneutrinos de Majorana pesados sería un buen candidato para explicar el por qué de un Higgs tan ligero.

En resumen, concluimos que las correcciones a un loop de neutrinos de Majorana pesados y sus compañeros supersimétricos a las masas de los bosones de Higgs son relevantes en este escenario MSSM-sesaw, y superan por muchos órdenes de magnitud las correcciones correspondientes en el caso de neutrinos de Dirac masivos. Estas correcciones han sido estimadas aquí y son extremadamente pequeñas, menores de 10^{-22} GeV.

- Hemos realizado un estudio comparativo de las desintegraciones semileptónicas LFV $\tau \to \mu f_0(980)$ y $\tau \to \mu\eta$ en el contexto de dos modelos SUSY-seesaw restringidos, el CMSSM-seesaw y el NUHM-seesaw, los cuales tienen un espectro de sector de Higgs muy distinto. Hemos explorado con especial interés la posible sensibilidad al sector de Higgs de estos canales de desintegración. En todo el análisis hemos exigido compatibilidad tanto con la cota superior experimental para ambos canales, como los datos actuales de las masas y oscilaciones de los neutrinos. Las cotas superiores actuales para ambas desintegraciones son $\mathrm{BR}(\tau \to \mu f_0(980)) < 3.4 \times 10^{-8}$(incl. $\mathrm{Br}(f^0 \to \pi^+\pi^-)$) y $\mathrm{BR}(\tau \to \mu\eta) < 2.3 \times 10^{-8}$ at the 90% C.L., dadas por la colaboración de BELLE [93, 94]. Estas cotas son muy competitivas con respecto a los demás canales LFV en el sector $\tau - \mu$, como la notable desintegración $\tau \to \mu\gamma$, con una cota superior $\mathrm{BR}(\tau \to \mu\gamma) < 4.4 \times 10^{-8}$ al 90% de nivel de confianza, dado por la colaboración BABAR [89].

  Hemos presentado un cálculo completo de $\mathrm{BR}(\tau \to \mu f_0(980))$, que tiene en cuenta el conjunto completo de diagramas SUSY a un loop en el vértice LFV $\tau\mu H$, donde H representa cualquiera de los bosones de Higgs neutros y pares bajo $\mathcal{CP}$, h^0 y H^0.

La hadronización de los bilineales de quarks se ha llevado a cabo usando las técnicas estándar de χPT y RχT. Dentro del enfoque chiral, los acoplamientos del Higgs al $f_0(980)$ y a η están dominados por sus componentes de quark extraño. Por otro lado, el acoplamiento $H^0 - f_0$ es más fuerte que el acoplamiento $h^0 - f_0$, debido a que el primero es proporcional a $\tan\beta$ en el límite de gran $\tan\beta$, al igual que ocurre con el acoplamiento $A^0 - \eta$, mientras que el segundo está suprimido en ese límite.

En la desintegración $\tau \to \mu\eta$ hemos comprobado que la contribución mediada por un Z es la dominante para valores de $\tan\beta < 20$. Por tanto, la contribución del A^0 sólamente domina para valores de $\tan\beta > 20$, a diferencia de la desintegración $\tau \to \mu f_0(980)$ que es sensible al sector de Higgs en todo el intervalo de valores de $\tan\beta$. Se han encontrado tasas de desintegración mucho más grandes en el modelo NUHM-Seesaw que en el CMSSM-Seesaw, debido principalmente a haber hallado masas de los bosones de Higgs m_{H^0}/m_{A^0} más ligeras en el primer caso, incluso para masas SUSY grandes de $\sim \mathcal{O}(1\,\text{TeV})$. Éste es precisamente el mayor interés de los canales mediados por el Higgs como $\tau \to \mu\eta$ y $\tau \to \mu f_0(980)$, a saber, el hecho de que sus tasas de desintegración pueden ser relevantes incluso para masas SUSY grandes, $M_{\text{SUSY}} \sim \mathcal{O}(1\,\text{TeV})$, a diferencia de otros canales del τ con violación de sabor importantes como, $\tau \to \mu\gamma$, cuyas tasas de desintegración decrecen como $1/M^2_{\text{SUSY}}$ y se encuentran por debajo de la presente cota experimental para un espectro SUSY tan pesado.

De hecho, es únicamente en el caso NUHM-Seesaw donde las predicciones para $\text{BR}(\tau \to \mu f_0(980))$ pueden alcanzar la precisión experimental actual. Hemos mostrado, que para obtener valores de $\text{BR}(\tau \to \mu f_0(980))$ al nivel de $10^{-8} - 10^{-7}$, se necesitan valores grandes de los parámetros relevantes, a saber, $m_{N_3} \sim 10^{14} - 10^{15}$ GeV, $|\theta_{1,2}| \sim 2 - 3$, $\pm \arg(\theta_{1,2}) \sim \pi/4 - 3\pi/4$, $\tan\beta \sim 50 - 60$ y $m_{H^0} \sim 100 - 200$ GeV. Además del resultado exacto de $\text{BR}(\tau \to \mu f_0(980))$, hemos proporcionado una fórmula aproximada sencilla de este proceso, que ha sido obtenida en el límite de gran M_{SUSY} y gran $\tan\beta$, y donde se ha usado la aproximación de la inserción de masas (MIA) para el parámetro LFV relevante δ_{32}. Hemos comprobado en este trabajo que el resultado aproximado concuerda bastante bien con el resultado exacto en casi todo el espacio de parámetros que hemos explorado.

La fórmula aproximada de la tasa de desintegración reproduce muy bien las características básicas más importantes de la predicción exacta, y sintetiza el rápido crecimiento con $\tan\beta$, como $(\tan\beta)^6$, con $1/m_{H^0}$, como $(1/m_{H^0})^4$, y siendo aprox-

imadamente constante con $M_{\rm SUSY}$. La dependencia con m_{N_3} y $\theta_{1,2}$ viene a través del parámetro δ_{32}, y los valores grandes de m_{N_3} son los que incrementan fundamentalmente la tasa de desintegración, que crece aproximadamente como BR $\sim |m_{N_3} \log m_{N_3}|^2$. La fórmula aproximada de BR($\tau \to \mu\eta$) en el mismo límite, presenta la misma dependencia con $\tan\beta$, el parámetro de mezcla δ_{32} y con la masa del bosón de Higgs, pero intercambiando m_{H^0} por m_{A^0}.

La conclusión más importante de este estudio es que las dos desintegraciones LFV del tau, $\tau \to \mu\eta$ y $\tau \to \mu f_0(980)$, son sensibles al sector de Higgs de los modelos NUHM-seesaw. Concretamente, la desintegración $\tau \to \mu\eta$ es sensible al bosón de Higgs impar bajo $\mathcal{CP}$, A^0, mientras que el canal $\tau \to \mu f_0(980)$ es fundamentalmente sensible al bosón de Higgs par bajo $\mathcal{CP}$, H^0, y ,por tanto, estos dos canales se complementan muy bien. Entre los distintos canales LFV del tau, los estudiados aquí son, sin duda, los más idóneos para buscar señales indirectas del Higgs. Estos dos canales son, sin duda, los más idoneos canales LFV del tau donde buscar señales indirectas del Higgs . Como colofón de nuestro análisis, hemos extraído algunas áreas excluídas del espacio de parámetros de estos modelos, haciendo uso de las fórmulas aproximadas correspondientes. La sensibilidad al sector de Higgs que hemos encontrado aquí mejorará probablemente en el futuro si el alcance experimental aumenta hasta $10^{-9} - 10^{-10}$, como parece ser el caso del futuro SuperB y factorías de *sabor* [195].

Para finalizar, espero que haya quedado claro a partir de esta tesis que los neutrinos y sneutrinos de Majorana pueden dejar huellas notables en los observables de baja energía sensibles al sector de Higgs.

Appendix A

New Feynman rules

In this appendix we collect the Feynman rules within the MSSM-seesaw that are relevant for the present work. These correspond to the interactions between the neutrinos and sneutrinos with the MSSM Higgs bosons and between the neutrinos and sneutrinos with the Z gauge bosons. We write all the Feynman rules here in the physical basis. Here $c_{\rm w} = \cos\theta_W$.

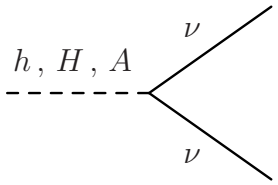

$$i\frac{g}{2M_W}m_D \sin 2\theta \left(\frac{\cos\alpha}{\sin\beta}, \frac{\sin\alpha}{\sin\beta}, -i\gamma_5 \cot\beta\right)$$

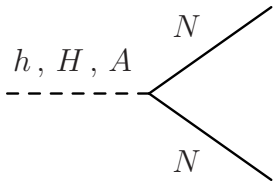

$$-i\frac{g}{2M_W}m_D \sin 2\theta \left(\frac{\cos\alpha}{\sin\beta}, \frac{\sin\alpha}{\sin\beta}, -i\gamma_5 \cot\beta\right)$$

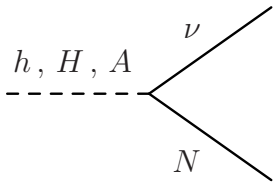

$$-i\frac{g}{2M_W}m_M \sin\theta\cos\theta \left(\frac{\cos\alpha}{\sin\beta}, \frac{\sin\alpha}{\sin\beta}, -i\gamma_5 \cot\beta\right)$$

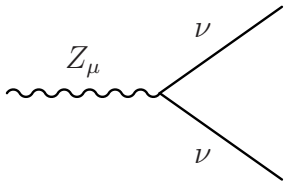

$$\frac{ig}{2c_{\rm w}} \cos^2\theta\, \gamma_\mu\gamma_5$$

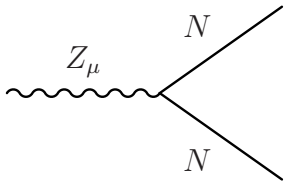

$$\frac{ig}{2c_{\rm w}} \sin^2\theta\, \gamma_\mu\gamma_5$$

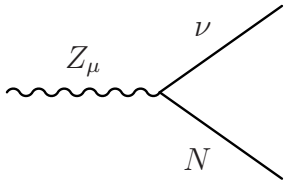

$$\frac{ig}{2c_{\rm w}} \sin\theta\cos\theta\, \gamma_\mu\gamma_5$$

Table A.1: Three-point couplings of two Majorana neutrinos to one MSSM Higgs boson and of two Majorana neutrinos to the Z gauge boson.

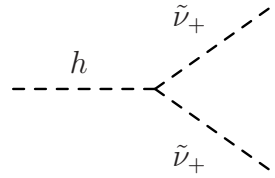

$$i\tfrac{g}{4c_{\rm w}M_W\sin\beta}[-4c_{\rm w}\cos\alpha\, m_D^2 + 2c_{\rm w}\cos\alpha\, m_D(A_\nu + m_M + \mu\tan\alpha\,)\sin 2\theta_+$$
$$+\tfrac{M_W^2}{c_{\rm w}}\sin\beta\,\sin(\alpha+\beta)\,(1+\cos 2\theta_+)\,]$$

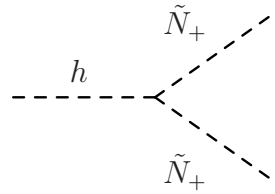

$$-i\tfrac{g}{4c_{\rm w}M_W\sin\beta}[4c_{\rm w}\cos\alpha\, m_D^2 + 2c_{\rm w}\cos\alpha\, m_D(A_\nu + m_M + \mu\tan\alpha\,)\sin 2\theta_+$$
$$-\tfrac{M_W^2}{c_{\rm w}}\sin\beta\,\sin(\alpha+\beta)\,(1-\cos 2\theta_+)\,]$$

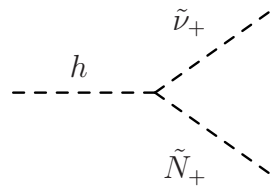

$$-i\tfrac{g}{2c_{\rm w}M_W\sin\beta}[c_{\rm w}\cos\alpha\, m_D(A_\nu + m_M + \mu\tan\alpha\,)\cos 2\theta_+$$
$$-\tfrac{M_W^2}{c_{\rm w}}\sin\beta\,\sin(\alpha+\beta)\,\cos\theta_+\sin\theta_+]$$

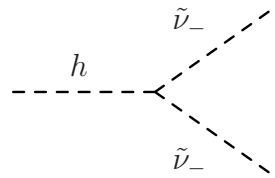

$$i\tfrac{g}{4c_{\rm w}M_W\sin\beta}[-4c_{\rm w}\cos\alpha\, m_D^2 + 2c_{\rm w}\cos\alpha\, m_D(A_\nu - m_M + \mu\tan\alpha\,)\sin 2\theta_-$$
$$+\tfrac{M_W^2}{c_{\rm w}}\sin\beta\,\sin(\alpha+\beta)\,(1+\cos 2\theta_-)\,]$$

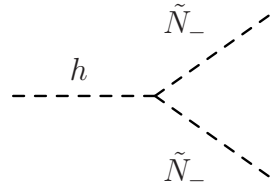

$$-i\tfrac{g}{4c_{\rm w}M_W\sin\beta}[4c_{\rm w}\cos\alpha\, m_D^2 + 2c_{\rm w}\cos\alpha\, m_D(A_\nu - m_M + \mu\tan\alpha\,)\sin 2\theta_-$$
$$-\tfrac{M_W^2}{c_{\rm w}}\sin\beta\,\sin(\alpha+\beta)\,(1-\cos 2\theta_-)\,]$$

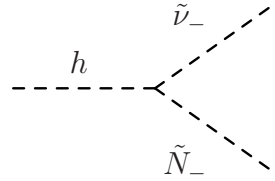

$$-i\tfrac{g}{2c_{\rm w}M_W\sin\beta}[c_{\rm w}\cos\alpha\, m_D\,(A_\nu - m_M + \mu\tan\alpha\,)\cos 2\theta_-$$
$$-\tfrac{M_W^2}{c_{\rm w}}\sin\beta\,\sin(\alpha+\beta)\,\cos\theta_-\sin\theta_-]$$

Table A.2: Three-point couplings of two sneutrinos to the Higgs boson h. The corresponding couplings to the Higgs boson H are obtained from the ones here by replacing $\cos\alpha \to \sin\alpha\,, \sin\alpha \to -\cos\alpha\,, \sin(\alpha+\beta) \to -\cos(\alpha+\beta)$. All the couplings not shown here vanish.

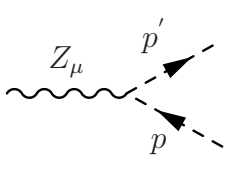

$\frac{g}{2c_\mathrm{w}} \cos\theta_+ \cos\theta_- \, (p+p')_\mu$

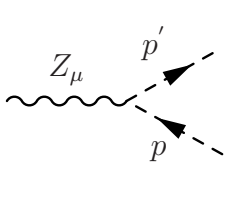

$\frac{g}{2c_\mathrm{w}} \sin\theta_+ \sin\theta_- \, (p+p')_\mu$

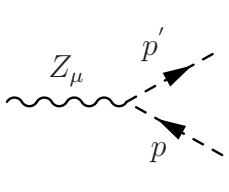

$\frac{g}{2c_\mathrm{w}} \sin\theta_+ \cos\theta_- \, (p+p')_\mu$

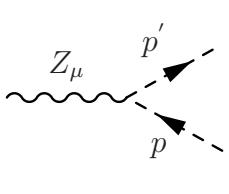

$\frac{g}{2c_\mathrm{w}} \cos\theta_+ \sin\theta_- \, (p+p')_\mu$

Table A.3: Three-point couplings of two sneutrinos to the Z gauge boson. All the couplings not shown here vanish.

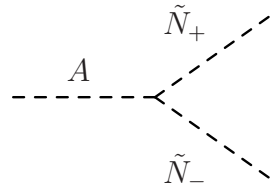

$$i\tfrac{g}{2M_W}\cot\beta\, m_D[(A_\nu+\mu\tan\beta)\sin(\theta_- -\theta_+)+m_M\sin(\theta_-+\theta_+)]$$

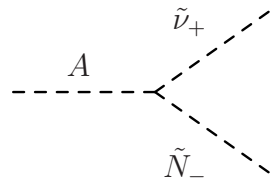

$$i\tfrac{g}{2M_W}\cot\beta\, m_D[-(A_\nu+\mu\tan\beta)\cos(\theta_- -\theta_+)+m_M\cos(\theta_-+\theta_+)]$$

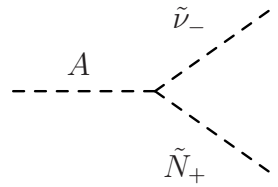

$$i\tfrac{g}{2M_W}\cot\beta\, m_D[(A_\nu+\mu\tan\beta)\cos(\theta_- -\theta_+)+m_M\cos(\theta_-+\theta_+)]$$

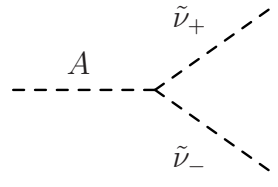

$$i\tfrac{g}{2M_W}\cot\beta\, m_D[(A_\nu+\mu\tan\beta)\sin(\theta_- -\theta_+)-m_M\sin(\theta_-+\theta_+)]$$

Table A.4: Three-point couplings of two sneutrinos to the Higgs boson A. All the couplings not shown here vanish.

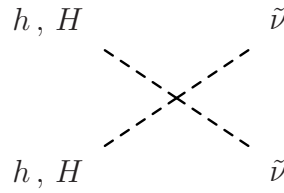

$$i\frac{g^2}{8c_{\rm w}^2 M_W^2 \sin^2\beta}[4(-\cos^2\alpha, \sin^2\alpha)c_{\rm w}^2 m_D^2 + \cos 2\alpha M_W^2 \sin^2\beta(1+\cos 2\theta_+)]$$

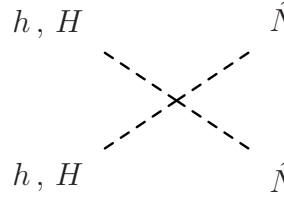

$$-i\frac{g^2}{8c_{\rm w}^2 M_W^2 \sin^2\beta}[4(\cos^2\alpha, \sin^2\alpha)c_{\rm w}^2 m_D^2(-,+)\cos 2\alpha M_W^2 \sin^2\beta(1-\cos 2\theta_+)]$$

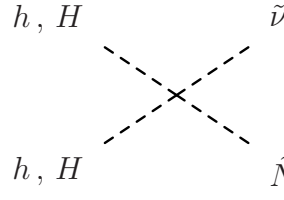

$$(+,-)\, i\frac{g^2}{4c_{\rm w}^2}\cos 2\alpha\, \cos\theta_+\, \sin\theta_+$$

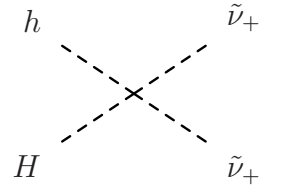

$$i\frac{g^2}{8c_{\rm w}^2 M_W^2 \sin^2\beta}\sin 2\alpha\,[-2c_{\rm w}^2 m_D^2 + M_W^2 \sin^2\beta\,(1+\cos 2\theta_+)]$$

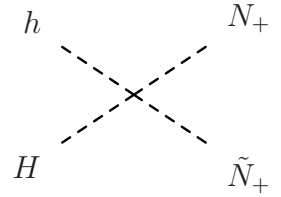

$$-i\frac{g^2}{8c_{\rm w}^2 M_W^2 \sin^2\beta}\,\sin 2\alpha\,[2c_{\rm w}^2 m_D^2 - M_W^2 \sin^2\beta\,(1-\cos 2\theta_+)]$$

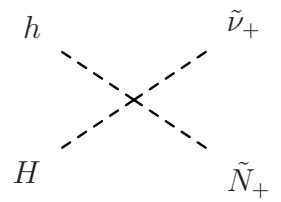

$$i\frac{g^2}{4c_{\rm w}^2}\sin 2\alpha\cos\theta_+\sin\theta_+$$

Table A.5: Four-point couplings of two sneutrinos to two $\mathcal{P}$-even Higgs bosons. The corresponding couplings for $\tilde{\nu}_-$ and $\tilde{N}_-$ can be obtained from these by replacing $\theta_+ \to \theta_-$. All the couplings not shown here vanish

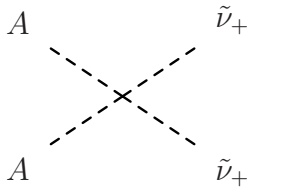

$$i\frac{g^2}{8c_{\rm w}^2 M_W^2 \sin^2\beta}[-4\cos^2\beta\, c_{\rm w}^2\, m_D^2 + \cos 2\beta\, M_W^2\, \sin^2\beta\,(1+\cos 2\theta_+)]$$

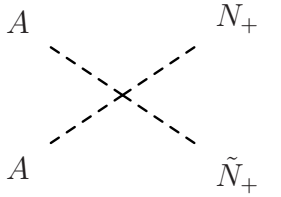

$$-i\frac{g^2}{8c_{\rm w}^2 M_W^2 \sin^2\beta}[4\cos^2\beta\, c_{\rm w}^2\, m_D^2 - \cos 2\beta\, M_W^2\, \sin^2\beta\,(1-\cos 2\theta_+)]$$

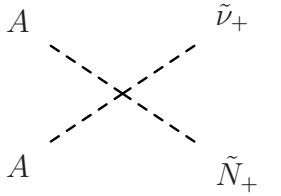

$$i\frac{g^2}{4c_{\rm w}^2}\cos 2\beta\, \cos\theta_+\, \sin\theta_+$$

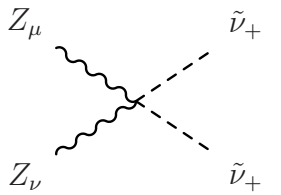

$$i\frac{g^2}{2c_{\rm w}}\cos^2\theta_+ g_{\mu\nu}$$

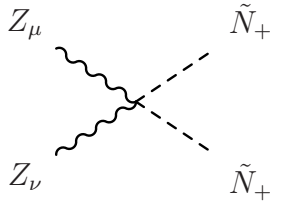

$$i\frac{g^2}{2c_{\rm w}}\sin^2\theta_+ g_{\mu\nu}$$

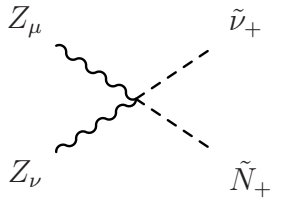

$$i\frac{g^2}{2c_{\rm w}}\cos\theta_+ \sin\theta_+ g_{\mu\nu}$$

Table A.6: Four-point couplings of two sneutrinos to two $\mathcal{P}$-odd Higgs bosons and of two sneutrinos to two Z gauge bosons. The corresponding couplings for $\tilde{\nu}_-$ and $\tilde{N}_-$ can be obtained from these by replacing $\theta_+ \to \theta_-$. All the couplings not shown here vanish.

Appendix B

Majorana case. One-loop neutrino/sneutrino corrections to the self-energies and tadpoles

In this Appendix we collect all the analytical results for the neutrino and sneutrino one-loop corrections to the Higgs boson tadpoles and unrenormalized self-energies, and to the Z self-energies, within the MSSM-seesaw. The contributions from neutrinos (ν) and sneutrinos ($\tilde{\nu}$) are presented separately for clearness. Here $c_{\rm w} = \cos\theta_W$.

$$T_h^{\nu} = \frac{g}{16 c_{\rm w} M_Z \pi^2} \frac{\cos\alpha \sin 2\theta}{\sin\beta} m_D (m_\nu A_0[m_\nu^2] - m_N A_0[m_N^2]) \tag{B.1}$$

$$\begin{aligned} T_h^{\tilde{\nu}} &= -\frac{g}{64 c_{\rm w} M_Z \pi^2} \frac{1}{\sin\beta} (A_0[m^2_{\tilde{\nu}_+}](M_Z^2 \cos^2\theta_+ \sin\beta \sin(\alpha+\beta) \\ &\quad + m_D \mu \sin\alpha \sin 2\theta_+ + m_D \cos\alpha(-2m_D + (A_\nu + m_M)\sin 2\theta_+)) \\ &+ A_0[m^2_{\tilde{\nu}_-}](M_Z^2 \cos^2\theta_- \sin\beta \sin(\alpha+\beta) \\ &\quad + m_D \mu \sin\alpha \sin 2\theta_- - m_D \cos\alpha(2m_D - (A_\nu - m_M)\sin 2\theta_-)) \\ &- A_0[m^2_{\tilde{N}_+}](-M_Z^2 \sin\beta \sin(\alpha+\beta)\sin^2\theta_+ \\ &\quad + 2m_D \cos\alpha(m_D + \frac{1}{2}(A_\nu + m_M)\sin 2\theta_+) + m_D \mu \sin\alpha \sin 2\theta_+) \\ &- A_0[m^2_{\tilde{N}_-}](-M_Z^2 \sin\beta \sin(\alpha+\beta)\sin^2\theta_- \\ &\quad + 2m_D \cos\alpha(m_D + \frac{1}{2}(A_\nu - m_M)\sin 2\theta_-) + m_D \mu \sin\alpha \sin 2\theta_-)) \end{aligned} \tag{B.2}$$

$$
\begin{aligned}
\Sigma^{\nu}_{hh}(p^2) &= -\frac{g^2}{64c_{\rm w}^2 M_Z^2\pi^2}\frac{\cos^2\alpha\sin^2 2\theta}{\sin^2\beta}\left[2m_D^2 A_0[m_\nu^2]+(2m_D^2+m_M^2)A_0[m_N^2]\right.\\
&+ 4m_D^2 m_\nu^2 B_0[p^2,m_\nu^2,m_\nu^2]+m_M^2(m_\nu^2+m_\nu m_N)B_0[p^2,m_\nu^2,m_N^2]\\
&+ 4m_D^2 m_N^2 B_0[p^2,m_N^2,m_N^2]\\
&+ \left. p^2(2m_D^2 B_1[p^2,m_\nu^2,m_\nu^2]+m_M^2 B_1[p^2,m_\nu^2,m_N^2]+2m_D^2 B_1[p^2,m_N^2,m_N^2])\right] \qquad \text{(B.3)}
\end{aligned}
$$

$$
\begin{aligned}
\Sigma^{\tilde{\nu}}_{hh}(p^2) &= \frac{g^2}{512c_{\rm w}^2 M_Z^2\pi^2\sin^2\beta}[-4A_0[m^2_{\tilde{\nu}_+}](-2m_D^2\cos^2\alpha+M_Z^2\sin^2\beta\cos 2\alpha\cos^2\theta_+)\\
&- 4A_0[m^2_{\tilde{N}_+}](-2m_D^2\cos^2\alpha+M_Z^2\sin^2\beta\cos 2\alpha\sin^2\theta_+)\\
&- 4A_0[m^2_{\tilde{\nu}_-}](-2m_D^2\cos^2\alpha+M_Z^2\sin^2\beta\cos 2\alpha\cos^2\theta_-)\\
&- 4A_0[m^2_{\tilde{N}_-}](-2m_D^2\cos^2\alpha+M_Z^2\sin^2\beta\cos 2\alpha\sin^2\theta_-)]\\
&+ 2B_0[p^2,m^2_{\tilde{N}_+},m^2_{\tilde{\nu}_+}](4m_D^2\cos^2 2\theta_+\cos^2\alpha\,(A_\nu+m_M+\mu\tan\alpha)^2\\
&\quad +M_Z^2\sin\beta\sin(\alpha+\beta)(M_Z^2\sin\beta\sin(\alpha+\beta)\sin^2 2\theta_+\\
&\quad -2m_D\cos\alpha(A_\nu+m_M+\mu\tan\alpha)\sin 4\theta_+)\\
&+ 2B_0[p^2,m^2_{\tilde{N}_-},m^2_{\tilde{\nu}_-}](4m_D^2\cos^2 2\theta_-\cos^2\alpha\,(A_\nu-m_M+\mu\tan\alpha)^2\\
&\quad +M_Z^2\sin\beta\sin(\alpha+\beta)(M_Z^2\sin\beta\sin(\alpha+\beta)\sin^2 2\theta_-\\
&\quad -2m_D\cos\alpha(A_\nu-m_M+\mu\tan\alpha)\sin 4\theta_-)\\
&+ 4B_0[p^2,m^2_{\tilde{N}_+},m^2_{\tilde{N}_+}](m_D\cos\alpha(2m_D+\sin 2\theta_+(A_\nu+m_M+\mu\tan\alpha))\\
&\quad -M_Z^2\sin\beta\sin(\alpha+\beta)\sin^2\theta_+)^2\\
&+ 4B_0[p^2,m^2_{\tilde{N}_-},m^2_{\tilde{N}_-}](m_D\cos\alpha(2m_D+\sin 2\theta_-(A_\nu-m_M+\mu\tan\alpha))\\
&\quad -M_Z^2\sin\beta\sin(\alpha+\beta)\sin^2\theta_-)^2\\
&+ 4B_0[p^2,m^2_{\tilde{\nu}_+},m^2_{\tilde{\nu}_+}](m_D\cos\alpha(-2m_D+\sin 2\theta_+(A_\nu+m_M+\mu\tan\alpha))\\
&\quad -M_Z^2\sin\beta\sin(\alpha+\beta)\cos^2\theta_+)^2\\
&+ 4B_0[p^2,m^2_{\tilde{\nu}_-},m^2_{\tilde{\nu}_-}](m_D\cos\alpha(-2m_D+\sin 2\theta_-(A_\nu-m_M+\mu\tan\alpha))\\
&\quad -M_Z^2\sin\beta\sin(\alpha+\beta)\cos^2\theta_-)^2] \qquad \text{(B.4)}
\end{aligned}
$$

The corresponding results for the tadpole T_H, and the unrenormalized self-energy Σ_{HH} are obtained from the above formulas by replacing $\cos\alpha\to\sin\alpha\,,\sin\alpha\to-\cos\alpha\,,\sin(\alpha+\beta)\to-\cos(\alpha+\beta)$.

$$
\begin{aligned}
\Sigma^{\nu}_{hH}(p^2) &= -\frac{g^2}{128c_{\rm w}^2 M_Z^2\pi^2}\frac{\sin 2\alpha\sin^2 2\theta}{\sin^2\beta}\left[2m_D^2 A_0[m_\nu^2]+(2m_D^2+m_M^2)A_0[m_N^2]\right.
\end{aligned}
$$

$$
\begin{aligned}
&+ \quad 4m_D^2 m_\nu^2 B_0[p^2, m_\nu^2, m_\nu^2] + m_M^2(m_\nu^2 + m_\nu m_N) B_0[p^2, m_\nu^2, m_N^2] \\
&+ \quad 4m_D^2 m_N^2 B_0[p^2, m_N^2, m_N^2]] \\
&+ \quad p^2(2m_D^2 B_1[p^2, m_\nu^2, m_\nu^2] + m_M^2 B_1[p^2, m_\nu^2, m_N^2] + 2m_D^2 B_1[p^2, m_N^2, m_N^2])\big] \qquad \text{(B.5)}
\end{aligned}
$$

$$
\begin{aligned}
\Sigma_{hH}^{\tilde{\nu}}(p^2) \;=\;& \frac{g^2}{512 c_{\rm w}^2 M_Z^2 \pi^2 \sin^2\beta}[4A_0[m_{\tilde{\nu}_+}^2]\sin 2\alpha(m_D^2 - M_Z^2 \sin^2\beta\cos^2\theta_+) \\
&+ \quad 4A_0[m_{\tilde{N}_+}^2]\sin 2\alpha(m_D^2 - M_Z^2 \sin^2\beta\sin^2\theta_+) \\
&+ \quad 4A_0[m_{\tilde{\nu}_-}^2]\sin 2\alpha(m_D^2 - M_Z^2 \sin^2\beta\cos^2\theta_-) \\
&+ \quad 4A_0[m_{\tilde{N}_-}^2]\sin 2\alpha(m_D^2 - M_Z^2 \sin^2\beta\sin^2\theta_-) \\
&+ \quad 2B_0[p^2, m_{\tilde{N}_+}^2, m_{\tilde{\nu}_+}^2] \times \\
&\quad (2m_D^2\cos^2 2\theta_+(-2(A_\nu + m_M)\mu\cos 2\alpha + ((A_\nu + m_M)^2 - \mu^2)\sin 2\alpha) \\
&\quad + M_Z^2 \sin\beta(-M_Z^2\sin\beta\sin(\alpha+\beta)\cos(\alpha+\beta)\sin^2 2\theta_+ \\
&\quad + m_D((A_\nu + m_M)\cos(2\alpha+\beta) + \mu\sin(2\alpha+\beta))\sin 4\theta_+)) \\
&+ \quad 2B_0[p^2, m_{\tilde{N}_-}^2, m_{\tilde{\nu}_-}^2] \times \\
&\quad (2m_D^2\cos^2 2\theta_-(-2(A_\nu - m_M)\mu\cos 2\alpha + ((A_\nu - m_M)^2 - \mu^2)\sin 2\alpha) \\
&\quad + M_Z^2 \sin\beta(-M_Z^2\sin\beta\sin(\alpha+\beta)\cos(\alpha+\beta)\sin^2 2\theta_- \\
&\quad + m_D((A_\nu - m_M)\cos(2\alpha+\beta) + \mu\sin(2\alpha+\beta))\sin 4\theta_-)) \\
&+ \quad 2B_0[p^2, m_{\tilde{N}_+}^2, m_{\tilde{N}_+}^2](m_D^2(-2\mu\cos 2\alpha\sin 2\theta_+(2m_D + (A_\nu + m_M)\sin 2\theta_+) \\
&\quad + \sin 2\alpha(4m_D^2 + 4m_D(A_\nu + m_M)\sin 2\theta_+ + ((A_\nu + m_M)^2 - \mu^2)\sin^2 2\theta_+)) \\
&\quad + M_Z^2 m_D \sin\beta\sin^2\theta_+(2\mu\sin(2\alpha+\beta)\sin 2\theta_+ \\
&\quad + 2(2m_D + (A_\nu + m_M)\sin 2\theta_+)\cos(2\alpha+\beta)) \\
&\quad - M_Z^4\sin^2\beta\sin^4\theta_+\sin 2(\alpha+\beta)) \\
&+ \quad 2B_0[p^2, m_{\tilde{N}_-}^2, m_{\tilde{N}_-}^2](-m_D^2(2\mu\cos 2\alpha\sin 2\theta_-(2m_D + (A_\nu - m_M)\sin 2\theta_-) \\
&\quad - \sin 2\alpha(4m_D^2 + 4m_D(A_\nu - m_M)\sin 2\theta_- + ((A_\nu - m_M)^2 - \mu^2)\sin^2 2\theta_-)) \\
&\quad + M_Z^2 m_D \sin\beta\sin^2\theta_-(2\mu\sin(2\alpha+\beta)\sin 2\theta_- \\
&\quad + 2(2m_D + (A_\nu - m_M)\sin 2\theta_-)\cos(2\alpha+\beta)) \\
&\quad - M_Z^4\sin^2\beta\sin^4\theta_-\sin 2(\alpha+\beta)) \\
&+ \quad 2B_0[p^2, m_{\tilde{\nu}_+}^2, m_{\tilde{\nu}_+}^2](-m_D^2(2\mu\cos 2\alpha\sin 2\theta_+(-2m_D + (A_\nu + m_M)\sin 2\theta_+) \\
&\quad - \sin 2\alpha(4m_D^2 - 4m_D(A_\nu + m_M)\sin 2\theta_+ + ((A_\nu + m_M)^2 - \mu^2)\sin^2 2\theta_+)) \\
&\quad + M_Z^2 m_D \sin\beta\cos^2\theta_+(-2\mu\sin(2\alpha+\beta)\sin 2\theta_+ \\
&\quad + 2(2m_D - (A_\nu + m_M)\sin 2\theta_+)\cos(2\alpha+\beta))
\end{aligned}
$$

$$
\begin{aligned}
& -M_Z^4 \sin^2\beta \cos^4\theta_+ \sin 2(\alpha+\beta)) \\
+ \;& 2B_0[p^2, m^2_{\tilde{\nu}_-}, m^2_{\tilde{\nu}_-}](-m_D^2(2\mu\cos 2\alpha \sin 2\theta_-(-2m_D + (A_\nu - m_M)\sin 2\theta_-) \\
& - \sin 2\alpha(4m_D^2 - 4m_D(A_\nu - m_M)\sin 2\theta_- + ((A_\nu - m_M)^2 - \mu^2)\sin^2 2\theta_-)) \\
& + M_Z^2 m_D \sin\beta\cos^2\theta_-(-2\mu\sin(2\alpha+\beta)\sin 2\theta_- \\
& + 2(2m_D - (A_\nu - m_M)\sin 2\theta_-)\cos(2\alpha+\beta)) \\
& - M_Z^4 \sin^2\beta\cos^4\theta_- \sin 2(\alpha+\beta))] \qquad \text{(B.6)}
\end{aligned}
$$

$$
\begin{aligned}
\Sigma^\nu_{AA}(M_A^2) &= -\frac{g^2}{64 c_{\rm w}^2 M_Z^2 \pi^2}\frac{\cos^2\beta \sin^2 2\theta}{\sin^2\beta}[2m_D^2 A_0[m_\nu^2] + (2m_D^2 + m_M^2)A_0[m_N^2] \qquad \text{(B.7)} \\
&+ m_M^2(m_\nu^2 - m_\nu m_N)B_0[M_A^2, m_\nu^2, m_N^2] \\
&+ M_A^2(2m_D^2(B_1[M_A^2, m_\nu^2, m_\nu^2] + B_1[M_A^2, m_N^2, m_N^2]) + m_M^2 B_1[M_A^2, m_\nu^2, m_N^2])]
\end{aligned}
$$

$$
\begin{aligned}
\Sigma^{\tilde{\nu}}_{AA}(M_A^2) &= \frac{g^2}{256 c_{\rm w}^2 M_Z^2 \pi^2}\frac{1}{\sin^2\beta}[A_0[m^2_{\tilde{\nu}_+}](4m_D^2\cos^2\beta - 2M_Z^2\cos 2\beta\sin^2\beta\cos^2\theta_+) \\
&+ A_0[m^2_{\tilde{N}_+}](4m_D^2\cos^2\beta - 2M_Z^2\cos 2\beta\sin^2\beta\sin^2\theta_+) \\
&+ A_0[m^2_{\tilde{\nu}_-}](4m_D^2\cos^2\beta - 2M_Z^2\cos 2\beta\sin^2\beta\cos^2\theta_-) \\
&+ A_0[m^2_{\tilde{N}_-}](4m_D^2\cos^2\beta - 2M_Z^2\cos 2\beta\sin^2\beta\sin^2\theta_-) \\
&+ 4m_D^2\left[B_0[M_A^2, m^2_{\tilde{\nu}_+}, m^2_{\tilde{\nu}_-}](\mu\sin\beta\sin(\theta_- - \theta_+)\right. \\
&\quad \left. + \cos\beta(A_\nu\sin(\theta_- - \theta_+) - m_M\sin(\theta_- + \theta_+)))^2\right. \\
&+ B_0[M_A^2, m^2_{\tilde{N}_+}, m^2_{\tilde{N}_-}](\mu\sin\beta\sin(\theta_- - \theta_+) \\
&\quad + \cos\beta(A_\nu\sin(\theta_- - \theta_+) + m_M\sin(\theta_- + \theta_+)))^2 \\
&+ B_0[M_A^2, m^2_{\tilde{N}_-}, m^2_{\tilde{\nu}_+}](\mu\sin\beta\cos(\theta_- - \theta_+) \\
&\quad + \cos\beta(A_\nu\cos(\theta_- - \theta_+) - m_M\cos(\theta_- + \theta_+)))^2 \\
&+ B_0[M_A^2, m^2_{\tilde{N}_+}, m^2_{\tilde{\nu}_-}](\mu\sin\beta\cos(\theta_- - \theta_+) \\
&\quad \left. + \cos\beta(A_\nu\cos(\theta_- - \theta_+) + m_M\cos(\theta_- + \theta_+)))^2\right]] \qquad \text{(B.8)}
\end{aligned}
$$

$$
\begin{aligned}
\Sigma^\nu_{ZZ}(M_Z^2) &= -\frac{g^2}{32 c_{\rm w}^2 \pi^2}\left[\cos^4\theta A_0[m_\nu^2] + \frac{1}{2}(3+\cos 2\theta)\sin^2\theta A_0[m_N^2]\right. \\
&+ 2\cos^4\theta\left(m_\nu^2 B_0[M_Z^2, m_\nu^2, m_\nu^2] - B_{00}[M_Z^2, m_\nu^2, m_\nu^2] + \frac{M_Z^2}{2}B_1[M_Z^2, m_\nu^2, m_\nu^2]\right) \\
&+ 2\sin^4\theta\left(m_N^2 B_0[M_Z^2, m_N^2, m_N^2] - B_{00}[M_Z^2, m_N^2, m_N^2] + \frac{M_Z^2}{2}B_1[M_Z^2, m_N^2, m_N^2]\right) \\
&+ \left.\frac{1}{2}\sin^2 2\theta\left(m_\nu(m_\nu + m_N)B_0[M_Z^2, m_\nu^2, m_N^2] - 2B_{00}[M_Z^2, m_\nu^2, m_N^2]\right.\right.
\end{aligned}
$$

$$+M_Z^2 B_1[M_Z^2, m_\nu^2, m_N^2])\Big] \tag{B.9}$$

$$\begin{aligned}
\Sigma_{ZZ}^{\tilde{\nu}}(M_Z^2) &= \frac{g^2}{64 c_{\rm w}^2 \pi^2}\Big[A_0[m_{\tilde{\nu}_-}^2]\cos^2\theta_- + A_0[m_{\tilde{\nu}_+}^2]\cos^2\theta_+ \\
&+ A_0[m_{\tilde{N}_-}^2]\sin^2\theta_- + A_0[m_{\tilde{N}_+}^2]\sin^2\theta_+ \\
&- 4(B_{00}[M_Z^2, m_{\tilde{\nu}_+}^2, m_{\tilde{\nu}_-}^2]\cos^2\theta_-\cos^2\theta_+ + B_{00}[M_Z^2, m_{\tilde{N}_-}^2, m_{\tilde{\nu}_+}^2]\cos^2\theta_+\sin^2\theta_- \\
&+ B_{00}[M_Z^2, m_{\tilde{N}_+}^2, m_{\tilde{\nu}_-}^2]\cos^2\theta_-\sin^2\theta_+ + B_{00}[M_Z^2, m_{\tilde{N}_+}^2, m_{\tilde{N}_-}^2]\sin^2\theta_-\sin^2\theta_+)\Big]
\end{aligned} \tag{B.10}$$

The definitions of the loop functions A_0, B_0, B_1 and B_{00} appearing in this and the next appendices can be found, for instance, in Ref. [196] (where $B_{00} = B_{22}$).

Appendix C

Dirac case. One-loop neutrino/sneutrino contributions to the h Higgs boson self-energy

We present here the result for the one-loop corrections from neutrinos (ν) and sneutrinos ($\tilde{\nu}$) to the renormalized hh self-energy in the case of Dirac neutrinos, obtained in the $\overline{\rm DR}$ scheme. Here $c_{\rm w} = \cos\theta_W$.

$$
\begin{aligned}
\hat{\Sigma}^{\nu}_{hh}(p^2)_{\rm Dirac} &= \frac{g^2}{32 c_{\rm w}^2 M_Z^2 \pi^2}\Big\{ A_0[m_D^2]\,(\sin^2(\alpha+\beta) M_Z^2 \\
&\quad + \frac{1}{\sin\beta}(\sin(2\alpha-3\beta) + 3\sin(2\alpha-\beta) - 2\sin\beta) m_D^2 \\
&+ \sin^2(\alpha+\beta) M_Z^2 (m_D^2 B_0[M_Z^2, m_D^2, m_D^2] \\
&\quad - 2B_{00}[M_Z^2, m_D^2, m_D^2] + M_Z^2 B_1[M_Z^2, m_D^2, m_D^2]) \\
&- 2\frac{\cos^2\alpha}{\sin^2\beta}(2m_D^4 B_0[p^2, m_D^2, m_D^2] + p^2 B_1[p^2, m_D^2, m_D^2]) \\
&+ 2M_A^2 m_D^2 \frac{\cos^2(\alpha-\beta)\cos^2\beta}{\sin^2\beta} B_1[M_A^2, m_D^2, m_D^2]\Big\} \qquad \text{(C.1)}
\end{aligned}
$$

$$
\begin{aligned}
\hat{\Sigma}^{\tilde{\nu}}_{hh}(p^2)_{\rm Dirac} &= -\frac{g^2}{256 c_{\rm w}^2 M_Z^2 \pi^2}\Bigg\{ A_0[m_{\tilde{\nu}_1}^2]\Big[8M_Z^2 \sin^2(\alpha+\beta)\cos^2\tilde{\theta} + 2m_D \frac{\sin(\alpha-\beta)\sin 2\tilde{\theta}}{\sin\beta} \times \\
&\qquad (\mu(3\sin\alpha - \sin(\alpha-2\beta)) + A_\nu(3\cos\alpha + \cos(\alpha-2\beta)))\Big] \\
&+ A_0[m_{\tilde{\nu}_2}^2]\Big[8M_Z^2 \sin^2(\alpha+\beta)\sin^2\tilde{\theta} - 2m_D \frac{\sin(\alpha-\beta)\sin 2\tilde{\theta}}{\sin\beta} \times
\end{aligned}
$$

$$
\begin{aligned}
& (\mu(3\sin\alpha - \sin(\alpha-2\beta)) + A_\nu(3\cos\alpha + \cos(\alpha-2\beta)))\Big] \\
- \quad & \frac{1}{16}\frac{1}{\sin^2\beta} B_0[p^2, m^2_{\tilde{\nu}_1}, m^2_{\tilde{\nu}_1}]\Big[2(8m_D^2 - M_Z^2)\cos\alpha \\
& +2M_Z^2(\cos(\alpha+2\beta) - 2\cos 2\tilde{\theta}\sin\beta\sin(\alpha+\beta)) \\
& -8m_D\sin 2\tilde{\theta}\cos\alpha(A_\nu + \mu\tan\alpha)\Big]^2 \\
- \quad & \frac{1}{16}\frac{1}{\sin^2\beta} B_0[p^2, m^2_{\tilde{\nu}_2}, m^2_{\tilde{\nu}_2}]\Big[2(8m_D^2 - M_Z^2)\cos\alpha \\
& +2M_Z^2(\cos(\alpha+2\beta) + 2\cos 2\tilde{\theta}\sin\beta\sin(\alpha+\beta)) \\
& +8m_D\sin 2\tilde{\theta}\cos\alpha(A_\nu + \mu\tan\alpha)\Big]^2 \\
- \quad & \frac{1}{8}\frac{1}{\sin^2\beta} B_0[p^2, m^2_{\tilde{\nu}_2}, m^2_{\tilde{\nu}_1}]\Big[-4M_Z^2\sin 2\tilde{\theta}\sin\beta\sin(\alpha+\beta) \\
& +8m_D\cos 2\tilde{\theta}\cos\alpha(A_\nu + \mu\tan\alpha)\Big]^2 \\
+ \quad & 8m_D^2\cos^2(\alpha-\beta)\cot^2\beta\, B_0[M_A^2, m^2_{\tilde{\nu}_2}, m^2_{\tilde{\nu}_1}]\,(A_\nu + \mu\tan\beta)^2 \\
- \quad & 8M_Z^2\sin^2(\alpha+\beta)\Big(2\cos^4\tilde{\theta}B_{00}[M_Z^2, m^2_{\tilde{\nu}_1}, m^2_{\tilde{\nu}_1}] + 2\sin^4\tilde{\theta}B_{00}[M_Z^2, m^2_{\tilde{\nu}_2}, m^2_{\tilde{\nu}_2}] \\
& + \sin^2 2\tilde{\theta}B_{00}[M_Z^2, m^2_{\tilde{\nu}_2}, m^2_{\tilde{\nu}_1}]\Big)\Bigg\}
\end{aligned}
\tag{C.2}
$$

Bibliography

[1] S. L. Glashow, Nucl. Phys. **22**, 579 (1961).

[2] M. Gell-Mann, Phys. Lett. **8**, 214 (1964).

[3] G. Zweig, "An SU(3) Model For Strong Interaction Symmetry And Its Breaking. 2," Preprint CERN-TH-412.

[4] S. Weinberg, Phys. Rev. Lett. **19**, 1264 (1967).

[5] A. Salam, *Originally printed in *Svartholm: Elementary Particle Theory, Proceedings Of The Nobel Symposium Held 1968 At Lerum, Sweden*, Stockholm 1968, 367-377*

[6] P. W. Higgs, Phys. Lett. **12**, 132 (1964).

[7] P. W. Higgs, Phys. Rev. **145**, 1156 (1966).

[8] F. Englert and R. Brout, Phys. Rev. Lett. **13**, 321 (1964).

[9] G. S. Guralnik, C. R. Hagen and T. W. B. Kibble, Phys. Rev. Lett. **13**, 585 (1964).

[10] B. W. Lee, C. Quigg, H. B. Thacker, Phys. Rev. Lett. **38** (1977) 883-885.

[11] M. Baak *et al.*, arXiv:1107.0975 [hep-ph].

[12] R. Barate *et al.* [LEP Working Group for Higgs boson searches and ALEPH Collaboration and and], Phys. Lett. B **565** (2003) 61 [arXiv:hep-ex/0306033].

[13] T. Aaltonen *et al.* [CDF and D0 Collaboration], [arXiv:1103.3233 [hep-ex]].

[14] [CDF and D0 Collaboration], [arXiv:1007.4587 [hep-ex]].

[15] ATLAS-CONF-2011-112

[16] CMS, CMS PAS HIG-11-011.

[17] Talk given by Gigi Rolandi, "Higgs status and combinations" Hadron Collider Physics Symposium, Paris, 14-18 November 2011

[18] T. Appelquist, J. Carazzone, Phys. Rev. **D11** (1975) 2856.

[19] M. J. G. Veltman, Nucl. Phys. **B123** (1977) 89.

[20] K. Nakamura et al. (Particle Data Group), J. Phys. G 37, 075021 (2010) and 2011 partial update for the 2012 edition.

[21] G. W. Bennett *et al.* [Muon G-2 Collaboration], Phys. Rev. **D73** (2006) 072003. [hep-ex/0602035].

[22] CMS and LHCb Collaborations, http://cdsweb.cern.ch/record/1374913/files/BPH-11-019-pas.pdf.

[23] A. J. Buras, PoS E **PS-HEP2009** (2009) 024 [arXiv:0910.1032 [hep-ph]].

[24] B. T. Cleveland *et al.*, Astrophys. J. **496** (1998) 505.

[25] Y. Fukuda *et al.* [Kamiokande Collaboration], Phys. Rev. Lett. **77** (1996) 1683.

[26] J. N. Abdurashitov *et al.* [SAGE Collaboration], Phys. Rev. C **80** (2009) 015807 [arXiv:0901.2200 [nucl-ex]].

[27] P. Anselmann *et al.* [GALLEX Collaboration], Phys. Lett. B **285** (1992) 376.

[28] W. Hampel *et al.* [GALLEX Collaboration], Phys. Lett. B **447** (1999) 127.

[29] M. Altmann *et al.* [GNO COLLABORATION Collaboration], Phys. Lett. B **616** (2005) 174 [arXiv:hep-ex/0504037].

[30] S. Fukuda *et al.* [Super-Kamiokande Collaboration], Phys. Lett. B **539** (2002) 179 [arXiv:hep-ex/0205075].

[31] Q. R. Ahmad *et al.* [SNO Collaboration], Phys. Rev. Lett. **87** (2001) 071301 [arXiv:nucl-ex/0106015].

[32] Q. R. Ahmad *et al.* [SNO Collaboration], Phys. Rev. Lett. **89** (2002) 011301 [arXiv:nucl-ex/0204008].

[33] Y. Fukuda *et al.* [Super-Kamiokande Collaboration], Phys. Rev. Lett. **81** (1998) 1562 [arXiv:hep-ex/9807003].

[34] Y. Ashie *et al.* [Super-Kamiokande Collaboration], Phys. Rev. Lett. **93** (2004) 101801 [arXiv:hep-ex/0404034].

[35] K. Eguchi *et al.* [KamLAND Collaboration], Phys. Rev. Lett. **90** (2003) 021802 [arXiv:hep-ex/0212021].

[36] T. Araki *et al.* [KamLAND Collaboration], Phys. Rev. Lett. **94** (2005) 081801 [arXiv:hep-ex/0406035].

[37] B. Pontecorvo, Sov. Phys. JETP **6** (1957) 429 [Zh. Eksp. Teor. Fiz. **33** (1957) 549].

[38] Z. Maki, M. Nakagawa and S. Sakata, Prog. Theor. Phys. **28** (1962) 870.

[39] M. H. Ahn *et al.* [K2K Collaboration], Phys. Rev. D **74** (2006) 072003 [arXiv:hep-ex/0606032].

[40] D. G. Michael *et al.* [MINOS Collaboration], Phys. Rev. Lett. **97** (2006) 191801 [arXiv:hep-ex/0607088].

[41] P. Adamson *et al.* [MINOS Collaboration], Phys. Rev. Lett. **101** (2008) 131802 [arXiv:0806.2237 [hep-ex]].

[42] S. M. Bilenky, J. Hosek and S. T. Petcov, Phys. Lett. B **94** (1980) 495.

[43] M. Doi, T. Kotani, H. Nishiura, K. Okuda and E. Takasugi, Phys. Lett. B **102** (1981) 323.

[44] S. Pascoli and S. T. Petcov, Phys. Lett. B **544** (2002) 239 [arXiv:hep-ph/0205022]. S. Pascoli and S. T. Petcov, Phys. Lett. B **580** (2004) 280 [arXiv:hep-ph/0310003].

S. Pascoli, S. T. Petcov and L. Wolfenstein, Phys. Lett. B **524** (2002) 319 [arXiv:hep-ph/0110287].

[45] S. M. Bilenky, S. Pascoli and S. T. Petcov, Phys. Rev. D **64** (2001) 053010 [arXiv:hep-ph/0102265].

[46] S. M. Bilenky, C. Giunti, C. W. Kim and S. T. Petcov, Phys. Rev. D **54** (1996) 4432 [arXiv:hep-ph/9604364].

[47] C. Aalseth *et al.*, arXiv:hep-ph/0412300.

[48] M. Czakon, J. Gluza and M. Zralek, arXiv:hep-ph/0003161.

[49] H. Murayama and C. Pena-Garay, Phys. Rev. D **69** (2004) 031301 [arXiv:hep-ph/0309114].

[50] P. Minkowski, *Phys. Lett.* **B 67** (1977) 421;
M. Gell-Mann, P. Ramond and R. Slansky, in *Complex Spinors and Unified Theories* eds. P. Van. Nieuwenhuizen and D. Z. Freedman, *Supergravity* (North-Holland, Amsterdam, 1979), p.315 [Print-80-0576 (CERN)];
T. Yanagida, in *Proceedings of the Workshop on the Unified Theory and the Baryon Number in the Universe*, eds. O. Sawada and A. Sugamoto (KEK, Tsukuba, 1979), p.95;
S. Glashow, in *Quarks and Leptons*, eds. M. Lévy et al. (Plenum Press, New York, 1980), p.687;
R. N. Mohapatra and G. Senjanović, *Phys. Rev. Lett.* **44** (1980) 912.

[51] R. Barbieri, D. V. Nanopolous, G. Morchio and F. Strocchi, Phys. Lett. B **90** (1980) 91; R. E. Marshak and R. N. Mohapatra, *Invited talk given at Orbis Scientiae, Coral Gables, Fla., Jan. 14-17, 1980*, VPI-HEP-80/02; T. P. Cheng and L. F. Li, Phys. Rev. D **22** (1980) 2860; M. Magg and C. Wetterich, Phys. Lett. B **94** (1980) 61; J. Schechter and J. W. F. Valle, Phys. Rev. D **22** (1980) 2227; G. Lazarides, Q. Shafi and C. Wetterich, Nucl. Phys. B **181** (1981) 287; R. N. Mohapatra and G. Senjanovic, Phys. Rev. D **23** (1981) 165. E. Ma and U. Sarkar, Phys. Rev. Lett. **80** (1998) 5716 [arXiv:hep-ph/9802445].

[52] S. Davidson and A. Ibarra, Phys. Lett. B **535** (2002) 25 [arXiv:hep-ph/0202239].

[53] Yu. A. Golfand and E. P. Likhtman, "Extension of the Algebra of Poincare Group Generators and Violation of p JETP Lett. **13**, 323 (1971) [Pisma Zh. Eksp. Teor. Fiz. **13**, 452 (1971)].

[54] D. V. Volkov and V. P. Akulov, Phys. Lett. B **46** (1973) 109.

[55] J. Wess and B. Zumino, Nucl. Phys. B **70**, 39 (1974).

[56] H. E. Haber and G. L. Kane, Phys. Rept. **117** (1985) 75.

[57] J. F. Gunion and H. E. Haber, Nucl. Phys. B **272** (1986) 1 [Erratum-ibid. B **402** (1993) 567].

[58] J. F. Gunion and H. E. Haber, Nucl. Phys. B **278** (1986) 449.

[59] L. Girardello, M. T. Grisaru, Nucl. Phys. **B194** (1982) 65.

[60] M. S. Carena, S. Heinemeyer, C. E. M. Wagner, G. Weiglein, [hep-ph/9912223].

[61] G. Degrassi, S. Heinemeyer, W. Hollik, P. Slavich, G. Weiglein, Eur. Phys. J. **C28** (2003) 133-143. [arXiv:hep-ph/0212020 [hep-ph]].

[62] A. Brignole, *Phys. Lett.* **B 281** (1992) 284;
P. Chankowski, S. Pokorski and J. Rosiek, *Phys. Lett.* **B 286** (1992) 307;
A. Dabelstein, *Nucl. Phys.* **B 456** (1995) 25 [arXiv:hep-ph/9503443];

[63] For a review see, for instance,
G. L. Kane, C. F. Kolda, L. Roszkowski and J. D. Wells, Phys. Rev. D **49** (1994) 6173 [arXiv:hep-ph/9312272].

[64] For a review see, for instance,
J. R. Ellis, T. Falk, K. A. Olive and Y. Santoso, Nucl. Phys. B **652** (2003) 259 [arXiv:hep-ph/0210205];

[65] CMS, CMS-PAS-SUS-11-003

[66] S. Chatrchyan *et al.* [CMS Collaboration], [arXiv:1109.2352 [hep-ex]].

[67] J. Cao and J. M. Yang, *Phys. Rev.* **D 71** (2005) 111701 [arXiv:hep-ph/0412315].

[68] G. Aad et al. [The ATLAS Collaboration], arXiv:0901.0512;
G. Bayatian et al. [CMS Collaboration], *J. Phys.* **G 34** (2007) 995.

[69] K. Cranmer, Y. Fang, B. Mellado, S. Paganis, W. Quayle and S. Wu, arXiv:hep-ph/0401148.

[70] S. Abdullin et al., *Eur. Phys. J.* **C 39S2** (2005) 41.

[71] S. Gennai, S. Heinemeyer, A. Kalinowski, R. Kinnunen, S. Lehti, A. Nikitenko and G. Weiglein, *Eur. Phys. J.* **C 52** (2007) 383 [arXiv:0704.0619 [hep-ph]].

[72] J. Aguilar-Saavedra et al., TESLA TDR Part 3: "Physics at an e^+e^- Linear Collider", arXiv:hep-ph/0106315, see: `tesla.desy.de/tdr/`;
K. Ackermann et al., DESY-PROC-2004-01, *prepared for 4th ECFA / DESY Workshop on Physics and Detectors for a 90-GeV to 800-GeV Linear e+ e- Collider, Amsterdam, The Netherlands, 1-4 Apr 2003.*

[73] T. Abe et al. [American Linear Collider Working Group Collaboration], arXiv:hep-ex/0106056.

[74] K. Abe et al. [ACFA Linear Collider Working Group Collaboration], arXiv:hep-ph/0109166.

[75] S. Heinemeyer et al., arXiv:hep-ph/0511332.

[76] G. Degrassi, S. Heinemeyer, W. Hollik, P. Slavich and G. Weiglein, *Eur. Phys. J.* **C 28** (2003) 133 [arXiv:hep-ph/0212020].

[77] F. Borzumati and A. Masiero, Phys. Rev. Lett. **57** (1986) 961.

[78] J. Hisano, T. Moroi, K. Tobe, M. Yamaguchi and T. Yanagida, Phys. Lett. B **357** (1995) 579 [arXiv:hep-ph/9501407];

[79] J. Hisano, T. Moroi, K. Tobe and M. Yamaguchi, Phys. Rev. D **53** (1996) 2442 [arXiv:hep-ph/9510309].

[80] J. Hisano and D. Nomura, "Solar and atmospheric neutrino oscillations and lepton flavor violation in supersymmetric models with the right-handed neutrinos," Phys. Rev. D **59** (1999) 116005 [arXiv:hep-ph/9810479].

[81] Y. Kuno and Y. Okada, Rev. Mod. Phys. **73** (2001) 151 [arXiv:hep-ph/9909265].

[82] J. R. Ellis, J. Hisano, M. Raidal, Y. Shimizu, Phys. Rev. **D66** (2002) 115013. [hep-ph/0206110].

[83] J. I. Illana and T. Riemann, Nucl. Phys. Proc. Suppl. **89** (2000) 64 [arXiv:hep-ph/0006055].

[84] A. Abada, C. Biggio, F. Bonnet, M. B. Gavela and T. Hambye, JHEP **0712** (2007) 061 [arXiv:0707.4058 [hep-ph]].

[85] J. Adam *et al.* [MEG collaboration], arXiv:1107.5547 [hep-ex].

[86] C. Dohmen *et al.* [SINDRUM II Collaboration.], Phys. Lett. B **317**, 631 (1993).

[87] W. Bertl *et al.* [SINDRUM II Collaboration], Eur. Phys. J. C **47**, 337 (2006).

[88] U. Bellgardt *et al.* [SINDRUM Collaboration], Nucl. Phys. B **299**, 1 (1988)

[89] B. Aubert *et al.* [BABAR Collaboration], Phys. Rev. Lett. **104** (2010) 021802. [arXiv:0908.2381 [hep-ex]].

[90] K. Hayasaka, K. Inami, Y. Miyazaki, K. Arinstein, V. Aulchenko, T. Aushev, A. M. Bakich, A. Bay *et al.*, Phys. Lett. **B687** (2010) 139-143. [arXiv:1001.3221 [hep-ex]].

[91] http://www.slac.stanford.edu/xorg/hfag/tau/HFAG-TAU-LFV.htm.

[92] D. Asner *et al.* [Heavy Flavor Averaging Group Collaboration], [arXiv:1010.1589 [hep-ex]].

[93] K. Hayasaka,

[arXiv:1010.3746 [hep-ex]].

[94] Y. Miyazaki *et al.* [Belle Collaboration], Phys. Lett. **B672** (2009) 317-322. [arXiv:0810.3519 [hep-ex]].

[95] M. Sher, Phys. Rev. D **66** (2002) 057301 [arXiv:hep-ph/0207136].

[96] A. Brignole and A. Rossi, Nucl. Phys. B **701** (2004) 3 [arXiv:hep-ph/0404211].

[97] E. Arganda, M. J. Herrero and J. Portoles, JHEP **0806**, 079 (2008) [arXiv:0803.2039 [hep-ph]].

[98] C. H. Chen and C. Q. Geng, Phys. Rev. D **74** (2006) 035010 [arXiv:hep-ph/0605299].

[99] E. Arganda and M. J. Herrero, Phys. Rev. D **73** (2006) 055003 [arXiv:hep-ph/0510405].

[100] E. Arganda, M. Herrero, J. Portoles, A. Rodriguez-Sanchez and A. M. Teixeira, Nucl. Phys. Proc. Suppl. **189** (2009) 134 [arXiv:0812.2692 [hep-ph]].

[101] S. Weinberg, Physica **A96** (1979) 327;

[102] J. Gasser and H. Leutwyler, Annals Phys. **158** (1984) 142.

[103] J. Gasser and H. Leutwyler, Nucl. Phys. B **250** (1985) 465.

[104] G. Ecker, J. Gasser, H. Leutwyler, A. Pich and E. de Rafael, Phys. Lett. B **223** (1989) 425; F. Guerrero and A. Pich, Phys. Lett. B **412** (1997) 382 [arXiv:hep-ph/9707347].

[105] G. Ecker, J. Gasser, A. Pich and E. de Rafael, Nucl. Phys. B **321** (1989) 311;

[106] A. Pich, in: R.F. Lebed (Ed.), Phenomenology of Large-N_C QCD, World Scientific, Singapore, 2002, arXiv:hep-ph/0205030.

[107] V. Cirigliano, G. Ecker, H. Neufeld and A. Pich, JHEP **0306** (2003) 012 [arXiv:hep-ph/0305311].

[108] V. Cirigliano, G. Ecker, M. Eidemuller, R. Kaiser, A. Pich and J. Portoles, Nucl. Phys. B **753** (2006) 139 [arXiv:hep-ph/0603205].

[109] M. J. Herrero, J. Portoles and A. M. Rodriguez-Sanchez, Phys. Rev. D **80** (2009) 015023 [arXiv:0903.5151 [hep-ph]].

[110] S. Heinemeyer, M. J. Herrero, S. Penaranda and A. M. Rodriguez-Sanchez, JHEP **1105** (2011) 063 [arXiv:1007.5512 [hep-ph]].

[111] B. O'Leary *et al.* [SuperB Collaboration], "SuperB Progress Reports – Physics," arXiv:1008.1541 [hep-ex].

[112] E. Arganda, M. J. Herrero, J. Portoles, A. Rodriguez-Sanchez and A. M. Teixeira, AIP Conf. Proc. **1078** (2009) 335 [arXiv:0810.0163 [hep-ph]].

[113] M. Herrero, J. Portoles and A. Rodriguez-Sanchez, AIP Conf. Proc. **1200** (2010) 908 [arXiv:0909.0724 [hep-ph]].

[114] S. Heinemeyer, M. J. Herrero, S. Penaranda and A. M. Rodriguez-Sanchez, "M_h in MSSM with Heavy Majorana Neutrinos," arXiv:1107.0241 [hep-ph].

[115] S. R. Coleman, J. Mandula, Phys. Rev. **159** (1967) 1251-1256.
R. Haag, J. T. Lopuszanski, M. Sohnius, Nucl. Phys. **B88** (1975) 257.

[116] S. P. Martin, In *Kane, G.L. (ed.): Perspectives on supersymmetry* 1-98. [hep-ph/9709356].

[117] L. E. Ibanez and G. G. Ross, arXiv:hep-ph/9204201.

[118] H. E. Haber, Y. Nir, Phys. Lett. **B306** (1993) 327-334. [hep-ph/9302228].

[119] S. Martin, *Phys. Rev.* **D 75** (2007) 055005 [arXiv:hep-ph/0701051];
R. Harlander, P. Kant, L. Mihaila and M. Steinhauser, *Phys. Rev. Lett.* **100** (2008) 191602 [*Phys. Rev. Lett.* **101** (2008) 039901] [arXiv:0803.0672 [hep-ph]]; arXiv:1005.5709 [hep-ph].

[120] A. Brignole, J. R. Ellis, G. Ridolfi, F. Zwirner, Phys. Lett. **B271** (1991) 123-132.

[121] J. R. Ellis, G. Ridolfi, F. Zwirner, Phys. Lett. **B262** (1991) 477-484.

[122] R. Barbieri, M. Frigeni, Phys. Lett. **B258** (1991) 395-398.

[123] M. S. Carena, H. E. Haber, Prog. Part. Nucl. Phys. **50** (2003) 63-152. [hep-ph/0208209].

[124] M. Carena, J.R. Espinosa, M. Quirós and C.E.M. Wagner, *Phys. Lett.* **B355** (1995) 209; M. Carena, M. Quirós and C.E.M. Wagner, *Nucl. Phys.* **B461** (1996) 407.

[125] H.E. Haber and R. Hempfling, *Phys. Rev.* **D48** (1993) 4280.

[126] S. Heinemeyer, W. Hollik and G. Weiglein, *Phys. Lett.* **B455** (1999) 179.

[127] M. Carena, H.E. Haber, S. Heinemeyer, W. Hollik, C.E.M. Wagner and G. Weiglein, *Nucl. Phys.* **B580** (2000) 29.

[128] ATLAS, ATLAS-CONF-2011-086.

[129] B. Abbott *et al.* [D0 Collaboration], Phys. Rev. Lett. **82** (1999) 29-34. [hep-ex/9808010].

[130] T. Affolder *et al.* [CDF Collaboration], Phys. Rev. Lett. **88** (2002) 041801 [arXiv:hep-ex/0106001].

[131] CMS-PAS-SUS-10-009.

[132] J. Abdallah *et al.* [DELPHI Collaboration], Eur. Phys. J. C **31** (2003) 421 [arXiv:hep-ex/0311019].

[133] Ch. Weinheimer et al., Phys. Lett. B**460** (1999) 219; Erratum ibid. 464 (1999) 332
M. Lobashev et al., Phys. Lett. B**464** (1999) 227.

[134] M. Fukugita and T. Yanagida, *Phys. Lett.* **B 174** (1986) 45.

[135] For a general overview and selected references therein, see, for instance:
M. Raidal et al., *Eur. Phys. J.* **C 57** (2008) 13 [arXiv:0801.1826 [hep-ph]].

[136] J. R. Ellis, J. Hisano, M. Raidal, Y. Shimizu, Phys. Lett. **B528** (2002) 86-96. [hep-ph/0111324].

[137] I. Masina, Nucl. Phys. **B671** (2003) 432-458. [hep-ph/0304299].

[138] Y. Farzan, M. E. Peskin, Phys. Rev. **D70** (2004) 095001. [hep-ph/0405214].

[139] Y. Grossman and H. Haber, *Phys. Rev. Lett.* **78** (1997) 3438 [arXiv:hep-ph/9702421].

[140] A. Dedes, H. Haber and J. Rosiek, *JHEP* **0711** (2007) 059 [arXiv:0707.3718 [hep-ph]].

[141] J. Gunion and H. Haber, *Nucl. Phys.* **B 272** (1986) 1 [Erratum-ibid. **B 402** (1993) 567].

[142] E. K. Akhmedov, [hep-ph/0001264].

[143] J. A. Casas and A. Ibarra, Nucl. Phys. B **618** (2001) 171 [arXiv:hep-ph/0103065].

[144] J. Küblbeck, M. Böhm and A. Denner, *Comput. Phys. Commun.* **60** (1990) 165;
T. Hahn, *Comput. Phys. Commun.* **140** (2001) 418 [arXiv:hep-ph/0012260];
T. Hahn and C. Schappacher, *Comput. Phys. Commun.* **143** (2002) 54 [arXiv:hep-ph/0105349].
The program and the user's guide are available via `www.feynarts.de` .

[145] Y. Farzan, *JHEP* **0502** (2005) 025 [arXiv:hep-ph/0411358].

[146] W. Siegel, Phys. Lett. **B84** (1979) 193.

[147] D. Stöckinger, *JHEP* **0503** (2005) 076 [arXiv:hep-ph/0503129].

[148] W. Hollik and D. Stöckinger, *Phys. Lett.* **B 634** (2006) 63 [arXiv:hep-ph/0509298].

[149] W. Hollik,

[150] J. R. Ellis, G. Ridolfi, F. Zwirner, Phys. Lett. **B257** (1991) 83-91.

[151] H. E. Haber, R. Hempfling, Phys. Rev. Lett. **66** (1991) 1815-1818.

[152] H. E. Haber, R. Hempfling, Phys. Rev. **D48** (1993) 4280-4309. [hep-ph/9307201].

[153] K. Sasaki, M. S. Carena, C. E. M. Wagner, Nucl. Phys. **B381** (1992) 66-86.

[154] A. Brignole, Phys. Lett. **B281** (1992) 284-294.

[155] P. H. Chankowski, S. Pokorski, J. Rosiek, Nucl. Phys. **B423** (1994) 437-496. [hep-ph/9303309].

[156] A. Dabelstein, Z. Phys. **C67** (1995) 495-512. [arXiv:hep-ph/9409375 [hep-ph]].

[157] A. Dabelstein and W. Hollik, In *Muenchen/Annecy/Hamburg 1992-93, Proceedings, e+ e- collisions at 500-GeV* 87-105. and Muenchen MPI Phys. - MPI-Ph-93-086 (93/11,rec.Feb.94) 20 p. C

[158] M. Frank, S. Heinemeyer, W. Hollik and G. Weiglein, "FeynHiggs1.2: Hybrid MS-bar / on-shell renormalization for the CP even Higgs boson sector in the MSSM," arXiv:hep-ph/0202166.

[159] A. Freitas and D. Stockinger, *Phys. Rev.* **D 66** (2002) 095014 [arXiv:hep-ph/0205281].

[160] M. Frank, T. Hahn, S. Heinemeyer, W. Hollik, H. Rzehak and G. Weiglein, *JHEP* **0702** (2007) 047 [arXiv:hep-ph/0611326].

[161] M. Frank, PhD thesis: "Radiative Corrections in the Higgs Sector of the MSSM with $\mathcal{CP}$ Violation", University of Karlsruhe, 2002, ISBN 3-937231-01-3.

[162] J. Collins, F. Wilczek and A. Zee, *Phys. Rev.* **D 18** (1978) 242.

[163] P. Nason, S. Dawson and R. K. Ellis, *Nucl. Phys.* **B 327** (1989) 49 [Erratum-ibid. **B 335** (1990) 260].

[164] T. Hahn and M. Pérez-Victoria, *Comput. Phys. Commun.* **118** (1999) 153 [arXiv:hep-ph/9807565].

[165] V. Büscher and K. Jakobs, *Int. J. Mod. Phys.* **A 20** (2005) 2523 [arXiv:hep-ph/0504099].

[166] M. Schumacher, *Czech. J. Phys.* **54** (2004) A103; arXiv:hep-ph/0410112.

[167] [LHC / ILC Study Group], G. Weiglein et al., *Phys. Rept.* **426** (2006) 47 [arXiv:hep-ph/0410364];
A. De Roeck et al., *Eur. Phys. J.* **C 66** (2010) 525 [arXiv:0909.3240 [hep-ph]].

[168] K. Desch, E. Gross, S. Heinemeyer, G. Weiglein and L. Zivkovic, *JHEP* **0409** (2004) 062 [arXiv:hep-ph/0406322].

[169] For reviews on radiative corrections to MSSM Higgs boson masses, see, for instance, A. Djouadi, *Phys. Rept.* **459** (2008) 1 [arXiv:hep-ph/0503173];
S. Heinemeyer, *Int. J. Mod. Phys.* **A 21** 2659 (2006) [arXiv:hep-ph/0407244], and references therein.

[170] S. Heinemeyer, W. Hollik and G. Weiglein, *Comput. Phys. Commun.* **124** (2000) 76 [arXiv:hep-ph/9812320]; see: `www.feynhiggs.de` .

[171] S. Heinemeyer, W. Hollik and G. Weiglein, *Eur. Phys. J.* **C 9** (1999) 343 [arXiv:hep-ph/9812472].

[172] E. Arganda, M. J. Herrero and A. M. Teixeira, JHEP **0710** (2007) 104 [arXiv:0707.2955 [hep-ph]].

[173] S. K. Kang, A. Kato, T. Morozumi and N. Yokozaki, Phys. Rev. D **81**, 016011 (2010) [arXiv:0909.2484 [hep-ph]];

[174] S. K. Kang, T. Morozumi and N. Yokozaki, arXiv:1005.1354 [hep-ph].

[175] Y. Farzan, Phys. Rev. **D69** (2004) 073009. [hep-ph/0310055]

[176] G. F. Giudice, P. Paradisi and A. Strumia, Phys. Lett. B **694** (2010) 26 [arXiv:1003.2388 [hep-ph]].

[177] S. M. Bilenky, S. T. Petcov and B. Pontecorvo, Phys. Lett. B **67** (1977) 309.

[178] T. P. Cheng, L. -F. Li, Phys. Rev. Lett. **45** (1980) 1908.

[179] W. J. Marciano and A. I. Sanda, Phys. Lett. B **67** (1977) 303.

[180] K. S. Babu and C. Kolda, Phys. Rev. Lett. **89** (2002) 241802 [arXiv:hep-ph/0206310].

[181] A. Dedes, J. R. Ellis and M. Raidal, Phys. Lett. B **549** (2002) 159 [arXiv:hep-ph/0209207].

[182] R. Kitano, M. Koike, S. Komine and Y. Okada, Phys. Lett. B **575** (2003) 300 [arXiv:hep-ph/0308021].

[183] A. Brignole and A. Rossi, Phys. Lett. B **566** (2003) 217 [arXiv:hep-ph/0304081];

[184] E. Arganda, A. M. Curiel, M. J. Herrero and D. Temes, Phys. Rev. D **71** (2005) 035011 [arXiv:hep-ph/0407302].

[185] P. Paradisi, JHEP **0510** (2005) 006 [arXiv:hep-ph/0505046].

[186] P. Paradisi, JHEP **0602** (2006) 050 [arXiv:hep-ph/0508054].

[187] S. Antusch, E. Arganda, M. J. Herrero and A. M. Teixeira, JHEP **0611** (2006) 090 [arXiv:hep-ph/0607263].

[188] T. Fukuyama, A. Ilakovac and T. Kikuchi, "Lepton flavour violating leptonic / semileptonic decays of charged leptons in the minimal supersymmetric standard model," Eur. Phys. J. C **56** (2008) 125 [arXiv:hep-ph/0506295].

[189] L. J. Hall, V. A. Kostelecky and S. Raby, Nucl. Phys. B **267** (1986) 415.

[190] W. Porod, Comput. Phys. Commun. **153** (2003) 275 [arXiv:hep-ph/0301101].

[191] G. 't Hooft, Nucl. Phys. B **72** (1974) 461; G. 't Hooft, Nucl. Phys. B **75** (1974) 461; E. Witten, Nucl. Phys. B **160** (1979) 57.

[192] S. Peris, M. Perrottet and E. de Rafael, JHEP **9805** (1998) 011 [arXiv:hep-ph/9805442]; M. Knecht, S. Peris, M. Perrottet and E. de Rafael, Phys. Rev. Lett. **83** (1999) 5230 [arXiv:hep-ph/9908283]; S. Peris, B. Phily and E. de Rafael, Phys. Rev. Lett. **86** (2001) 14 [arXiv:hep-ph/0007338]; B. Moussallam, Nucl. Phys. B **504** (1997) 381 [arXiv:hep-ph/9701400]; B. Moussallam, Phys. Rev. D **51** (1995) 4939 [arXiv:hep-ph/9407402]; M. Knecht and A. Nyffeler, Eur. Phys. J. C **21** (2001) 659 [arXiv:hep-ph/0106034]; P. D. Ruiz-Femenía, A. Pich and J. Portolés, JHEP **0307** (2003) 003 [arXiv:hep-ph/0306157]; V. Cirigliano, G. Ecker, M. Eidemüller, A. Pich and J. Portolés, Phys. Lett. B **596** (2004) 96 [arXiv:hep-ph/0404004]; V. Cirigliano, G. Ecker, M. Eidemüller, R. Kaiser, A. Pich and J. Portolés, JHEP **0504** (2005) 006 [arXiv:hep-ph/0503108]; V. Mateu and J. Portolés, Eur. Phys. J. C **52** (2007) 325 [arXiv:0706.1039 [hep-ph]].

[193] J. Bijnens, E. Gamiz, E. Lipartia and J. Prades, JHEP **0304** (2003) 055 [arXiv:hep-ph/0304222]; P. Masjuan and S. Peris, JHEP **0705** (2007) 040 [arXiv:0704.1247 [hep-ph]].

[194] R. Kaiser and H. Leutwyler, arXiv:hep-ph/9806336; F. G. Cao and A. I. Signal, Phys. Rev. D **60** (1999) 114012 [arXiv:hep-ph/9908481].

[195] T. E. Browder, T. Gershon, D. Pirjol, A. Soni and J. Zupan, arXiv:0802.3201 [hep-ph].

[196] W. Beenakker, PhD thesis: "Electroweak Corrections: Techniques and Applications", University of Leiden, 1989;
W. Hollik, "Precision Tests of the Electroweak Theory, Part 1". Lectures given at the CERN-JINR School of Physics 1989. CERN-TH-5661/90